CECW-ET Engineer Manual 1110-2-6050	Department of the Army U.S. Army Corps of Engineers Washington, DC 20314-1000	EM 1110-2-6050 30 June 1999
	Engineering and Design RESPONSE SPECTRA AND SEISMIC ANALYSIS FOR CONCRETE HYDRAULIC STRUCTURES	
	Distribution Restriction Statement Approved for public release; distribution is unlimited.	

EM 1110-2-6050
30 June 1999

US Army Corps
of Engineers

ENGINEERING AND DESIGN

Response Spectra and Seismic Analysis for Concrete Hydraulic Structures

ENGINEER MANUAL

DEPARTMENT OF THE ARMY
U.S. Army Corps of Engineers
Washington, DC 20314-1000

EM 1110-2-6050

CECW-ET

Manual
No. 1110-2-6050

30 June 1999

Engineering and Design
RESPONSE SPECTRA AND SEISMIC ANALYSIS FOR CONCRETE HYDRAULIC STRUCTURES

1. Purpose. This manual describes the development and use of response spectra for the seismic analysis of concrete hydraulic structures. The manual provides guidance regarding how earthquake ground motions are characterized as design response spectra and how they are then used in the process of seismic structural analysis and design. The manual is intended to be an introduction to the seismic analysis of concrete hydraulic structures. More detailed seismic guidance on specific types of hydraulic structures will be covered in engineer manuals and technical letters on those structures.

2. Applicability. This manual applies to all USACE Commands having responsibilities for the design of civil works projects.

3. Scope of Manual. Chapter 1 provides an overview of the seismic assessment process for hydraulic structures and the responsibilities of the project team involved in the process, and also briefly summarizes the methodologies that are presented in Chapters 2 and 3. In Chapter 2, methodology for seismic analysis of hydraulic structures is discussed, including general concepts, design criteria, structural modeling, and analysis and interpretation of results. Chapter 3 describes methodology for developing the earthquake ground motion inputs for the seismic analysis of hydraulic structures. Emphasis is on developing response spectra of ground motions, but less detailed guidance is also provided for developing acceleration time-histories.

4. Distribution Statement. Approved for public release; distribution is unlimited.

FOR THE COMMANDER:

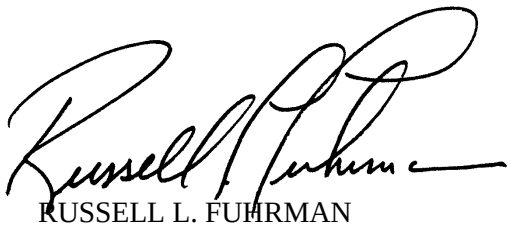

RUSSELL L. FUHRMAN
Major General, USA
Chief of Staff

DEPARTMENT OF THE ARMY
U.S. Army Corps of Engineers
Washington, DC 20314-1000

CECW-ET

EM 1110-2-6050

Manual
No. 1110-2-6050

30 June 1999

Engineering and Design
RESPONSE SPECTRA AND SEISMIC ANALYSIS FOR CONCRETE HYDRAULIC STRUCTURES

Table of Contents

Chapter 1
Introduction

1-1. Purpose

This manual describes the development and use of response spectra for the seismic analysis of concrete hydraulic structures. The manual provides guidance regarding how earthquake ground motions are characterized as design response spectra and how they are then used in the process of seismic structural analysis and design. The manual is intended to be an introduction to the seismic analysis of concrete hydraulic structures. More detailed seismic guidance on specific types of hydraulic structures will be covered in engineer manuals and technical letters on those structures.

1-2. Applicability

This manual applies to all USACE Commands having responsibilities for the design of civil works projects.

1-3. Scope of Manual

Chapter 1 provides an overview of the seismic assessment process for hydraulic structures and the responsibilities of the project team involved in the process, and also briefly summarizes the methodologies that are presented in Chapters 2 and 3. In Chapter 2, methodology for seismic analysis of hydraulic structures is discussed, including general concepts, design criteria, structural modeling, and analysis and interpretation of results. Chapter 3 describes methodology for developing the earthquake ground motion inputs for the seismic analysis of hydraulic structures. Emphasis is on developing response spectra of ground motions, but less detailed guidance is also provided for developing acceleration time-histories.

1-4. References

References are listed in Appendix A.

1-5. Responsibilities of Project Team

The development and use of earthquake ground motion inputs for seismic analysis of hydraulic structures require the close collaboration of a project team that includes the principal design engineer, seismic structural analyst, materials engineer, and geotechnical specialists. The principal design engineer is the leader of the project team and has overall responsibility for the design. The seismic structural analyst plans, executes, and evaluates the results of seismic analyses of the structure for earthquake ground motions for the design earthquakes. The materials engineer characterizes the material properties of the structure. The geotechnical specialists conduct evaluations to define the design earthquakes and input ground motions and also characterize the properties of the soils or rock foundation for the structure. Any potential for seismically induced failure of the foundation is evaluated by the geotechnical specialists. The geotechnical evaluation team typically involves the participation of geologists, seismologists, and geotechnical engineers.

1-6. Overview of Seismic Assessment

The overall process of seismic assessment of concrete hydraulic structures consists of the following steps: establishment of earthquake design criteria, development of design earthquakes and characterization of earthquake ground motions, establishment of analysis procedures, development of structural models, prediction of earthquake response of the structure, and interpretation and evaluation of the results. The following paragraphs present a brief description of each step, the objectives, and the personnel needed to accomplish the tasks.

a. Establishment of earthquake design criteria. At the outset, it is essential that the lead members of the project team (principal design engineer, seismic structural analyst, materials engineer, and lead geotechnical specialist) have a common understanding of the definitions of the project operating basis earthquake (OBE) and maximum design earthquake (MDE). Structure performance criteria for each design earthquake should also be mutually understood. Having this understanding, the geotechnical team can then proceed to develop an overall plan for developing design earthquakes and associated design response spectra and acceleration time-histories, while the structural team begins establishing conceptual designs and analysis and design methods leading to sound earthquake-resistant design or safety evaluation.

b. Development of design earthquakes and characterization of earthquake ground motions.

(1) Assessing earthquake potential. The project geologist and seismologist must initially develop an understanding of the seismic environment of the site region. The seismic environment includes the regional geology, regional tectonic processes and stress conditions leading to earthquakes, regional seismic history, locations and geometries of earthquake sources (faults or source areas), and the type of faulting (strike slip, reverse, or normal faulting). Analysis of remote imagery and field studies to identify active faults may be required during this step. Next, maximum earthquake sizes of the identified significant seismic sources must be estimated (preferably in terms of magnitude, but in some cases in terms of epicentral Modified Mercalli intensity). Earthquake recurrence relationships (i.e., the frequency of occurrence of earthquakes of different sizes) must also be established for the significant seismic sources.

(2) Determining earthquake ground motions. After the geologist and seismologist have characterized the seismic sources, the geotechnical engineer and/or strong-motion seismologist members of the geotechnical team can then proceed to develop the design (OBE and MDE) ground motions, which should include response spectra and, if needed, acceleration time-histories as specified by the principal design engineer. The design ground motions should be based on deterministic and probabilistic assessments of ground motions. These design ground motions should be reviewed and approved by the principal design engineer.

c. Establishment of analysis procedures.

(1) Basic entities of analysis procedures. The establishment of analysis procedures is an important aspect of the structural design and safety evaluation of hydraulic structures subjected to earthquake excitation. The choice of analysis procedures may influence the scope and nature of the seismic input characterization, design procedures, specification of material properties, and evaluation procedures of the results. The basic entities of analysis procedures described in this manual are as follows: specification of the form and point of application of seismic input for structural analysis, selection of method of analysis and design, specification of material properties and damping, and establishment of evaluation procedures.

(2) Formulation of analysis procedures. The analysis procedures and the degree of sophistication required in the related topics should be established by the principal design engineer. In formulating rational structural analysis procedures, the principal design engineer must consult with experienced seismic structural, materials, and geotechnical specialists to specify the various design and analysis parameters as well as the type of seismic analysis required. The seismic structural specialist should review the completed design criteria for adequacy and in the case of major projects may work directly with the engineering seismologists and the geotechnical engineers in developing the seismic input. The physical properties of the construction materials and the foundation supporting the structure are determined in consultation with the materials, geotechnical engineer, and the engineering geologist (for the rock foundation).

d. Development of structural models. The task of structural modeling should be undertaken by an engineer (seismic structural analyst) who is familiar with the basic theory of structural dynamics as well as the finite element structural analysis. The structural analyst should work closely with the principal design engineer in order to develop an understanding of the basic functions and the dynamic interactions among the various components of the structure. In particular, interaction effects of the foundation supporting the hydraulic structure and of the impounded, surrounding, or contained water should be accounted for. However, the structural model selected should be consistent with the level of refinement used in specifying the earthquake ground motion, and should always start with the simplest model possible. Classifications, unit weights, and dynamic modulus and damping properties of the backfill soils and the soil or rock foundation are provided by the geotechnical engineer or engineering geologist member of the project team. Various aspects of the structural modeling and the way seismic input is applied to the structure are discussed in Chapter 2.

e. Prediction of earthquake response of structure. After constructing the structural models, the seismic structural analyst should perform appropriate analyses to predict the earthquake response of the structure. Prediction of the earthquake response includes the selection of a method of analysis covered in paragraph 1-7, formulation of structural mass and stiffness to obtain vibration properties, specification of damping, definition of earthquake loading and combination with static loads, and the computation of response quantities of interest. The analysis should start with the simplest method available and progress to more refined types as needed. It may begin with a pseudo-static analysis performed by hand or spreadsheet calculations, and end with more refined linear elastic response-spectrum and time-history analyses carried out using appropriate computer programs. The required material parameters are formulated initially based on preliminary values from the available data and past experience, but may need adjustment if the analysis shows strong sensitivity to certain parameters, or new test data become available. Damping values for the linear analysis should be selected consistent with the induced level of strains and the amount of joint opening or cracking and yielding that might be expected. Seismic loads should be combined with the most probable static loads, and should include multiple components of the ground motion when the structure is treated as a two-dimensional (2-D) or three-dimensional (3-D) model. In the modal superposition method of dynamic analysis, the number of vibration modes should be selected according to the guidelines discussed in Chapter 2, and response quantities of interest should be determined based on the types of information needed for the design or the safety evaluation. In simplified procedures, the earthquake loading is represented by the equivalent lateral forces associated with the fundamental mode of vibration, where the resultant forces are computed from the equations of equilibrium.

f. Interpretation and evaluation of results.

(1) Responsibilities. The seismic structural analyst and the principal design engineer are the primary personnel responsible for the interpretation and evaluation of the results. The final evaluation of seismic

performance for damaging earthquakes should include participation by experienced structural earthquake engineers.

(2) Interpretation and evaluation. The interpretation of analysis results should start with the effects of static loads on the structure. The application of static loads and the resulting deflections and stresses (or forces) should be thoroughly examined to validate the initial stress conditions. The earthquake performance of the structure is then evaluated by combining the initial static stresses (or forces) with the dynamic stresses (or forces) due to the earthquake. The evaluation for the linear elastic analysis is carried out by comparing computed stresses for unreinforced concrete (URC) or section forces and deformations for reinforced concrete (RC) with the allowable stress values or the supplied capacities, in accordance with the performance goals set forth in Chapter 2. However, in view of the fact that the predicted earthquake response of the structure is based on numerous assumptions, each of which has a limited range of validity, the evaluation procedure should not be regarded as absolute. The final evaluation therefore should consider the uncertainties associated with the earthquake ground motions, accuracy of the analysis techniques, level of foundation exploration, testing, and confidence in material properties, as well as limitations of the linear analysis and engineering judgment to predict nonlinear behavior.

1-7. Summary of Seismic Analysis of Concrete Hydraulic Structures

a. General. Hydraulic structures traditionally have been designed based on the seismic coefficient method. This simple method is now considered inadequate because it fails to recognize dynamic behavior of the structures during earthquake loading. The seismic coefficient method should be used only in the preliminary design and evaluation of hydraulic structures for which an equivalent static force procedure based on the vibration properties of the structure has not yet been formulated. The final design and evaluation of hydraulic structures governed by seismic loading should include response spectra and, if needed, acceleration time-histories as the seismic input and response spectrum or time-history method of analysis for predicting the dynamic response of the structure to this input. With recent advances in the estimation of site-specific ground motions and in structural dynamic computer analysis techniques, the ability to perform satisfactory and realistic analyses has increased. This manual presents improved guidelines for the estimation of site-specific ground motions and the prediction of dynamic response for the design and seismic safety evaluation of hydraulic structures.

b. Types of hydraulic structures. The general guidelines provided in this manual apply to concrete hydraulic structures including locks, intake towers, earth retaining structures, arch dams, conventional and Roller Compacted Concrete (RCC) gravity dams, powerhouses, and critical appurtenant structures.

c. Design criteria. The design and evaluation of hydraulic structures for earthquake loading must be based on appropriate criteria that reflect both the desired level of safety and the nature of the design and evaluation procedures (ER 1110-2-1806). The first requirement is to establish earthquake ground motions to be used as the seismic input by considering safety, economics, and the designated operational functions. The second involves evaluating the earthquake performance of the structure to this input by performing a linear elastic dynamic analysis based on a realistic idealization of the structure, foundation, and water.

d. Design earthquakes. The design earthquakes for hydraulic structures are the OBE and the MDE. The actual levels of ground motions for these earthquakes depend on the type of hydraulic structure under consideration, and are specified in the seismic design guidance provided for a particular structure in conjunction with ER 1110-2-1806.

(1) Operating basis earthquake (OBE). The OBE is an earthquake that can reasonably be expected to occur within the service life of the project, that is, with a 50 percent probability of exceedance during the

service life. The associated performance requirement is that the project function with little or no damage, and without interruption of function.

(2) Maximum design earthquake (MDE). The MDE is the maximum level of ground motion for which the structure is designed or evaluated. The associated performance requirement is that the project performs without catastrophic failure, such as uncontrolled release of a reservoir, although severe damage or economic loss may be tolerated. The MDE is set equal to the maximum credible earthquake (MCE) or to a lesser earthquake, depending on the critical nature of the structure (see ER 1110-2-1806 and paragraph 2-4b).

(3) The MCE is defined as the greatest earthquake that can reasonably be expected to be generated by a specific source on the basis of seismological and geological evidence.

e. Earthquake ground motion(s). The ground motions for the design earthquakes are defined in terms of smoothed elastic response spectra and, if required, also in terms of acceleration time-histories. Standard ground motions selected from published ground motion maps can be used in preliminary and screening studies, and for final design or evaluation in areas of low to moderate seismicity where the earthquake loading does not control the design. Site-specific ground motions, as described in Chapter 3, are required for projects with high to significant hazard potential in case of failure and located in areas of high seismicity, and in areas of moderate seismicity where the earthquake loading controls the design (ER 1110-2-1806).

f. Structural idealization. The structural idealization should start with the simplest model possible and, if required, progress to a 2-D or a more comprehensive 3-D model. The structural model should represent the important features of the dynamic behavior of the structure including its interaction with the foundation and the water. It should also be consistent with the design and evaluation objectives, that is, to reflect the relative accuracy suitable for the type of seismic input used as well as the type of studies performed, i.e., feasibility, preliminary, or final study. For example, one-dimensional (1-D) models are used for the preliminary design and evaluation, whereas depending on geometry of the structure, 2-D or 3-D models are used in the final phase of the study.

(1) Simplified models. Simplified models are based on the equivalent lateral force procedures, where the earthquake response of the structure is obtained directly from the response spectra. In most cases only the fundamental mode of vibration, but sometimes the second mode as well, is considered. However, only the fundamental mode is adjusted to account for the effects of structure-foundation and structure-water interaction.

(2) Two-dimensional models. 2-D models including the structure-foundation and structure-water interaction effects are developed using the finite element (FE) procedures. They are employed in the final or preliminary study of structures for which simplified models have not yet been formulated. The seismic input consists of response spectra (or acceleration time-histories) for the vertical and one horizontal components of ground motion. The seismic input is applied either at the base of the composite structure-foundation model or at the base of the structure if the substructure method of analysis is used.

(3) Three-dimensional models. Hydraulic structures with complicated 3-D geometry should be idealized as 3-D models and analyzed for all three components of the earthquake ground motion. The model should be developed using FE procedures and account for the effects of structure-foundation and structure-water interaction. The seismic input in the form of response spectra or acceleration time-histories is applied along three principal axes of the structure either at the base of the composite structure-foundation model or at the base of the structure if the foundation region is analyzed separately.

g. Dynamic analysis procedures. Linear dynamic analysis procedures are presently used for earthquake-resistant design and safety evaluation of hydraulic structures. The linear dynamic analysis is performed using the response spectrum or the time-history modal superposition method. The primary feature of the modal analysis is that the total response of a structure is obtained by combining the response of its individual modes of vibration, calculated separately. The response spectrum analysis is adequate for structures whose responses to earthquakes are within the linear elastic range. But for structures for which the cracking strength of the concrete and yield strength of the reinforcing steels may be exceeded under a major earthquake, a linear time-history analysis provides additional information that is essential to approximating the damage or expected level of inelastic response behavior.

(1) Response spectrum analysis. In the response spectrum analysis, the maximum response of the structure to earthquake excitation is evaluated by combining the maximum responses from individual modes and multicomponent input. All response quantities computed in this manner are positive and require careful examination and interpretation. The accuracy of the results depends on the number of vibration modes considered and the methods of combination used for the modal and multicomponent earthquake responses.

(2) Time-history analysis. Linear time-history analysis involves computation of the complete response history of the structure to earthquakes, and not just the maximum values. The results of such analysis serve to demonstrate the general behavior of the seismic response, and combined with rational interpretation and judgment can provide a reasonable estimate of the expected inelastic behavior or damage, when the cracking or other form of nonlinearity is considered to be slight to moderate. Prediction of the actual damage that could occur during major earthquakes can only be estimated using more complicated nonlinear analyses, but approximate assessment can still be made using the analysis discussed in paragraph 2-4b(3)(a) and (b). The complete nonlinear analysis of hydraulic structures is not currently practical; only limited aspects of the nonlinear response behavior such as joint opening and sliding of blocks can be considered.

h. Interpretation and evaluation of results. The evaluation of earthquake performance of hydraulic structures is currently based on the numerical results of linear dynamic analyses, in which the calculated stresses for URC or section forces and deformations for RC are compared with the allowable stress values or the supplied moment and shear capacities. New hydraulic structures should resist the OBE excitation within the elastic range of the element stresses (or section forces) to avoid structural damage or yielding. However, existing hydraulic structures in high seismic hazard regions may be allowed to respond to the OBE excitation within the *nearly elastic* range; that is, minor local damage or yielding is permitted if retrofit to preclude damage is deemed uneconomical. The evaluation for the severe MDE excitation is more complicated because the dynamic response is expected to exceed the linear elastic limits, resulting in damage and inelastic behavior. In such cases, the extent of damage for URC hydraulic structures is normally estimated based on the results of linear response history analysis together with engineering judgment and other considerations discussed in paragraph 2-8a(4). For RC hydraulic structures undergoing inelastic deformations, approximate postelastic dynamic analyses are performed to ensure that the inelastic demands of the severe MDE excitation can be resisted by the available capacity of the structure. The postelastic analysis discussed in paragraph 2-4b(3)(b) is a step-by-step linear analysis with revised stiffness or resistance characteristics of all structural members that have reached their yielding capacities. The stiffness modification and analysis of the modified structure are repeated until no further yielding will occur or the structure reaches a limit state with excessive distortions, mechanism, or instability.

1-8. Summary of Development of Site-Specific Response Spectra for Seismic Analysis of Structures

a. Factors affecting earthquake ground motion. It has been well recognized that earthquake ground motions are affected by earthquake source conditions, source-to-site transmission path properties, and site conditions. The source conditions include stress conditions, source depth, size of rupture area, amount of rupture displacement, rise time, style of faulting, and rupture directivity. The transmission path properties include the crustal structure and the shear wave velocity and damping characteristics of the crustal rock. The site conditions include the rock properties beneath the site to depths of up to 2 km, the local soil conditions at the site for depths of up to several hundred feet, and the topography of the site. In current ground motion estimation relationships, the effects of source, path, and site are commonly represented in a simplified manner by earthquake magnitude, source-to-site distance, and local subsurface conditions. Due to regional differences in some of the factors affecting earthquake ground motions, different ground motion attenuation relationships have been developed for western United States (WUS) shallow crustal earthquakes, eastern United States (EUS) earthquakes, and subduction zone earthquakes (which, in the United States, can occur in portions of Alaska, northwest California, Oregon, and Washington). It is also recognized that ground motions in the near-source region of earthquakes may have certain characteristics not found in ground motions at more distant sites, especially a high-energy intermediate-to-long-period pulse that occurs when fault rupture propagates toward a site.

b. Basic approaches for developing site-specific response spectra. There are two basic approaches to developing site-specific response spectra: deterministic and probabilistic. In the deterministic approach, termed deterministic seismic hazard analysis, or DSHA, typically one or more earthquakes are specified by magnitude and location with respect to a site. Usually, the earthquake is taken as the MCE and assumed to occur on the portion of the source closest to the site. The site ground motions are then estimated deterministically, given the magnitude and source-to-site distance. In the probabilistic approach, termed probabilistic seismic hazard analysis, or PSHA, site ground motions are estimated for selected values of the probability of ground motion exceedance in a design time period or for selected values of return period of ground motion exceedance. A PSHA incorporates the frequency of occurrence of earthquakes of different magnitudes on the various seismic sources, the uncertainty of the earthquake locations on the sources, and the ground motion attenuation including its uncertainty. Guidance for using both of these approaches is presented in Chapter 3 and is briefly summarized below.

(1) Deterministic approach for developing site-specific response spectra. Deterministic estimates of response spectra can be obtained by either Approach 1, anchoring a response spectral shape to the estimated peak ground acceleration (PGA); or Approach 2, estimating the response spectrum directly. When Approach 1 is followed, it is important to consider the effects of various factors on spectral shape (e.g., regional tectonic environment, earthquake magnitude, distance, local soil or rock conditions). Because of the significant influence these factors have on spectral shape and because procedures, data, and relationships are now available to estimate response spectra directly, Approach 2 should be used. Approach 1 can be used for comparison. The implementation of Approach 2 involves the following:

(a) Using response spectral attenuation relationships of ground motions (attenuation relationships are now available for directly estimating response spectral values at specific periods of vibration).

(b) Performing statistical analyses of response spectra of ground motion records.

(c) Applying theoretical (numerical) ground motion modeling.

When soil deposits are present at a site and response spectra on top of the soil column are required (rather than or in addition to spectra on rock), then either empirically based approaches and/or analytical procedures can be used to assess the local soil amplification effects. Empirically based approaches rely on recorded ground motion data and resulting empirical relationships for similar soil conditions. Analytical procedures involve modeling the dynamic properties of the soils and using dynamic site response analysis techniques to propagate motions through the soils from the underlying rock.

(2) Probabilistic approach for developing site-specific response spectra. Similar to a deterministic analysis, a probabilistic development of a site-specific response spectrum can be made by either Approach 1, anchoring a spectral shape to a PGA value, or Approach 2, developing the spectrum directly. In Approach 1, PSHA is carried out for PGA, and an appropriate spectral shape must then be selected. The selection of the appropriate shape involves the analysis of earthquake sizes and distances contributing to the seismic hazard. In Approach 2, the PSHA is carried out using response spectral attenuation relationships for each of several periods of vibration. Drawing a curve connecting the response spectral values for the same probability of exceedance gives a response spectrum having an equal probability of exceedance at each period of vibration. The resulting spectrum is usually termed an equal-hazard spectrum. Approach 2 should be used because response spectral attenuation relationships are now available and the use of these relationships directly incorporates into the analysis the influence of different earthquake magnitudes and distances on the results for each period of vibration.

c. Developing acceleration time-histories. When acceleration time-histories are required for the structure dynamic analysis, they should be developed to be consistent with the design site-specific response spectrum. They should also have an appropriate duration of shaking (duration of shaking is strongly dependent on earthquake magnitude). The two general approaches to developing acceleration time-histories are selecting a suite of recorded motions that, in aggregate, have spectra that envelope the design spectrum; or synthetically modifying one or more recorded motions to produce motions having spectra that are a close match to the design spectrum ("spectrum matching" approach). For either approach, when near-source ground motions are modeled, it is desirable to include a strong intermediate-to-long-period pulse to model this characteristic that is observed in near-source ground motions.

1-9. Terminology

Appendix I contains defiinitions of terms that relate to Response Spectra and Seismic Analysis for Hydraulic Structures.

Chapter 2
Seismic Analysis of Concrete Hydraulic Structures

2-1. Introduction

a. General. This chapter provides structural guidance for the use of response spectra for the seismic design and evaluation of the Corps of Engineers hydraulic structures. These include locks, intake towers, earth retaining structures, arch dams, conventional and RCC gravity dams, powerhouses, and critical appurtenant structures. The specific requirements are provided for the structures built on rock, such as the arch and most gravity dams, as well as for those built on soil or pile foundations, as in the case of some lock structures. The response spectrum method of seismic design and evaluation provisions for building-type structures are summarized in paragraph 2-10.

b. Interdisciplinary collaboration. A complete development and use of response spectra for seismic design and evaluation of hydraulic structures require the close collaboration of a project team consisting of several disciplines.

(1) Project team. The specialists in the disciplines of seismology, geophysics, geology, and geotechnical engineering develop design earthquakes and the associated ground motions, with the results presented and finalized in close cooperation with structural engineers. The materials engineer and geotechnical specialists specify the material properties of the structure and of the soils and rock foundation. The structural engineer in turn has the special role of explaining the anticipated performance and the design rationale employed to resist the demands imposed on the structure by the earthquake ground motions.

(2) Ground motion studies. As discussed in Chapter 3, the seismic input in the form of site-specific response spectra is developed using a deterministic or a probabilistic approach. Both methods require the following three main items to be clearly addressed and understood so the project team members have a common understanding of the design earthquakes: seismic sources, i.e., faults or source areas that may generate earthquakes; maximum earthquake sizes that can occur on the identified sources and their frequency of occurrence; and attenuation relationships for estimation of ground motions in terms of magnitude, distance, and site conditions. The results of ground motion studies should be presented as required in ER 1110-2-1806. For a DSHA mean and 84^{th} percentile, response spectra for the MCE should be presented. For a PSHA, response spectra should be presented as equal hazard spectra at various levels of probability and damping, as described in ER 1110-2-1806 and Chapter 3. Acceleration time-histories based on natural or synthetic accelerograms may also be required. The assumptions and methodology used to perform a DSHA and PSHA should be explained, and the uncertainties associated with the selection of input parameters should be presented in the report.

2-2. General Concepts

Two essential problems must be considered in the seismic analysis and design of structures: definition of the expected earthquake input motion and the prediction of the response of the structure to this input. The solutions to these problems are particularly more involved for the structures founded on soil or pile foundations and for those built on rock sites with complicated topography as in the case of arch dams.

a. Input motion(s). A general description of the factors affecting the earthquake input motions to be used in the design and evaluation of structures is demonstrated in Figure 2-1. The base rock motion

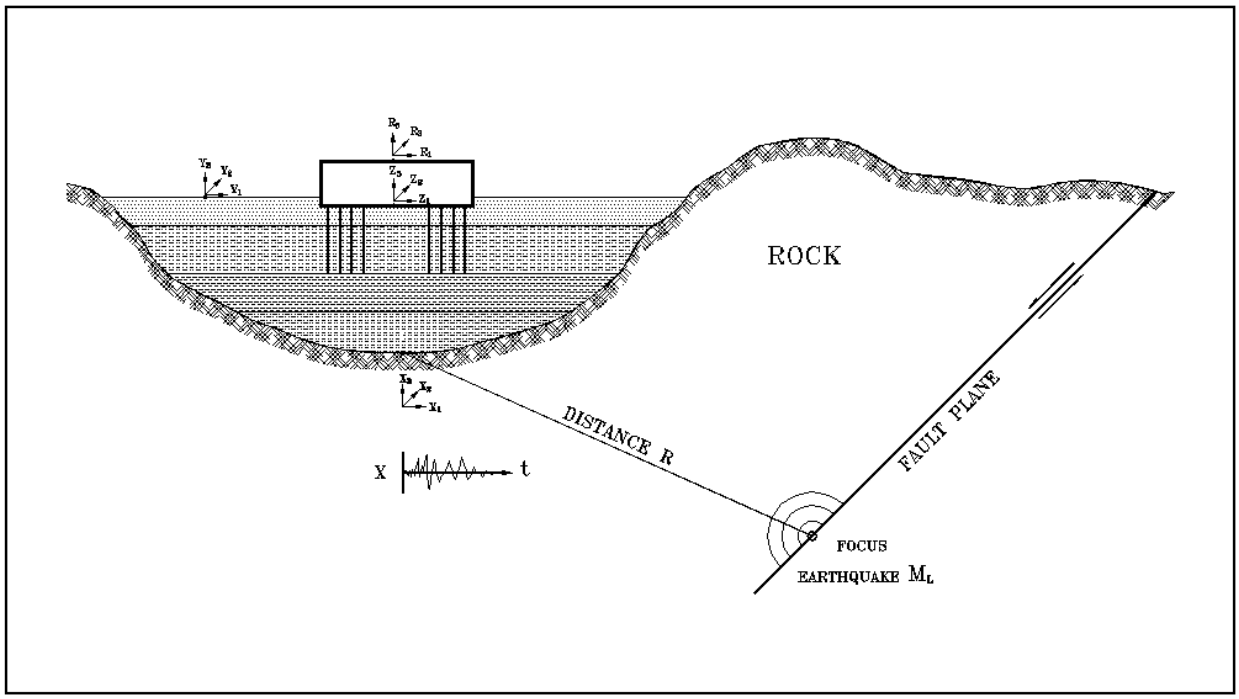

Figure 2-1. Factors affecting seismic input motion for a structure founded on soil-pile foundation

X_i(i = 1,2,3) is estimated from the study of regional geologic setting, historic seismicity of the area, and the geologic structure along the path from source to site. The characteristics of this motion, however, are affected by the local soil conditions as it travels to the free ground surface. Thus, the resulting free-field motion Y_i (i = 1,2,3), in the absence of the structure, differs from X_i in terms of the peak amplitude, the frequency content, and the spatial distribution of the motion characteristics. In addition, the dynamic interaction of the structure with the soil foundation produces a further change of the seismic motions, leading to Z_i (i = 1,2,3) at the soil-structure interface. Depending on the method of analysis adopted, one of these motions is selected as the earthquake input in the actual dynamic analysis of the structure. If X_i or Y_i is selected, the soil foundation is modeled as part of the structure, and a direct method of soil-structure interaction (SSI) analysis is performed. Alternatively, the structure and the soil region may be treated as two separate substructures. First the soil region is analyzed with the mass of the structure set to zero, to obtain ground motion Z_i at the soil-structure interface (kinematic interaction). The same model is also used to determine the dynamic stiffness of the soil region. Then Z_i is used as the input motions in the subsequent earthquake response analysis of the structure whose stiffness is now being combined with the dynamic stiffness of the soil region, and its mass being considered. To estimate these ground motions, however, many aspects of the problem such as the seismic environment, dynamic soil properties, site response, and the structural analysis must be considered. The solution thus requires close cooperation among the geologist, seismologist, and geotechnical and structural engineers to achieve satisfactory results.

b. Structural response. The second problem involves prediction of the response of the structure to the specified input motion. This requires development of a structural model, specification of material properties and damping, and calculation of the response, taking into account the dynamic interactions with the foundation, the water, and the backfill soils. Depending on complexity of the structure and intensity of the earthquake, a simple or more advanced modeling and analysis may be required. In either case the analysis should consist of the following steps, except that the level of effort may be different for simple and more refined analyses:

(1) Establishment of earthquake design criteria.

(2) Development of design earthquakes and associated ground motions.

(3) Establishment of analysis procedure.

(4) Development of structural models.

(5) Prediction of earthquake response of the structure.

(6) Interpretation and evaluation of results.

2-3. Design Criteria

The design and evaluation of hydraulic structures for earthquake loading must be based on appropriate criteria that reflect both the desired level of safety and the choice of the design and evaluation procedures (ER 1110-2-1806). The first requirement is to establish design earthquake ground motions to be used as the seismic input by giving due consideration to the consequences of failure and the designated operational function. Then the response of the structure to this seismic input must be calculated taking into account the significant interactions with the rock, soil, or pile foundation as well as with the impounded, or surrounding and contained water. The analysis should be formulated using a realistic idealization of the structure-water-foundation system, and the results are evaluated in view of the limitations, assumptions, and uncertainties associated with the seismic input and the method of analysis.

2-4. Design Earthquakes

a. Operating basis earthquake (OBE).

(1) Definition and performance. The OBE is an earthquake that can reasonably be expected to occur within the service life of the project, that is, with a 50 percent probability of exceedance during the service life. (This corresponds to a return period of 144 years for a project with a service life of 100 years.) The associated performance requirement is that the project function with little or no damage, and without interruption of function. The purpose of the OBE is to protect against economic losses from damage or loss of service. Therefore alternative choices of return period for the OBE may be based on economic considerations. In a site-specific study the OBE is determined by a PSHA (ER 1110-2-1806).

(2) Analysis. For the OBE, the linear elastic analysis is adequate for computing seismic response of the structure, and the simple stress checks in which the predicted elastic stresses are compared with the expected concrete strength should suffice for the performance evaluation. Structures located in regions of high seismicity should essentially respond elastically to the OBE event with no disruption to service, but limited localized damage is permissible and should be repairable. In such cases, a low to moderate level of damage can be expected, but the results of a linear time-history analysis with engineering judgment may still be used to provide a reasonable estimate of the expected damage.

b. Maximum design earthquake (MDE).

(1) Definition and performance. The MDE is the maximum level of ground motion for which a structure is designed or evaluated. The associated performance requirement is that the project performs without catastrophic failure, such as uncontrolled release of a reservoir, although severe damage or economic loss may be tolerated. The MDE can be characterized as a deterministic or probabilistic event (ER 1110-2-1806).

(a) For critical structures the MDE is set equal to the MCE. Critical structures are defined in ER 1110-2-1806 as structures of high downstream hazard whose failure during or immediately following an earthquake could result in loss of life. The MCE is defined as the greatest earthquake that can reasonably be expected to be generated by a specific source on the basis of seismological and geological evidence (ER 1110-2-1806).

(b) For other than critical structures the MDE is selected as a lesser earthquake than the MCE, which provides for an economical design meeting specified safety standards. This lesser earthquake is chosen based upon an appropriate probability of exceedance of ground motions during the design life of the structure (also characterized as a return period for ground motion exceedance).

(2) Nonlinear response. The damage during an MDE event could be substantial, but it should not be catastrophic in terms of loss of life, economics, and social and environmental impacts. It is evident that a realistic design criterion for evaluation of the response to damaging MDEs should include nonlinear analysis, which can predict the nature and the extent of damage. However, a complete and reliable nonlinear analysis that includes tensile cracking of concrete, yielding of reinforcements, opening of joints, and foundation failure is not currently practical. Only limited aspects of the nonlinear earthquake response behavior of the mass concrete structures such as contraction joint opening in arch dams, tensile cracking in concrete gravity dams, and sliding of concrete monoliths have been investigated previously. There is a considerable lack of knowledge with respect to nonlinear response behavior of the hydraulic structures. Any consideration of performing nonlinear analysis for hydraulic structures should be done in consultation with CECW-ED.

(3) Performance evaluation. The earthquake performance evaluation of the response of hydraulic structures to a damaging MDE is presently based on the results of linear elastic analysis. In many cases, a linear elastic analysis can provide a reasonable estimate of the level of expected damage when the cracking, yielding, or other forms of nonlinearity are considered to be slight to moderate.

(a) URC. For URC hydraulic structures subjected to a severe MDE, the evaluation of damage using the linear time-history analysis may still continue. The evaluation, however, must be based on a rational interpretation of the results by giving due consideration to several factors including number and duration of stress excursions beyond the allowable limits, the ratio of computed to allowable values, simultaneous stress distributions at critical time-steps, size and location of overstressed area, and engineering judgment.

(b) RC. Such evaluation for the RC hydraulic structures should include approximate postelastic analysis of the system considering ductility and energy dissipation beyond yield. First the section forces for critical members are computed using the linear elastic analysis procedure described in this manual. These forces are defined as the force *demands* imposed on the structure by the earthquake. Next the yield or plastic capacities at the same locations are computed and defined as the force *capacities*. Finally, the ratio of force demands to force capacities is computed to establish the *demand-capacity ratios* for all the selected locations. The resulting demand-capacity ratios provide an indication of the ductility that may be required for the structural members to withstand the MDE level of ground motion. If the computed demand-capacity ratios for a particular structure exceed the limits set forth in the respective design documents for that structure, approximate postelastic analyses should be performed to ensure that the inelastic demands of the MDE excitation on the structure can be resisted by the supplied capacity. This evaluation consists of several equivalent linear analyses with revised stiffness or resistance characteristics of all structural members that have reached their yielding capacities. The stiffness modification and analysis of the modified structure are repeated until no further yielding will occur or the structure reaches a limit state with excessive distortions, mechanism, or instability.

2-5. Earthquake Ground Motions

Earthquake ground motions for analysis of hydraulic structures are usually characterized by peak ground acceleration, response spectra, and acceleration time-histories. The peak ground acceleration (usually as a fraction of the peak) is the earthquake ground motion parameter usually used in the seismic coefficient method of analysis. The earthquake ground motions for dynamic analysis, as a minimum, should be specified in terms of response spectra (Figure 2-2). A time-history earthquake response analysis, if required, should be performed using the acceleration time-histories. The standard response spectra are described in the following paragraphs, and procedures for estimating site-specific response spectra are discussed in Chapter 3.

a. Elastic design response spectra. Elastic design response spectra of ground motions can be defined by using standard or site-specific procedures. As illustrated in Figure 2-2, elastic design response spectra represent maximum responses of a series of single-degree-of-freedom (SDOF) systems to a given ground motion excitation (Ebeling 1992; Chopra 1981; Clough and Penzien 1993; Newmark and Rosenblueth 1971). The maximum displacements, maximum pseudo-velocities, and maximum pseudo-accelerations presented on a logarithmic tripartite graph provide advance insight into the dynamic behavior of a structure. For example, Figure 2-2 shows that at low periods of vibration (<0.05 sec), the spectral or pseudo-accelerations approach the PGA, an indication that the rigid or very short period structures undergo the same accelerations as the ground. This figure also shows that structures with periods in the range of about 0.06 to 0.5 sec are subjected to amplified accelerations and thus higher earthquake forces, whereas the earthquake forces for flexible structures with periods in the range of about 1 to 20 sec are reduced substantially but their maximum displacements exceed that of the ground. In the extreme, when the period exceeds 20 sec, the structure experiences the same maximum displacement as the ground. The response spectrum amplifications depend on the values of damping and are significantly influenced by the earthquake magnitude, source-to-site distance, and the site conditions (Chapter 3).

(1) Standard or normalized response spectra. The standard response spectra described in this section are to be used in accord with ER 1110-2-1806 and follow-up guidance. The development starts with the spectral acceleration ordinates obtained from the National Earthquake Hazards Reduction Program (NEHRP) hazard maps. The site coefficients to be used with the hazard maps to develop standard response spectra for various soil profiles, as well as the methodology to construct response spectra at return periods other than those given in NEHRP, are provided in the guidance in ER 1110-2-1806.

(2) Site-specific response spectra.

(a) Site-specific procedures to produce design response spectra are to be used in accord with ER 1110-2-1806. Site-specific response spectra correspond to those expected on the basis of the seismological and geological calculations for the site. The procedures described in Chapter 3 use either the deterministic or probabilistic method to develop site-specific spectra.

(b) While the deterministic method provides a single estimate of the peak ground acceleration and response spectral amplitudes, the probabilistic method estimates these parameters as a function of probability of exceedance or return period. To select the return period to use for the OBE and MDE, see the definitions of these design earthquakes in paragraphs 2-4a and 2-4b, respectively. The resulting response spectra for the selected return period should then be used as input for quantifying the seismic loads required for the design and analysis of structures.

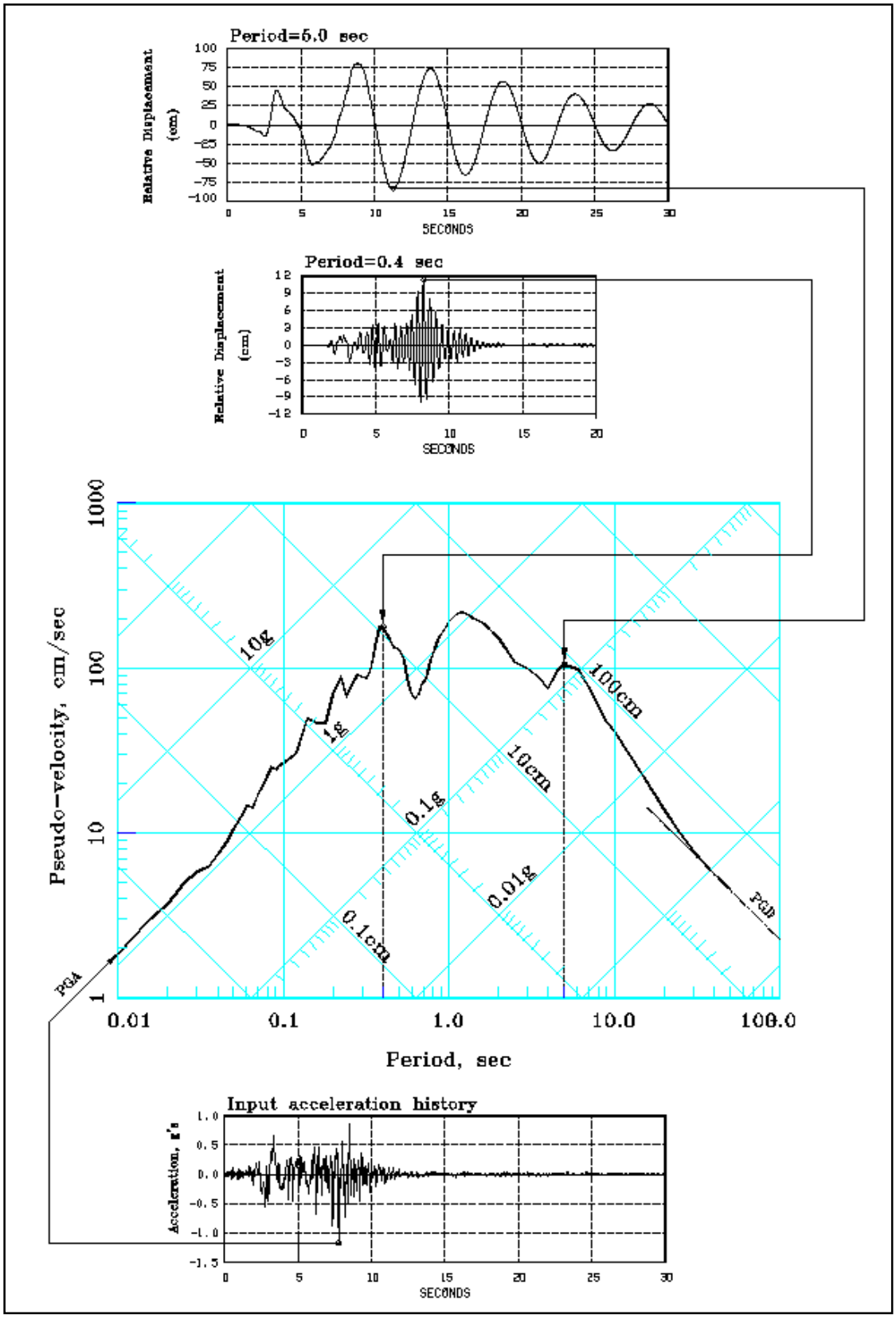

Figure 2-2. Construction of tripartite elastic design response spectrum

b. Acceleration time-histories. Various procedures for developing representative acceleration time-histories at a site are described in Chapter 3. Whenever possible, the acceleration time-histories should be selected to be similar to the design earthquake in the following aspects: tectonic environment, earthquake magnitude, fault rupture mechanism (fault type), site conditions, design response spectra, and duration of strong shaking. Since it is not always possible to find records that satisfy all of these criteria, it is often necessary to modify existing records or develop synthetic records that meet most of these requirements.

2-6. Establishment of Analysis Procedures

Seismic analysis of hydraulic structures should conform to the overall objectives of new designs and satisfy the specific requirements of safety evaluation of existing structures. The choice of analysis procedures may influence the scope and nature of the seismic input characterization, design procedures, specification of material properties, and evaluation and interpretation of the results. Simple procedures require fewer and easily available parameters, while refined analyses usually need more comprehensive definition of the seismic input, structural idealization, and material properties. The analysis should begin with the simplest procedures possible and then, if necessary, progress to more refined and advanced types. Simplified procedures are usually adequate for the feasibility and preliminary studies, whereas refined procedures are more appropriate for the final design and safety evaluation of structures. The simplified analysis also serves to assess the need for a more elaborate analysis and provide a baseline for comparison with the results obtained from the more elaborate analyses.

2-7. Structural Idealization

Structural models should be developed by giving careful consideration to the geometry, stiffness, and mass distributions, all of which affect the dynamic characteristics of the structure. The engineering judgment and knowledge of the dynamics of structures are required to develop a satisfactory model that is both simple and representative of the most important dynamic behavior of the structure. Depending on its level of complexity, a hydraulic structure may be represented by a simplified one-dimensional model, a planar or 2-D model whose deformations are restricted in a plane, or by a more elaborate 3-D model to account for its 3-D behavior.

a. Simplified models. Structures with regular geometry and mass distribution along one axis may be idealized by simplified models using the beam theory. The simplified model should approximately represent the significant features of the dynamic response of the structure including the fundamental period and mode shape, as well as the effects of structure-foundation and structure-water interaction. Two such simplified models have been developed for the free-standing intake towers and the nonoverflow gravity dam sections. In both cases, the simplified models were formulated based on the results of finite element analyses that rigorously accounted for the structure-water-foundation interaction effects, as well as for the reservoir bottom energy absorption for the gravity dams.

(1) Simplified model for intake towers. The preliminary design and safety evaluation of the free-standing and regular intake towers may be conducted using the simplified model shown in Figure 2-3. A step-by-step analysis procedure for this cantilever beam model is provided in Goyal and Chopra (1989) and Appendix H. Some important features and assumptions of this approximate model are as follows:

(a) It is applicable to towers with regular geometry in plan and elevation.

(b) Only flexural deformations are considered.

(c) Seismic response is calculated for the first two modes of vibration.

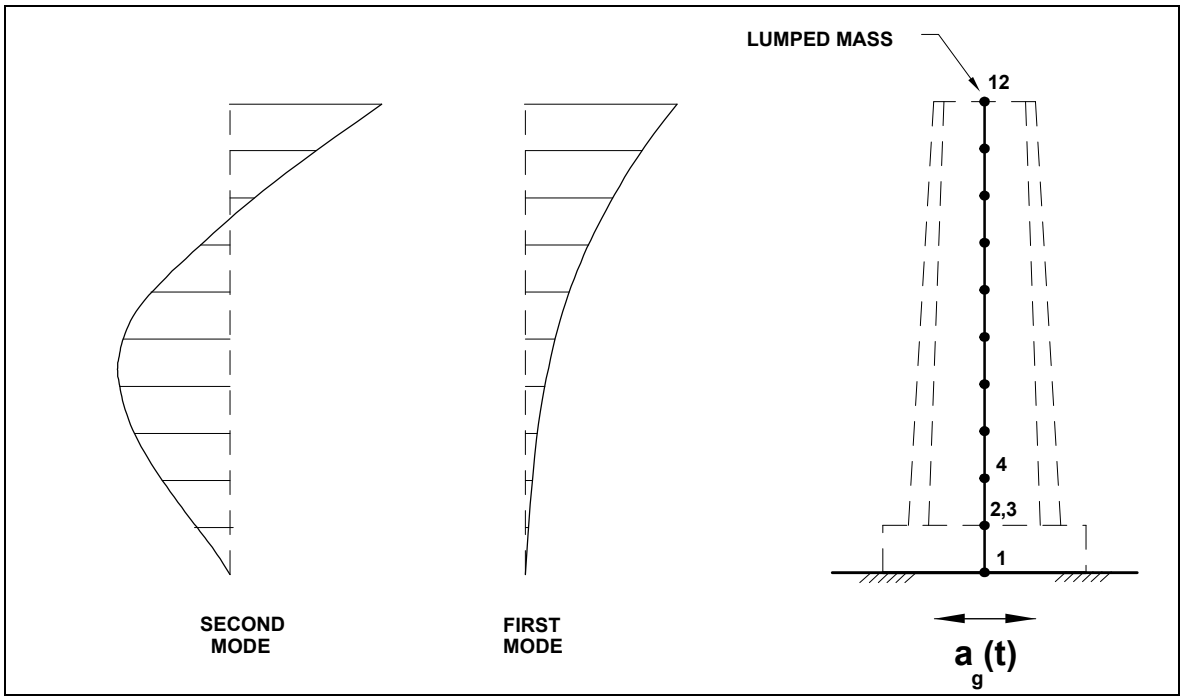

Figure 2-3. Simplified model of intake tower ($a_g(t)$ = ground motion acceleration)

(d) Foundation-structure interaction effects are considered only for the first mode of vibration.

(e) Interaction between the tower and the inside and outside water is represented by the added mass assumption.

(f) The effects of vertical component of ground motion are ignored.

Note that slender towers with cross-section dimensions 10 times less than the height of the structure can usually be adequately represented solely by the flexural deformations of the tower. However, the effects of shear deformations on vibration frequencies and section forces, especially for higher modes, are significant when the cross-section dimensions exceed 1/10 of the tower height and should be included in the analysis. The effects of shear deformation can be incorporated in the analysis if a computer program with beam elements including shear deformation is used. The earthquake response for this simplified model should be calculated for the combined effects of the two horizontal components of the ground motions. The maximum shear forces, moments, and stresses for each lateral direction are computed separately using the specified response spectrum and the calculated vibration properties associated with that direction. The total response values of the tower are then obtained by combining the responses caused by each of the two components of the earthquake ground motion, as discussed in paragraph 2.8a(2)(f).

(2) Simplified model for gravity dams. The preliminary design and safety evaluation of gravity dams may start with a simplified model developed by Fenves and Chopra (1986), as shown in Figure 2-4. In this procedure, deformations of the dam monolith are restricted to the fundamental mode of vibration of the dam on rigid foundation rock. Standard values are provided for the fundamental vibration period and mode shape of typical nonoverflow gravity sections. But they are not available for the nonstandard or spillway sections whose geometries substantially differ from that of a typical nonoverflow section. In such cases, the fundamental vibration period and mode shape for the nonstandard section should be

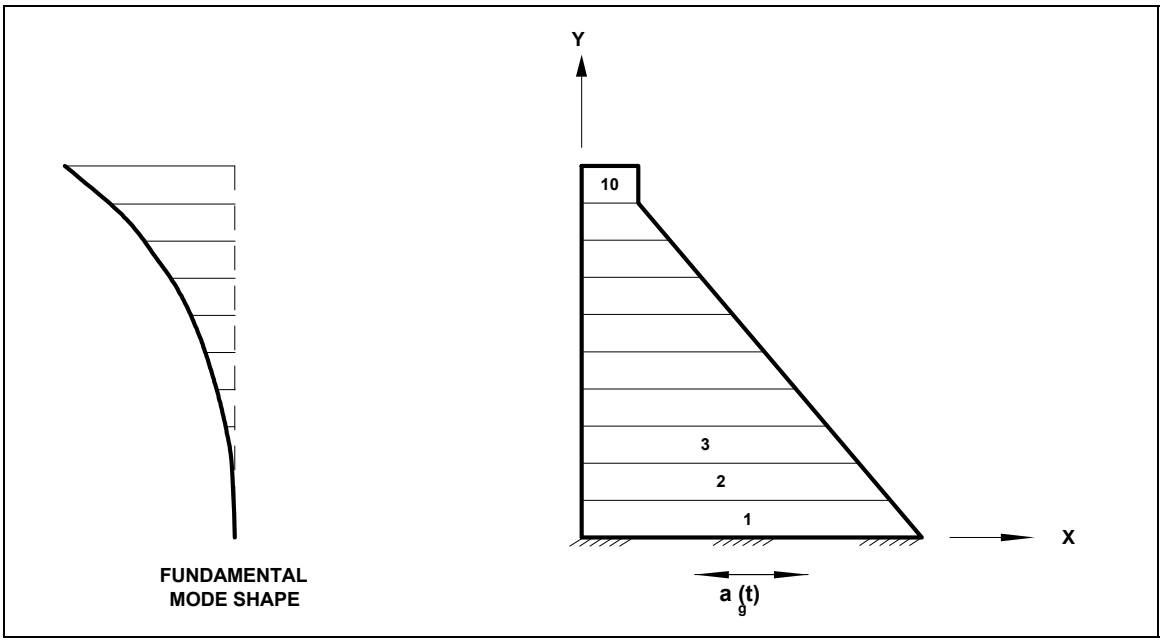

Figure 2-4. Simplified model of gravity dam monolith (Fenves and Chopra (1986), courtesy of Earthquake Engineering Research Center, University of California at Berkeley)

estimated using other procedures before this simplified method could be applied. The most important features of the simplified model are summarized as follows.

(a) Only fundamental mode of vibration is considered; contributions due to higher modes are accounted for by static correction.

(b) The upstream face of the dam is assumed to be vertical or nearly vertical.

(c) The effects of vertical ground motion are ignored.

(d) The interactions with the foundation rock and water are accounted for by adjustment of the vibration period and damping of the fundamental mode. The inertial effects of the added mass of water are considered in terms of additional lateral hydrodynamic forces.

b. Two-dimensional models. 2-D idealization is used to model planar or very long structures. Most Corps of Engineers hydraulic structures are of the latter type such as the retaining walls, gravity dams, outlet tunnels, and lock structures. These structures are usually made of independent segments separated by construction joints, and the loads perpendicular to the long axis are assumed not to vary along each segment. Under these conditions, the structure may be modeled as a 2-D slice using either the plane stress or plane strain elements, as shown in Figure 2-5. The choice of plane stress or plane strain elements depends on whether the stress or strain in the out-of-plane direction can be neglected. In either case, plane strain models should be used to idealize the foundation supporting the structure. 2-D models should be analyzed for two components of the earthquake ground motion applied in the vertical and one horizontal direction. However, the way the seismic input is applied to the structure depends on the type of foundation model being used. Three commonly used foundation models and their associated seismic input for the analysis of typical hydraulic structures are discussed in the following paragraphs.

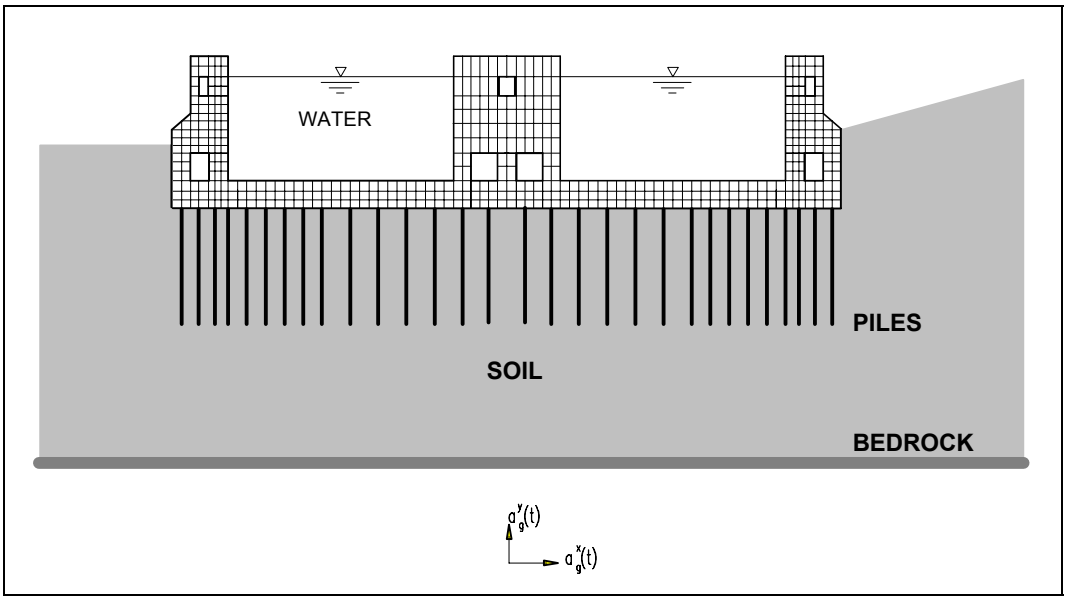

Figure 2-5. 2-D model of W-frame lock

(1) Rigid rock-base excitation. The standard approach to accounting for the effects of the foundation interaction is to analyze the combined structure-foundation system by including an appropriate region of the rock in the finite element idealization, as shown in Figure 2-6a. In this approach, the earthquake motion is represented as a rigid body translation a_R of the basement rock, and either the response spectra or acceleration time-histories are used as input to the model. The characteristics of the specified earthquake ground motion should be similar to the motions recorded on the rock sites. The location of the rigid boundary at the base of the model should be selected consistent with the size and type of the structure being analyzed. The mass of foundation rock should be ignored so that the free-field motions recorded at ground surface are directly applied to the structure without changes, and the spurious reflection effects caused by the rigid boundary assumption are eliminated.

(2) Free-field earthquake excitation. For rock and firm soil sites where similar foundation materials extend to large depths, the foundation region may be idealized as a homogeneous, isotropic, viscoelastic

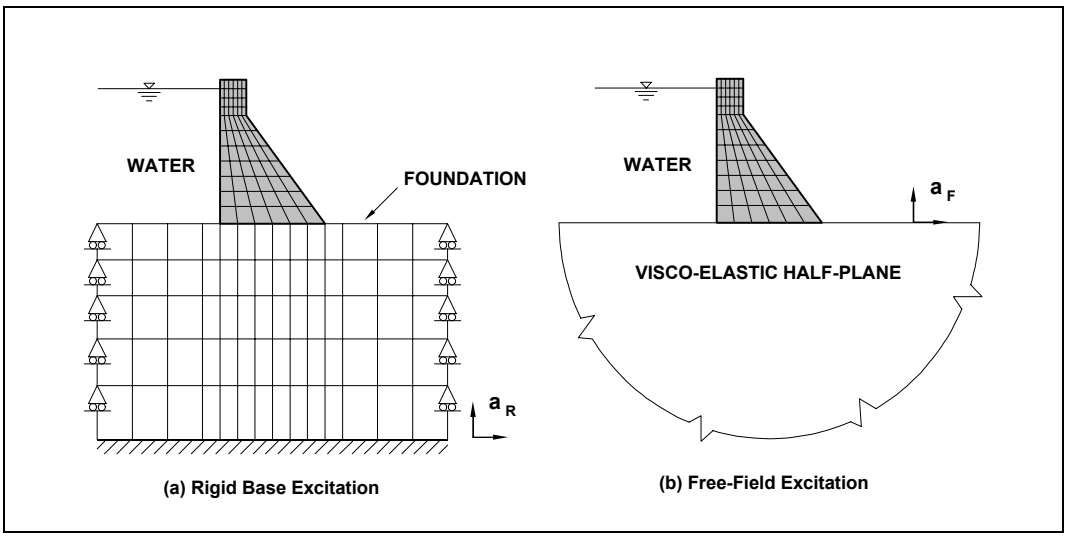

Figure 2-6. Earthquake excitation for rock or firm soil sites

half-plane (Dasgupta and Chopra 1979), as shown in Figure 2-6b. In this case, the structure is supported on the horizontal surface of the foundation, and the earthquake response is formulated with respect to the free-field definition of the ground motion a_F rather than the basement rock input. The interaction effects of the foundation are represented by a frequency-dependent dynamic stiffness matrix defined with respect to the degrees of freedom on the structure-foundation interface. The seismic input for this idealization is in the form of acceleration time-histories of the free-field motion; the response spectrum method of analysis is not applicable. This method is currently used in the analysis of gravity dams and free-standing intake towers when the foundation material can be assumed homogeneous.

(3) Soil-pile-structure earthquake excitation. Unlike the gravity dams and intake towers, lock structures may be supported on pile groups embedded in nonhomogeneous soil media. In such cases, the soil-pile-structure interaction significantly affects the earthquake response of the structure and piles and should be considered in the analysis. Figure 2-7 schematically presents two methods for the earthquake analysis of structures founded on the soil-pile foundations (Wass and Hartmann 1984). In the direct method illustrated in Figure 2-7a, the piles and the soil up to the transmitting boundaries are modeled as part of the structure. The nonlinear soil behavior may be represented by the equivalent linear method (Seed and Idriss 1969). The seismic input in the form of acceleration time-histories is applied at the rock basement (rock-soil interface), and the earthquake response of the structure and the pile forces are determined. Alternatively, the analysis may be performed in two steps consisting of the kinematic and inertial parts, with the total motion a divided into a_k and a_i caused by kinematic and inertial interactions, respectively, as shown in Figures 2-7b and 2-7c. First the kinematic interaction is evaluated using the same model employed in the direct method, except that the mass of the structure is set to zero (M = 0). This analysis provides the ground motions a_k at the structure-soil interface, the required seismic input for the subsequent dynamic analysis for the inertial-interaction effects. The dynamic stiffness matrix of the soil-pile foundation needed for the inertial interaction analysis is also determined from the analysis of the same model employed in the kinematic interaction analysis. However, the resulting dynamic stiffness (or impedance function) for the soil-pile region is a complex valued matrix that requires solution in the frequency domain. The 2-D direct method and kinematic interaction analysis described above have been used for the analysis of pile foundation with backfill soils using the FLUSH program (Olmsted Locks and Dam, Design Memorandum No. 7, U.S. Army Engineer District, Louisville 1992). These analyses also provide response spectrum seismic input at the pile tips required for performing 3-D rigid-cap pile-group dynamic analysis using the Computer-Aided Structural Engineering (CASE) computer program, X0085 (CPGD), Dynamic Analysis of Pile Groups.

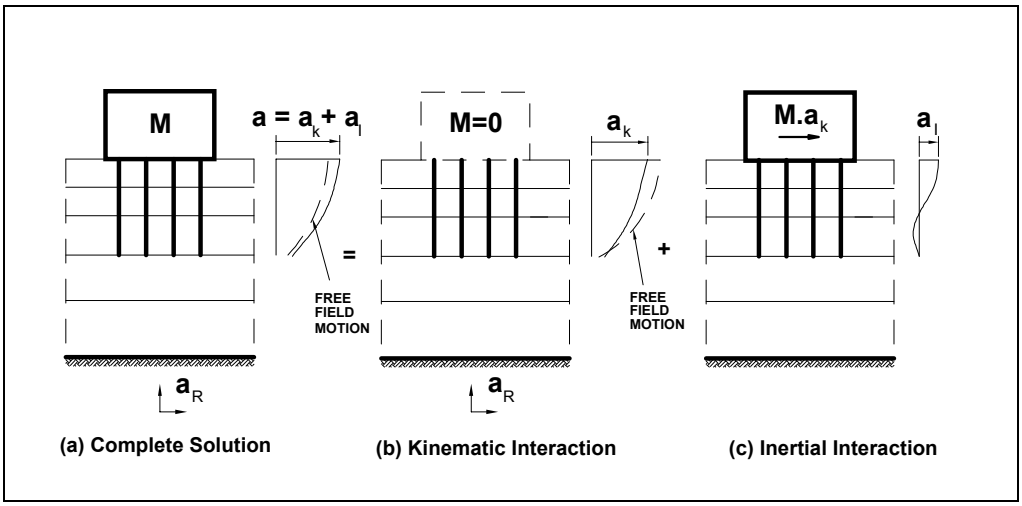

Figure 2-7. Schematic of earthquake response analysis for soil-pile-structure interaction

c. Three-dimensional (3-D) models. 3-D finite-element models are used to analyze hydraulic structures with complex geometry or nonuniform loading. Such structures include the arch dams, inclined intake towers supported on the abutment foundations, irregular free-standing intake towers with significant torsional behavior, gravity dams built in narrow canyons, and certain lock monoliths with complicated components and loading conditions. Arch dams must be treated as 3-D systems consisting of the concrete arch, foundation rock, and the impounded water (Figure 2-8). The inclined intake towers should be treated as 3-D structures to account for not only their complicated geometry and torsional behavior, but also for ground motions that must be applied at the tower base and along the entire tower-abutment interface. The irregular free-standing towers exhibiting dominant torsional modes of vibration should also be analyzed using 3-D models. Gravity dams built in narrow canyons are another example requiring 3-D treatment, because the customary assumption that dam monoliths behave independently is no longer valid—the movements of each monolith under these conditions are restrained by the adjacent ones, causing torsional moments or twists that would affect the manner in which the loads are distributed. The pile-founded lock structures with complicated geometry and structural components usually feature complicated soil-pile-structure interaction, which may require 3-D treatment. The specification of earthquake input for analysis of 3-D structures depends on the level of sophistication and capabilities used in modeling the dynamic behavior of the structure. The basic procedures are based on the general concepts described by Clough et al. (1985). These are summarized in the following paragraphs.

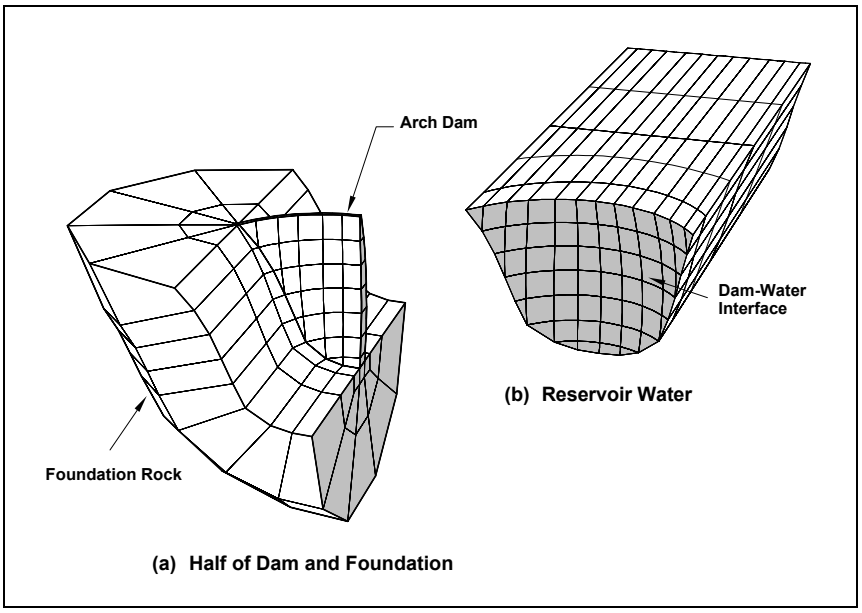

Figure 2-8. 3-D model of arch dam-water-foundation system

(1) Standard base input model. It is assumed that 3-D structures built on rock sites are supported by a large volume of deformable rock, which in turn is supported by a rigid boundary. The seismic input in the form of response spectra or acceleration time-histories is defined as the motion of this rigid base, but it should be noted that the motions applied to the rigid base differ from the free-field motions recorded at ground surface.

(2) Massless foundation rock model. An improved version of the model described in (1) above is obtained by neglecting the mass of the deformable foundation region. In this case no wave propagation takes place through the foundation rock; thus the prescribed motions at the rigid base are directly transmitted to the structure interface. With this assumption it is reasonable to use the earthquake motions

recorded at the ground surface as the rigid base input as for the 2-D analysis in Figure 2-6a. This procedure is commonly used in the practical analysis of 3-D structures built on rock sites. GDAP (Ghanaat 1993) and ADAP-88 (Fenves, Mojtahedi, and Reimer 1989) and other arch dam analysis programs commonly use this type of foundation model.

(3) Deconvolution base rock input model. In this approach the recorded free-field surface motions are deconvolved to determine the motions at the rigid base boundary. The deconvolution analysis is performed on a horizontally uniform layer of deformable rock or soil deposits using the one-dimensional wave propagation theory. For the soil sites, however, the strain-dependent nature of the nonlinear soil should be considered. The resulting rigid base motion is then applied at the base of the 3-D foundation-structure system, in which the foundation model is assumed to have its normal mass as well as stiffness properties. This procedure permits the wave propagation in the foundation rock, but requires an extensive model for the foundation rock, which computationally is inefficient.

(4) Free-field input model. A more reasonable approach for defining the seismic input would be to apply the deconvolved rigid base motion to a foundation model without the structure in place and to calculate the free-field motions at the interface positions, where the structure will be located. These interface free-field motions would be used as input to the combined structure-foundation model, which employs a relatively smaller volume of the rock region. It should be noted that the resulting seismic input at the interface varies spatially due to the scattering effects of canyon walls (in the case of arch dams) in addition to the traveling wave effects that also take place in the relatively long structures, even when the contact surface is flat. In either case, the computer program used should have capabilities to permit multiple support excitation. The application of this procedure has not yet evolved to practical problems.

(5) Soil-pile-structure interaction model. The seismic input for 3-D structures supported on pile foundations may be evaluated using a 3-D extension of the procedure discussed in b(3) above. However, the soil-pile-structure interaction analysis should also consider the inclined propagating body and surface waves if the structure is relatively long and is located close to a potential seismic source, or if it is supported on a sediment-filled basin. In particular, long-period structures with natural periods in the predominant range of surface waves should be examined for the seismic input that accounts for the effects of surface waves. One limiting factor in such analyses is the maximum number of piles that can be considered in the analysis of structures on a flexible base. For example a pile-founded lock structure may include a monolith having more than 800 piles. 3-D soil-structure interaction analysis programs such as SASSI (Lysmer et al. 1981) with pile groups analysis capability may not be able to handle such a large problem without some program modifications or structural modeling assumptions that could lead to a reduced number of piles for the idealized monolith.

2-8. Dynamic Analysis Procedures

The idealized model of structures and the prescribed earthquake ground motions are used to estimate the dynamic response of structures to earthquakes. The dynamic analysis is performed using the response spectrum or time-history method. The response spectrum method is usually a required first step in a dynamic analysis for the design and evaluation of hydraulic structures. In many cases it suffices for the structures located in low seismic hazard regions. It is also the preferred design tool, because the maximum response values for the design can be obtained directly from the earthquake response spectrum. However, the response spectrum procedure is an approximate method for calculating only the maximum response values and is restricted to the linear elastic analysis. The time-history method, on the other hand, is applicable to both linear elastic and nonlinear response analyses and is used when the time-dependent response characteristics or the nonlinear behavior is important, as explained later.

a. Modal analysis procedure. The modal superposition method is used to compute the earthquake response of structures within their linear elastic range of behavior. This procedure is especially applicable to the majority of Corps of Engineers hydraulic structures that are designed to remain essentially elastic when subjected to the medium intensity ground motions, such as the OBE. The modal analysis is also used for the MDE excitation, except that the computed linear elastic response is permitted to exceed the concrete cracking and yield stress levels for a limited amount in order to account for energy absorption of the structure. As illustrated in Figure 2-9, the primary feature of the modal analysis is that the total response of a structure is obtained by combining the response of its individual modes of vibration calculated separately. Furthermore, only the response in the first few modes need be calculated, because the response of structures to earthquakes is essentially due to the lower modes. The response of each individual mode is computed from the analysis of an SDOF system, according to the procedures described in the following paragraphs.

(1) Simplified Response Spectrum Analysis. The simplified response spectrum analysis (SRSA) is used for dynamic analysis of structures for which a simplified model of the types described in paragraph 2-7a can be developed. Whenever possible, this approximate analysis should be attempted to provide a preliminary estimate of the seismic response, as well as a basis for comparison with the results of a more refined analysis. The SRSA is normally employed for the analysis of structures whose dynamic behavior can be represented by an equivalent SDOF system. The maximum response of an idealized structure by the SRSA procedure is estimated as follows:

(a) Design response spectrum. For a preliminary analysis the standard response spectra described in paragraph 2-5a(1) should be used when a site-specific response spectrum does not exist.

(b) Natural frequencies and vibration mode shapes. Use the standard simplified procedures (Fenves and Chopra 1986, Goyal and Chopra 1989) to calculate the fundamental natural period and mode shape for the nonoverflow gravity dam sections and the regular intake towers. For other structures idealized by an equivalent SDOF system, the fundamental frequency and mode shape may be computed using the iterative methods described by Clough and Penzien (1993).

(c) Damping. Energy dissipation in the form of a damping ratio is included as part of the response spectrum curves. For the linear elastic or nearly elastic response during an OBE event, the damping value should be limited to 5 percent. For the MDE excitation, a damping constant of 7 or 10 percent may be used depending on the level of strains and the amount of inelastic response developed in the structure.

(d) Maximum modal displacement. The spectral acceleration, S_{an} (T_n ξ_n) corresponding to the nth mode (here nth mode is assumed to be the fundamental mode) period of vibration, T_n, and the specified damping ratio, ξ_n, is directly obtained from the prescribed response spectrum. The maximum modal displacement in terms of S_{an} (T_n, ξ_n) is given by:

$$Y_n = \frac{L_n}{M_n \omega_n^2} S_{an}\left(T_n, \xi_n\right) \tag{2-1}$$

where

$L_n = \sum_{j=1}^{K} m_j \phi_{jn}$ is the modal earthquake-excitation factor

$M_n = \sum_{j=1}^{K} m_j \phi_{jn}^2$ is the modal mass

RESPONSE SPECTRUM ANALYSIS

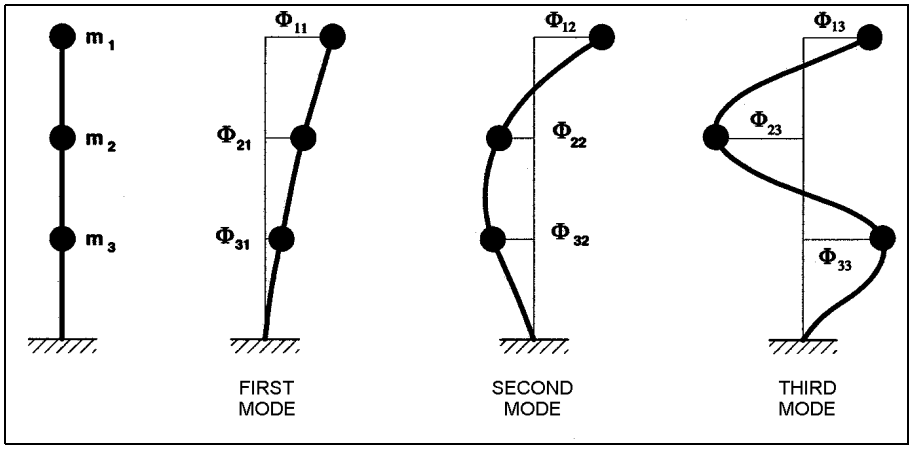

(1) Compute mode shapes [ϕ_{j1}, ϕ_{j2}, ϕ_{j3}] and natural periods [T_1, T_2, T_3]

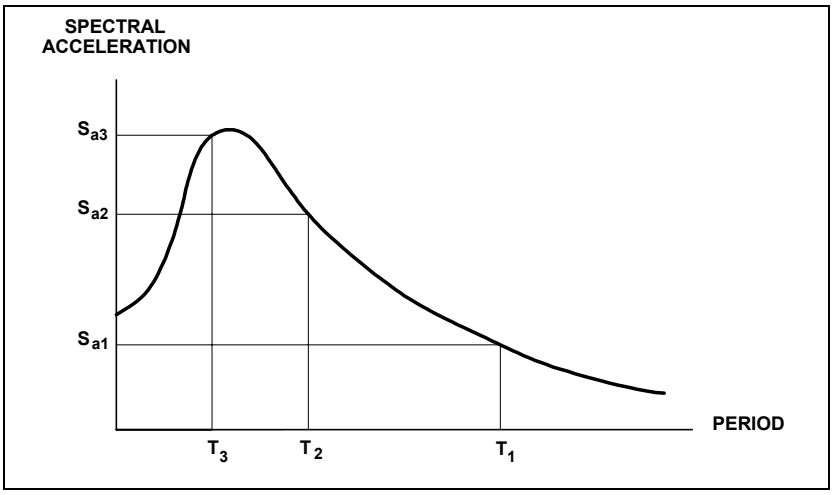

(2) Obtain spectral accelerations [S_{a1}, S_{a2}, S_{a3}] for all modes

$$L_n = \sum_{j=1}^{3} \phi_{jn} m_j \quad ; \quad M_n = \sum_{j=1}^{3} \phi_{jn}^2 m_j$$

$$PF_n = L_n / M_n$$

$$Y_n = \frac{PF_n}{\omega_n^2} \cdot S_{an} \qquad where \quad n = 1,2,3$$

(3) Compute modal participation factor PF_n and maximum modal response Y_n

Figure 2-9. Illustration of response spectrum mode-superposition analysis (Continued)

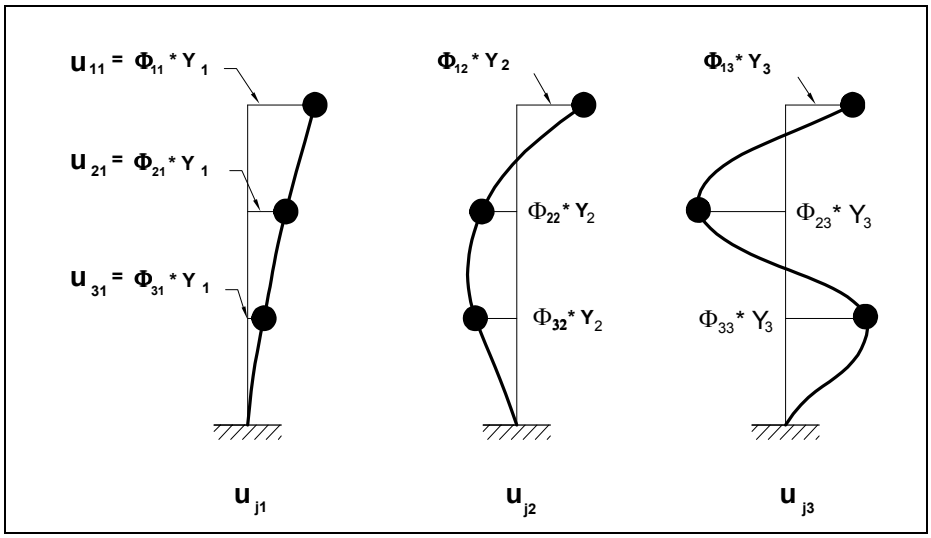

(4) Compute maximum response of structure in each mode from $u_n=\Phi_{n*}Y_n$

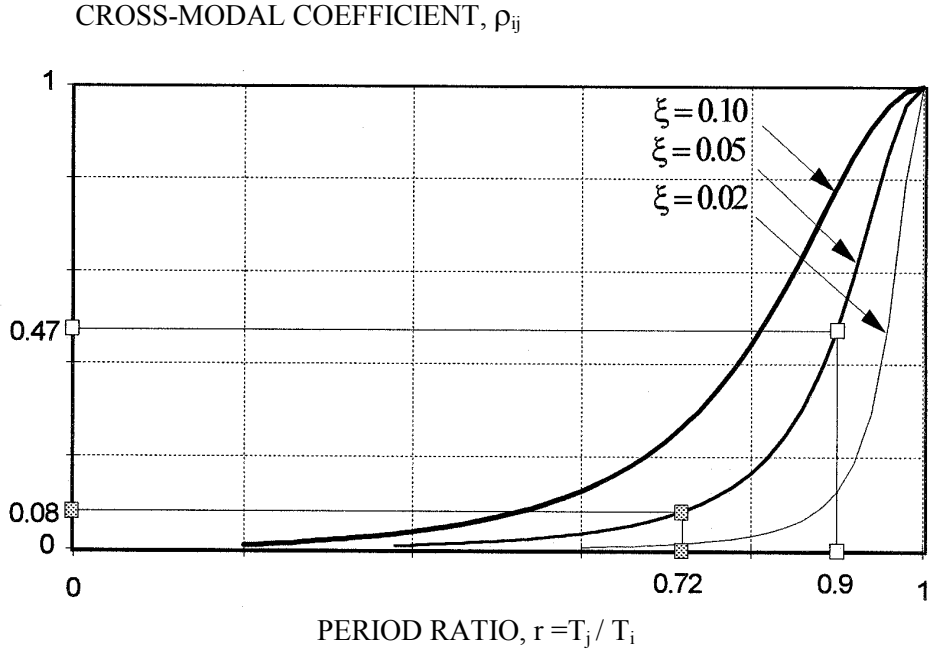

(5) Obtain cross-modal coefficients ρ_{ij}

$$u_k = \left[\sum_{i=1}^{3} \sum_{j=1}^{3} u_{ki} \rho_{ij} u_{kj} \right]^{1/2}$$

(6) Compute total response u_k due to earthquake in direction *k*

Figure 2-9. (Concluded)

$\omega_n = 2\pi/T_n$ is the circular frequency

K = number of degrees of freedom in structural model

The ratio L_n/M_n is the modal participation factor PF_n indicating the degree to which mode n is excited by the ground motion.

(e) Maximum displacement. With the maximum modal displacement being computed in step (d), the maximum displacement of the structure is computed as

$$u_{jn} = \frac{L_n}{M_n \omega^2} \phi_{jn} S_{an}\left(T_n, \xi_n\right) \tag{2-2}$$

where ϕ_{jn} is the assumed or calculated mode shape of the structure.

(f) Maximum shear and moment. The shear forces and moments at sections along the height of the structure are obtained by static analysis from the equivalent lateral forces as follows:

$$f_{jn} = \frac{L_n}{M_n} m_j \phi_{jn} S_{an}\left(T_n, \xi_n\right) \tag{2-3}$$

$$V_n = \sum f_{jn} \tag{2-4}$$

$$M_n = \sum h_j f_{jn} \tag{2-5}$$

where

f_{jn} = maximum value of equivalent lateral force at the j^{th} section

h_j = associated moment arm

(2) Response spectrum modal superposition method. The estimation of maximum response of a hydraulic structure to earthquake excitation usually involves many modes of vibration, which may contribute significantly to the response. The contributions of various modes to the total displacements, forces, and stresses depend on a number of factors including the response spectrum ordinates, natural periods of vibration, and mode shapes, which in turn depend on the mass and stiffness properties of the structure. The seismic responses of such structures are further complicated by the dynamic interaction with the foundation supporting the structure and the impounded water. In general, the simplified SDOF procedures described above may not be applicable in most cases or may provide only a very crude estimate of the response. In these situations, the structure is analyzed using the response-spectrum modal-superposition method illustrated in Figure 2-9. The response-spectrum modal-superposition analysis is usually carried by standard or specialized programs following the same analysis steps described in a(1), but additional factors including the number of modes, combination of modal responses, and the effects of multiple components of earthquake input should also be considered.

(a) Number of modes. There are no guidelines for determining in advance how many modes should be included in a response spectrum analysis, because it depends on the dynamic characteristics of the structure and the response spectrum ordinates. However, the analysis should include a sufficient number

of modes until the calculated response quantities are at least within 10 percent of the "exact" values. Since the "exact" response values are not known, a trial and error procedure may be adapted, in which analyses are repeated with addition of modes until it is seen that the addition of modes does not significantly affect the results. Alternatively, it may be demonstrated that the participating effective modal masses are at least within 90 percent of the total mass of the structures.

(b) Combination of modal responses. The response spectrum analysis procedure described above provides only the maximum response in each mode of vibration. The response quantities of interest, such as the peak displacements, element stresses, element forces, and moments, evaluated for each significant mode of vibration should be combined to obtain the total response of the structure. Since modal responses do not occur at the same time during the earthquake excitation, they should be combined using the complete quadratic combination (CQC) or the square root of the sum of the squares (SRSS) method described below.

(c) CQC method. The CQC modal combination method (Wilson, Der Kiureghian, and Bayo 1981) is based on random vibration theory and can be used in the response spectrum analysis if the duration of the strong motion portion of the earthquake shaking is several times longer than the fundamental period of the structure and if the design response spectrum ordinates vary slowly over a wide range of periods that include the dominant modes of the structure. Both conditions are easily met for short-period hydraulic structures and smooth design response spectra with 5 percent damping or more. The CQC formula for the maximum combined displacements u_k to an earthquake in direction k is given by

$$u_k = \left[\sum_{i=1}^{N} \sum_{j=1}^{N} u_{ki} \rho_{ij} u_{kj} \right]^{1/2} \tag{2-6}$$

where u_{ki} and u_{kj} are the maximum modal displacements corresponding to the vibration modes i and j, respectively, and N is the number of modes. The cross-modal coefficients ρ_{ij} for the above two conditions and for the constant modal damping ξ are expressed by

$$\rho_{ij} = \frac{8\xi^2 (1+r) r^{3/2}}{(1-r^2)^2 + 4\xi^2 r (1+r)^2} \tag{2-7}$$

where r is the ratio of natural period of j^{th} mode, T_j, to the natural period of the i^{th} mode, T_i. As illustrated in Figure 2-9, this equation indicates a significant interaction between closely spaced modes, especially at high damping values.

(d) SRSS method. For the structures for which the modal periods are well separated, ρ_{ij} approaches zero (for $i \neq j$), and the CQC method degenerates into the familiar SRSS method. The maximum total response for a single earthquake response spectrum in direction k is then given by

$$u_k = \left[\sum_{i=1}^{N} u_{ki}^2 \right]^{1/2} \tag{2-8}$$

The SRSS method leads to conservative results for the well-separated vibration modes, but is inappropriate when they are closely spaced, because it ignores the contribution due to the cross-modal terms.

(e) Calculation of section forces and moments. The output of most computer response-spectrum analyses usually includes nodal displacements and element stresses only. The section forces and moments required for the design of structures are not readily available, except when beam elements are used to idealize the structure. For nonbeam elements, the combined maximum stress values have no sign, and thus evaluation of section forces from these stresses, if not interpreted properly, may lead to incorrect results. Like the element stresses, section forces and moments should first be evaluated for the individual modes and then combined by the CQC or SRSS method to obtain the maximum shears, thrusts, and moments at a specified cross section.

(f) Combining for multicomponent earthquake input. Three-dimensional structures are analyzed for three orthogonal components of the earthquake ground motions applied in two horizontal and vertical direction. The maximum response quantity of interest due to each component of the earthquake ground motion is estimated separately as described above. The maximum responses due to all three components of the earthquake ground motion are then combined according to the SRSS method:

$$u = \left[\sum_{k=1}^{3} u_k^2 \right]^{1/2} \tag{2-9}$$

The SRSS combination of the multicomponent earthquake responses can be used with either the SRSS or CQC modal combination method. With the SRSS modal combination, the summation for multi-component input can be performed before or after combination of the modal responses, but with the CQC method it should always be applied after the modal responses have been combined. Regular intake towers with a circular or rectangular cross section are usually analyzed for two horizontal components of the ground motion and not the vertical. For such towers in addition to the SRSS method, the peak value of any resultant response quantity due to the combined gravity and two horizontal components of ground motion may also be obtained from the largest of the values given by the following equations:

$$R = R_0 \pm R_x \pm \alpha R_y \tag{2-10}$$

$$R = R_0 \pm \alpha R_x \pm R_y \tag{2-11}$$

where R_x is the peak response due to the x-component; R_y the y-component of horizontal ground motion; and R_0, gravity loads. Equations 2-10 and 2-11 are usually used in conjunction with the standard response spectra, and the SRSS method is employed with the site-specific response spectra. The value of α for circular towers is taken equal to 0.40 and for rectangular towers equal to 0.3.

(g) Interpretation of analysis results. The basic results of response spectrum analysis consist of the maximum nodal displacements and element stresses (or forces). As discussed previously, these maximum responses are estimated by combining responses from individual modes and multicomponent input. The resulting dynamic responses obtained in this manner have no sign and may be interpreted as positive or negative. For example, the maximum element dynamic stresses σ_d are assumed to be either tension (positive) or compression (negative). Furthermore, the maximum values associated with each response quantity are not concurrent and usually occur at different instants of time. Thus static equilibrium checks cannot be performed to validate the results. Most computer programs used to perform response spectrum analysis do not compute section thrusts, shears, and moments for elements other than beam elements. To obtain section moments and forces from the computed stress results, the analyst should assign stress signs that would produce the correct stress distribution across a specified section. This is done by a careful examination of the shape of the predominant response modes, from which the actual deflected shape

of a member and the associated stress distributions can be predicted. As discussed previously, a better approach is first to compute modal section forces and moments from the modal stresses, and then combine them using the CQC or SRSS method.

(h) Combining static and dynamic stresses. For the evaluation of earthquake performance of hydraulic structures, the response-spectrum estimate of the dynamic stresses σ_d should be combined with the effects of the static loads σ_s. Since response spectrum stresses have no sign, combination of static and dynamic stresses should consider dynamic stresses to be either positive or negative, leading to the maximum values of the total tensile or compressive stresses:

$$\sigma_{max} = \sigma_s \pm \sigma_d \tag{2-12}$$

It should be noted that only the similarly oriented components of σ_s and σ_d can be combined.

(3) Time-history method. The linear response of structures to earthquakes can also be computed using the time-history method of analysis. In the time-history analysis normally the acceleration time-histories are used as the seismic input. Procedures for developing acceleration time-history input consistent with the design response spectrum are described in Chapter 3. The idealized structural models used in the time-history analysis are essentially identical to those described previously for the response spectrum analysis. The response history is computed using a step-by-step numerical integration procedure applied either to the original equations of motion (direct method) or to the transformed equations in modal coordinates (mode superposition) (Bathe and Wilson 1976). In the more efficient mode superposition approach, first the response history for each mode is evaluated at each integration time-step, and then the modal response histories for all significant modes of vibration are combined to determine the dynamic response of the structure.

(4) Need for time-history analysis. Linear time-history analysis is required when the results of response spectrum analysis indicate that the computed maximum total stresses (or forces) exceed the allowable values, or when special conditions exist. The time-history analysis is performed to estimate the deformations and stresses (or forces) more accurately by considering the time-dependent nature of the dynamic response to earthquake motions. The results of such analysis serve to demonstrate the general behavior of the dynamic response, and combined with rational interpretation and judgment can provide a preliminary estimate of the level of inelastic behavior. Most Corps hydraulic structures are designed essentially to respond within their linear range when subjected to low to moderate intensity earthquakes. For this level of ground motions, the linear time-history analysis provides satisfactory results. For major earthquakes it is probable that the elastic capacity of the mass concrete would be exceeded, and some cracking and crushing of the concrete and yielding of reinforcing steels could occur. Prediction of the actual response and estimation of the expected damage and inelastic behavior under severe earthquakes can be evaluated only using a more complicated nonlinear analysis. However, linear analysis can still be very valuable for a preliminary assessment of the damage and the level of postelastic response and can help to decide whether a nonlinear analysis should be performed. As part of this evaluation, the results of linear analysis for the URC hydraulic structures should be examined in a systematic manner to identify the extent of overstressed regions at any particular point in time, to produce plots showing time-histories of stresses and other response quantities of interest, and to determine statistics on the number of stress cycles exceeding the allowable values and the corresponding excursions of these stress cycles beyond the specified limits.

b. Nonlinear time-history.

(1) Need for nonlinear analysis. A nonlinear time-history analysis may be necessary when the results of a linear analysis show that the structure could suffer significant damage during a major earthquake.

Minor local damages have little effect on the overall integrity of the structure and can still be evaluated by proper interpretation of the results of linear analysis. However, when the calculated tensile stresses (or forces) are significantly greater than the tensile strength of the concrete (or section capacity) over a large region and are repeated several times during the earthquake excitation, severe cracking of the concrete, joint slippage, and yielding of reinforcements can be expected. Under these conditions, the dynamic behavior of the structure is drastically different from the linear response, and a valid estimate of the damage is possible only if a true nonlinear performance is incorporated in the analysis.

(2) Realistic nonlinear analysis. A reasonable nonlinear analysis should take into account all sources of nonlinearity that contribute significantly to the nonlinear response behavior. The damage caused by earthquake shaking is normally associated with significant loss in the structural stiffness resulting from the concrete cracking, yielding of steel, opening of construction joints, slippage across the construction joints or cracking planes, and the nonlinear material behavior. Additional sources of nonlinearity arise from the nonlinear soil and the fractured foundation rock supporting the structure, as well as the separation of the structure and the foundation at the contact surface. At the present time, analytical techniques for a complete nonlinear earthquake analysis of hydraulic structures, including the interaction with foundation and water, are not available. Only limited aspects of the nonlinear behavior such as the contraction joint opening in arch dams, tensile cracking of gravity dams, sliding of blocks, and approximate postelastic analyses have been considered in practice. A realistic nonlinear analysis for the seismic safety evaluation of hydraulic structures depends on a great deal of new developments in the following topics: definition of seismic input, identification and specification of significant nonlinear mechanisms (joint opening and sliding, tensile cracking of the concrete, yielding and slippage of reinforcing steel, nonlinear material behavior under cyclic loads, etc.), development of idealized models representing the nonlinear behavior, numerical techniques and solution strategies for computing the nonlinear response, and development of criteria for acceptable performance and identification of possible modes of failure. The seismic input for a nonlinear analysis is in the form of acceleration time-histories. The key issues in developing time-histories for nonlinear analysis are duration of strong shaking, energy and pulse sequencing, special near-fault characteristics such as the source "fling," and the number of sets of time-histories required for the analysis. The main difficulty in effective nonlinear analysis at the present is the lack of or limited knowledge on the actual nonlinear material properties of the mass and reinforced concrete under cyclic loading.

2-9. Sliding and Rotational Stability During Earthquakes

a. Sliding stability. The sliding stability evaluation of hydraulic structures under earthquake loading can be made according to the traditional static equilibrium (seismic coefficient) and permanent displacement approaches described in Ebeling and Morrison (1992). In the traditional approach, the sliding stability is expressed in terms of a prescribed factor of safety against sliding, whereas in the permanent displacement approach the structure is permitted to slide along its base but the accumulated displacement during the ground shaking should be limited to a specified allowable value.

(1) Seismic coefficient approach. In the seismic coefficient approach, the safety against sliding is determined on the basis of shear-friction factor of safety (Ebeling and Morrison 1992). The shear-friction factor of safety is defined as the ratio of the resisting to driving forces along a potential failure surface

$$FS = \frac{CA + \left(\sum N - \sum U\right)\tan\phi}{\sum V} \tag{2-13}$$

where

C = unit cohesion

A = area of base

$\sum N$ = summation of normal forces

$\sum U$ = summation of uplift forces

$\tan \phi$ = coefficient of internal friction

$\sum V$ = summation of shear or driving forces

(a) The driving forces acting on the structure include the static and seismic inertia forces due to weight of the structure and to hydrodynamic pressures. Treating the system above the failure surface as a rigid block, the inertia force associated with the mass of the structure is computed as the product of the seismic coefficient, as specified in ER 1110-2-1806, and the weight of the block. Similarly, the product of the seismic coefficient and the added mass of water moving with the structure produces inertia force due to the hydrodynamic pressure. The added mass of water may be computed using the Westergaard method (Westergaard 1933) or the equation given by Chopra (Chopra 1967):

$$M_a = 0.54\rho h^2 \tag{2-14}$$

where ρ is the density and h is the depth of water. The motion of the structure relative to the failure surface is resisted by the shear strength mobilized between the structure and the surface by the friction and cohesion, as shown in Equation 2-13. For example, the shear friction factor of safety for sliding of the gravity dam shown in Figure 2-10 is given by

$$FS = \frac{CA + (W - U)\tan\phi}{\pm H_s + H_d + \left(\frac{W}{g}\right)a} \tag{2-15}$$

where

W = weight of dam

H_s = hydrostatic force

H_d = hydrodynamic force (i.e., M_a . a)

g = gravitational acceleration

a = ground motion acceleration or some fraction thereof

The ± sign is for sliding in the downstream or upstream direction with the plus sign indicating downstream.

(b) When the earthquake forces are included in the sliding stability analysis, the calculated factor of safety against sliding may become less than one. A factor of safety of less than one indicates a transient sliding. The sliding is assumed to occur for as long as the ground acceleration is greater than the critical value required for the driving force to exceed the resistance. However, due to the oscillatory nature of the earthquake ground motion, the sliding displacement is expected to be limited but could lead to excessive permanent displacements.

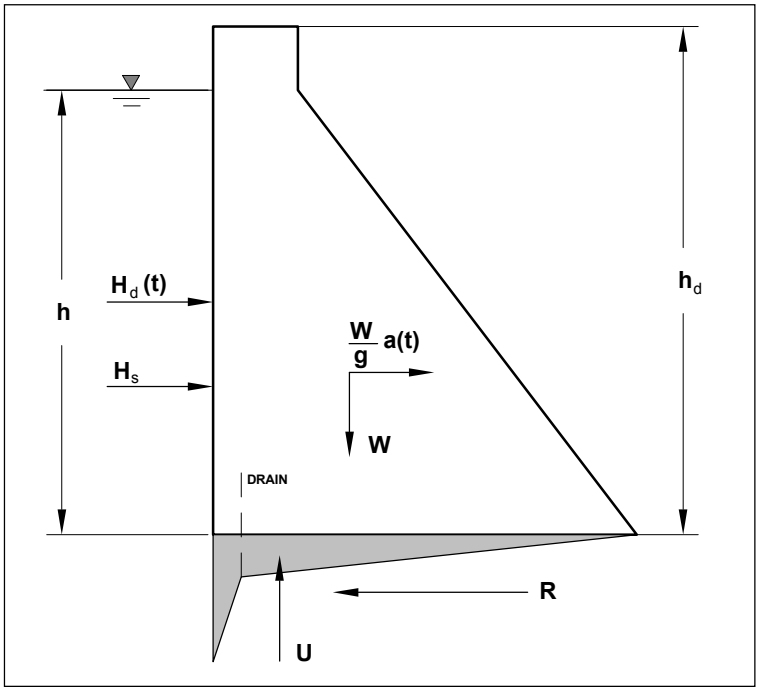

Figure 2-10. Forces acting on gravity dam monolith

(2) Permanent displacement approach. The traditional sliding stability criteria described above were developed for unrealistically small seismic forces based on a seismic coefficient of 0.1 or less. The factor of safety against sliding required by the traditional approach may not be attainable for larger seismic forces representative of the moderate- to high-intensity earthquake ground motions. In such cases, the sliding may occur but it takes place only during a short period of time associated with the acceleration cycles exceeding a critical acceleration, a_c, and diminishes during the remainder of these cycles when the acceleration is less than a_c and the relative velocity between the structure and the base is zero. Treating a gravity dam monolith as a rigid body supported on horizontal ground, and assuming that the motion of the dam relative to the ground is resisted by the friction between the dam and the ground surface, the critical acceleration a_c is given by (Chopra and Zhang 1991)

$$\frac{a_c}{g} = \frac{1}{W + W_{a0}}\left[\mu_s (W - U) \pm H_s\right] \tag{2-16}$$

where μ_s is the coefficient of static friction, and W_{a0} is the weight of water which represents the hydrodynamic force. The ± sign in this equation is for sliding in the upstream or downstream direction. It is apparent from Equation 2-16 that the critical acceleration required to slide the dam downstream is smaller than that needed to move the dam upstream. Similarly, the critical acceleration a_c necessary to initiate sliding in other hydraulic structures can be derived by considering the equilibrium of forces involved in each particular structure. Knowing the critical acceleration a_c, the permanent sliding displacements can be estimated using the Newmark's rigid block model (Newmark 1965). According to Newmark's concepts, also discussed by Chopra and Zhang (1991), the upper bounds for permanent displacements of the sliding rigid mass subjected to earthquake ground motion with peak velocity v_m and peak acceleration a_m can be estimated from :

$$s_m = \frac{v_m^2}{2a_c}\left(1 - \frac{a_c}{a_m}\right)\frac{a_m}{a_c} \tag{2-17}$$

$$s_m = \frac{v_m^2}{2a_c} \cdot \frac{a_m}{a_c} \tag{2-18}$$

$$s_m = \frac{v_m^2}{2a_c} 6 \tag{2-19}$$

These equations, plotted in nondimensional form in Figure 2-11, show that Equation 2-18 provides more conservative values than Equation 2-17, and Equation 2-19 is intended for systems with the small values of a_c/a_m. The portion of the curve for each equation where the equation is recommended for use is a thick line. Newmark's model provides an easy means for approximate estimation of the upper bounds for permanent sliding displacements, but it is based on certain assumptions that ignore the true dynamic response behavior of the sliding. More accurate estimates of the sliding displacements can be made from the response history analysis proposed by Chopra and Zhang (1991).

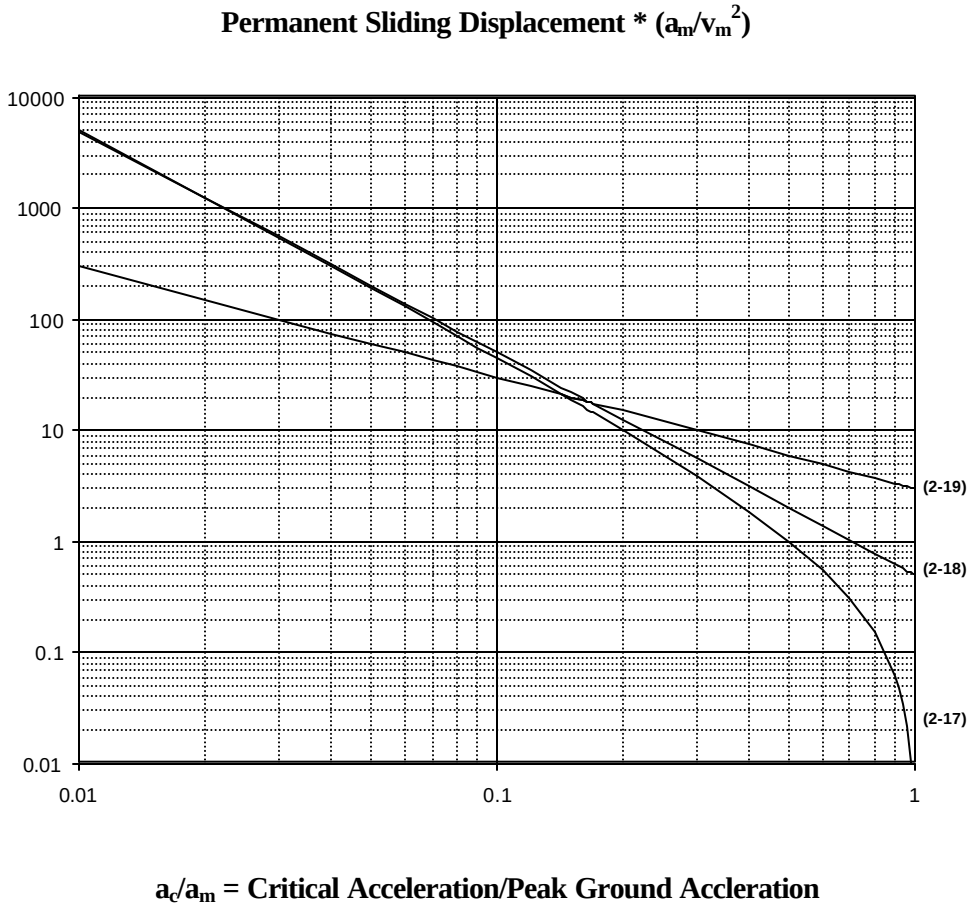

Figure 2-11. Newmark's upper bounds for permanent sliding displacement (Chopra and Zhang (1991), courtesy of Earthquake Engineering Research Center, University of California, Berkeley)

b. Rotational stability. Hydraulic structures subjected to large lateral forces produced by major earthquakes may tip and start rocking when the resulting overturning moment becomes so large that the structure breaks contact with the ground.

(1) Intake towers. For an intake tower idealized as a nearly rigid or flexible equivalent SDOF system (Figure 2-12), the tipping occurs when the overturning moment exceeds the resisting moment due to the weight of the structure. This condition is expressed by:

$$mS_a h > mgb \tag{2-20}$$

$$S_a > g\,(b/h) \tag{2-21}$$

where

m = mass of structure

S_a = spectral acceleration of the earthquake ground motion

h = one-half height of structure

b = one-half base width of structure

Similar expressions can also be derived for other hydraulic structures, except that the moments due to hydrostatic and hydrodynamic forces should be included ((2) below). In both cases it is assumed that the structure is not bonded to the ground, but it may be keyed into the soil with no pulling resistance. It should be noted that the structure will eventually overturn if the moment $M > mgb$ is applied and sustained, where mgb represents the resisting moment due to the weight of the structure. However, under earthquake excitation large overturning moments occur for only a fraction of a second in each cycle, with intermediate opportunities to unload. By comparing the earthquake average energy input with the required average energy for overturning the structure, Housner provided the following relationship as a criterion for the rotational stability of a rocking structure (Housner 1963):

$$\alpha = S_v \sqrt{\frac{mr}{gI_0}} \tag{2-22}$$

where

α = an angle defined in Figure 2-12

S_v = spectral velocity of the earthquake ground motion

m = mass of structure

r = radial distance from the center of gravity to tipping edge

I_0 = moment inertia about the corner

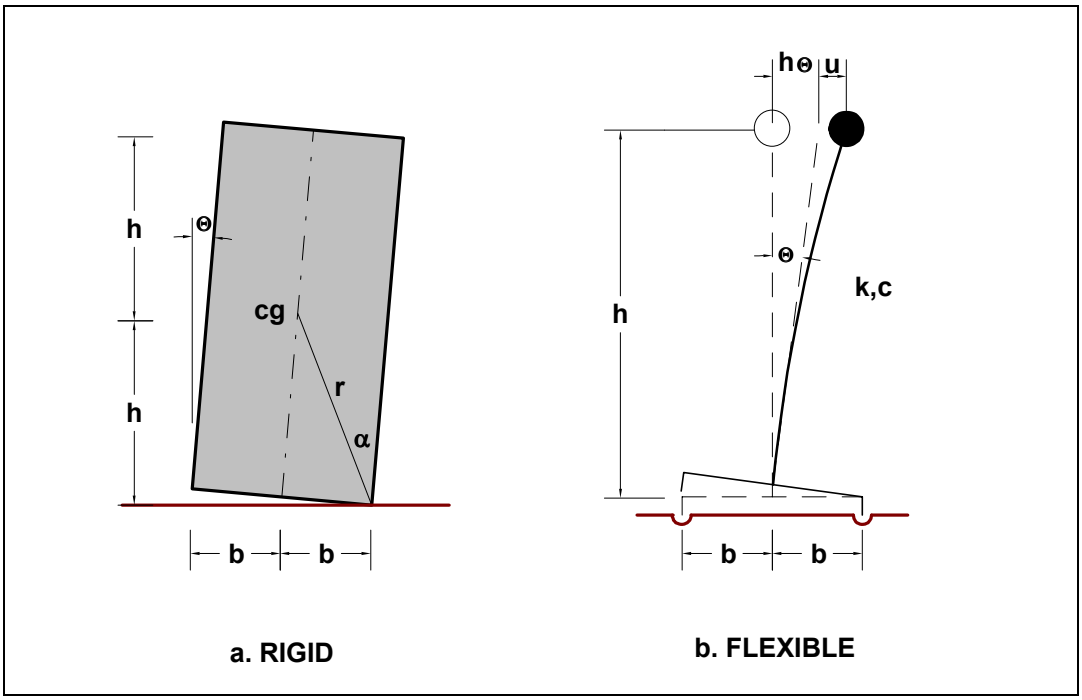

Figure 2-12. Rigid block and SDOF models for rigid and flexible structures

Based on the average energy formulation used, this equation is interpreted as stating that for a given spectral velocity S_v, a block having an angle of α given by Equation 2-22 will have approximately a 50 percent probability of being overturned (Housner 1963). For slender structures such as intake towers, Equation 2-22 can be approximated by

$$\alpha = \frac{S_v}{\sqrt{gr}} \tag{2-23}$$

By combining Equations 2-21 and 2-23 and using the relationships among the spectral acceleration, velocity, and displacement, Scholl (Applied Technology Council (ATC) 1984) found that consideration of one spectral parameter alone as the earthquake demand is not sufficient for evaluating overturning and suggested the following relationships:

$$S_d = b \quad \text{when} \quad S_a = g\frac{b}{h} \tag{2-24}$$

These equations show that when S_a is just sufficient to cause tipping, the structure will start rocking, but its displacement approximated by spectral displacement S_d must reach the value of b before it can overturn. These equations also demonstrate why larger structures such as buildings do not overturn during earthquakes, whereas smaller rigid blocks having the same aspect ratios are expected to overturn. This is because, in general, S_d is never large enough to tip over a building, but it can approach the one-half base width (i.e., b) of smaller rigid blocks such as tombstones.

(2) Gravity dams. A preliminary study of the rotational stability of a gravity dam may be carried out as described by Chopra and Zhang (1991). The dam is assumed to be rigid and subjected to both the horizontal and vertical components of earthquake ground motion. The dam starts tipping in the

downstream direction if the overturning moment due to upstream ground acceleration and water pressures exceeds the restoring moment (Figure 2-13) as follows:

$$M|a_x(t)|y_c + M_d(t) + \frac{1}{3}hH_s + U(b - b_U) \geq M\left[g + a_y(t)\right](b - x_c) \tag{2-25}$$

where parameters are shown in Figure 2-13 and $M_d(t)$ is the moment due to hydrodynamic pressure given by

$$M_d(t) = -M_{d0}a_x(t) + \frac{1}{6}\rho h^3 a_y(t) \tag{2-26}$$

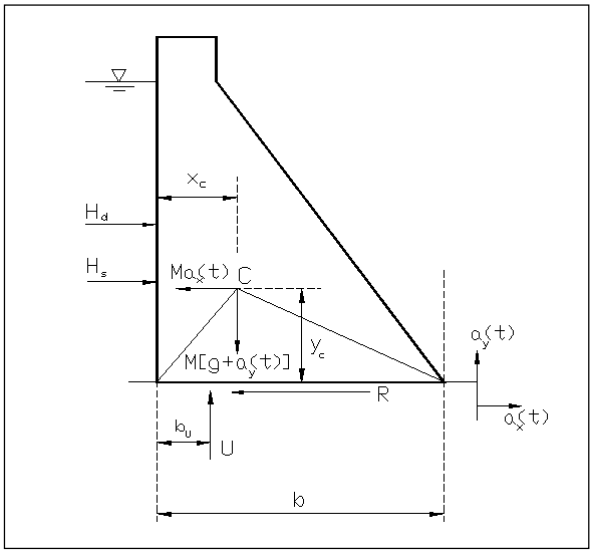

Figure 2-13. Rigid gravity dam on horizontal ground

The first term, $M_{d0} = \int_0^h p_0(y)y\,dy$, is moment due to hydrodynamic pressure generated by the horizontal ground motion. The pressure $p_0(y)$ may be obtained using either the Westergaard (1933) or Chopra (1967) formula. The second term in Equation 2-26 is the moment due to hydrodynamic pressure, $\rho(h - y)$ $a_y(t)$, produced by the vertical motion. Substituting Equation 2-26 into 2-25 gives the critical upstream acceleration a_c required to initiate downstream tipping of the dam about its toe:

$$a_c = \frac{1}{My_c + M_{d0}} \times \left\{\left[M(b - x_c) - \frac{1}{6}\rho h^3\right]\left[g + a_y(t)\right] - U(b - b_u)\right\} \tag{2-27}$$

Similarly, tipping about the heel of the dam initiates when the critical downstream acceleration a_c reaches

$$a_c = \frac{1}{My_c + M_{d0}}\left\{\left(Mx_c + \frac{1}{6}\rho h^3\right)\left[g + a_y(t)\right] - Ub_u\right\} \tag{2-28}$$

When subjected to strong ground motions, a rigid dam may move with ground, slide only, rock only, and rock and slide. Comparison of critical accelerations for sliding and tipping can show which motion will

start first. The parameter studies by Chopra and Zhang (1991) over a wide range of parameters indicate that downstream sliding of the dam will initiate before tipping or upstream sliding. Large downstream accelerations will usually cause upstream tipping of the dam about its heel before upstream sliding. In most cases, the more likely type of motion is the downstream sliding of the dam. The effect of rocking on the sliding motion is considered to be negligible and may be ignored in the evaluation of sliding response.

2-10. Current Practice on Use of Response Spectra for Building-Type Structures

a. General. The design requirements of the Structural Engineers Association of California (SEAOC) are the most current state of practice for the earthquake-resistant design of buildings in California. SEAOC also includes provisions for lower seismic hazard regions in California, which may be suitable for use in regions outside of California. A summary of the SEAOC's use of design response spectra and the similarities and differences between the SEAOC's recommendations and the procedures used for the hydraulic structures are described in this section.

b. Criteria for dynamic analysis. According to SEAOC's recommendations, dynamic analysis procedures should be used for the design and analysis of certain building structures. This includes buildings 73.2 m (240 ft or more) in height, except for those located in Seismic Zone 1 and standard occupancy structures in Zone 2, buildings with irregular stiffness, mass, or vertical geometry, buildings over five stories or 20 m (65 ft) in height located in Seismic Zones 3 and 4, or buildings founded on soft soils (type S4) with fundamental period of vibration greater than 0.7 sec. The dynamic analysis procedures for buildings are based on the same general concepts described for the hydraulic structures. The response spectrum analysis is the preferred method for most buildings. The time-history analysis is employed to study inelastic response characteristics or to incorporate time-dependent effects in the elastic dynamic response. However, structural modeling, design earthquakes, and acceptable level of nonlinear response for buildings are different from those for hydraulic structures.

c. Structural modeling. The obvious differences between building and hydraulic structures are the structural system and the function. While buildings are made primarily of frame systems with shear walls and braces, hydraulic structures are built as massive plain or lightly reinforced concrete monoliths to contain or retain water. The idealized model of a building usually consists of beam and column elements with the mass of the building lumped at a few selected nodes. Most regular buildings can be adequately idealized by one- or two-dimensional models. Very complex and highly irregular buildings or those with large eccentricies between the center of mass and resistance require 3-D analysis. The majority of hydraulic structures, on the other hand, are modeled as planar or 3-D models using 2-D or 3-D solid and shell elements as discussed previously. Furthermore, interactions with the water and foundation are important aspects of the dynamic characteristics of hydraulic structures that need to be included in the analysis.

d. Design response spectra. Hydraulic structures and civil works buildings are analyzed for two levels of design earthquakes (as described previously and in reference to ER 1110-2-1806, respectively). SEAOC requires a single design earthquake that as a minimum should have a 10 percent probability of exceedance in 50 years, which gives a return period of 475 years. The ground motion for buildings may be represented by normalized response spectra, site-specific response spectra, or time-histories. The normalized response spectra, shown in Figure 2-14, are permitted for the soil profiles S_1, S_2, and S_3 defined in Table 2-1. Site-specific response spectra are required if the site condition significantly differs from those used to develop the normalized shapes, or if the structure is founded on soil profile S4, or the structure is seismically isolated. The time-histories of the ground motions are usually developed for inelastic analysis and for the seismic-isolated structures. The probabilistic seismic hazard analysis is commonly used to develop site-specific response spectra for building sites in Zones 3 and 4.

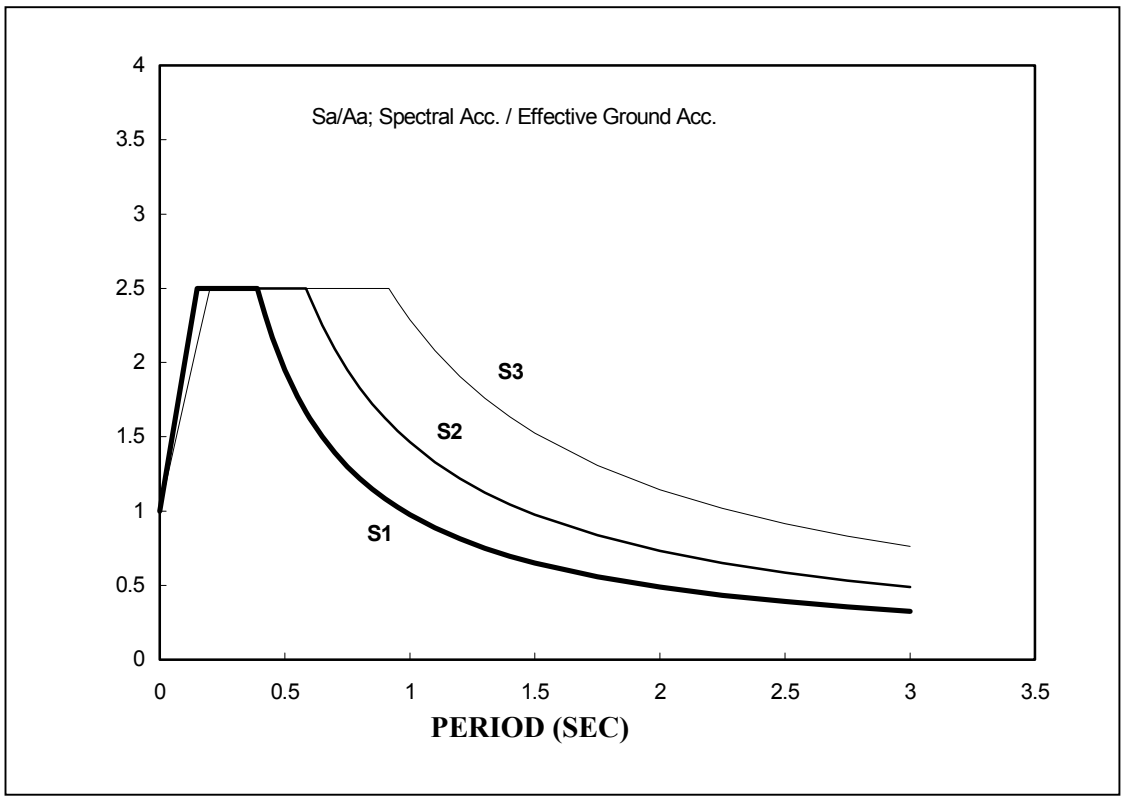

Figure 2-14. Normalized SEAOC's design response spectra

Table 2-1
SEAOC's Site Coefficients

Type	Description	S Factor
S1	A soil profile with either: 1 A rock-like material characterized by a shear wave velocity greater than 762 m/sec (2,500 fps) or by other suitable means of classification, or 2 Medium-stiff to stiff or medium dense to dense soil conditions where soil depth is less than 70 m (200 ft).	1.0
S2	A soil profile with predominantly medium dense to dense or medium stiff to stiff soil conditions where soil depth exceeds 70 m (200 ft) or more.	1.2
S3	A soil profile containing more than 6 m (20 ft) of soft to medium stiff clay but not more than 12 m (40 ft) of soft clay.	1.5
S4	A soil profile characterized by a shear wave velocity less than 152 m/sec (500 fps) and containing more than 12 m (40 ft) of soft clay.	2.0

1 Reprinted from SEAOC's Recommended Lateral Force Requirements and Commentary, 1996 (SEAOC 1996).

e. Nonlinear response of buildings. The design practice for buildings permits the structure to respond inelastically during a major earthquake but suffer only acceptable and predictable amounts of damage without collapse. The energy dissipated through such inelastic deformations is utilized to reduce the level of seismic design forces. According to the SEAOC's Commentary, structures designed in conformance with its recommendations should, in general, be able to

(1) Resist a minor level of earthquake ground motion without damage.

(2) Resist a moderate level of earthquake ground motion without structural damage, but possibly experience some nonstructural damage.

(3) Resist a major level of earthquake ground motion having an intensity equal to the strongest either experienced or forecast at the building site, without collapse, but possibly with some structural as well as nonstructural damage. To achieve such performance goals, SEAOC recommends that the design forces be determined by reducing the elastic forces obtained from linear analysis by the system quality factor R_w. The structural system quality factor R_w represents the overall ductility and energy dissipation capacity of the system when strained beyond its elastic limit. The R_w values are selected according to the ability of a particular system to sustain cyclic inelastic deformations without collapse. Factors contributing to the actual selection of R_w include redundancy, reliability of as-built performance, inelastic load-deformation behavior, and changed damping and period modification with deformation. Experience indicates that buildings designed based on this procedure have exhibited adequate performance in most cases. In addition to the ductility requirement, most seismic codes require a limitation on the story drift to limit nonstructural damage during more frequent earthquakes and to ensure building stability under the major earthquakes. For tall buildings, the drift limitations may dictate an elastic design, even for MCE ground motions.

f. Inelastic design response spectra. For regular buildings, the code specified design seismic forces can be estimated from

$$V = C_S W = \frac{\left(S_a / g\right)}{R_w} \cdot W \tag{2-29}$$

where

V = base shear

C_s = design seismic coefficient

W = weight of building

S_a = linear elastic response spectral acceleration

R_w = the structural system quality factor intended to account for ductility and energy dissipation when the structure deforms beyond the yield point

The design seismic coefficient C_s can be obtained from a reduced response spectrum that can be considered to be the inelastic design response spectrum (IDRS). However, recent statistical studies have shown that the shape of IDRS significantly differs from the shape of elastic response spectra (Miranda 1992; Krawinkler and Rahnama 1992), and is strongly influenced by the level of inelastic

deformation, local site conditions, and the period of vibration. Until more data become available, the most reliable procedure for establishing an IDRS is to perform nonlinear dynamic time-history analyses of structures with different degrees of ductility ratios using the available recorded ground motions.

g. Nonlinear inelastic response of reinforced concrete hydraulic structures.

(1) Free-standing intake towers. The response of a free-standing intake tower to earthquake ground shaking is similar to that of a cantilever wall that resists earthquake forces by flexural and shear deformations. Thus, the principles of inelastic design of reinforced concrete walls are generally applicable to free-standing towers, provided that the response is consistent with the post-yield capacity of reinforced tower structure. Similar to the structural walls with limited ductility, intake towers should be designed such that flexural yielding controls the strength, the inelastic deformations, and thus the energy dissipation in the entire structure (Pauly 1986). Failure modes due to diagonal tension or diagonal compression caused by shear and sliding shear along the base of the structure should be avoided. The main source of energy dissipation should be yielding of flexural reinforcement in the region where the plastic hinges are expected to develop. Recent research at CEWES has demonstrated that a lightly reinforced rectangular intake tower possesses sufficient ductility to allow formation of a plastic hinge at the base of the tower with a limited amount of inelastic behavior. The ability of such plastic hinges to sustain the repeated cycles of inelastic demands imposed on them, the expected length of the plastic hinge, and the acceptable level of damage during major earthquakes are being investigated at CEWES. Until these have been established, preliminary design and screening evaluations for retangular intake towers should be limited to an inelastic response not greater than twice the yield deflection in accordance with the design provisions of EM 1110-2-2400.

(2) Other reinforced concrete hydraulic structures. For other reinforced concrete hydraulic structures with structural configurations and systems different from those of buildings and intake towers, postelastic analyses should be performed to establish appropriate ductility for the members so that the structure will undergo controlled levels of nonlinearity without compromising structural safety. Designing for to MDE take advantage of the ability of the structures to dissipate energy through inelastic deformations should produce uniform patterns of yielding and energy absorption. While the initial forces are distributed through the structure according to the elastic stiffness of the various members and connections, partially developed plastic hinges in the critical members will redistribute forces to the stiffer members and may not follow the load paths envisioned in the initial design. If the desired level of ductility is not reached or the forces are not distributed appropriately, then it is possible that the actual member forces may exceed the design values. In addition, the possibility that all cycles of nonlinear response (i.e., hysteretic energy demand), and not just the maximum response cycle, may cause damage should also be investigated. In other words, it is important to note that the specified ductility may be reached either once or several times during the ground shaking, and to ensure that the lightly reinforced concrete hydraulic structure has sufficient ductility to resist such repeated demands. These considerations indicate that the inelastic design of hydraulic structures requires careful attention to the actual postelastic behavior of the structure and should be done in consultation with and approved by CECW-ET.

Chapter 3
Development of Site-Specific Response Spectra for Seismic Analysis of Concrete Hydraulic Structures

Section I
Introduction

3-1. Purpose and Scope

This chapter describes procedures for developing site-specific response spectra of ground motions throughout the United States for seismic analyses of hydraulic structures. Also covered, but in less detail, are approaches for developing acceleration time-histories of ground motions. Section I provides an overview of the general approaches to developing site-specific response spectra, a brief discussion of factors influencing earthquake ground motions, and a brief discussion of differences in ground motion characteristics in different regions of the United States. This is followed in Sections II and III by descriptions of procedures for developing site-specific response spectra using deterministic and probabilistic approaches, respectively.

3-2. General Approaches for Developing Site-Specific Response Spectra

The two general approaches for developing site-specific response spectra are the deterministic and probabilistic approaches.

a. Deterministic approach.

(1) General. In this approach, often termed a deterministic seismic hazard analysis, or DSHA, site ground motions are deterministically estimated for a specific, selected earthquake, that is, an earthquake of a certain size on a specific seismic source occurring at a certain distance from the site. The earthquake size may be characterized by magnitude or by epicentral intensity. In the WUS, the practice has been to use magnitude, whereas in the EUS, both magnitude and Modified Mercalli Intensity (MMI) have been used. However, in the EUS, magnitude is increasingly being used as the measure of earthquake size, and ground motions are correspondingly being estimated using correlations with magnitude. In this manual, ground motions are estimated using relationships with magnitude. For procedures for estimating ground motions as a function of intensity, reference should be made to the state-of-the-art publication by Krinitzsky and Chang (1987).

(2) Size and location of design earthquakes. In the deterministic approach, earthquake magnitude is typically selected to be the magnitude of the largest earthquake judged to be capable of occurring on the seismic source, i.e., MCE. The selected earthquake is usually assumed to occur on the portion of the seismic source that is closest to the site (an exception is the “random earthquake” analysis described in Section II and Appendix D). After the earthquake magnitude and distance are selected, the site ground motions are then estimated using ground motion attenuation relationships or other techniques. Procedures for deterministically estimating earthquake ground motions are described in Section II.

b. Probabilistic approach. In the probabilistic approach, often termed a probabilistic seismic hazard analysis, or PSHA, site ground motions are estimated for selected values of the probability of ground motion exceedance in a design time period or for selected values of annual frequency or return period for ground motion exceedance. As an example, ground motions could be estimated for a 10

percent probability of exceedance in 100 years or for a return period of 950 years. The probabilistic approach thus provides an expression of potential earthquake loading in terms analogous to those used for other environmental loads in civil engineering design such as wind and flood loading. A probabilistic ground motion assessment incorporates the frequency of occurrence of earthquakes of different magnitudes on the seismic sources, the uncertainty of the earthquake locations on the sources, and the ground motion attenuation including its uncertainty. Section III describes the procedures for probabilistically estimating earthquake ground motions.

3-3. Factors Affecting Earthquake Ground Motions

a. General. As stated in paragraph 1-8, It has been well-recognized that earthquake ground motions are affected by earthquake source conditions, source- to-site transmission path properties, and site conditions. The source conditions include the stress drop, source depth, size of the rupture area, slip distribution (amount and distribution of static displacement on the fault plane), rise time (time for the fault slip to complete at a given point on the fault plane), type of faulting, and rupture directivity. The transmission path properties include the crustal structure and the shear-wave velocity and damping characteristics of the crustal rock. The site conditions include the rock properties beneath the site to depths of up to about 2 km, the local soil conditions at the site to depths of up to several hundred feet, and the topography of the site. In developing relationships for estimating ground motions, the effects of source, path, and site have been commonly represented in a simplified manner by earthquake magnitude, source-to-site distance, and local subsurface conditions. The important influences of these factors on ground motion are summarized below.

b. Effects of earthquake magnitude and distance on ground motions.

(1) General. The effects of earthquake magnitude and distance on the amplitude of ground motions are well known; ground motion amplitudes tend to increase with increasing magnitude and decreasing distance. However, the effects of magnitude and source-to-site distance on relative frequency content (response spectral shape) and duration of ground motions are not as well known and therefore are briefly reviewed below.

(2) Effects of magnitude. The Guerrero, Mexico, accelerograph array data illustrate the large effect of magnitude on the relative frequency content and duration of earthquake ground motions. The Guerrero array has provided recordings of rock motions over a wide range of magnitudes. Figures 3-1 and 3-2 show the accelerograms and the corresponding response spectra for six recordings selected by Anderson and Quaas (1988) to be approximately equally spaced in magnitude from the smallest event of magnitude 3.1 to the largest of magnitude 8.1. Figure 3-1 illustrates the effect of magnitude on the duration of the strong shaking part of an accelerogram; with increasing magnitude, duration rapidly increases. All events have epicenters about 25 km from the station, and all stations are on hard rock (Anderson and Quaas 1988). Figure 3-2 illustrates that the larger magnitude events have somewhat larger spectral amplitudes at high frequencies and much larger spectral amplitudes at long periods. In other words, increasing magnitude results in greatly enriched relative frequency content (higher spectral shapes) at long periods. Figure 3-3 illustrates a generalization of the effect of magnitude on response spectral shape, in this case, from the empirically based attenuation relationships for rock developed by Sadigh et al. (1993).

(3) Effects of distance. Data from the Loma Prieta earthquake of October 17, 1989, provide an example of the effect of distance on response spectral shape. Figure 3-4 shows that the spectral shape of the recordings obtained on rock during this earthquake reduce in the high-frequency range and increase in the long-period range with increasing distance. A generalization of the effect of distance on spectral

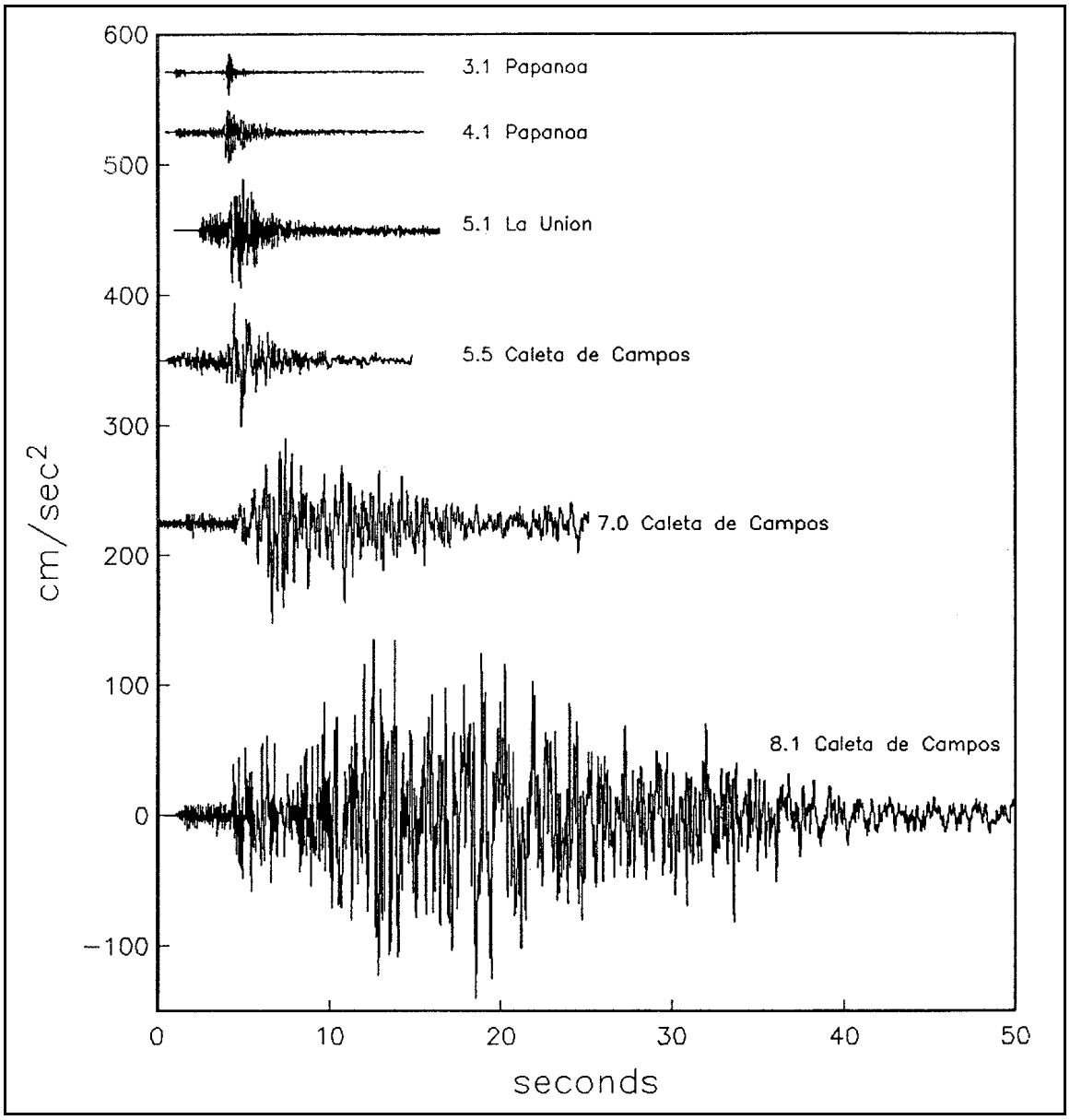

Figure 3-1. An example of accelerograms recorded in 1985 and 1986 on the Guerrero accelerograph array (Anderson and Quaas (1988), courtesy of Earthquake Engineering Research Institute, Oakland, CA)

shape, in this case from the theoretically based relationships for rock of Silva and Green (1989), is illustrated in Figure 3-5. In general, within source-to-site distances of about 50 km, the effect of distance on spectral shape is much smaller than the effect of magnitude. Similarly, although the relative duration of the strong shaking part of an accelerogram tends to increase with increasing distance (e.g., Dobry, Idriss, and Ng 1978), this effect appears to be relatively small within 50 km of an earthquake source.

(4) Special effects of near-source earthquakes. Near the earthquake source (within approximately 10 to 15 km of the source), earthquake ground motions often contain a high-energy pulse of medium-to-long-period ground motion (at periods in the range of approximately 0.5 to 5 sec) that occurs when fault

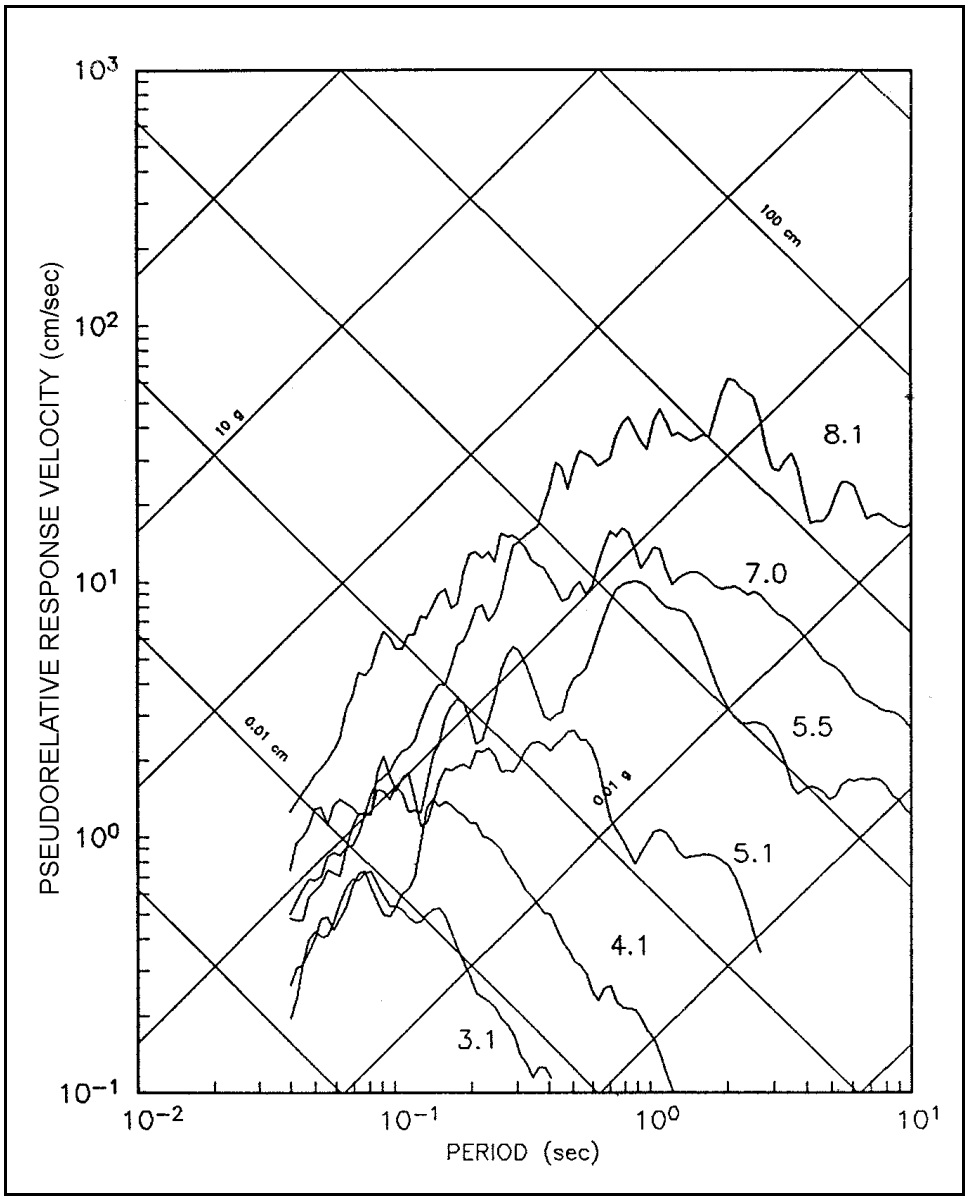

Figure 3-2. Response spectra (5 percent damped, pseudo-relative velocity) corresponding to the acceleration traces in Figure 3-1 (Anderson and Quaas (1988), courtesy of Earthquake Engineering Research Institute, Oakland, CA)

rupture propagates toward a site. It has also been found that these pulses exhibit a strong directionality, with the component of motion perpendicular (normal) to the strike of the fault being larger than the component parallel to the strike (see, for example, Sadigh et al. 1993; Somerville and Graves 1993; Somerville et al. 1997). These characteristics of near-source ground motions are illustrated by the Rinaldi recording obtained during the 1994 Northridge earthquake (Figure 3-6). These characteristics should be included in ground motion characterization for near-source earthquakes.

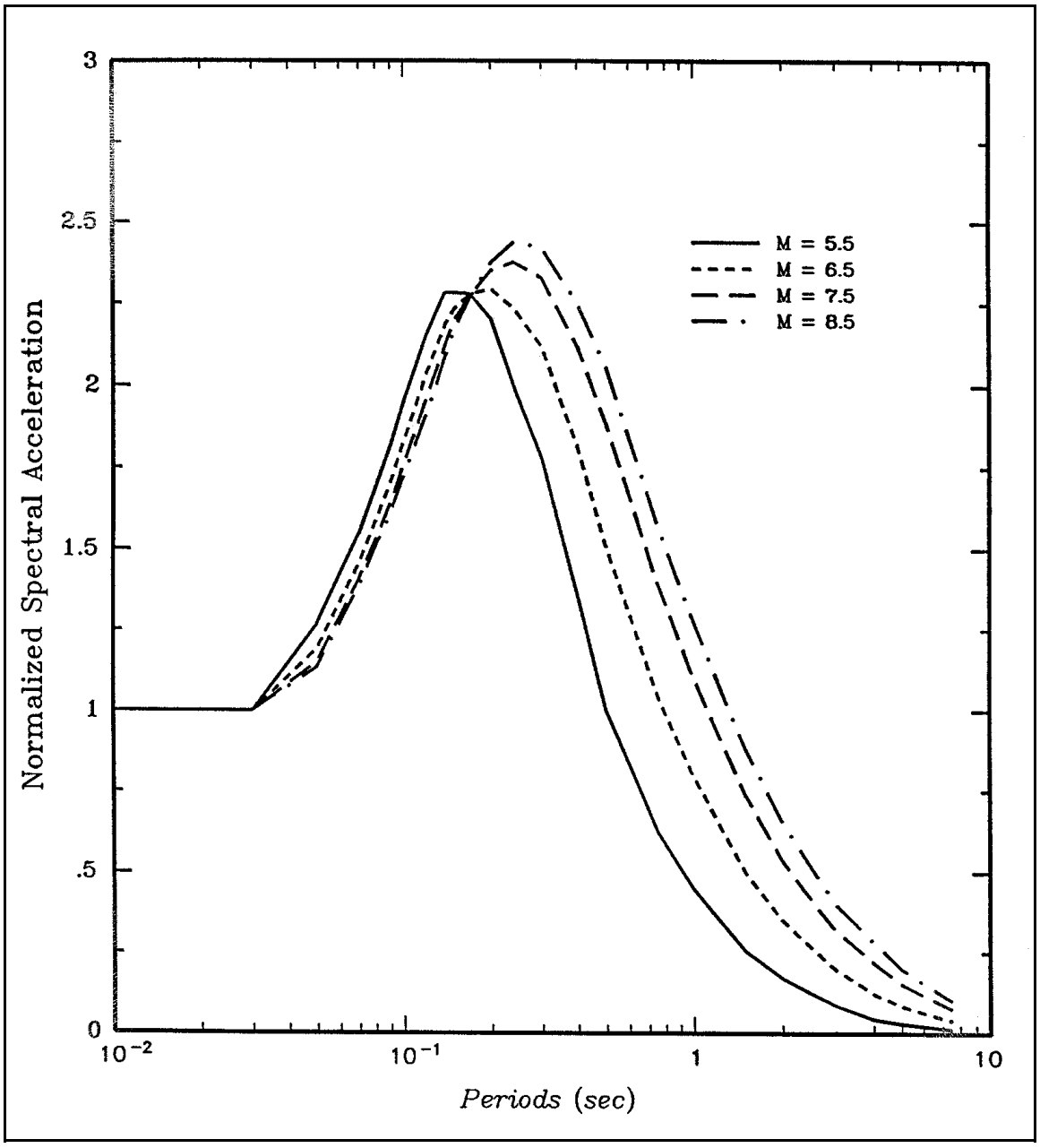

Figure 3-3. Effect of magnitude *M* on response spectral shape of rock motions based on attenuation relationships of Sadigh et al. (1993), 30-km distance from source to site, 5 percent damping

c. Effect of local subsurface conditions on ground motions.

(1) General. It is well established that local soil conditions have a major effect on the amplitude and response spectral characteristics of earthquake ground motions. It was demonstrated again by the dramatic differences in ground motions in different parts of Mexico City in the 1985 Mexico earthquake, and in different locations in the San Francisco Bay Area in the 1989 Loma Prieta earthquake.

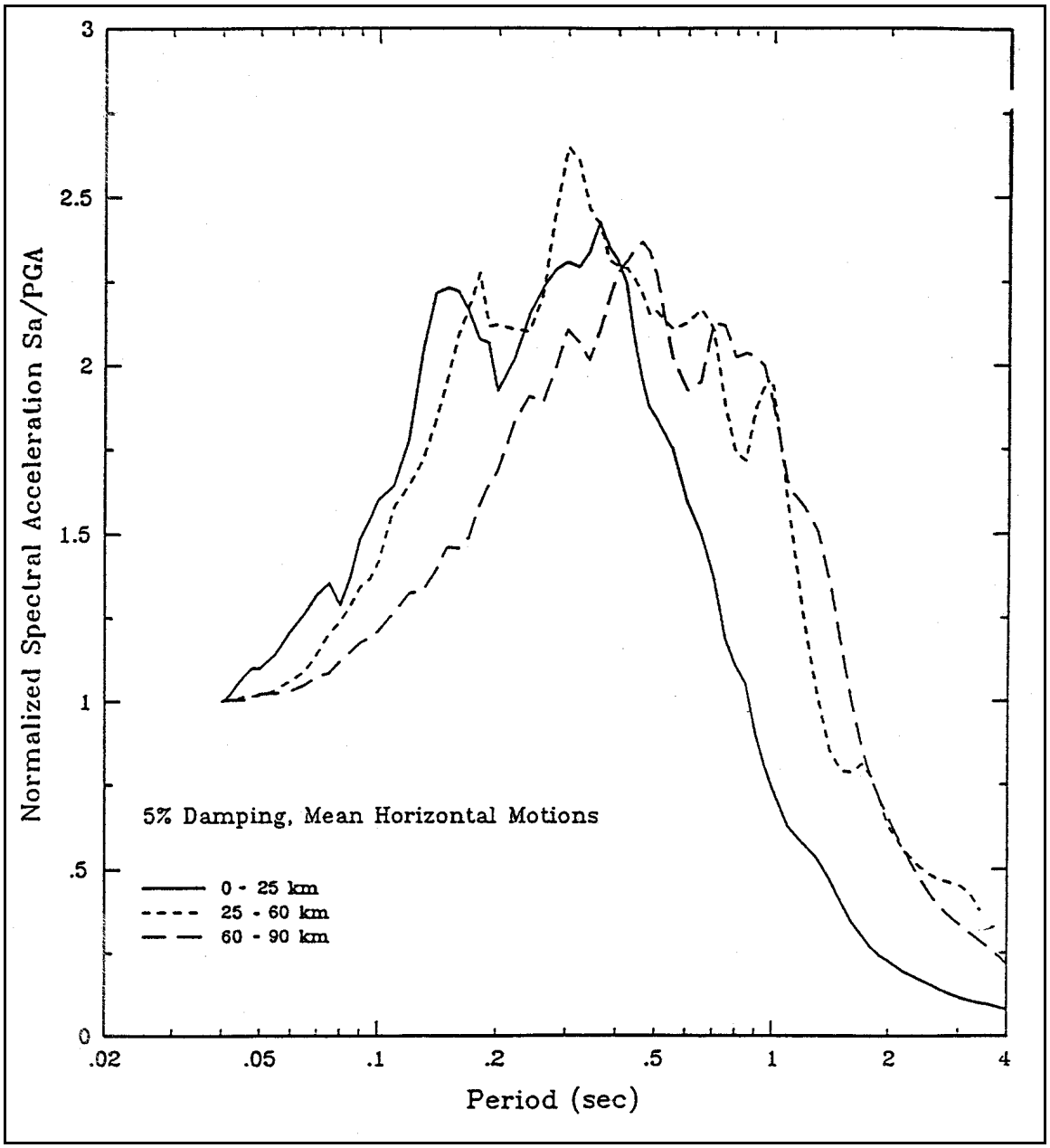

Figure 3-4. Variation of spectral shape with distance for rock recordings of the October 17, 1989, Loma Prieta earthquake

(2) Site amplification effects. Recordings obtained on different soil conditions and analytical studies indicate that soil amplification is dependent on the type and depth of soil. Figure 3-7 illustrates the amplification of response spectra of a soft soil site recording (Treasure Island site) relative to an adjacent rock site recording (Yerba Buena site) during the Loma Prieta earthquake. The effects illustrated in Figure 3-7 are qualitatively typical of those expected in soft soil for relatively low levels of ground motion (peak rock acceleration less than about 0.4 g). However, for higher levels of ground motion, higher soil damping due to nonlinear soil behavior tends to result in deamplification of high-frequency response spectra and peak ground accelerations a_{max} while longer period components continue to be amplified but

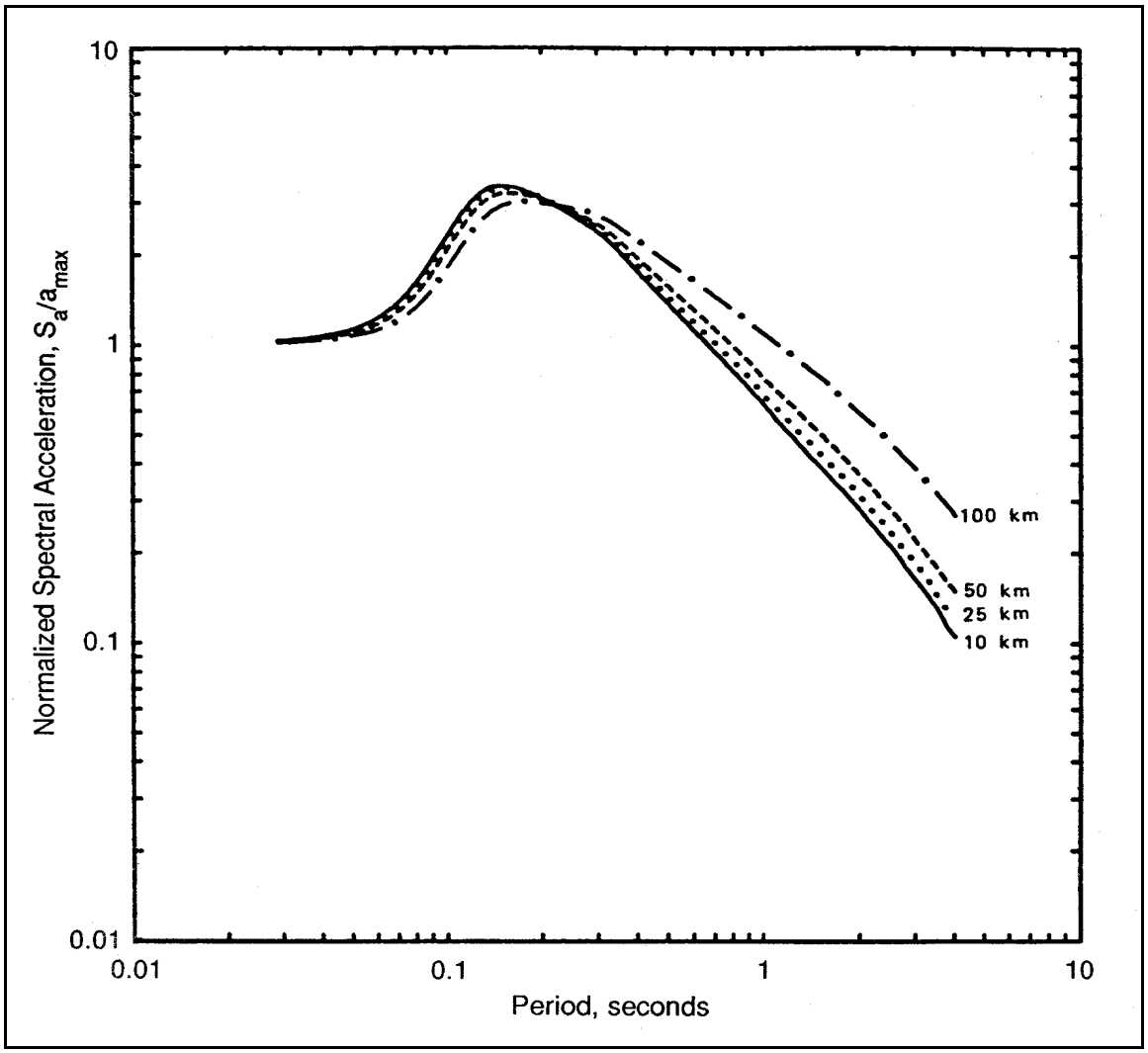

Figure 3-5. Effect of distance on response spectral shapes for a moment magnitude M_w 6.5 earthquake using western North American parameters (Silva and Green 1989, courtesy of Earthquake Engineering Research Institute, Oakland, CA)

by smaller amounts than for low levels of ground motion. Thus, site amplification effects are dependent on the level of ground motion as well as the soil characteristics. For peak ground acceleration, this dependence of amplification on ground motion level is illustrated by the relationship for soft soil developed by Idriss (1991a) shown in Figure 3-8. For response spectral values, the dependence of spectral amplifications on soil type and ground motion level are illustrated by the curves in Figure 3-9, which were the result of the National Center for Earthquake Engineering Research (NCEER)/Structural Engineers Association of California (SEAOC)/Building Seismic Safety Council (BSSC) workshop on site response held in 1992. The response spectral ratios shown in Figure 3-9 have been adopted into the NEHRP Provisions (BSSC 1994) and the Uniform Building Code (International Conference of Building Officials 1997).

(3) Effects on response spectral shape. The shape of the response spectrum is greatly influenced by the local subsurface conditions. This is illustrated in Figure 3-10 by the site-dependent spectral shapes developed by Seed, Ugas, and Lysmer (1976) for four different subsurface site classifications on the basis of statistical analysis of ground motion data. Although these spectral shapes could be updated

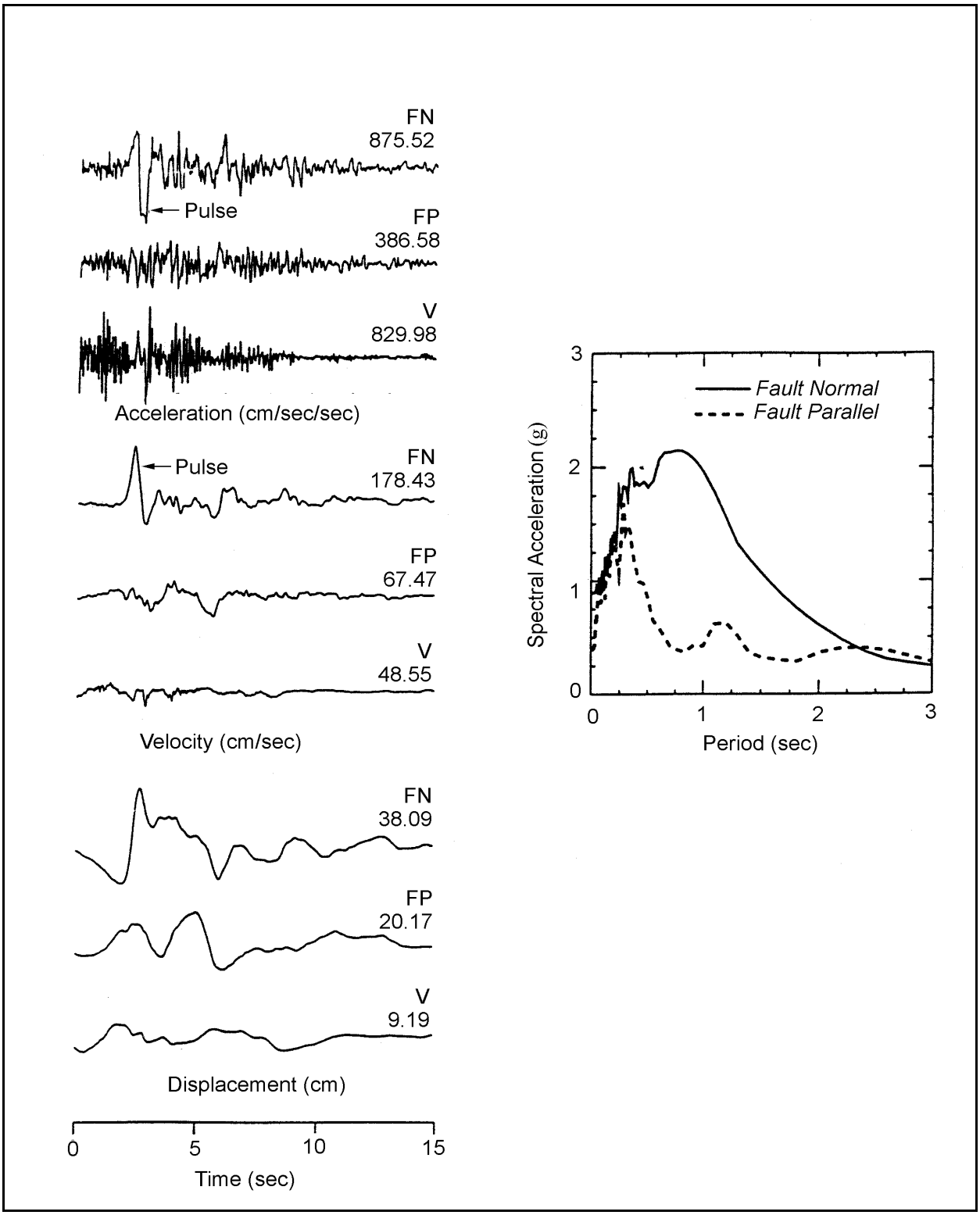

Figure 3-6. Time-histories and horizontal response spectra (5 percent damping) for the fault strike-normal (FN) and fault strike-parallel (FP) components of ground motion (V = vertical) for the Rinaldi recording obtained 7.5 km from the fault rupture during the 1994 Northridge, California, earthquake (Somerville (1997), courtesy of Multidisciplinary Center for Earthquake Engineering Research, State University of New York at Buffalo)

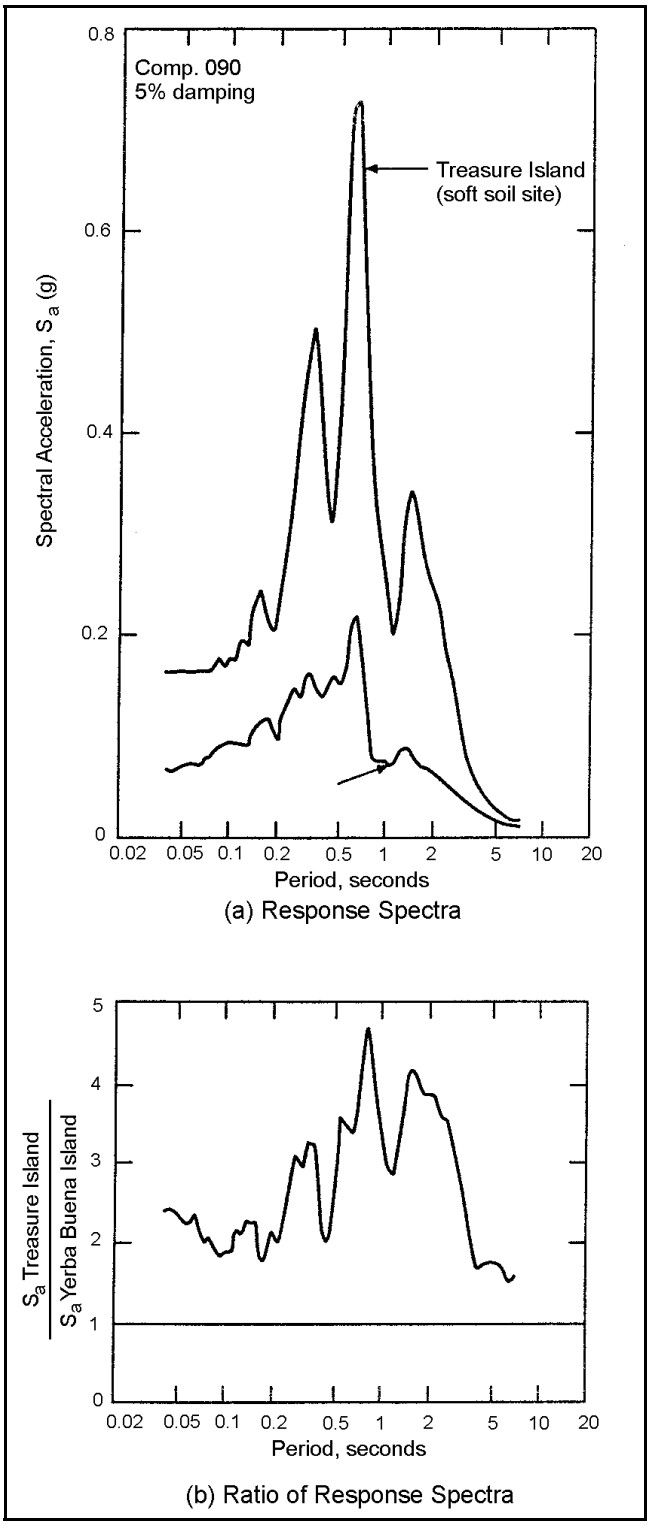

Figure 3-7. Response spectra and ratio of response spectra for ground motions recorded at a soft and nearby rock site during the 1989 Loma Prieta earthquake

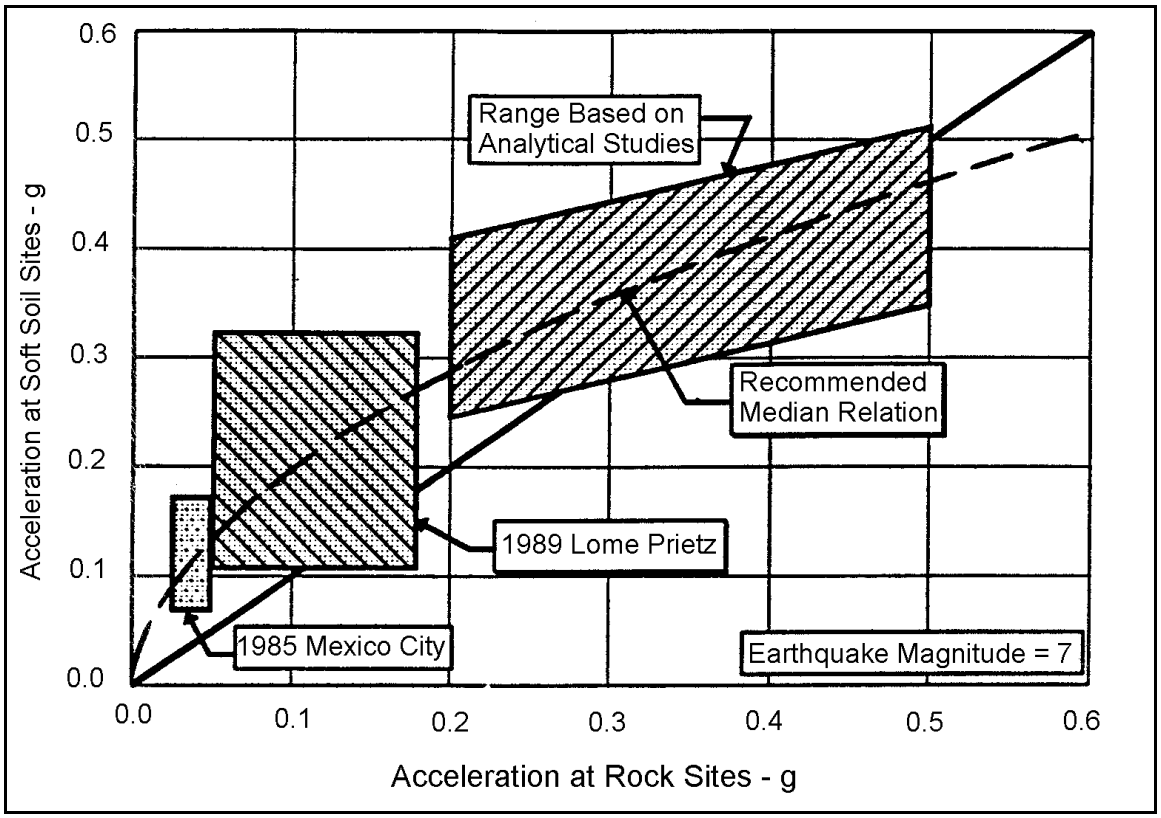

Figure 3-8. Variation of accelerations on soft soil sites versus rock sites (Idriss 1991a, courtesy of I. M. Idriss and Shamsher Prakesh, ed.)

using data from more recent earthquakes and specialized to different magnitudes, the spectral shapes developed by Seed, Ugas, and Lysmer (1976) have been widely used and have provided the basis for quantification of spectral shapes in building codes (Applied Technology Council 1978; Uniform Building Code (International Conference of Building Officials 1994).

3-4. Differences in Ground Motion Characteristics in Different Regions of the United States

a. Eastern versus western United States. Differences in strong ground motions between the WUS and EUS are due somewhat to earthquake source differences (somewhat higher stress drops in the EUS) but are currently believed to be due primarily to differences in travel path and site effects. In the stable intraplate region of the EUS, crustal rocks have higher shear wave velocities and lower damping than crustal rocks in the tectonically active interplate regions of the WUS. As a result, ground motions tend to attenuate more slowly with distance in the EUS than in the WUS. At the same time, the softer rocks within the upper 1 to 2 km of the crust in the WUS exhibit different site effects from those of the harder rocks of the EUS. Specifically, the WUS rocks, having higher damping and steeper velocity gradients with depth than EUS rocks, tend to damp out high-frequency components of motion while amplifying long-period components relative to EUS rocks. As a result of the interaction of these travel path and site effects, rock motions at relatively close source-to-site distances (within about 50 km) exhibit increased high-frequency motions (frequencies greater than about 5 to 10 Hz) but somewhat reduced long-period motions at EUS sites compared to WUS sites. Illustration of these differences in terms of response spectral shapes is shown by comparison of recorded ground motion data from California and Nahanni,

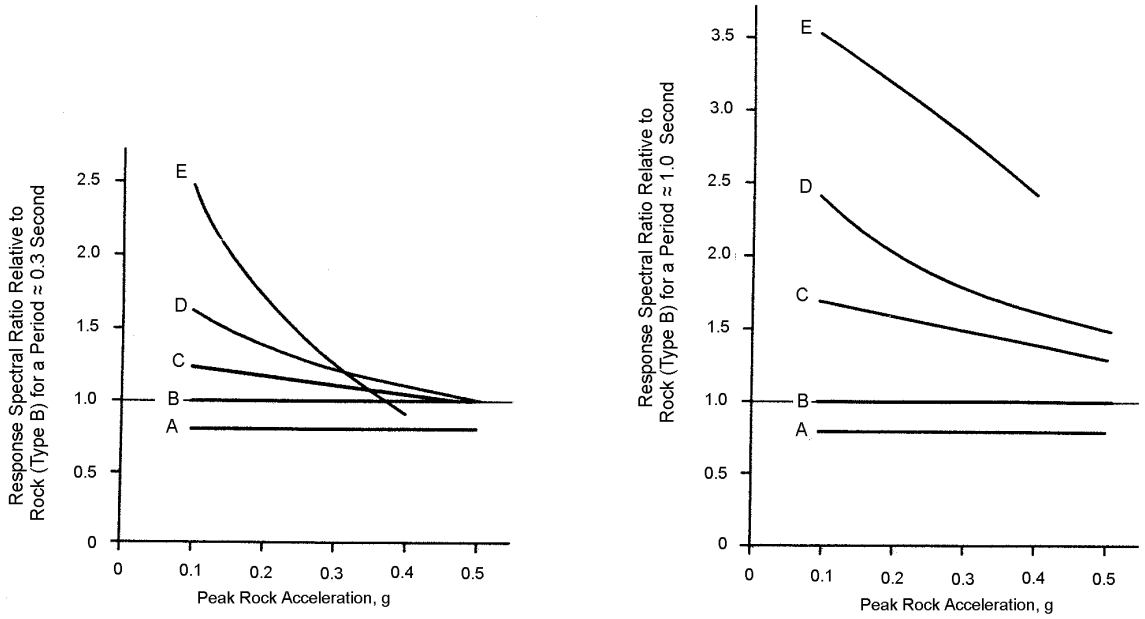

Site Classification	Description
A	Hard rock, shear wave velocity, v_s > 1500 m/sec (5000 fps)
B	Rock, v_s 760 to 1500 m/sec (2500 to 5000 fps)
C	Very dense soil and soft rock, v_s 360 to 760 m/sec (1200 to 2500 fps)
D	Stiff soils, v_s 180 to 360 m/sec (600 to 1200 fps)
E	Soil profile with v_s <180 m/sec (600 ft/sec) or more than 3 m (10 ft) of soft clay with PI > 20, w ≥ 40%, and s_u <25 kPa (500 psf)

Note: v_s = weighted average shear wave velocity for the top 30 m (100 ft) of the soil profile

PI = plasticity index

w = water content

s_u = undrained shear strength

Figure 3-9. Response spectral ratios relative to rock for different site classifications and ground motion levels (BSSC 1994)

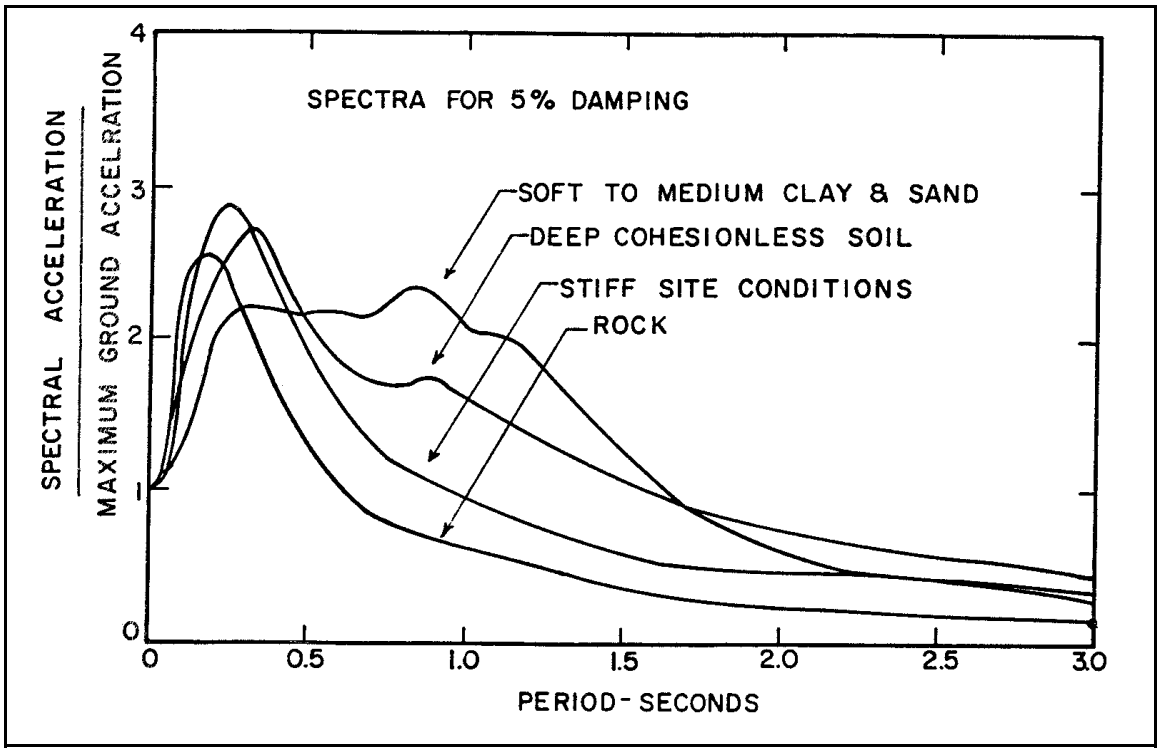

Figure 3-10. Average acceleration spectra for different site conditions (Seed, Ugas, and Lysmer 1976, courtesy of Seismological Society of America)

Canada, in Figure 3-11 (Nahanni is located in an EUS-like tectonic environment). In terms of absolute response spectra, these differences are illustrated in Figures 3-12 and 3-13, where response spectra for relatively close source-to-site distances have been calculated using the theoretical model of Silva and Green (1989). As distance increases, the effects of travel path attenuation begin to dominate over the local site effects, leading to higher ground motions in the EUS over a broader frequency range.

b. Subduction zone versus shallow crustal earthquakes. The collision of tectonic plates of the earth in subduction zones has caused numerous large and relatively deep earthquakes (e.g., in subduction zones in Japan; west coast of Central and South America; coastal northwest California, Oregon, and Washington; Alaska; Puerto Rico; and many other areas). Analyses of ground motion data from subduction zone earthquakes indicate that the main difference between ground motions from subduction zone earthquakes and ground motions from WUS shallow crustal earthquakes is a slower rate of attenuation for the subduction zone events. This is illustrated in Figure 3-14 in which attenuation of peak rock acceleration from shallow crustal WUS earthquakes is compared with that from subduction zone earthquakes as determined by Youngs et al. (1993a). Attenuation curves for two types of subduction zone earthquakes are shown in Figure 3-14—interface earthquakes occurring at the interface between the subducting tectonic plate and the overriding plate, and intraslab earthquakes occurring within the subducting plate. Analyses by Youngs, Day, and Stevens (1988) and Youngs et al. (1993a) also suggest that ground motions from subduction zone earthquakes have response spectral shapes that are lower in the long-period range than response spectral shapes for WUS shallow crustal earthquakes (Figure 3-15).

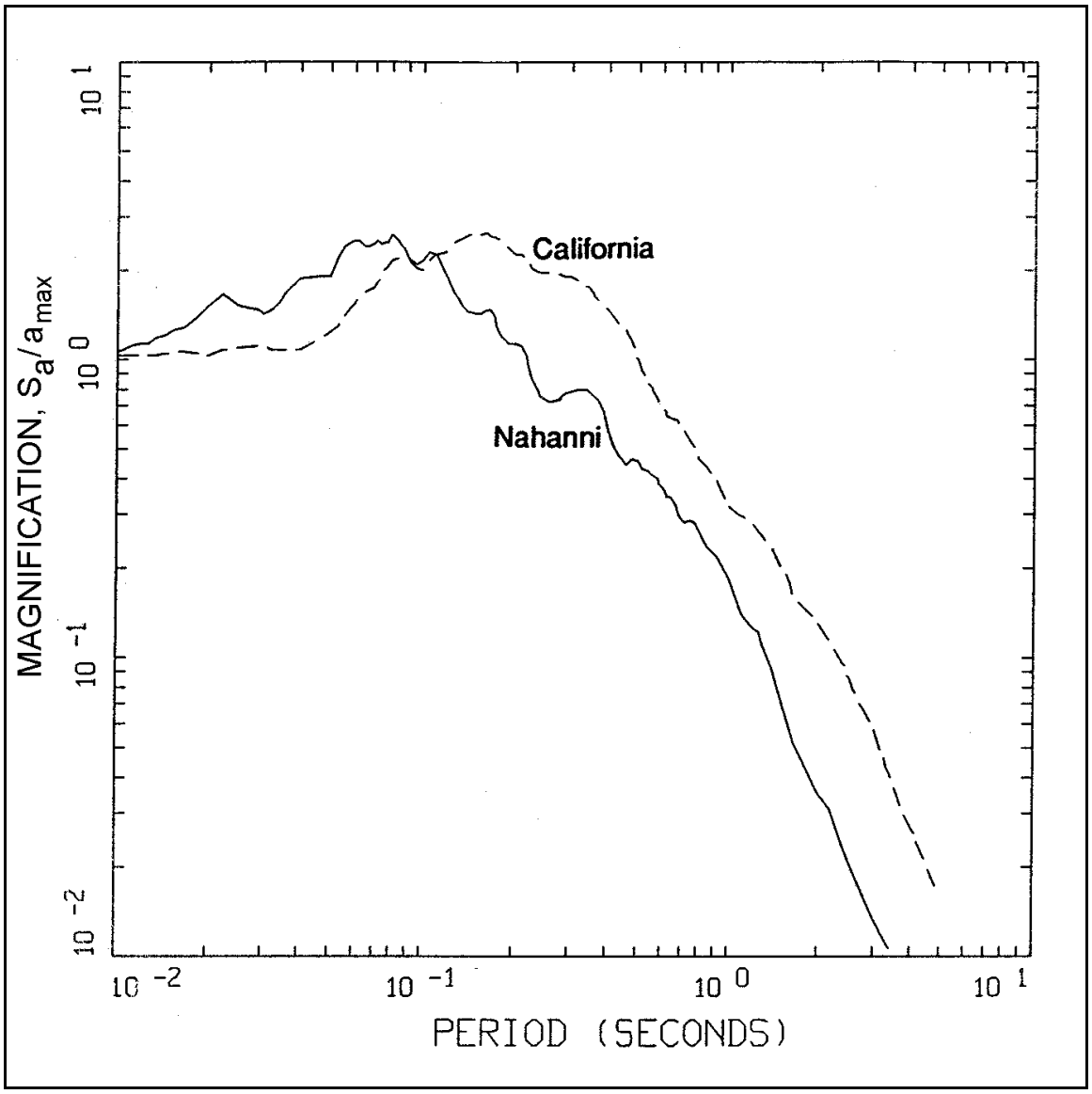

Figure 3-11. Comparison of average 5 percent damped response spectral shapes (S_a /a_{max}) computed from strong-motion data recorded at rock sites in Nahanni, Canada, and California for M_w 5.3 earthquakes (Darragh et al. 1989)

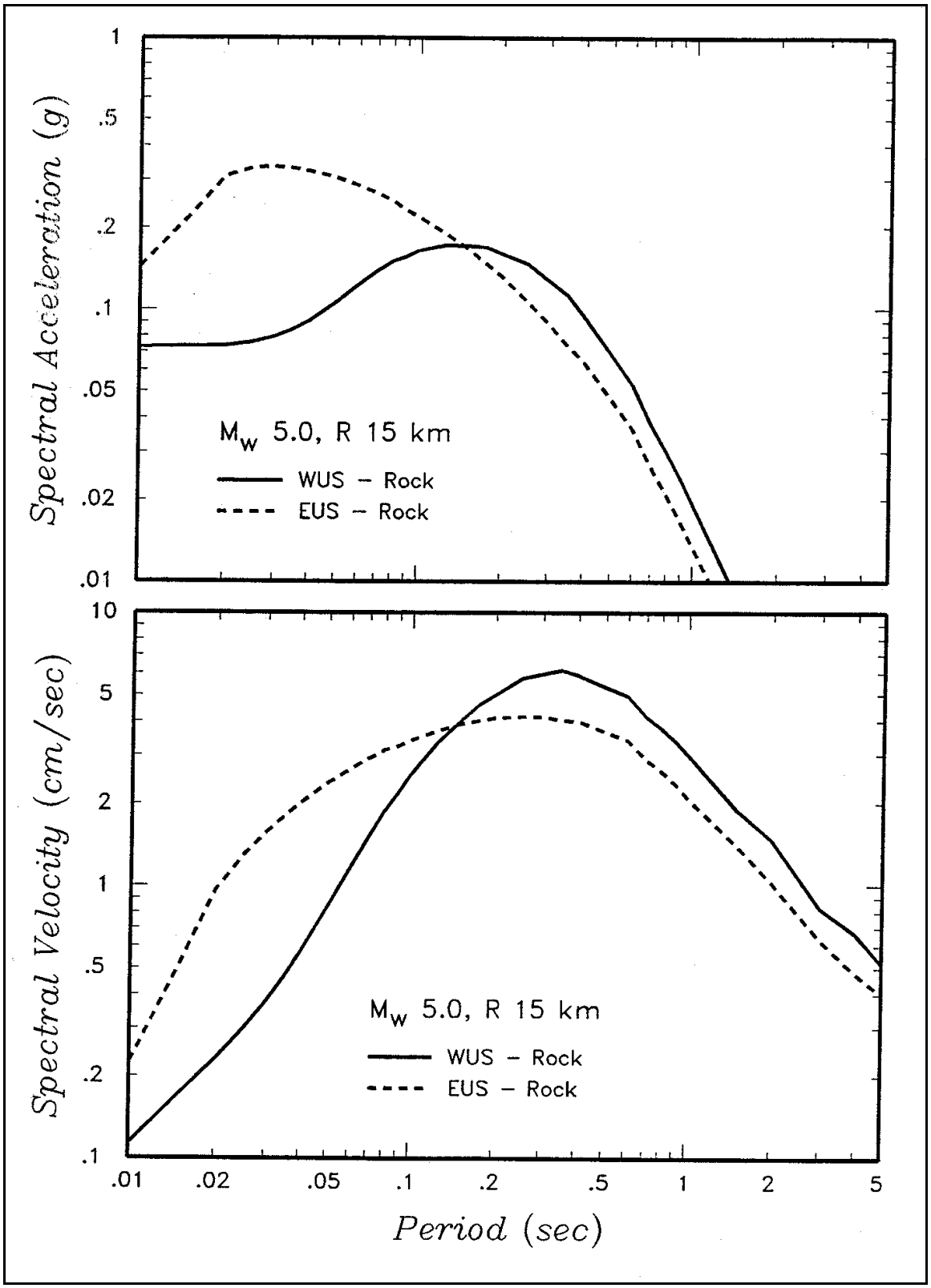

Figure 3-12. Comparison of response spectra for a magnitude 5 earthquake at 15 km using WUS and EUS attenuation relationships (calculated using Band-Limited-White-Noise/Random Vibration Theory (BLWN/RVT) model as formulated by Silva and Green 1989)

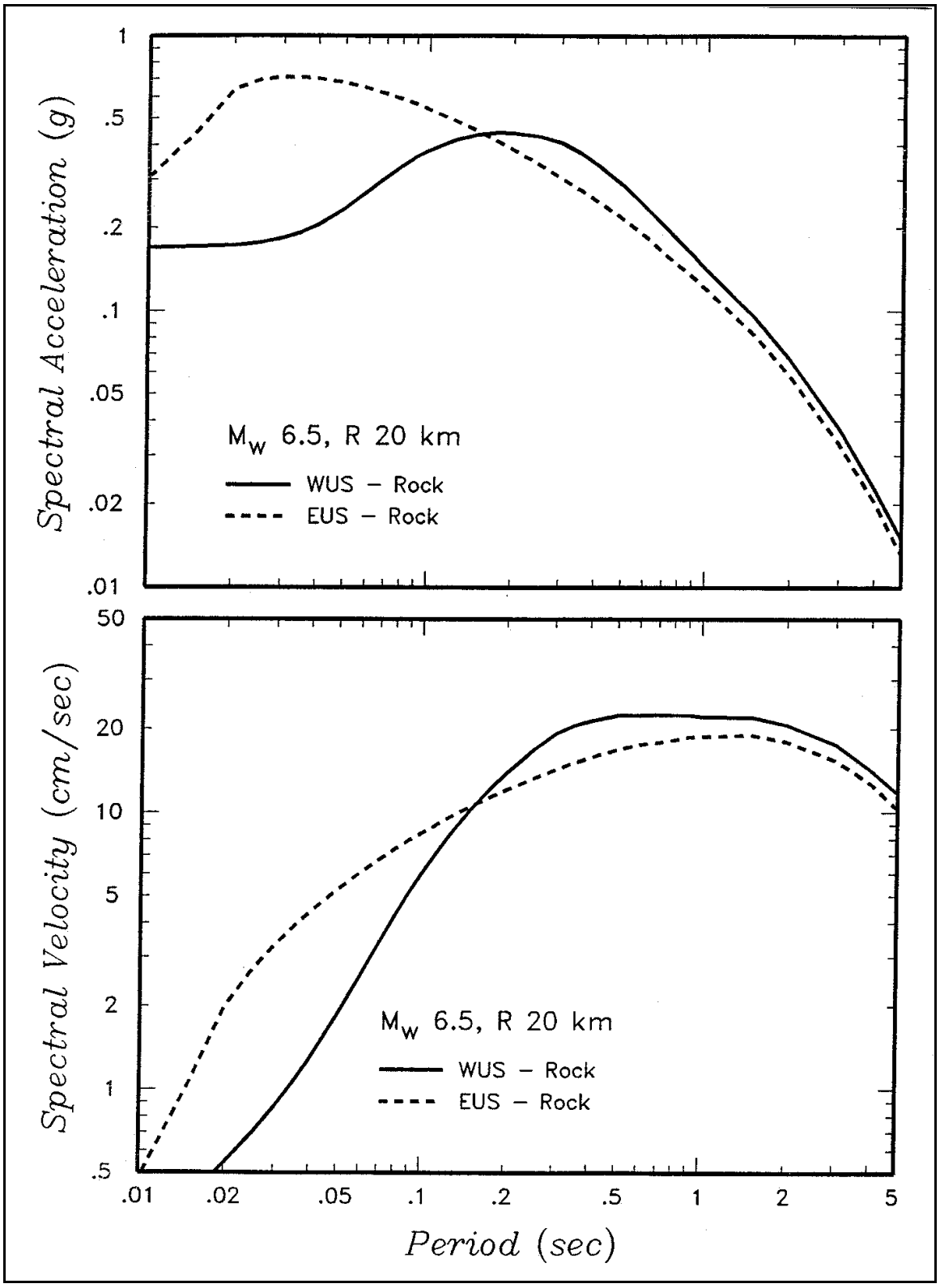

Figure 3-13. Comparison of response spectra for a magnitude 6.5 earthquake at 20 km using WUS and EUS attenuation relationships (calculated using BLWN/RVT model as formulated by Silva and Green 1989)

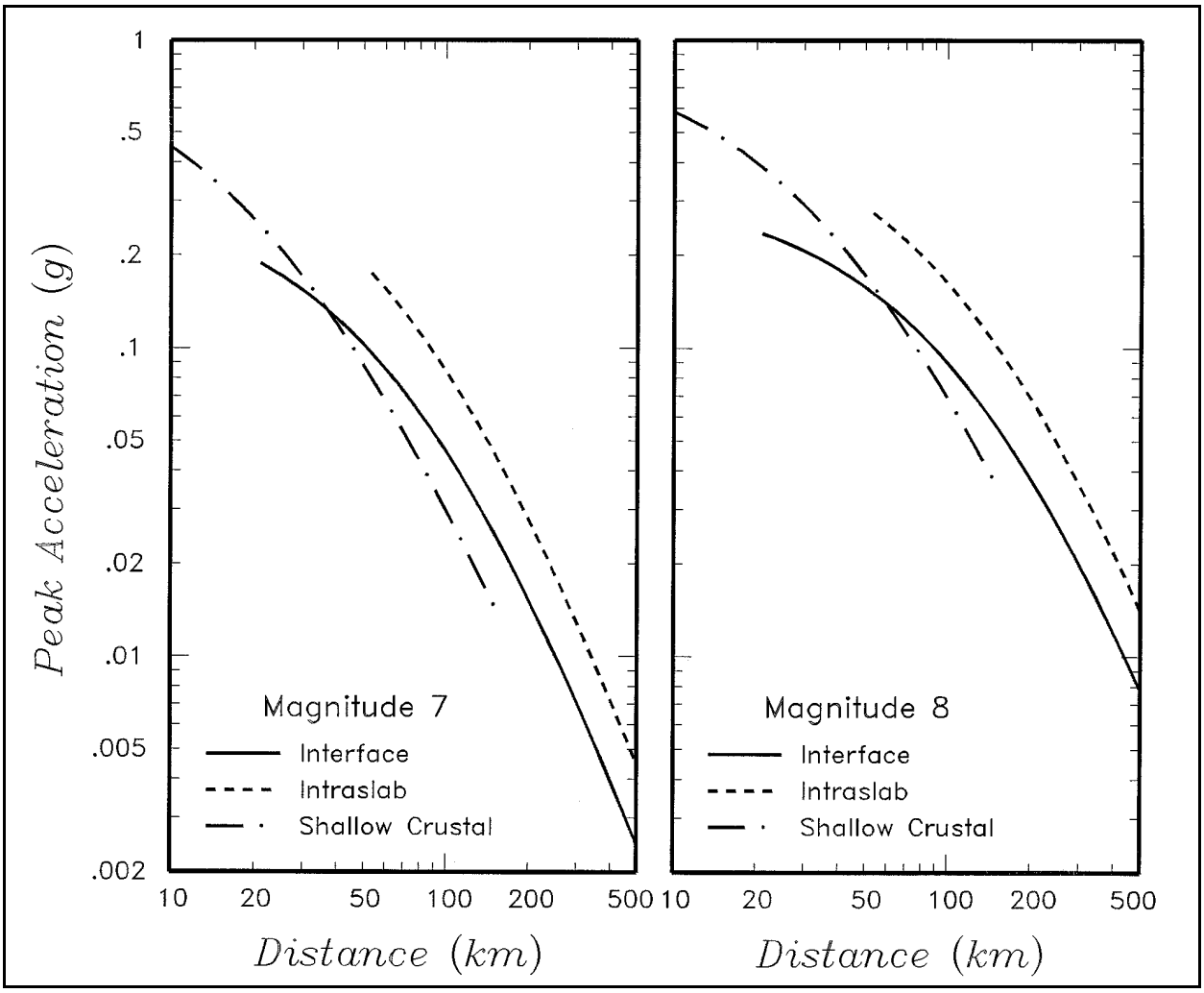

Figure 3-14. Comparison of median peak accelerations on rock from subduction zone earthquakes with peak accelerations from WUS shallow crustal earthquakes

Section II
Deterministic Procedures for Developing
Site-Specific Response Spectra

3-5. Summary of Alternative Procedures

Two basic approaches can be considered in developing design response spectra using a deterministic approach (deterministic seismic hazard analysis, or DSHA): Approach 1, anchoring response spectral shape to peak ground acceleration, and Approach 2, estimating the spectrum directly. These basic approaches are described below. This is followed in paragraphs 3-6 and 3-7 by an elaboration of the application of the two approaches to rock sites and soil sites, respectively.

a. Approach 1 - Anchoring response spectral shape to peak ground acceleration. Approach 1 is a three-part procedure in which peak ground acceleration is estimated, a response spectral shape is selected, and the shape is then multiplied by the peak ground acceleration to obtain the response spectrum, i.e.,

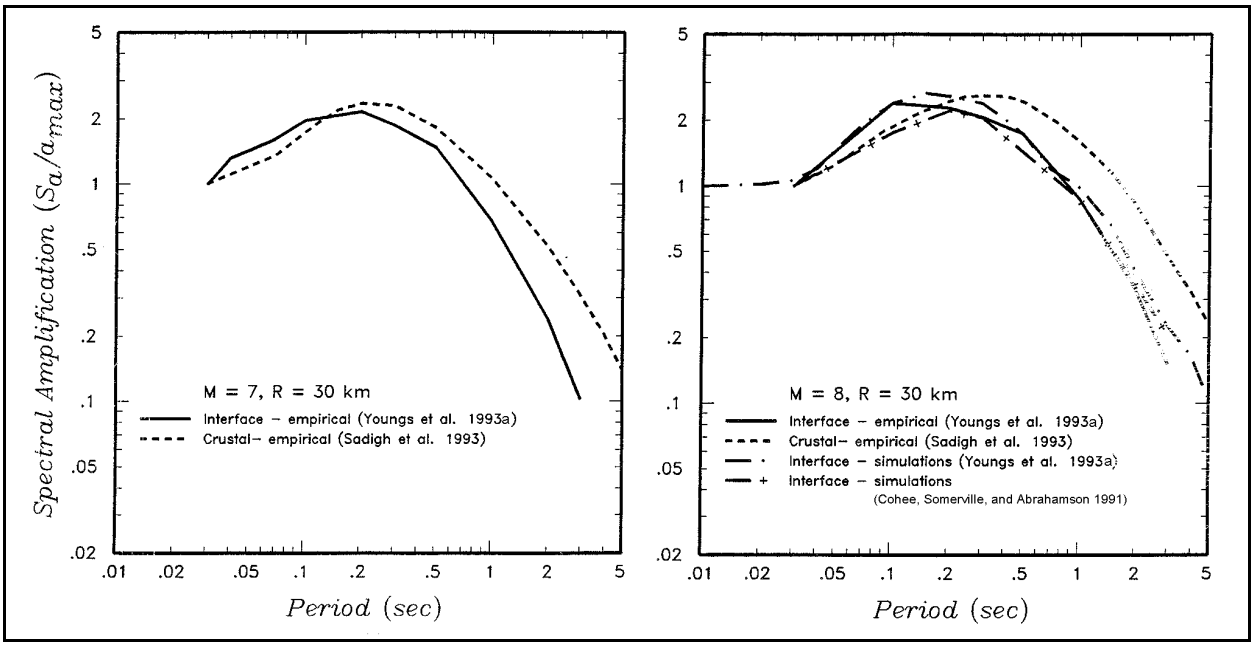

Figure 3-15. Comparison of spectral shapes using WUS and subduction zone attenuation relationships

(1) Step 1: Estimate peak ground acceleration (PGA).

(2) Step 2: Select response spectral shape, which is the curve of spectral amplification factors, (SA_T/PGA), where SA_T is spectral acceleration at period T.

(3) Step 3: Obtain response spectrum as the product of the peak ground acceleration and the spectral shape, SA_T = PGA × (SA_T/PGA). This approach is often referred to as "anchoring" the spectral shape to the peak ground acceleration. A variation on this approach is to estimate peak ground velocity (and, if desired, peak ground displacement) as well as peak ground acceleration and multiply these ground motion parameters by the appropriate spectral amplification factors (Newmark and Hall 1978, 1982); the Newmark and Hall procedure is summarized in Appendix B.

b. Approach 2 - estimating the spectrum directly. In Approach 2 the response spectrum ordinates are estimated directly as a single process. In general, there are three different approaches within Approach 2 for directly estimating response spectra: using response spectral attenuation relationships; performing statistical analysis of spectra from selected ground motion records; and theoretical (numerical) modeling. These approaches are briefly outlined below.

(1) Using response spectral attenuation relationships. Attenuation relationships have been developed by several investigators for response spectral values of ground motions (spectral acceleration or spectral pseudo-relative velocity) at selected periods of vibration by performing statistical regression analyses of ground motion data and by conducting theoretical analyses. Relationships have been developed for different site conditions and tectonic environments. Specific relationships are presented in paragraph 3-6 for rock sites and paragraph 3-7 for soil sites. These relationships can be used to make period-by-period estimates of response spectral values, given the design earthquake magnitude and distance. (The zero-period spectral value is obtained from the corresponding attenuation relationship for the peak ground acceleration, i.e., zero-period spectral acceleration (ZPA) = PGA.)

Typically, these relationships have been developed for 5 percent damping; and ratios between spectral values at different damping ratios (e.g., Newmark and Hall 1978, 1982; Appendix B) are used to obtain the corresponding spectra for other damping ratios.

(2) Performing statistical analysis of ground motion data. Spectral attenuation relationships discussed above are based on all the available applicable ground motion data, and they typically cover a wide range of earthquake magnitudes and distances. However, for a specific magnitude and distance, it may be possible to obtain an improved or a comparative estimate of the response spectrum by performing statistical analysis using a set of response spectra of ground motion records from earthquakes having magnitudes and distances that are close to the design magnitude and distance. The data set is typically a subset of the data used to develop attenuation relationships. The analysis may consist of direct, period-by-period statistical analysis of the data. However, it is also possible to "scale" or adjust each response spectral value of each record to values for the design magnitude and distance and then do statistical analysis of the scaled data set. The attenuation relationships for response spectral values (discussed in (1) above) are used to perform the scaling. This approach of scaling before performing statistical analyses is recommended unless the magnitudes and distances for the data set are closely bunched around the design magnitude and distance. Appendix C illustrates the approach of statistical analyses of a set of scaled response spectra. A particular type of statistical analysis that has been used for many nuclear power plant sites in the EUS and for other sites and locations as well is termed a "random earthquake" analysis. This analysis is performed to estimate the response spectrum at a site due to a randomly located ("floating") earthquake within the vicinity of the site, i.e., when its location cannot be assigned to a specific geologic structure at a specific distance from the site. After the design magnitude of the random earthquake is selected, a statistical analysis is made of response spectra of ground motion records from earthquakes having magnitudes close to the design magnitude, recorded on site conditions similar to those for the actual site, and recorded within a selected source-to-site distance, typically 25 km. A random earthquake analysis can also be performed using attenuation relationships. Appendix D illustrates a random earthquake analysis.

(3) Performing theoretical (numerical) ground motion modeling. The state of the art for theoretical (numerical) modeling of ground motions is being vigorously advanced and is being increasingly used for site-specific project applications. Various methods attempt to simulate the earthquake rupture, the propagation of seismic waves from earthquake source to site, and/or the effect of local site conditions. A number of methods have been developed. These methods warrant consideration as a supplementary means for ground motion estimation. They can be particularly useful for extrapolating to conditions that lie outside those represented by the database of strong motion recordings. The methods vary considerably in degree of complexity and sophistication. One relatively simple model that has been used increasingly to simulate earthquake rupture and source-to-site wave propagation is the Band Limited White Noise/Random Vibration Theory (BLWN/RVT) Model (Atkinson 1984; Atkinson and Boore 1995; Boore 1983, 1986; Boore and Atkinson 1987; Boore and Joyner 1991; Hanks and McGuire 1981; McGuire, Toro, and Silva 1988; Silva and Green 1989). This method has been applied particularly in the EUS because of the relative scarcity of ground motion data in the EUS, and attenuation relationships for the EUS have been developed using this model. A particular form of theoretical analysis applicable to soil sites is "site response analysis," or "ground response analysis" in which the objective is to assess the modifying influence of the local soil conditions on rock motions estimated for the site and, in this manner, estimate the motions at the ground surface of the soil site. Site response analyses are discussed in paragraph 3-7 in the context of their use in estimating response spectra for soil sites.

c. Relative advantages of Approach 1 and Approach 2. Approach 2, estimating the spectrum directly, should be used rather than Approach 1, anchoring spectral shape to peak ground acceleration,

because, as was outlined in Section I, spectral shapes depend on more than just the site conditions (i.e., on tectonic environment, earthquake magnitude, and other factors), yet the readily available and widely used spectral shapes generally incorporate only the effect of the local site conditions. Currently available procedures, relationships, and data enable response spectra to be estimated as a single process in Approach 2. When spectra are estimated using Approach 2, it is often useful to make comparative estimates using Approach 1. In paragraph 3-6 procedures and relationships for Approaches 1 and 2 for developing response spectra for rock sites are discussed. A similar presentation is made in paragraph 3-7 for soil sites.

3-6. Developing Site-Specific Spectra for Rock Sites

a. Using Approach 1 - Anchoring rock response spectral shape to peak rock acceleration.

(1) Estimating peak rock acceleration. Recently developed attenuation relationships for estimating peak rock acceleration for shallow crustal earthquakes in the WUS, for the EUS, and for subduction zones are summarized in Table 3-1. The relationships for the WUS shallow crustal earthquakes are better constrained than those for the other tectonic environments because of the relative abundance of strong motion data for WUS shallow earthquakes. The peak acceleration attenuation relationships in Table 3-1 generally include the standard deviations of the estimates, from which 84th percentile values may be obtained.

Table 3-1
Summary of Recently Developed Attenuation Relationships for Peak Ground Acceleration

Tectonic Environment	Relationship	Site Condition
WUS shallow earthquakes	Idriss (1991b)[1]	Rock
	Idriss (1991a)[1]	Soft soil
	Sadigh et al. (1993)[1,2]	Rock
	Abrahamson and Silva (1997)[1,2]	Rock and deep firm soil
	Campbell (1997)[1,2]	Alluvium, soft rock, hard rock
	Boore, Joyner, and Fumal (1997)[1]	Four site classifications based on shear wave velocity
	Sadigh et al. (1997) [1]	Rock and deep firm soil
EUS	Boore and Joyner (1991)	Deep soil
	Frankel et al. (1996)	Hard rock
	Atkinson and Boore (1997)	Hard rock
	Toro, Abrahamson, and Schneider (1997)	Hard rock
Subduction zone	Crouse (1991)	Firm soil
	Molas and Yamazaki (1995)	Rock; hard soil; medium soil; soft soil
	Youngs et al. (1997)	Rock and deep soil
Subduction zone and shallow earthquakes (no distinction)	Fukushima and Tanaka (1990)	Rock; hard soil; medium soil; soft soil
	Krinitzsky, Chang, and Nuttli (1987)	Hard site and soft site

[1] Includes a factor for type of faulting.
[2] Including vertical ground motions.

(2) Estimating response spectral shape and the response spectrum. Available spectral shapes for rock site conditions are summarized in Table 3-2. Multiplying spectral shape times peak ground acceleration results in the absolute response spectrum. Using the Newmark and Hall (1978, 1982) approach (Appendix B), peak ground acceleration is multiplied by the acceleration amplification factor, peak ground velocity by the velocity amplification factor, and peak ground displacement by the displacement amplification factor. Newmark and Hall's recommended relationships between peak ground acceleration, peak ground velocity, and peak ground displacement for rock site conditions may be used to estimate peak ground velocity and peak ground displacement, given peak ground acceleration; or peak ground velocity and peak ground displacement may be independently estimated. Note that the relationships in Table 3-2 of Seed, Ugas, and Lysmer (1976), Mohraz (1976), Applied Technology Council (1978), and Newmark and Hall (1978, 1982), do not explicitly incorporate the important effects of magnitude on spectral shape. The relationships of Mohraz (1976) and Newmark and Hall (1978, 1982) can indirectly incorporate the effects of magnitude through its effect on peak ground velocity and peak ground displacement if these parameters are estimated independently from peak ground acceleration (Appendix B).

Table 3-2
Summary of Available Response Spectral Shapes of Ground Motions

Tectonic Environment	Relationship	Site Conditions
WUS shallow earthquakes	Seed, Ugas, and Lysmer (1976)	Rock; stiff soil; deep cohesionless soil; soft to medium clay and sand
	Mohraz (1976)	Rock; shallow alluvium; moderately deep alluvium; alluvium
	Applied Technology Council (1978)[1]	Rock or shallow stiff soil; deep stiff soil; soft soil
	Newmark and Hall (1978, 1982)	Rock; firm soil
	Sadigh et al. (1997)	Rock and deep firm soil
WUS shallow earthquakes; EUS	Silva and Green (1989)	Rock
Subduction zones	Youngs et al. (1997)	Rock and deep soil

[1] These spectral shapes are based primarily on Seed, Ugas, and Lysmer (1976). The Applied Technology Council (1978) spectral shapes are also the spectral shapes that appear in the 1994 Uniform Building Code (International Conference of Building Code Officials 1994) and the 1995 Recommended Lateral Force Requirements and Commentary ("Blue Book") of the Seismology Committee of the Structural Engineers Association of California (SEAOC 1996).

(3) Uncertainty in response spectral prediction. Response spectra obtained using the median or mean peak ground acceleration attenuation relationships and the median or mean spectral shapes summarized above result in median (50th percentile) or mean ground motion estimates, given a design earthquake magnitude and distance. Additional consideration must be given if a higher percentile ground motion is to be predicted, for example the 84th percentile (median plus standard deviation) ground motion. Spectra for the 84th percentile can be estimated by multiplying median or mean peak ground acceleration by 84th percentile spectral shapes. For example, Seed, Ugas and Lysmer (1976) present 84th percentile shapes as well as mean shapes. However, this procedure results in a lesser degree of conservatism in the very short period part of the spectrum because the anchor value of peak ground acceleration (equal to the zero-period spectral acceleration, ZPA) is at the median or mean level. In order to have a uniform degree of conservatism throughout the period range, the peak ground acceleration and the very short period part of the spectrum should be adjusted upward to the 84th percentile level. Alternatively, the entire median response spectrum may be scaled upward by a factor to the approximate 84th percentile level. When the entire spectrum is scaled, often the standard deviation in peak ground acceleration is used to obtain a scaling factor. This is an approximation, since the standard deviation has

been found to vary with period of vibration. (The period dependence can be directly accounted for when using Approach 2.) The 84th percentile amplification factors of the Newmark and Hall (1978, 1982) approach can be applied to median estimates of peak ground acceleration, velocity, and displacement to obtain 84th percentile spectral values (Appendix B, Table B-1). Again, a separate adjustment should be applied to raise the peak ground acceleration and very short period part of the spectrum to the 84th percentile level.

(4) Estimating vertical ground motion response spectra. Ratios of vertical to horizontal response spectral amplitudes can be used to estimate vertical response spectra, given an estimate of horizontal response spectra. Recent studies (e.g., Silva 1997) indicate that vertical-to-horizontal response spectral ratios are a function of period of vibration, earthquake source to site distance, earthquake magnitude, tectonic environment (WUS and EUS), and subsurface conditions (soil and rock). Figure 3-16 provides a guideline for ratios of vertical to horizontal spectral values on rock sites that is generally conservative for earthquake magnitudes equal to or less than about 6.5. However, if a facility is sensitive to short-period (less than 0.3 sec) vertical motions, and is located within 10 km of the earthquake source or the magnitude exceeds 6.5, further evaluation of vertical response spectra on rock is recommended because vertical response spectra can significantly exceed horizontal response spectra for these conditions.

b. Using Approach 2 - Estimating the rock response spectrum directly.

(1) General. The three approaches discussed in paragraph 3-5*b* can be used: using response spectral attenuation relationships, performing statistical analyses of ground motion response spectra, and theoretical (numerical) modeling. The following paragraphs refer to particular relationships or methods.

(2) Using response spectral attenuation relationships. Recently developed attenuation relationships that can be used to predict horizontal rock response spectral values for WUS shallow crustal earthquakes, for EUS earthquakes, and for subduction zone earthquakes are summarized in Table 3-3. The spectral acceleration attenuation relationships summarized in Table 3-3 generally include the standard deviations of the estimates, from which 84th percentile values may be obtained. As illustrated in Figures 3-12 and 3-13, EUS attenuation models characteristically estimate much higher spectral response in the short-period range (less than 0.1 to 0.2 sec) than estimated by relationships for the WUS. As discussed in paragraph 3-4*a* the higher short-period response is attributed to the hardness of the rock in the EUS. Such short-period (high-frequency) motions may or may not be significant to the response and performance of hydraulic structures. The assessment of the significance of such motions should be made by the principal design engineer in collaboration with the seismic structural analyst and the materials engineer.

(3) Using statistical analyses of response spectra. Abundant strong motion data are available to permit statistical analyses of data sets for many design earthquake scenarios for WUS shallow crustal earthquakes. As noted in paragraph 3-5*b*(2), statistical “random earthquake” analyses have been made at many EUS sites because, in general, discrete faults have not been identified in the EUS. Yet it was desired to model the possibility of an earthquake (usually of moderate magnitude, in the range of magnitude 5 to 6) occurring near the site. Many of these analyses have been carried out using WUS ground motion data because only a few records from moderate magnitude earthquakes are available in the EUS. Such analyses may be reasonable for estimating longer period rock motions but would apparently underestimate shorter period (less than 0.1 to 0.3 sec) ground motions at hard rock sites. In this case, an adjustment should be made for the short-period response spectral values, if these short-period motions are of significance to the structure under consideration. The adjustment can be made by comparing

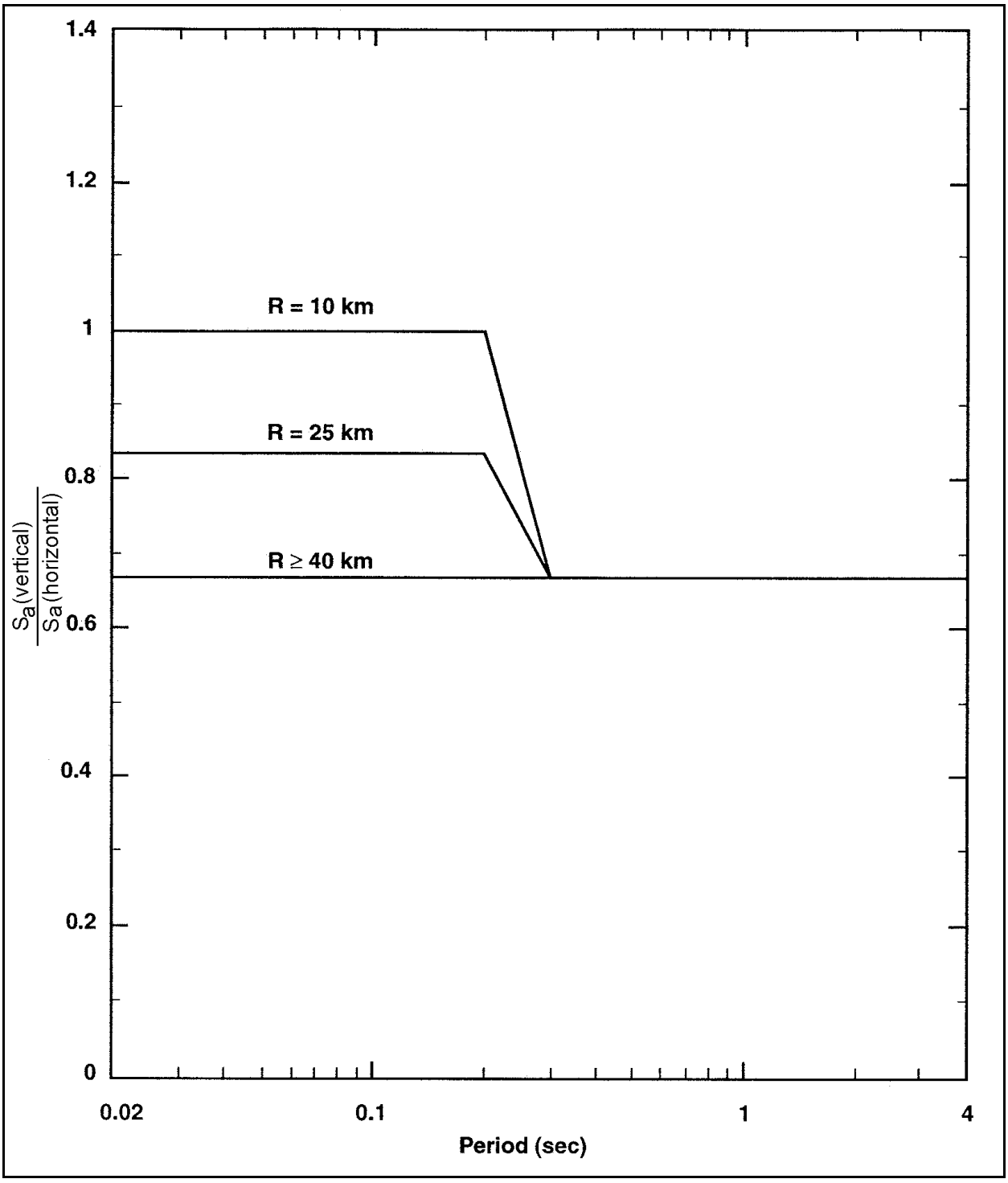

Figure 3-16. Simplified relationships between vertical and horizontal response spectra as a function of distance *R*

Table 3-3
Summary of Recently Developed Attenuation Relationships for Response Spectral Values of Ground Motions

Tectonic Environment	Relationship	Site Conditions
WUS shallow earthquakes	Idriss (1991b)[1]	Rock
	Sadigh et al. (1993)[1,2]	Rock
	Abrahamson and Silva (1997)[1,2]	Rock and deep firm soil
	Campbell (1997)[1,2]	Alluvium, soft rock, hard rock
	Boore, Joyner, and Fumal (1997)[1]	Four site classifications based on shear wave velocity
	Sadigh et al. (1997)[1]	Rock and deep firm soil
EUS	Boore and Joyner (1991)	Deep soil
	Frankel et al. (1996)	Hard rock
	Atkinson and Boore (1997)	Hard rock
	Toro, Abrahamson, and Schneider (1997)	Hard rock
Subduction zone	Crouse (1991)	Firm soil
	Youngs et al. (1997)	Rock and deep soil

[1] Includes a factor for type of faulting.
[2] Including vertical ground motions.

response spectrum amplitudes predicted by EUS and WUS attenuation relationships for rock (Table 3-3). As illustrated in Appendix D, a random earthquake analysis can also be carried out using attenuation relationships. Thus this analysis can be performed using the EUS spectral attenuation relationships that predict higher short-period motions at hard rock sites.

(4) Using theoretical (numerical) modeling techniques. The techniques discussed in paragraph 3-5*b*(3) can be used. These techniques attempt to simulate the earthquake rupture and the propagation of seismic waves from the earthquake source to the site.

(5) Estimating vertical ground motion response spectra. The available recently developed attenuation relationships for response spectral values of vertical rock motions are summarized in Table 3-3. These relationships can be used directly to estimate vertical rock response spectra. The vertical to horizontal spectral ratios discussed in paragraph 3-6*a*(4) and shown in Figure 3-16 can be used as a guide in estimating vertical response spectra, given an estimate of the horizontal spectra.

c. Developing acceleration time-histories of rock motions consistent with the design response spectrum.

(1) General. When acceleration time-histories of ground motions are required for the dynamic analysis of a structure, they should be developed to be consistent with the design response spectrum over the period range of significance for the structure, as well as have an appropriate strong motion duration for the particular design earthquake. Two general approaches to developing acceleration time-histories are selecting a suite of recorded motions and synthetically developing or modifying one or more motions.

These approaches are discussed below. For either approach, when near-source earthquake ground motions are modeled, it may be desirable that an acceleration time-history include a strong intermediate- to long-period pulse to model this particular characteristic of ground motion often observed in the near field (paragraph 3-3*b*(4) and Figure 3-6).

(2) Selecting recorded motions. Every earthquake produces a unique set of acceleration time-histories having characteristics that depend on the earthquake magnitude and other source characteristics, distance, attenuation and other travel path characteristics, and local site conditions. The response spectrum of any individual ground motion accelerogram has peaks and valleys that occur at different periods of vibration. Thus, the response spectrum of any single accelerogram is unlikely to match the developed smooth design response spectrum. Typically, when recorded motions are selected, it is necessary to choose a suite of time-histories (typically at least four) such that, in aggregate, valleys of individual spectra that fall below the design curve are covered by peaks of other spectra and (preferably) the exceedance of the design spectrum by individual spectral peaks is not excessive. For nonlinear analyses, it may be desirable to have additional time-histories because of the importance of pulse sequencing to nonlinear response (see also comments in (3) below). In the approach of selecting recorded motions, simple scaling of individual accelerograms by a constant factor is done to improve the spectral fit, but the wave form and the relative spectral content of the accelerograms are not modified. The advantage of selecting recorded motions is that each accelerogram is an actual recording, and thus the structure is analyzed for natural motions that are presumably most representative of what the structure could experience. The approach has the following disadvantages: multiple dynamic analyses are needed for the suite of accelerograms selected; although a suite of accelerograms is selected, there will typically be substantial exceedances of the smooth design spectrum by individual spectrum peaks; and although a reasonably good spectral fit may be achieved for one horizontal component, when the same simple scaling factors are applied to the other horizontal components and the vertical components for the records selected, the spectral fit is usually not as good for the other components.

(3) Synthetically developing or modifying motions. A number of techniques and computer programs have been developed either to completely synthesize an accelerogram or modify a recorded accelerogram so that the response spectrum of the resultant accelerogram closely fits or matches the design spectrum. It is preferred to use techniques that modify a recorded accelerogram rather than completely synthesize a motion since the recorded motion will have time-domain characteristics representative of actual ground motions. Two techniques that have been found to do a good job of spectrally modifying recorded motions are the frequency-domain RASCAL computer code developed for the Corps of Engineers by Silva and Lee (1987) and the time-domain technique developed by Lilhanand and Tseng (1988). These techniques preserve the basic time-domain character of the accelerogram yet provide an excellent match to a smooth spectrum. An example of the spectral matching technique is given in Figures 3-17 and 3-18. The RASCAL computer code was used in this case. Figure 3-17 illustrates the initial (recorded) acceleration, velocity, and displacement time-histories and the time-histories after the spectral matching process. Figure 3-18 illustrates the initial (recorded) acceleration response spectra, the smooth design response spectrum, and the response spectrum of the acceleration time-history after the spectral matching process. Figure 3-18 illustrates the very close spectral match that was achieved, while Figure 3-17 illustrates that the modified time-histories preserve the basic time-domain character of the original record. Synthetic techniques for developing time-histories have the following advantages: a good fit to the design spectrum can be achieved with a single accelerogram; the natural appearance and strong motion duration can be maintained in the accelerograms; and three component motions (two horizontal and one vertical) each providing a good spectral match can be developed, and these can be made statistically independent if desired; and the process is relatively efficient.

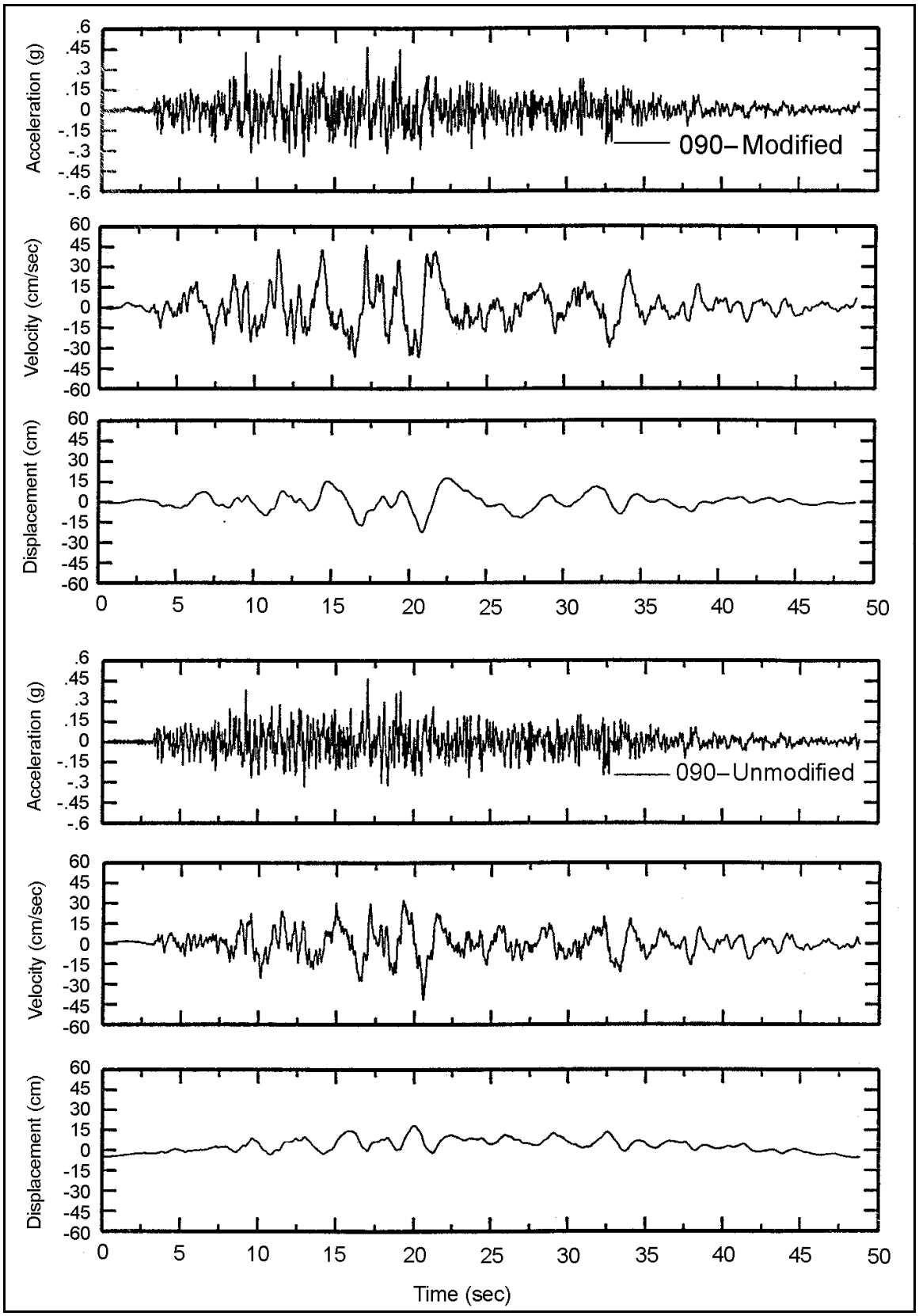

Figure 3-17. Example of original time-histories and time-histories after a spectral matching process

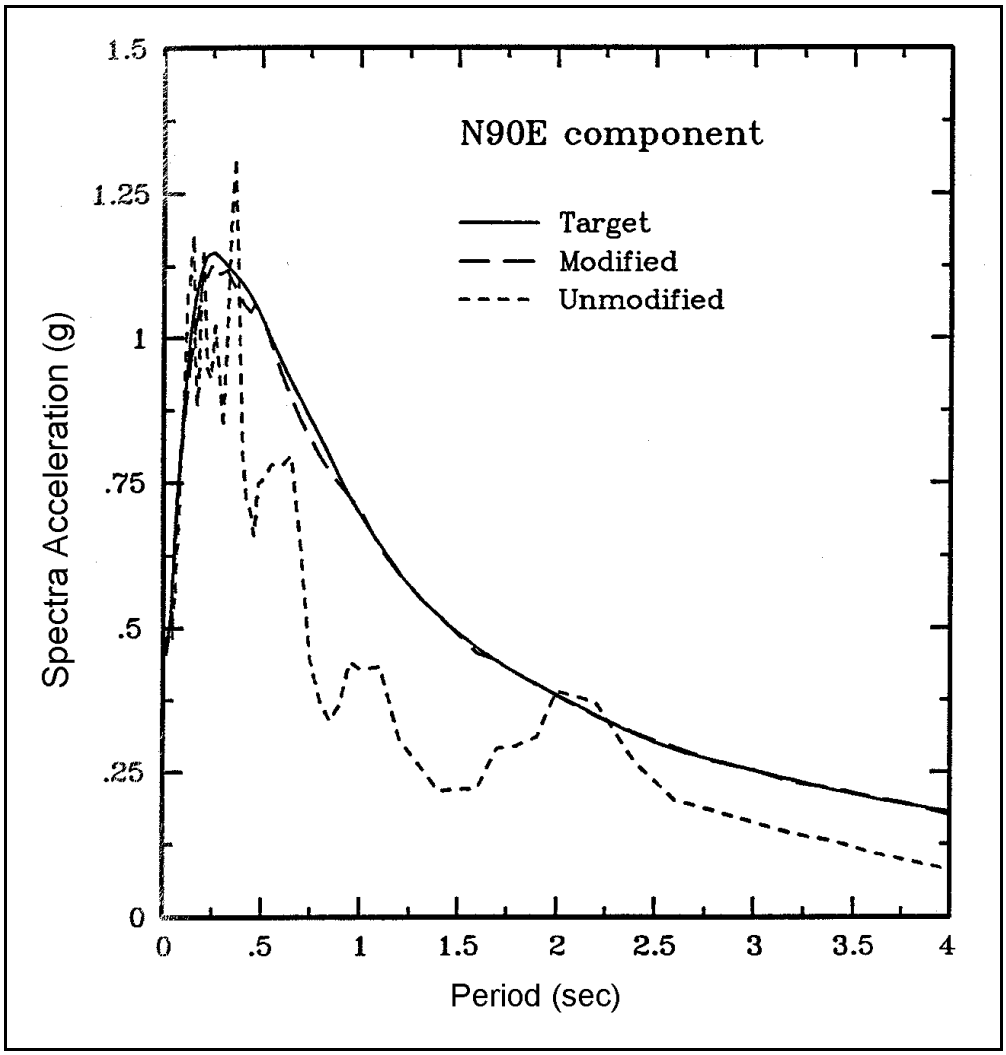

Figure 3-18. Example of response spectrum of time-history matched to a design response spectrum and spectrum of original time-history

The disadvantage is that the motions are not "real" motions, which would not exhibit smooth design spectra. Also "real" motions may contain less energy than synthetic spectrum-matched motions of similar amplitude. Although a good fit to a design spectrum can be attained with a single accelerogram, it may be desirable in some cases to fit the spectrum using more than one accelerogram. For nonlin ear analysis applications, it is particularly desirable to have multiple accelerograms because different accelerograms may have different pulse sequencing characteristics of importance to nonlinear response yet have essentially identically response spectra. Numerical ground motion modeling methods can also be used to produce synthetic accelerograms. Such motions have the character of recorded motions since the modeling procedures are intended to simulate the earthquake rupture and wave propagation process.

3-7. Developing Site-Specific Spectra for Soil Sites

As is the case for developing site-specific rock spectra, either the approach of anchoring spectral shapes to a peak ground acceleration (Approach 1) or the approach of directly estimating the spectra (Approach 2) can be used for soil sites. The implementation of these approaches is outlined below.

a. Approach 1 - Anchoring the response spectral shape to the peak ground acceleration.

(1) Estimating peak ground acceleration. Table 3-1 summarizes recently developed attenuation relationships for estimating peak ground acceleration. For WUS shallow crustal faulting earthquakes, several recent attenuation relationships are available to estimate top-of-soil peak ground accelerations for firm soil conditions, and Idriss (1991a) has developed a peak acceleration attenuation relationship for soft soil sites. Combining the BLWN/RVT method for rock motion estimation with a site response analysis for a deep soil column, Boore and Joyner (1991) developed a peak ground acceleration attenuation relationship for deep soil sites in the EUS. For subduction zone earthquakes, attenuation relationships have been developed for firm soil conditions and in some cases for soft soil conditions (Table 3-1). As is the case for rock attenuation relationships, the soil attenuation relationships are better constrained by data for WUS shallow crustal earthquakes than for EUS or subduction zone earthquakes.

(2) Estimating response spectral shape and the response spectrum. Spectral shapes that have been developed for soil sites for WUS shallow crustal earthquakes and for subduction zone earthquakes on the basis of statistical analyses of ground motion data are summarized in Table 3-2. Spectral shapes have not been developed for soil sites for EUS earthquakes. Using the Newmark and Hall (1978, 1982) approach (Appendix B), the effect of soil is accounted for by estimating values of peak ground velocity and peak ground displacement directly, or by using Newmark and Hall's relationships between peak ground acceleration, peak ground velocity, and peak ground displacement for firm soil to estimate peak ground velocity and peak ground displacement, given peak ground acceleration. Peak ground acceleration, velocity, and displacement then are multiplied by Newmark and Hall's amplification factors to obtain the absolute response spectrum.

(3) Uncertainty in response spectra predictions. The comments made in paragraph 3-6*a*(3) regarding estimating 84th percentile response spectra for rock also apply to response spectra for soil.

(4) Estimating vertical ground motion response spectra. Recent studies (e.g., Silva 1997) indicate that vertical-to-horizontal ratios of response spectra of ground motions are higher on soil than on rock for short periods of vibration. Figure 3-16 provides a guideline for ratios of vertical-to-horizontal spectral ratios on firm soil sites that is generally conservative. However, if a facility is sensitive to short-period (less than 0.3 sec) vertical motions, and is located within 25 km of the earthquake source or the magnitude exceeds 6.5, further evaluation of vertical response spectra on soil is recommended because vertical response spectra can significantly exceed horizontal response spectra for these conditions.

b. Using Approach 2 - Estimating the soil response spectrum directly.

(1) General. The three approaches discussed in paragraph 3-5*b* can be used for soil sites. These approaches are using response spectral attenuation relationships, performing statistical analysis of ground motion response spectra, and theoretical (numerical) modeling.

(2) Using response spectral attenuation relationships. Recently developed response spectral attenuation relationships for soil are summarized in Table 3-3. The spectral attenuation relationships in

Table 3-3 generally include the standard deviations of the estimates, from which 84th percentile values may be obtained.

(3) Using statistical analyses of response spectra. Abundant ground motion data for firm soil sites in the WUS are available to permit statistical analyses of data sets for many design earthquakes. Although such data are not available for EUS earthquakes, the WUS data can be used, recognizing that the analyses may underestimate short-period (less than 0.1 to 0.3 sec) response spectra. (Refer to discussion for rock sites in paragraph 3-6*b*(3).) The degree of underestimation should be less at soil sites than at rock sites because soils will tend to damp out the short-period motions.

(4) Using theoretical (numerical) modeling techniques. The techniques discussed in paragraph 3-5*b*(3) can be used to simulate the earthquake rupture and propagation of seismic waves from the earthquake source to the site. In addition, site response analyses may be carried out to estimate top-of-soil response spectra, given a response spectrum in rock. With this approach, rock motions, including response spectra, are first defined for the site (using procedures and relationships described in paragraph 3-6). The soil profile between the ground surface and the underlying rock is modeled. The rock motions are assigned to a hypothetical rock outcrop at the site rather than to the rock at depth beneath the soil column. This is because rock motion recordings are obtained at the ground surface rather than at depth, and unless the rock is rigid, the rock motion beneath the soil column will differ somewhat from the rock outcrop motion. Then, using nonlinear or equivalent linear soil response analytical methods, rock motions are propagated through the soils column and top-of-soil motions are estimated. The site response analysis process is schematically illustrated in Figure 3-19. This figure illustrates the commonly used one-dimensional site response analysis method applicable where the soil stratigraphy is relatively uniform and flat-lying and the ground surface topography is relatively level. Two-dimensional site response analysis methods are available for situations where these conditions are not sufficiently met. Just as in other types of theoretical modeling and numerical analyses, results of site response analyses are sensitive to the details of the analytical procedures, modeling of the process, and inputs to the analysis. Broad guidelines for conducting these analyses are listed below:

(a) More than one input rock acceleration time-history should be used, and the selected motions should be reasonably representative of the rock motions in terms of spectra and duration.

(b) Parametric analyses for variations in the dynamic soil properties should be made to examine the sensitivity of the response to uncertainties in the soil properties. This is particularly important when soil properties are based on generalized correlations rather than on a program of field shear wave velocity measurements.

(c) It is useful to compute ratios of response spectra of top-of-soil motion to input rock motion for each analysis that is carried out. The ratios are much less sensitive to the actual input motion than is the absolute top-of-soil motion. The spectral ratios can then be examined and smoothed and multiplied by the rock smooth spectrum to obtain a top-of-soil spectrum, which can be further smoothed.

An illustration of a site response analysis is presented in Appendix E. Articles by Seed and Sun (1989), Chang et al. (1990), and Ahmad, Gazetas, and Desai (1991) provide useful background information on site response analysis methodologies. Site response analyses are needed relatively more for soft soil sites than for firm soil sites because the site response effects are greater for soft soils and because ground motion data and empirically based ground motion relationships are relatively scarce for soft soil sites.

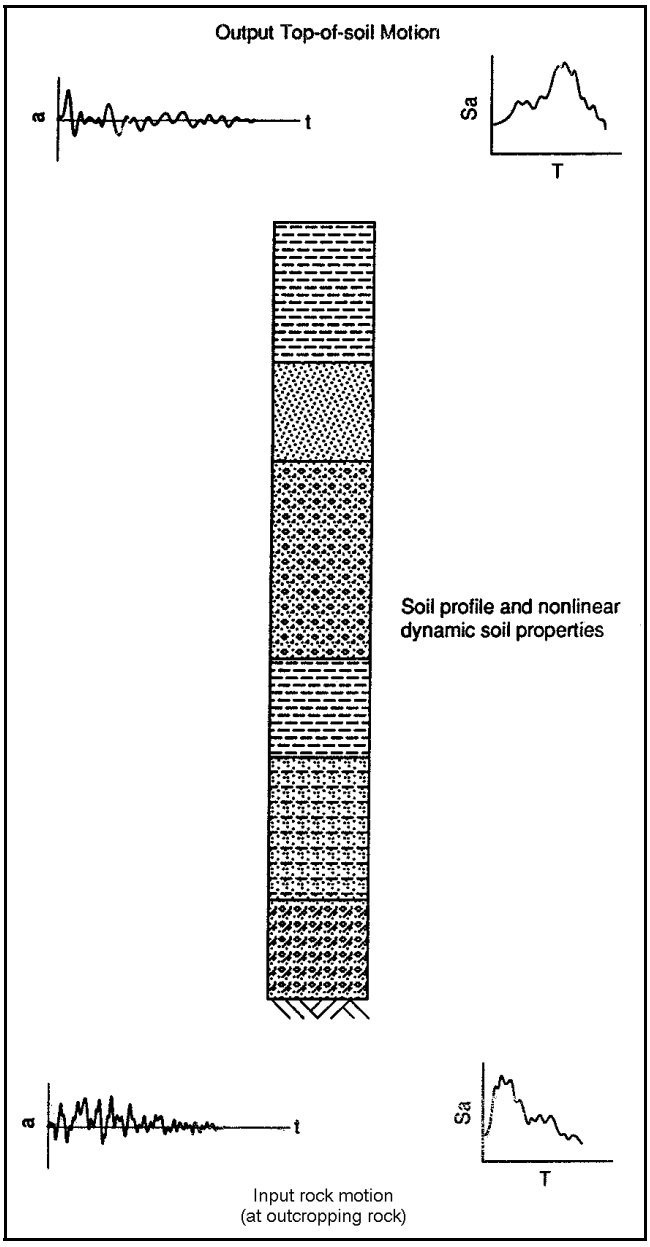

Figure 3-19. Schematic of one-dimensional site response analysis

(5) Estimating vertical ground motion response spectra. The available recently developed attenuation relationships for response spectral accelerations of vertical firm-soil site motions are summarized in Table 3-3. These relationships can be used directly to estimate vertical response spectra on firm soils sites. The vertical to horizontal response spectral ratios discussed in paragraph 3-7*a*(4) and shown in Figure 3-16 can be used as a guide in estimating vertical response spectra, given an estimate of horizontal response spectra.

c. Developing acceleration time-histories of soil motions consistent with design response spectrum. The two alternatives for developing acceleration time-histories for rock motions that were discussed in

paragraph 3-6*c*, namely, selecting recorded motions and synthetically developing or modifying motions, can also be used to develop time-histories for top-of-soil motions. In the case where site response analyses are carried out to define top-of-soil motions, there is a third alternative, which is to obtain the time-histories directly from the site response analyses.

Section III
Probabilistic Approach for Developing Site-Specific Response Spectra

3-8. Overview of Probabilistic Seismic Hazard Analysis (PSHA) Methodology

a. General. PSHA takes the elements of a deterministic assessment of earthquake ground shaking hazard—identification of seismic sources; specification of limiting earthquake sizes; assessment of ground motions as a function of earthquake magnitude; source-to-site distance; and site conditions—and adds an assessment of the likelihood that ground shaking will occur during a specified time period. Figure 3-20 shows a typical result of PSHA, termed a hazard curve, that relates the level of ground shaking to the annual frequency of exceedance of that level. The ground motion parameter for the example in Figure 3-20 is peak ground acceleration. PSHA may be conducted for other ground motion parameters, such as peak ground velocity or response spectral values for specific periods of vibration and damping ratios. If a PSHA is carried out for response spectral values at a number of periods of vibration, then response spectra having selected probabilities of exceedance (i.e., "equal hazard" response spectra) may be constructed, as will be discussed later.

b. Elements of a PSHA. Evaluation of the frequency or probability of exceedance of ground motions at a site is a function of earthquake source definition (distance of the sources from the site, source geometries, and frequencies of occurrence (recurrence) of earthquakes of different magnitudes on each source), and ground motion attenuation (amplitudes of ground motion as a function of earthquake magnitude and distance). These basic inputs to a PSHA are then combined in a probabilistic model to obtain hazard curves and (if desired) equal-hazard response spectra as discussed above. The basic elements of a PSHA are illustrated in Figure 3-21 for peak ground acceleration and in Figure 3-22 for equal hazard response spectra.

c. Formulation of PSHA methodology.

(1) Formulation. The methodology used to conduct PSHA was initially developed by Cornell (1968). Current practice is described in several publications, such as National Research Council (1988) and Earthquake Engineering Research Institute Committee on Seismic Risk (1989). Using a Poisson probability model (paragraph 3-9*d*), the probability of exceedance $p_E(z)$ of a ground motion level z in an exposure time or design time period t at a site is related to the annual frequency of ground motion exceedance at the site, ν_z, by:

$$p_E(z) = 1 - e^{-(\nu_z \cdot t)} \tag{3-1}$$

A PSHA is carried out to obtain ν_z, and $p_E(z)$ can then be obtained using Equation 3-1. The return period (RP) for ground motion exceedance at a site is equal to the reciprocal of ν_z. The results of a PSHA are, in practice, expressed in terms of one or more of the parameters, $p_E(z)$, ν_z, and RP. Using Equation 3-1, the interrelationship between these fundamental parameters is illustrated in graphical form in Figure 3-23 and in tabular form in Table 3-4. Note that when $(\nu_z \cdot t)$ is small (approximately ≤ 0.1), $p_E(z)$ is approximately equal to $\nu_z \cdot t$. For larger values of $\nu_z \cdot t$, $p_E(z)$ is less than $(\nu_z \cdot t)$. The basic formulation for ν_z is:

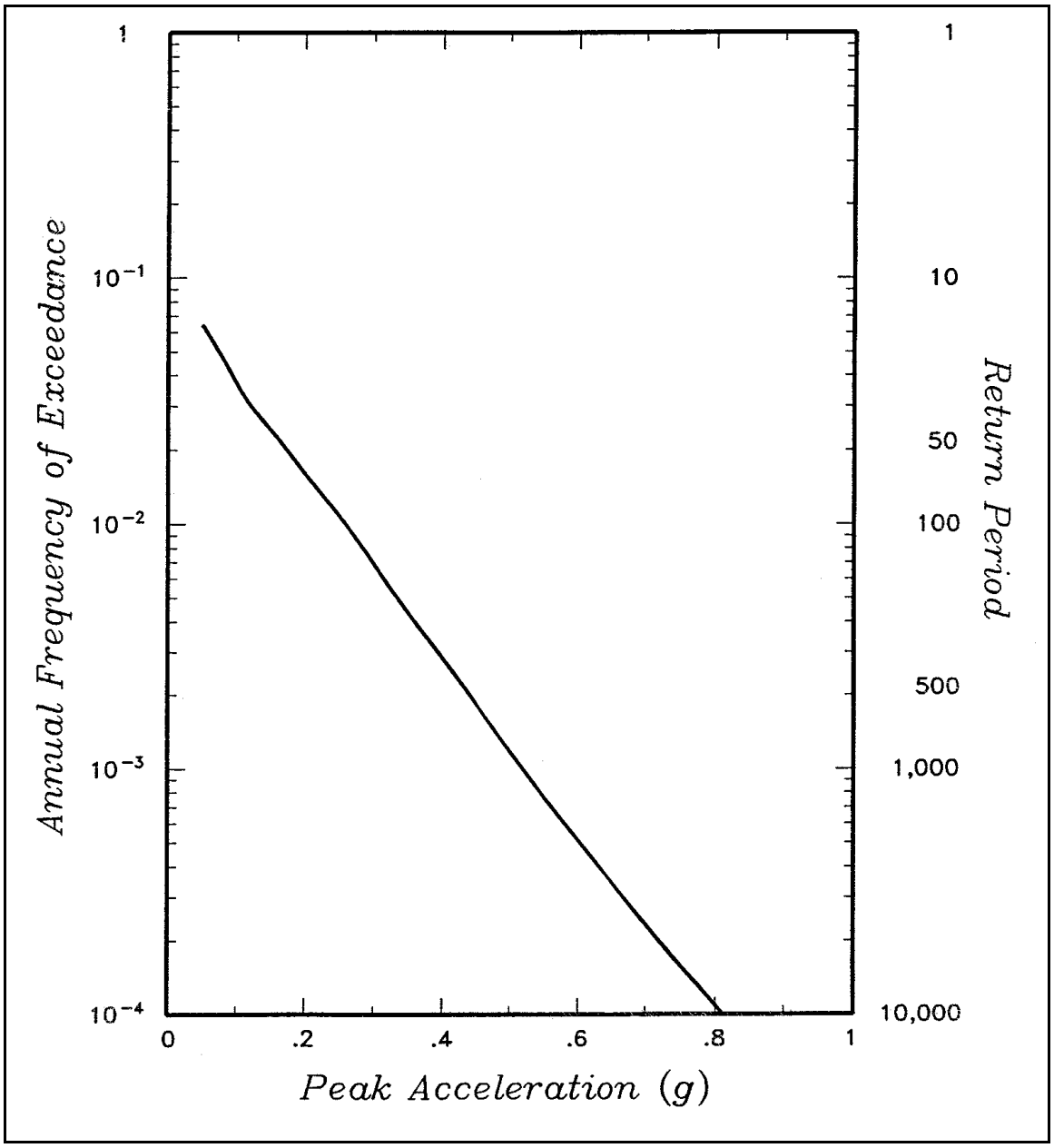

Figure 3-20. Example seismic hazard curve showing relationship between peak ground acceleration and probability (annual frequency) of exceedance

$$v_z = \sum_N \left[\sum_M \lambda\,(m_i) \bullet \sum_R P\,(R = r_j \,|\, m_i) \bullet P\,(Z > z \,|\, m_i\ r_j) \right]_n \tag{3-2}$$

where

$\sum_N$ = summation over all (N) seismic sources

$\lambda(m_i)$ = the annual frequency of occurrence of earthquakes of magnitude m_i (above a certain minimum size of engineering significance) on seismic source n

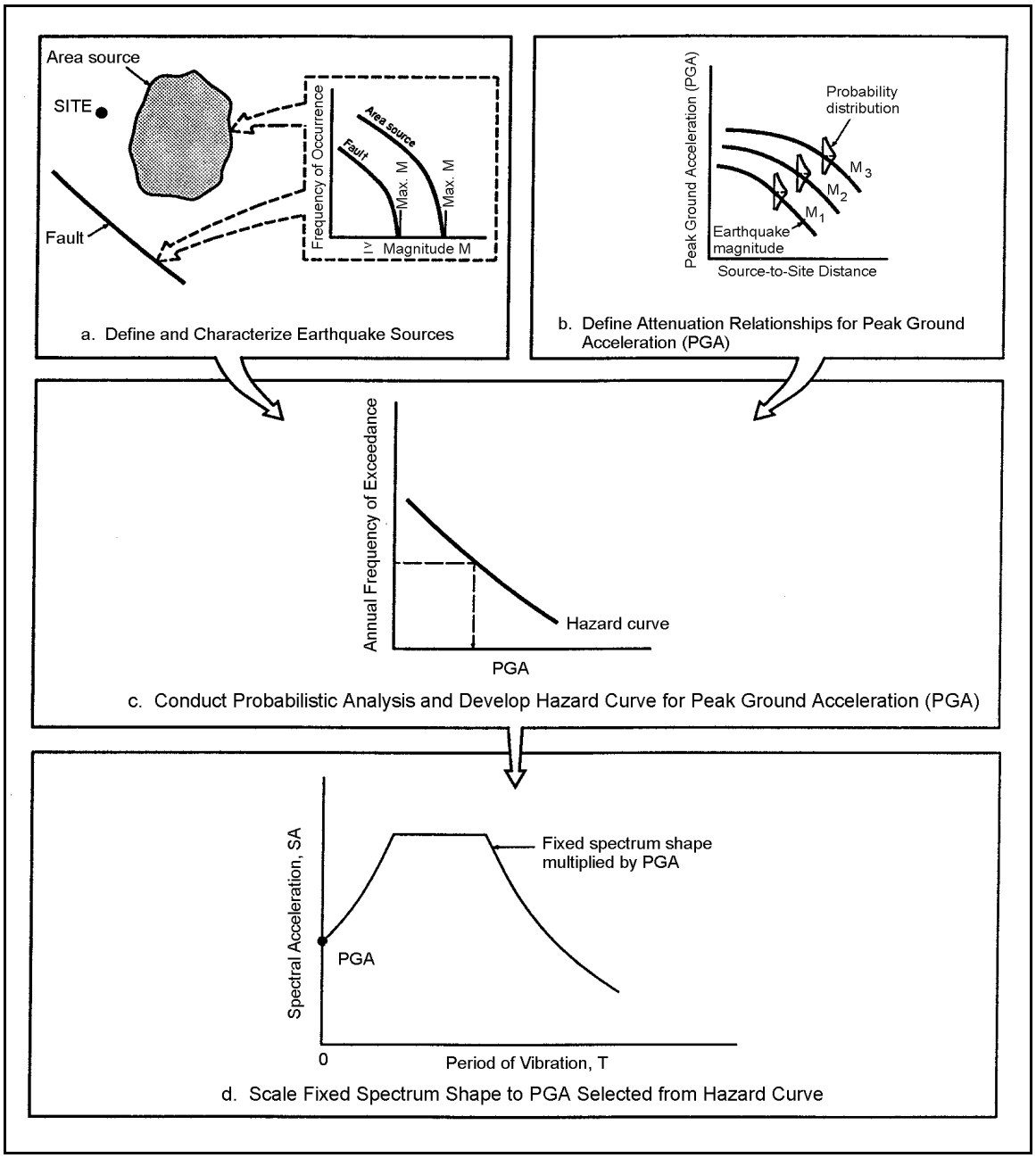

Figure 3-21. Development of response spectrum based on a fixed spectrum shape and a probabilistic seismic hazard analysis for peak ground acceleration

$P\,(R{=}r_j \mid m_i)$ = the probability of an earthquake of magnitude m_i on source n occurring at a certain distance r_j from the site

$P\,(Z{>}z \mid m_i, r_j)$ = the probability that ground motion level z will be exceeded, given an earthquake of magnitude m_i on source n at distance r_j from the site

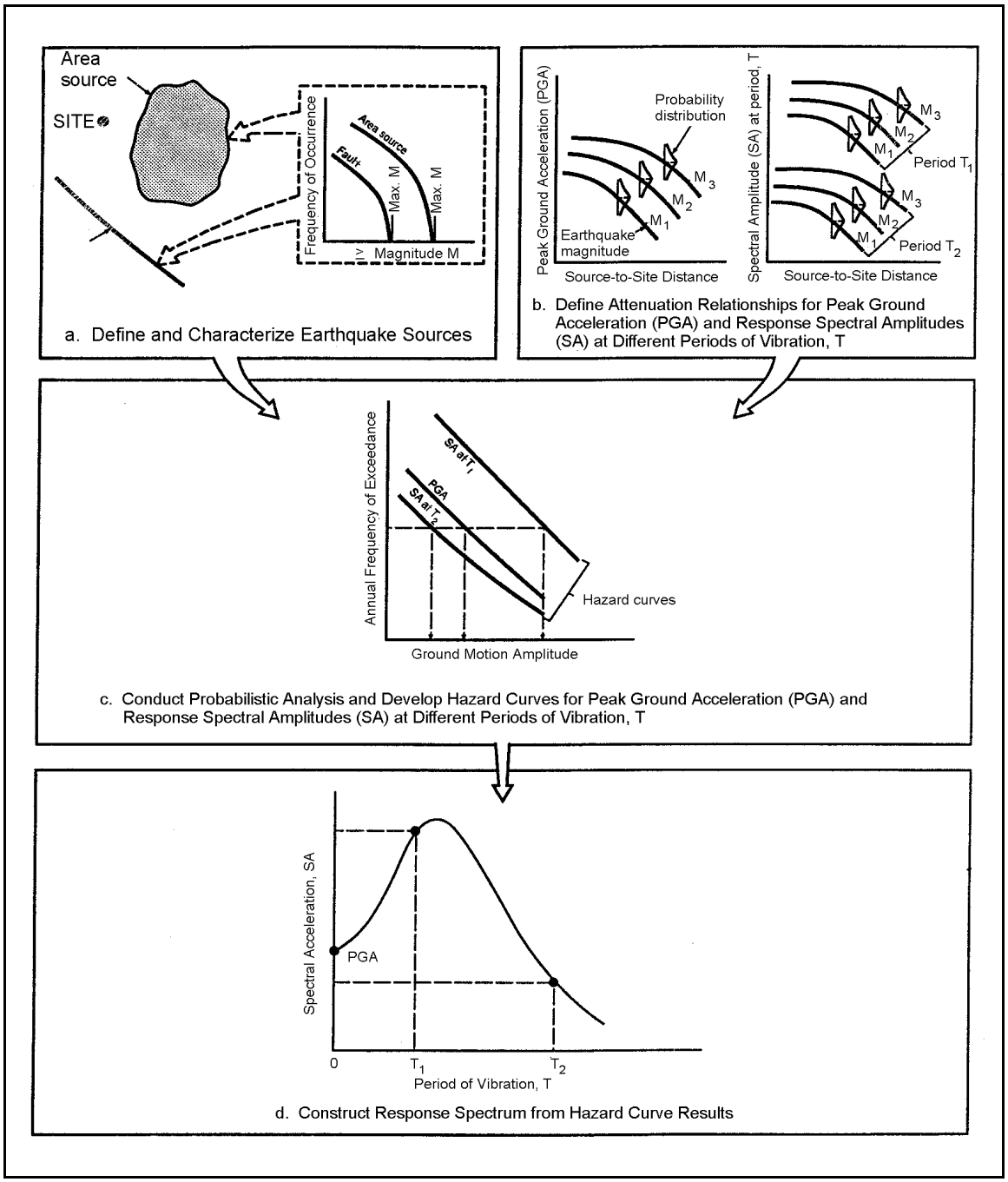

Figure 3-22. Development of equal-hazard response spectrum from probabilistic seismic hazard analysis for response spectral values

Thus, for a given source, the annual frequency or rate of exceeding a certain ground motion level at the site is obtained by summing over all magnitudes and source-to-site distances for that source. Then, the total rate of ground motion exceedance at the site ν_z is obtained by adding the rates for all the sources. The components of Equation 3-2 are discussed in (2), (3), and (4) below. A simplified example of a PSHA illustrating the calculation process using Equation 3-2 is presented in Appendix G (Example G-1).

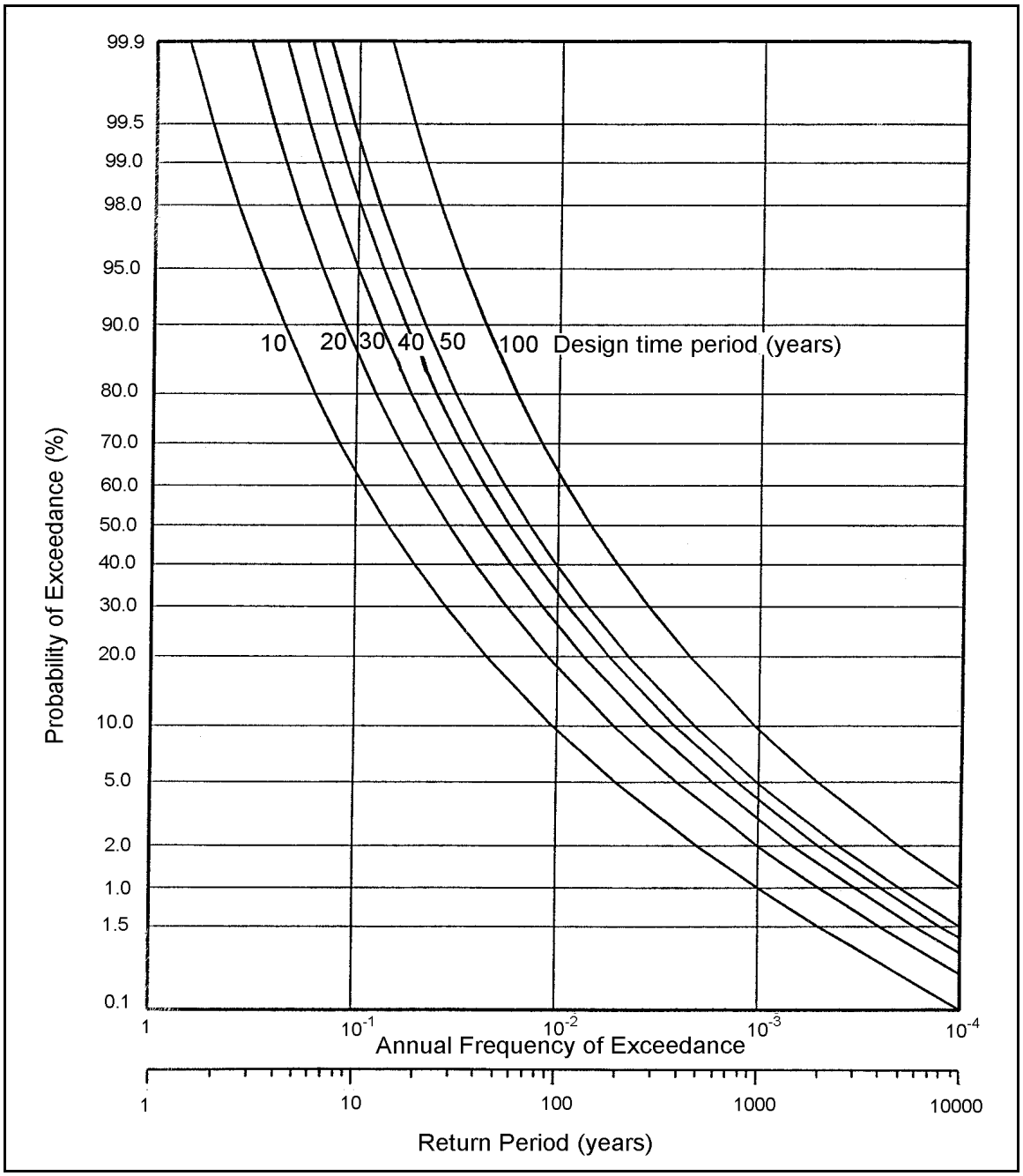

Figure 3-23. Relationship between annual frequency of exceedance/return period and probability of exceedance for different design time periods

(2) Rate of occurrence of earthquakes. The rate of occurrence of earthquakes $\lambda(m_i)$ is obtained based on earthquake recurrence assessments. Typical earthquake recurrence curves for earthquake sources are illustrated in the upper part of Figure 3-24. As shown, recurrence curves express the rate of occurrence of earthquakes equal to or greater than a certain magnitude. $\lambda(m_i)$ is obtained by discretizing the recurrence curves into narrow magnitude intervals as illustrated in the lower part of Figure 3-24. The two different types of magnitude distributions shown in Figure 3-24, exponential and characteristic, are discussed in paragraph 3-9(d).

Table 3-4
Relationship Between Return Period and Probability of Exceedance for Different Time Periods

	Return Period, Years, for Different Design Time Periods *t*					
Probability of Exceedance, %	***t* = 10 years**	***t* = 20 years**	***t* = 30 years**	***t* = 40 years**	***t* = 50 years**	***t* = 100 years**
1	995	1,990	2,985	3,980	4,975	9,950
2	495	990	1,485	1,980	2,475	4,950
5	195	390	585	780	975	1,950
10	95	190	285	380	475	950
20	45	90	135	180	225	450
30	28	56	84	112	140	280
40	20	39	59	78	98	195
50	14	29	43	58	72	145
60	11	22	33	44	55	110
70	8.3	17	25	33	42	83
80	6.2	12	19	25	31	62
90	4.3	8.7	13	17	22	43
95	3.3	6.7	10	13	17	33
99	2.2	4.3	6.5	8.7	11	22
99.5	1.9	3.8	5.7	7.5	9.4	19

(3) Distance probability distribution. The distance probability distribution, $P(R=r_j \mid m_i)$, depends on the geometry of earthquake sources and their distance from the site; an assumption is usually made that earthquakes occur with equal likelihood on different parts of a source. The function $P(R=r_j \mid m_i)$ also should incorporate the magnitude-dependence of earthquake rupture size; larger magnitude earthquakes have larger rupture areas, and thus have higher probability of releasing energy closer to a site than smaller magnitude earthquakes on the same source. An example of probability distributions for the closest distance to an earthquake source is shown in Figure 3-25. In this particular example, the source (fault) is characterized as a line source, and the probability distributions are based on the formulations presented by Der Kiureghian and Ang (1977). Figure 3-25a illustrates the probability distributions for a fault rupture length of 5 km; Figure 3-25b illustrates the probability distributions for a fault rupture length of 25 km. The longer rupture length corresponds to a larger magnitude. The figure shows the distributions for both the probability of the closest distance to the fault rupture R being less than a certain value $P(R<r_j \mid m_i)$, and the probability of earthquakes occurring at a certain distance ($P(R=r_j \mid m_i)$, which is obtained by discretizing the curves for $P(R<r_j \mid m_i)$. The higher probability for earthquakes to occur at closer distances for longer rupture lengths (larger magnitudes) can be noted by comparing Figure 3-25b with 3-25a. It can also be observed in Figure 3-25 that there is zero probability of earthquake occurrence either closer than the closest distance to the earthquake source (10 km in the example) or farther than the closest distance to the rupture placed at the farthest end of the fault (farther than a distance of approximately 61 km $[10^2 + (65 - 5)^2]^{½}$ for a 5-km rupture and a distance of approximately 41 km $[10^2 + (65 - 25)^2]^{½}$ in the case of the 25-km rupture length). The probability abruptly changes at a closest distance equal to the distance defined by placing the fault rupture at the nearest end of the fault (distance of approximately 32 km $[10^2 + (35 - 5)^2]^{½}$ for a 5-km rupture and a distance of approximately 14 km $[10^2 + (35 - 25)^2]^{½}$ for a 25-km rupture). Note that the distance to the earthquake rupture must be

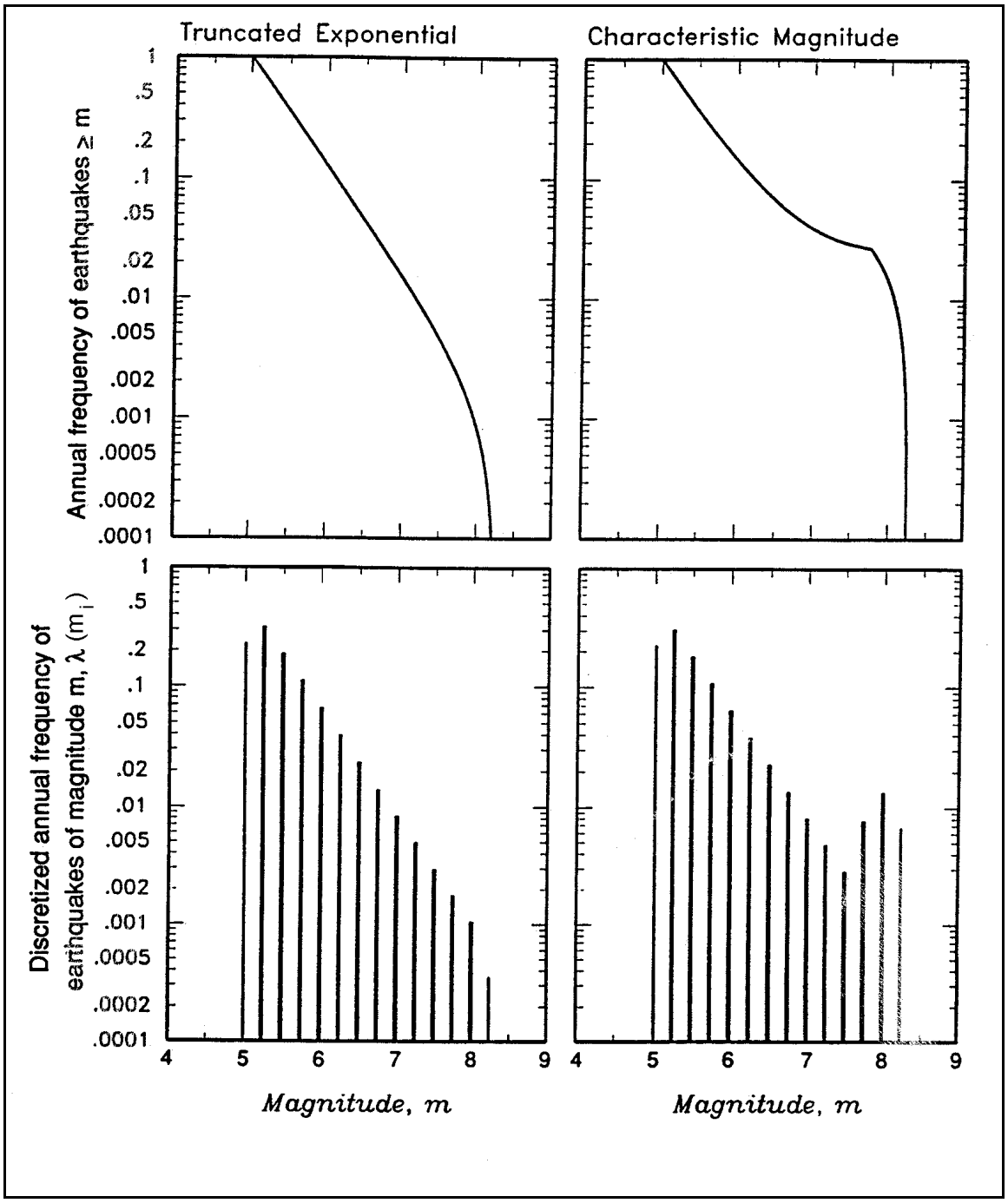

Figure 3-24. Typical earthquake recurrence curves and discretized occurrence rates

expressed in terms of the same definition of distance as used in the ground motion attenuation relationships. Typically, some form of closest distance to rupture definition is used for attenuation relationships (variations in this definition include closest distance to rupture, closest distance to rupture of the seismogenic zone, closest horizontal distance to surface projection of rupture, etc.).

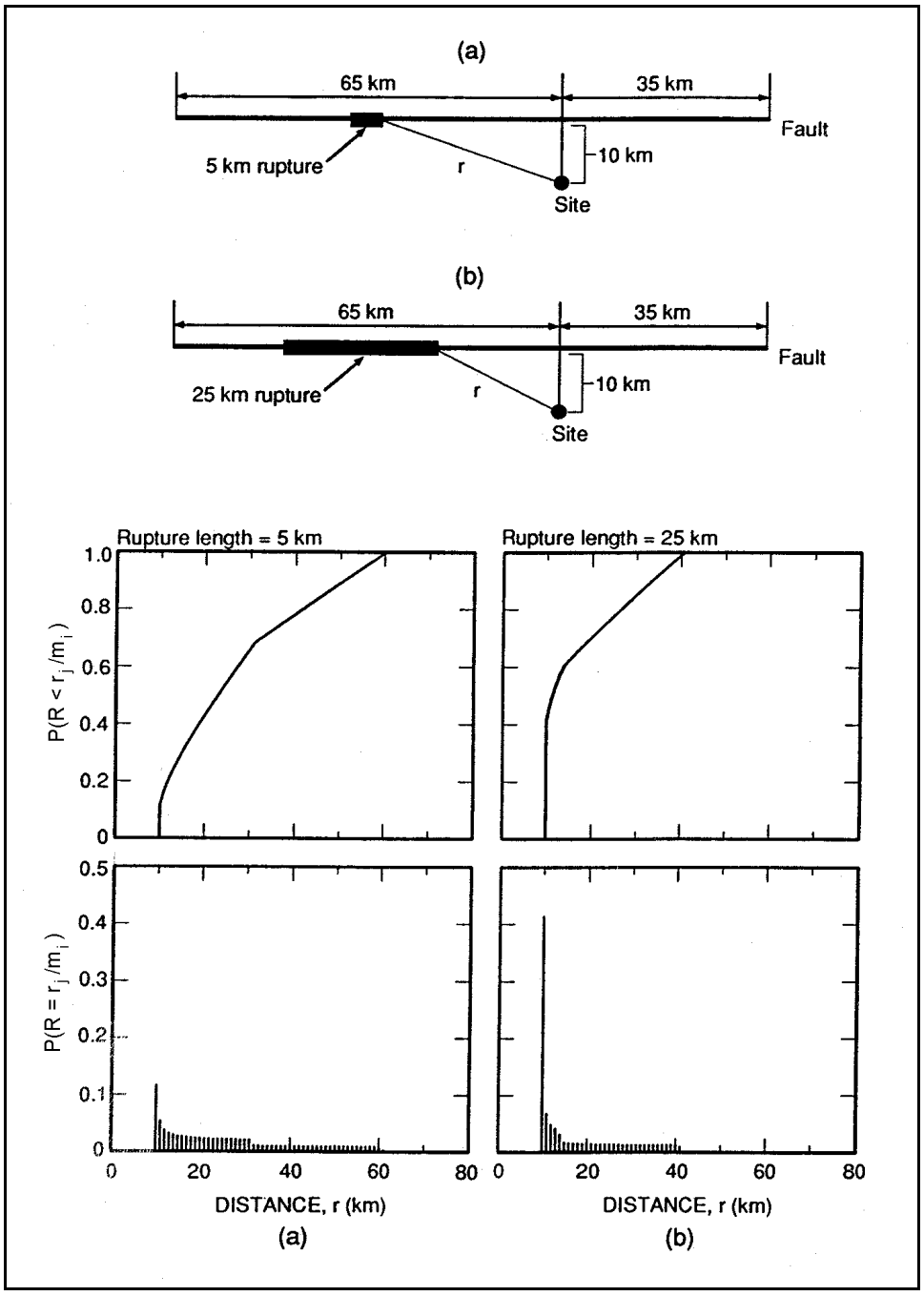

Figure 3-25. Illustration of distance probability distribution

(4) Conditional probability of ground motion exceedance. The conditional probability of exceeding a ground motion level for a certain earthquake magnitude and distance $P(Z>z|m,r)$ is determined from the ground motion attenuation relationships selected for the site. (Available relationships are discussed in Section II.) These relationships incorporate the uncertainty in ground motion estimation given m and r (see Figures 3-21 and 3-22). The function $P(Z>z|m,r)$ is usually evaluated assuming that ground motion values are log normally distributed about the median value; the calculation of this function is illustrated in Figure 3-26.

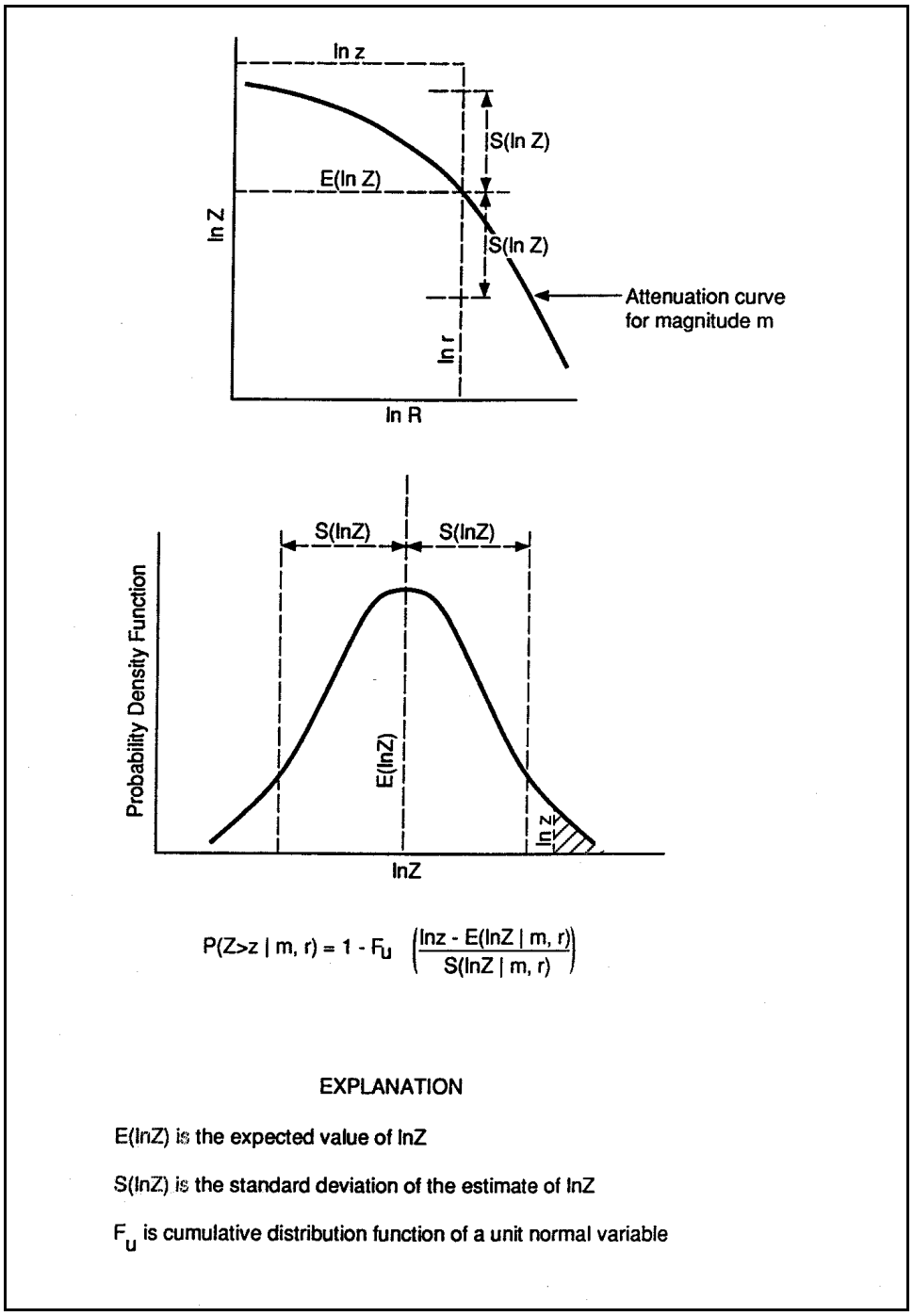

Figure 3-26. Ground motion estimation conditional probability function

3-9. Characterizing Seismic Sources for PSHA

Although the following discussion is oriented toward probabilistic approaches for characterizing seismic sources, much of the discussion is applicable to deterministic approaches as well.

a. Source identification.

(1) Seismic source. A seismic source represents a region of the earth's crust where the characteristics of earthquake activity are recognized to be different from those of the adjacent crust. Seismic sources are identified on the basis of geological, seismological, and geophysical data. An understanding of the regional tectonics, local Quaternary geologic history, and seismicity of an area leads to the identification of seismic sources. The development of tectonic models for crustal deformation and the assessment of the tectonic role of individual geologic structures are useful for both identifying potential sources and assessing their characteristics. Geologic studies can be used to assess the location, timing, and style of crustal deformation. The association of geologic structures with historic or instrumental seismicity may clarify their role within the present tectonic stress regime. Characteristics of seismicity, including epicenter locations, focal depths, and source mechanisms, also aid in identifying potential sources.

(2) Faults. Because earthquakes occur as a result of differential slip on faults, modeling of seismic sources as individual faults is the most physically realistic model for seismic hazard analysis. Under favorable conditions, individual faults can be identified and treated as distinct seismic sources. Active faults are usually identified on the basis of geomorphic expression and stratigraphic displacements but can also be identified by lineations of seismicity, by geophysical measurements, or by inference from detailed investigations of related geologic structures, such as active folding or crustal plate subduction. A fault model for individual sources allows the use of geologic data on fault behavior, as well as seismicity data, to characterize earthquake activity.

(3) Seismic source zones. In areas with low rates of crustal deformation away from plate margins, such as the EUS, seismic sources are often defined as seismic source zones. Seismic source zones are used to model the occurrence of seismicity in areas where specific faults cannot be identified and where the observed seismicity exhibits a diffuse pattern not clearly associated with individual faults. These conditions are typical of areas with lower rates of crustal deformation, such as regions away from plate margins (e.g., EUS). Seismic source zones can be defined based either on historical seismicity patterns or geology and tectonics. When defined based on historical seismicity patterns, a large region can be subdivided into small regular areas that are treated as individual source zones (Electric Power Research Institute (EPRI) 1987; U.S. Geological Survey (USGS) 1996). With this approach, it is assumed that the spatial variation in the occurrence rate of future earthquakes is similar to the historical pattern of seismicity. Due to the relatively short historical period and low rates of seismicity, the seismicity patterns are usually determined by small earthquakes. It is not clear whether this pattern reflects the likelihood of future earthquakes of engineering significance (generally taken to be earthquakes of magnitude approximately equal to or greater than 5). The alternative approach is to define areas thought to have homogeneous earthquake potential characteristics (in terms of rate of earthquake occurrence and maximum earthquake size) on the basis of the geology and tectonics of the region. For example, recent evidence from studies of global earthquakes in stable continental regions such as the EUS has shown that most larger earthquakes occur through reactivation of faults in geologically ancient rift zones (Johnston et al. 1994). Where available, paleoseismological data (e.g., spatial and temporal distribution of liquefaction features) should be used to identify source regions for large-magnitude earthquakes. Because of uncertainty regarding the most appropriate model for earthquake occurrence, both seismicity-based and geologically based seismic source zones should be included in a probabilistic analysis.

b. Source geometry.

(1) General. Description of the geometry of a seismic source is necessary to evaluate the distances from the site at which future earthquakes could occur. In addition, source geometry can place physical constraints on the maximum size earthquake that can occur on a source.

(2) Faults. Seismic sources defined as faults are modeled in a PSHA as segmented linear or planar features. Earthquake ruptures on fault sources are modeled as rupture lengths or rupture areas, with the size of rupture defined on the basis of empirical relationships between earthquake magnitude and rupture size (Wyss 1979; Wells and Coppersmith 1993).

(3) Seismic source zones. For seismic sources defined as geologic structures suspected to contain faults, the distribution of earthquakes can be modeled as rupture surfaces occurring on multiple fault planes distributed throughout the source volume if the general trend of such planes is known or can be inferred. Alternatively, earthquake locations can be modeled as random point sources within the source volume if the orientation of potential fault planes is unknown. The spatial distribution of seismicity within large areal sources can be modeled similarly.

c. Maximum earthquake magnitude.

(1) Faults. The limiting size earthquake that can occur on each seismic source is an important parameter, especially in evaluating seismic hazard at low probability levels. The maximum magnitude can most easily be estimated when the seismic source is defined on the basis of an identifiable fault. For faults, the maximum earthquake magnitude is related to fault geometry and fault behavior through an assessment of the maximum dimensions of a single rupture. Evaluation of fault segmentation can play a key role in identifying portions of a fault zone likely to represent the largest size of a single rupture (Schwartz and Coppersmith 1986; Schwartz 1988). The maximum magnitude is related to the maximum rupture size through empirical relationships (Slemmons 1982; Bonilla, Mark, and Lienkaemper 1984; Wells and Coppersmith 1994). Because these relationships are subject to uncertainty, the use of a number of magnitude estimation techniques can result in more reliable estimates of maximum magnitude than the application of a single relationship.

(2) Seismic source zones. The assessment of maximum magnitude is more difficult when seismic sources are defined on the basis of large-scale tectonic features or crustal blocks, as is typically done in the EUS. In such cases the maximum magnitude is often estimated to be the maximum historical earthquake magnitude plus an increment, or is estimated to be a magnitude having a specified return period. The chief weakness of these approaches is the generally short period of historical observations compared with the likely return period of a maximum event for an individual source. Another approach that attempts to extend the generally short observational period for individual sources is based in augmenting the assessment using data from analogous structures worldwide. This approach identifies analogous features for which the maximum magnitude is better defined or identifies the largest event that has occurred on such features. In the application of analogies, the seismicity of similar structures on a worldwide basis can be examined to supplement the limited local historical record. Recent efforts have been made to use a global earthquake database to identify the factors that control or limit the maximum size of earthquakes within stable continental regions like the EUS to develop a formal method for estimating maximum magnitude in such regions (Johnston et al. 1994)

d. Rate of earthquake occurrence and distribution in earthquake size.

(1) Estimating recurrence rates. Earthquake recurrence rates are estimated from historical seismicity, from geological data on rates of fault movement, and from paleoseismic data on the timing of large prehistoric events. For areal sources, historical seismicity is usually used to estimate earthquake recurrence rates. When recurrence for small, regular source zones (cells) is analyzed (*a*(3) above), procedures can be employed to smooth seismicity rates among adjoining cells (EPRI 1987; USGS 1996). In an analysis of the earthquake catalog of historical seismicity, it is important to translate the data into a common magnitude scale consistent with the magnitude scale used in the ground motion attenuation

relationships, and to account for completeness in earthquake reporting as a function of time and location. Straightforward statistical techniques can then be used to estimate earthquake recurrence parameters (Weichert 1980).

(2) Use of geologic data for faults. For sources defined as individual faults, the available historical seismicity is usually insufficient to characterize the earthquake recurrence. Geologic data on fault slip rates can be used to estimate the rate of seismic moment release, leading to the rate of earthquake recurrence. In addition, paleoseismic studies of the occurrence of large prehistoric events can be used to estimate recurrence of larger magnitude earthquakes on a fault. Predictions of recurrence rates for larger events from fault-specific geologic data have been shown to match well with observed historical rates on a regional basis (Youngs and Coppersmith 1985b; Youngs, Swan, and Power 1988; Youngs et al. 1987; Youngs et al. 1993b). The rate of earthquake occurrence may not be uniform along the strike or dip of an earthquake fault. Evaluation of fault segmentation can be used to characterize variations in recurrence along the length of a fault. The depth distribution of historical seismicity can be used to specify down-dip variations in recurrence.

(3) Recurrence models. The relative frequency of various size earthquakes has usually been specified by the truncated exponential recurrence model (Cornell and Van Marke 1969) based on Gutenberg and Richter's (1954) recurrence law. This model was developed on the basis of observations of global seismicity. It has been found to work well on a regional basis and for modeling seismicity for nonfault specific sources such as distributed seismicity zones and generalized tectonic structures. Recent advances in understanding of the earthquake generation process have indicated that earthquake recurrence on individual faults may not conform to the exponential model. Instead, individual faults or fault segments may tend to rupture in what have been termed “characteristic” magnitude events at or near the maximum magnitude (Schwartz and Coppersmith 1984). This has led to the development of fault-specific recurrence models such as the maximum moment model (Wesnousky et al. 1983) and the characteristic magnitude recurrence model (Youngs and Coppersmith 1985a, 1985b). Figure 3-27 illustrates a characteristic magnitude recurrence model. Figure 3-28 compares exponential and characteristic earthquake recurrence relationships. The figure illustrates the differences between the two recurrence models depending on how the earthquake recurrence rate is specified. Figure 3-28a shows recurrence curves if the total rate of seismic moment release is specified to be the same for each model; Figure 3-28b shows recurrence curves if the rate of large-magnitude earthquakes is specified to be the same for each model. Detailed studies of earthquake recurrence in the Wasatch fault region, Utah, and in the San Francisco Bay region have shown excellent matches between regional seismicity rates and recurrence modeling when combining the characteristic recurrence model for individual faults with the exponential model for distributed source areas (Youngs et al. 1987; Youngs, Swan, and Power 1988; Youngs et al. 1993b).

(4) Poisson versus real-time recurrence. Nearly all PSHA's assume that earthquake occurrence in time is a random and memoryless (Poisson) process. In the Poisson process, it is assumed that the probability of an event in a specified period is completely determined by the average frequency of occurrence of events, and the probability of occurrence of the next event is independent of when the last event occurred. While the observed seismicity data on a regional basis have been shown to be consistent with the Poisson model, the model does not conform to the physical process believed to result in earthquakes, one of a gradual, relatively uniform rate of strain accumulation followed by sudden release. Detailed paleoseismic studies of several faults as well as historical seismicity from very active subduction zones have indicated that the occurrence of the larger events on a source tends to be more cyclic in nature. These observations have led to the use of nonstationary or “real-time” recurrence models that predict the probability of events in the next period, rather than any period. Typically, a

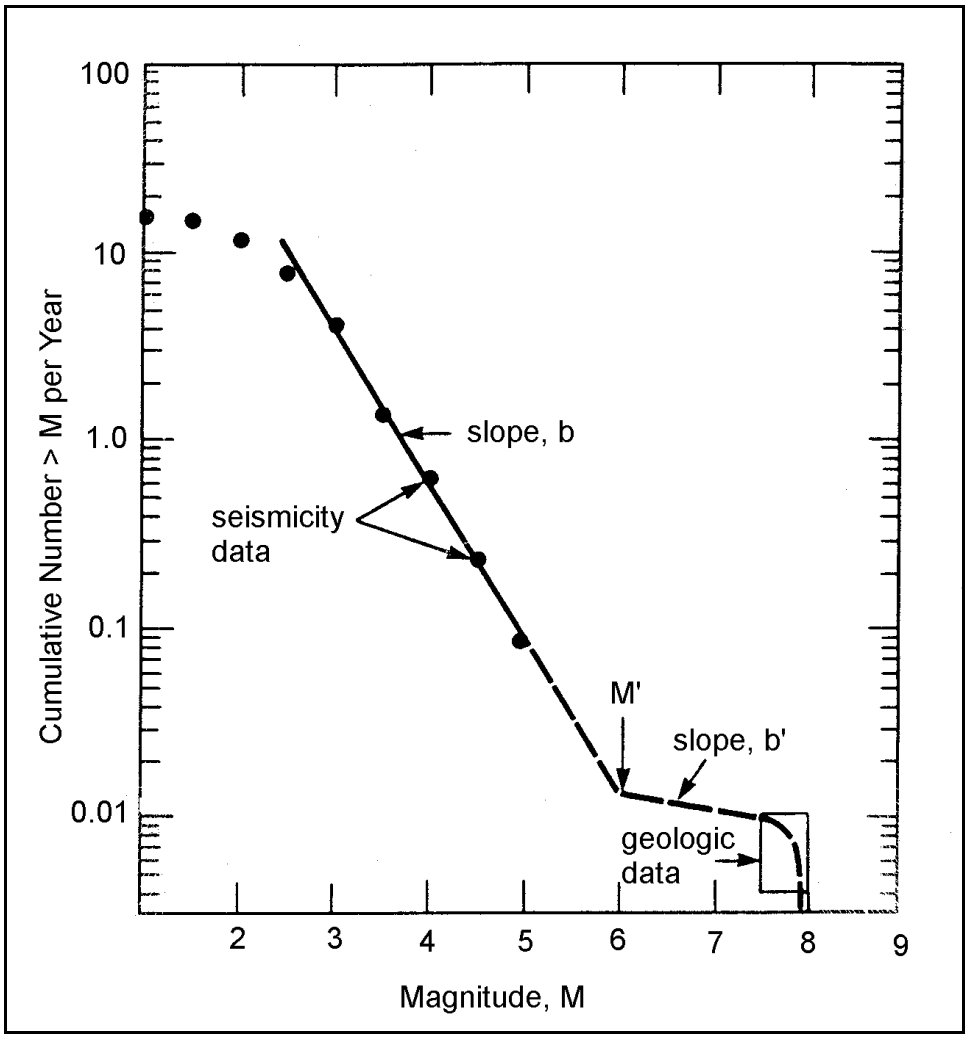

Figure 3-27. Diagrammatic characteristic earthquake recurrence relationship for an individual fault or fault segment. Above magnitude *M*' a low *b* value (*b*') is required to reconcile the small-magnitude recurrence with geologic recurrence, which is represented by the box (Schwartz and Coppersmith 1984; National Research Council 1988)

simple "renewal model" is used to evaluate the likelihood of events within specified future periods. A recent example of the use of a renewal model was a study of the probabilities of large earthquakes on the San Andreas fault system in northern California for use in regional planning (Working Group on California Earthquake Probabilities 1990). Consideration may be given to such time-dependent models in the few cases where there is sufficient information to develop the required parameters.

3-10. Ground Motion Attenuation Characterization for PSHA

Specification of ground motions for PSHA is subject to all of the requirements discussed in Section II for deterministic ground motion assessments. The analysis requires ground motion attenuation relationships for the full range of magnitudes and distances considered. Recently developed attenuation relationships for peak ground acceleration and response spectral values of ground motion are listed in Tables 3-1 and 3-3, respectively. The uncertainties in the level of a ground motion parameter given a certain

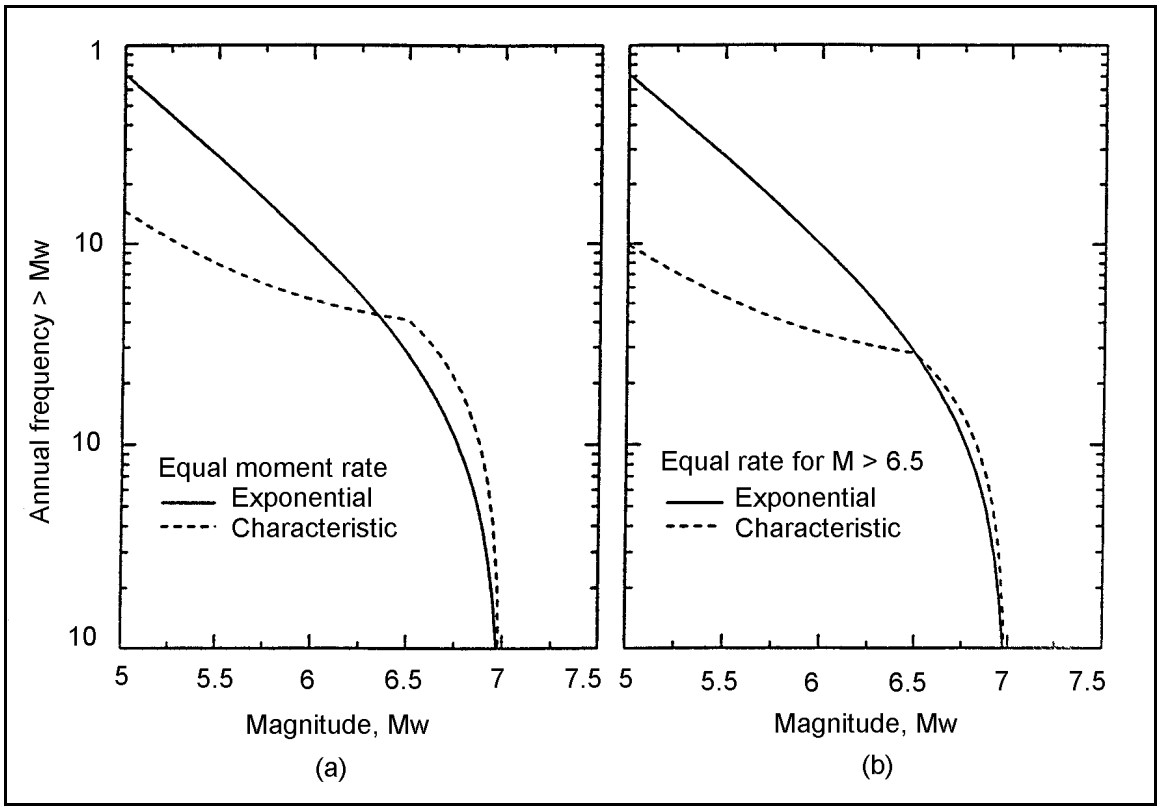

Figure 3-28. Comparison of truncated exponential and characteristic earthquake recurrence relationships

earthquake magnitude and distance (modeled by the probability distribution for the attenuation relationship (Figure 3-26)) are of considerable importance in influencing the results of a PSHA and should be included in the analysis.

3-11. Treatment of Scientific Uncertainty in PSHA

The basic probability formulations in Equations 3-1 and 3-2 incorporate the randomness of the physical process of earthquake generation and seismic wave propagation. Although these formulations incorporate the inherent uncertainty due to randomness, they do not incorporate additional sources of uncertainty that may be associated with the choice of particular models or model parameters. For example, there could be uncertainty about which ground motion attenuation relationship is most applicable to a site, whether an exponential or characteristic earthquake recurrence model is most applicable, the most appropriate model for seismic source zones, the geometry of earthquake sources, the values of maximum earthquake magnitude, or earthquake recurrence parameters. In a deterministic analysis, these uncertainties, which are termed scientific or epistemic uncertainties, are usually treated by applying conservatism in selecting design earthquakes and estimating ground motions. In PSHA, these uncertainties can be directly modeled within the analysis framework to provide an assessment of the uncertainty in the result. The technique of “logic trees” has been widely used to incorporate scientific uncertainty in a PSHA (Kulkarni, Youngs, and Coppersmith 1984; Youngs et al. 1985; Coppersmith and Youngs 1986; National Research Council 1988). Figure 3-29 shows an example of a logic tree used in a PSHA. Although only a few branches of the logic tree are shown, there may be many thousands of branches in the tree. Each path through the tree to an end branch (on the right side of Figure 3-29)

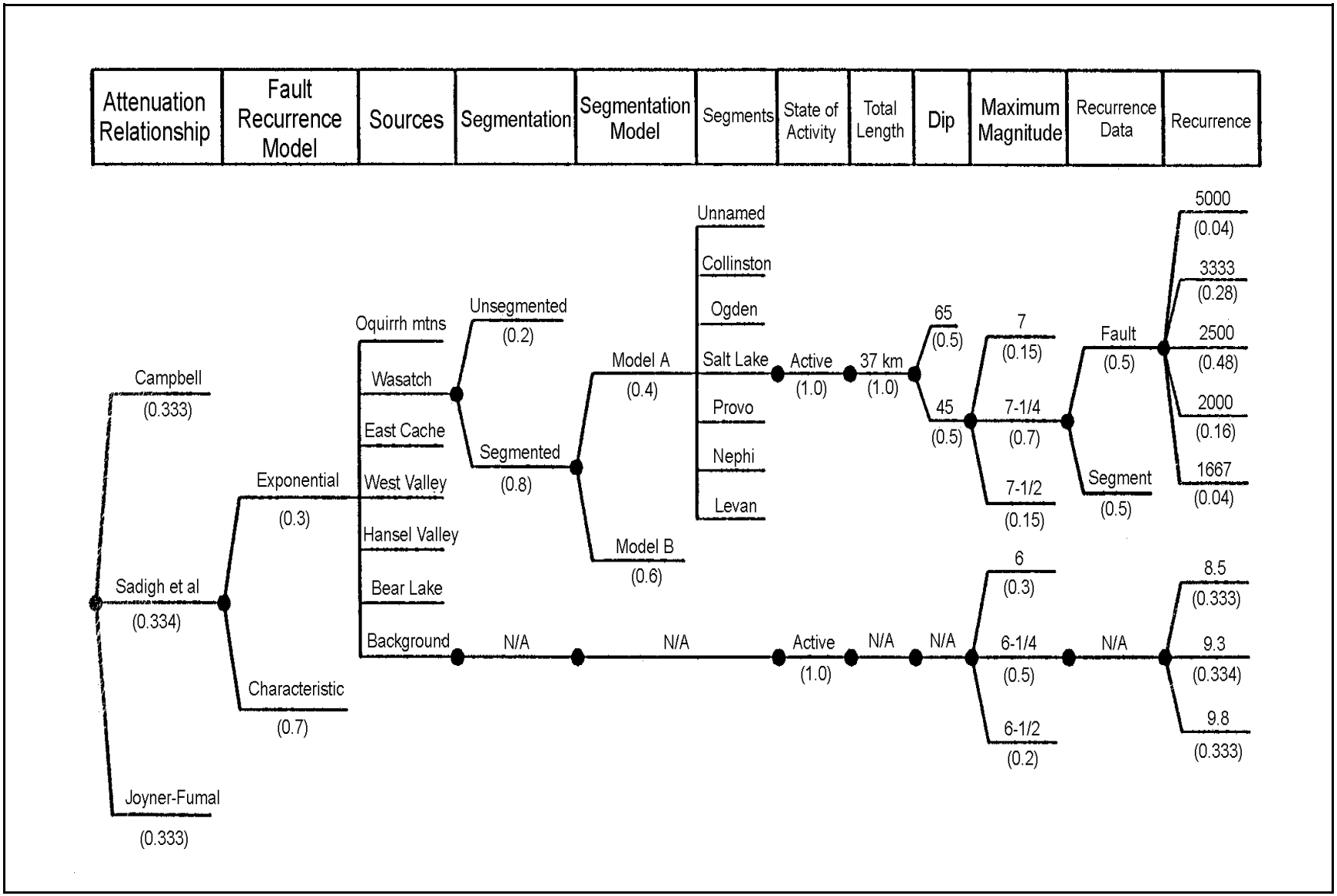

Figure 3-29. Example of logic tree for characterizing uncertainty in seismic hazard input (Youngs, Swan, and Power 1988, reprinted by permission of ASCE)

defines a set of parameters that are used to conduct a basic seismic hazard analysis for that path and end branch using Equation 3-2. Basic hazard analyses are carried out for each path. Each path also has an associated probability or weight that is determined by the product of the relative probabilities or weights assigned to the various models and parameters along the path. (The relative probabilities or weights of the alternative models and parameters are illustrated by the numbers in parentheses in Figure 3-29.) The relative probabilities or weights assigned to alternative models or parameter values are often assigned subjectively, on the basis of the preponderance of scientific evidence or judgment. The sensitivity of the PSHA to changes in the weights can be tested. For some parameters, such as earthquake recurrence based on observed seismicity, the relative weights assigned to different recurrence rates and b-values can be derived from statistical analysis of the seismicity data. The basic hazard analysis results for all the paths in the logic tree are combined using the associated weights to arrive at best estimates (mean or median values) for the frequencies of exceedance of ground motions as well as uncertainty bands for the estimates. Through the approach of incorporating scientific uncertainty, PSHA incorporates the alternative hypotheses and data interpretations that may significantly affect the computed results. The use of logic trees in PSHA, including the mathematical formulation, is discussed in more detail in Appendix F. A simplified example of a PSHA illustrating the calculation process using logic trees is presented in Appendix G (Example G-1).

3-12. Development of Site-Specific Response Spectra from PSHA

The approaches that can be followed in specifying site-specific spectra on the basis of a probabilistic seismic hazard analysis mirror those outlined in Section II for deterministic analyses and involve either anchoring a spectral shape to a peak acceleration level determined from a PSHA for peak acceleration (Figure 3-21) or estimating the entire spectrum on the basis of PSHA for response spectral values at a number of periods of vibration (i.e., developing an equal-hazard spectrum, Figure 3-22). For soil sites, the ground motions can be obtained either by conducting the PSHA using attenuation relationships for soil sites or by conducting the PSHA for rock site conditions and then using site response analyses to evaluate the effects of the site soil column on the ground motions.

a. Approach 1 - Anchoring spectral shape to peak ground acceleration determined from PSHA. In this approach a probabilistic seismic hazard analysis is conducted to establish the relationship between peak ground acceleration and frequency of exceedance. The design peak acceleration level is specified by selecting an appropriate frequency, return period, or probability level. For example, Figure 3-20 shows a typical result of a PSHA for peak ground acceleration. If the exceedance frequency is taken to be 0.001 (return period of 1,000 years), then the corresponding peak acceleration level would be approximately 0.5 g for the example in Figure 3-20. A site-specific spectrum could then be constructed by anchoring an appropriate spectral shape to this acceleration level. As discussed in Section II, it is desirable to select a spectral shape appropriate for the earthquake size and distance producing the hazard as well as the local subsurface conditions. Consideration of earthquake size and distance is less straightforward in a PSHA than in a deterministic analysis because the hazard is the result of the possible occurrences of many different earthquakes of varying sizes and distances from the site. Thus, the hazard analysis results must be examined to identify the major contributors to the hazard at the ground motion level of interest. As an example, Figure 3-30 shows the relative contribution of earthquakes of various magnitudes and distances from three different return periods. As indicated in the figure, the major contribution to seismic hazard shifts to larger magnitudes and closer distances as the return period increases. The example also indicates that a wide range of magnitudes can contribute to the hazard at a selected probability level. This suggests that more than one spectral shape may be appropriate in particular circumstances to address the different types of events that may affect the site.

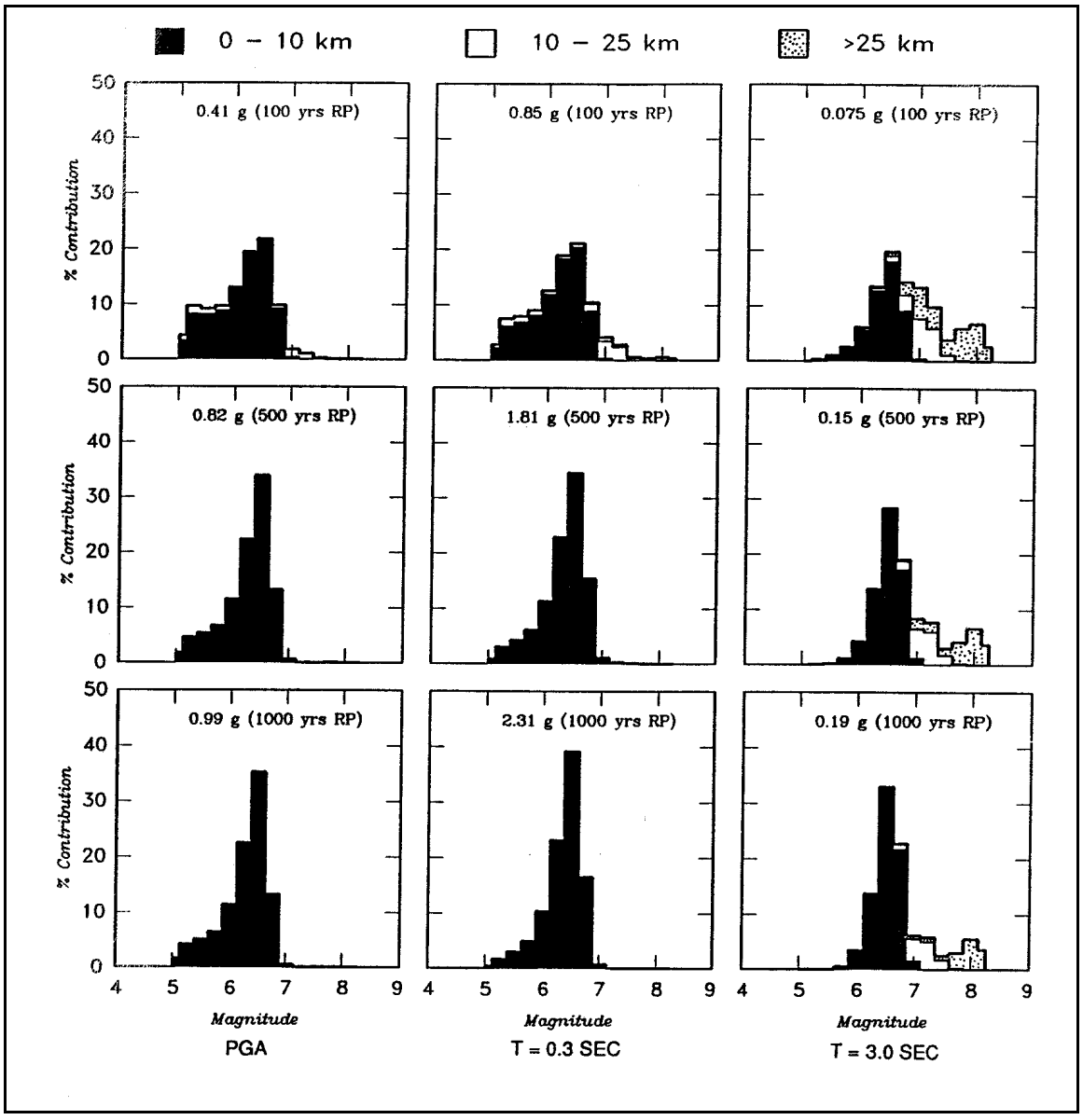

Figure 3-30. Example of contributions of events in various magnitude and distance intervals to mean hazard for peak acceleration and 5 percent damped spectral acceleration at periods of 0.3 and 3 sec

b. Approach 2 - Development of equal-hazard spectra. In this approach, PSHA's are conducted for response spectral values covering the range of vibrational periods of interest for the project. Figure 3-31a shows the results of PSHA's for peak ground acceleration and for 5 percent-damped spectral ordinates at seven selected periods of vibration for the example site used in Figure 3-20. When the appropriate exceedance frequency or return period to use for design is specified, spectral ordinates are read off each hazard curve and are plotted against frequency as shown in Figure 3-31b. (Note that peak ground acceleration is equal to zero-period response spectral acceleration, which, in this example, is equal to response spectral acceleration at 0.03-sec period.) A smooth spectral shape is then drawn through these points to construct the equal-hazard spectrum, a spectrum that has the same probability of exceedance at each frequency. As was the case for the peak ground acceleration hazard results, the

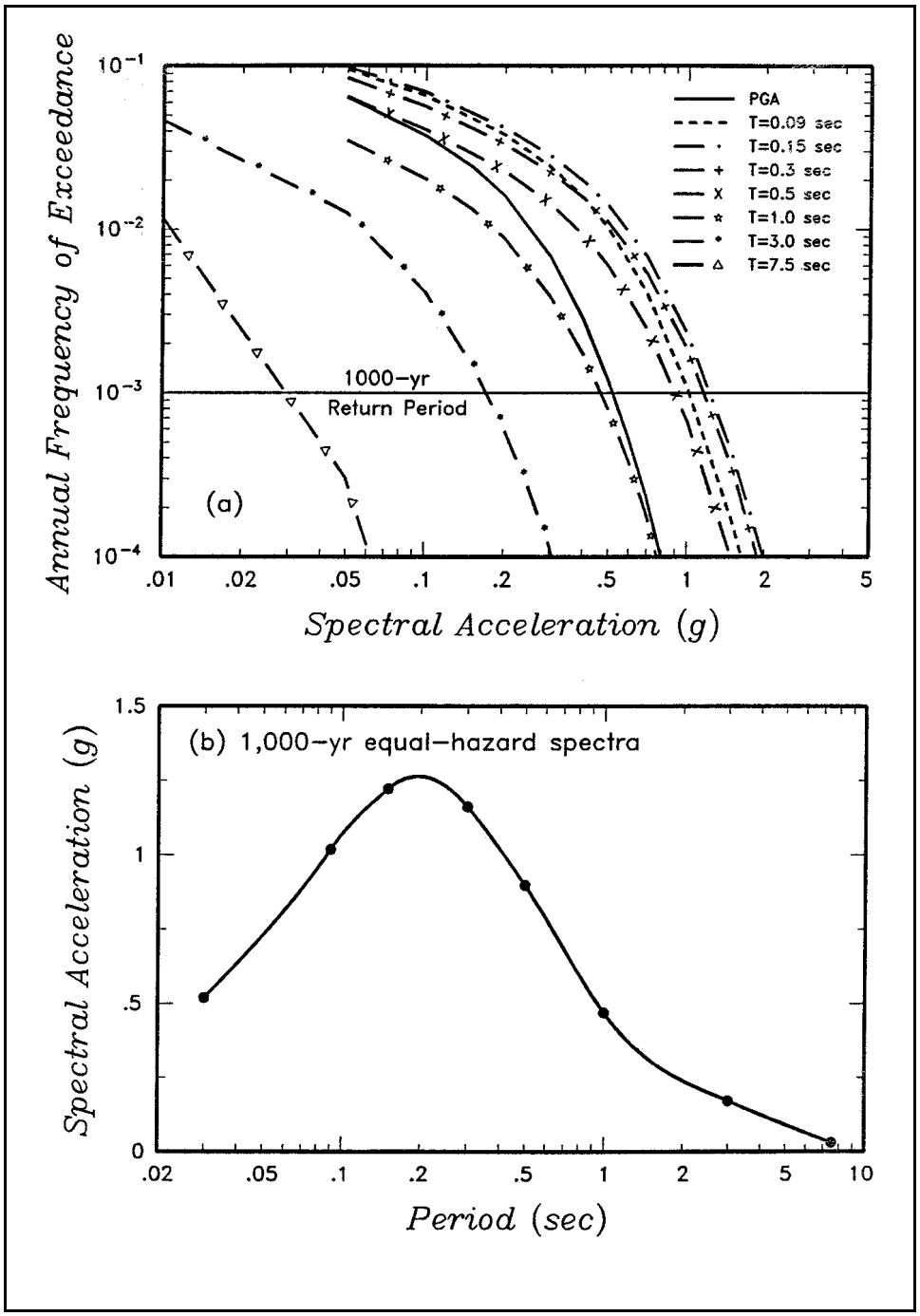

Figure 3-31. Construction of equal-hazard spectra. Top plot (a) shows hazard curves for a range of spectral periods. Bottom plot (b) shows equal hazard spectrum for a period of 1,000 years

equal-hazard spectrum is the result of many possible earthquakes of different sizes and locations. This is illustrated in Figure 3-30, which shows the relative contributions of different magnitude earthquakes to the hazard as a function of return period for spectral values at two periods of vibration as well as for peak ground acceleration. As can be seen, for the same probability of exceedance, the contributions shift to larger magnitudes as the spectral period of vibration increases. This is because the ground motion attenuation relationships are more strongly a function of magnitude at long periods than short periods of vibration.

c. Preferred approach. Approach 2 is recommended over Approach 1 because it is not straightforward to select appropriate spectral shapes in Approach 1. It will be feasible to develop an equal-hazard response spectra from a PSHA using Approach 2. Response spectral value attenuation relationships are available for both the EUS and WUS (Section II and Table 3-3) that are as reliable as those developed for peak ground acceleration. The computation of equal-hazard spectra using these spectral attenuation relationships directly accounts for the changes in contributions to the hazard from different magnitudes and source-to-site distances. The use of equal-hazard spectra also accounts for the change in spectral shape with change in return period or probability level, as is illustrated in Figure 3-32 showing an example of equal-hazard response spectral shapes for three probability levels. These are compared in the figure to a standard spectral shape for a similar site condition.

3-13. Development of Accelerograms

Appropriate accelerograms for use with probabilistically based response spectra can be developed using the same two methods described in Section II for deterministic analyses. The additional step required for probabilistically based response spectra is identification of the appropriate magnitude and distance range from which candidate accelerograms may be selected. This information is obtained by deaggregation of the composite hazard to identify the contributions of various magnitudes and distances, as illustrated in Figure 3-30. Suites of natural accelerograms representing the range of events with major contributions to the hazard may be selected and scaled to approximately correspond to the level of the equal-hazard spectrum. Alternatively, synthetically modified accelerograms can be generated to provide a close match to the equal-hazard spectrum (paragraph 3-6c).

3-14. Summary of Strengths and Limitations of DSHA and PSHA

a. DSHA.

(1) Strengths.

(a) The concept of the design maximum earthquake (MCE) is straightforward and readily understood by the engineer. The MCE represents an estimate of the maximum earthquake size on a source and is located a defined distance from the site.

(b) Provided an appropriate degree of conservatism is incorporated in defining the earthquake magnitude, source-to-site distance, and resulting site ground motions, design for the MCE should provide an appropriately high level of safety.

(2) Limitations.

(a) The frequency of earthquakes and resulting ground motions is not explicitly considered. As a result, a deterministic estimate for a maximum earthquake will have a lower probability of being exceeded in a low-seismicity environment than in a high-seismicity environment.

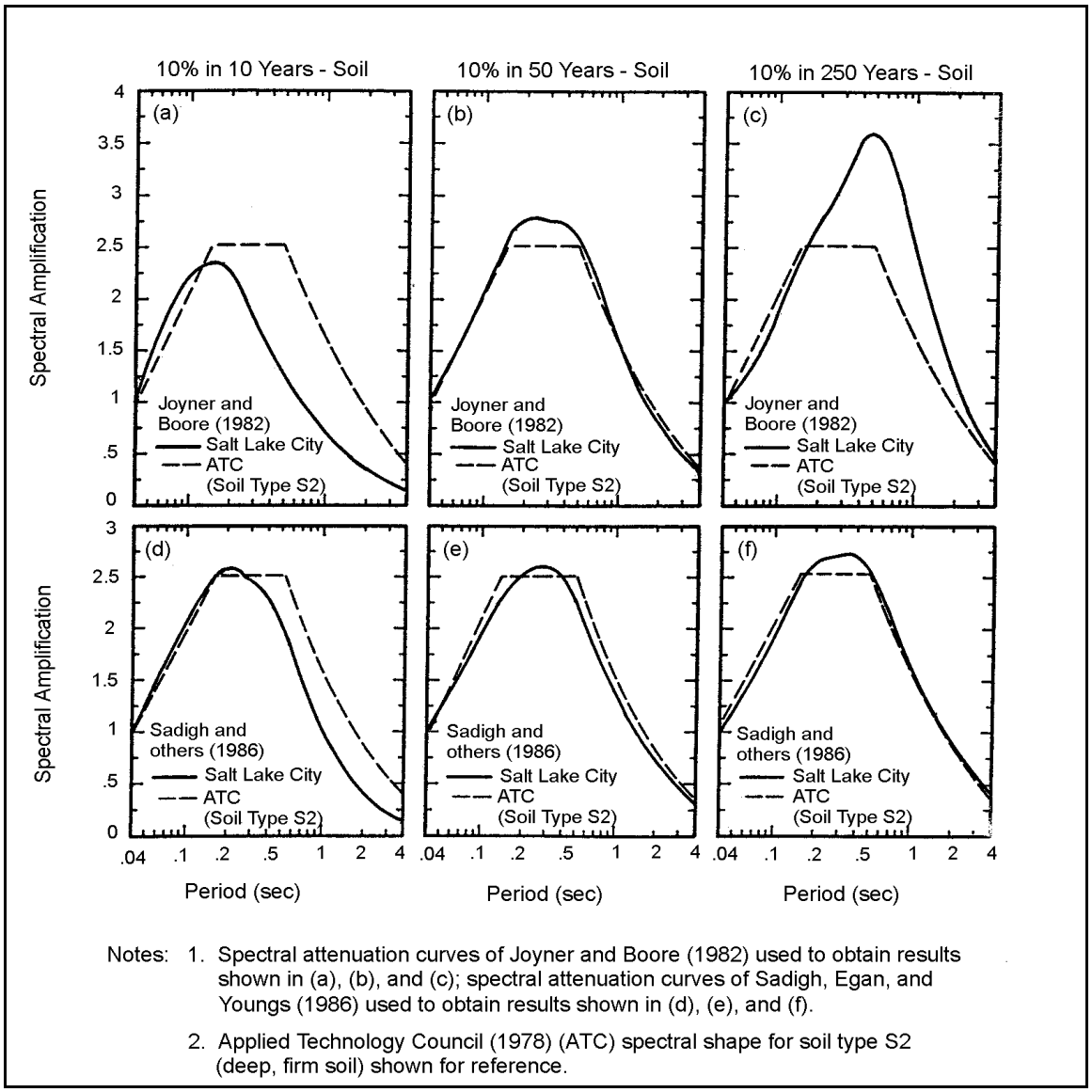

Notes: 1. Spectral attenuation curves of Joyner and Boore (1982) used to obtain results shown in (a), (b), and (c); spectral attenuation curves of Sadigh, Egan, and Youngs (1986) used to obtain results shown in (d), (e), and (f).

2. Applied Technology Council (1978) (ATC) spectral shape for soil type S2 (deep, firm soil) shown for reference.

Figure-3-32. Response spectral shapes for different probability levels resulting from probabilistic hazard analysis for a deep soil site in Utah

(b) The uncertainties and scientific judgments that are present in a DSHA may not be explicitly recognized or quantified (e.g., uncertainties and judgments in assigning the MCE). As a result, the degree of uncertainty or conservatism in a deterministic estimate is not always known or apparent.

(c) For regions in which active faults have not been identified and sites are located within seismic source zones (e.g., EUS), there is not a standard approach or clear basis for selecting the distance to the design earthquake.

b. PSHA

(1) Strengths.

(a) A PSHA allows the designer to balance risk and cost for a project in a manner similar to that used for other environmental loadings such as flood or wind loadings. The reduction in risk by selecting a lower probability level (longer return period) and correspondingly higher seismic loading may be compared to the increased project cost involved with designing for the higher loading.

(b) The frequency of occurrence of earthquakes is explicitly incorporated in a PSHA. As such, regions of greater seismic activity (thus higher probabilities of earthquake occurrence) will have higher ground motion levels for given probabilities or return periods.

(c) The uncertainty or randomness in earthquake location is explicitly incorporated in a PSHA. Thus, the conservatism of assuming that the earthquake occurs at the closest location on the source to the site is not necessary in a PSHA. For sites located within low-seismicity seismic source zones in the EUS, it is usually very conservative to "float" the earthquake to the site or even within a small radius of the site.

(d) Uncertainties in the earthquake occurrence and ground motion estimation process are explicitly considered in a PSHA.

(2) Limitations.

(a) The fact that there are significant scientific uncertainties in earthquake source characterization and ground motion estimation means that there is not a unique result for the relationship between ground motion level and probability of exceedance. In fact, there is usually a significant range of possible ground motion levels for a given probability of exceedance. Usually, the mean estimate from a logic tree analysis is used as a basis for selecting project design criteria.

(b) Probability of exceedance versus ground motion relationships and equal hazard spectra from PSHA's involve contributions from multiple earthquake sources, magnitudes, and distances. As a result, the concept of a design earthquake is not as straightforward as in a DSHA. Furthermore, the evaluation of the duration of shaking and selection of acceleration time-histories based on probabilistic results are more difficult than for a deterministic analysis because of the multiple contributions. Therefore, it is important to deaggragate the results of a PSHA so that the primary contributors (earthquake sources, magnitude ranges, distance ranges) are known.

(c) While uncertainties are incorporated in the analysis (e.g., by the logic tree approach), nevertheless the weights assigned to alternative models and parameter values generally involve subjective judgment. The basis for these judgments should be fully documented.

c. Summary. Both deterministic and probabilistic ground motion analyses have their place in developing earthquake ground motions for seismic design. These two approaches should be used to complement each other as specified in ER 1110-2-1806. It is usually appropriate to carry out both types of analyses to aid the design engineer in developing the project seismic design criteria. Of paramount importance in either deterministic or probabilistic analyses is the expertise of the individuals conducting the analyses.

3-15. Examples of PSHA

Appendix G presents examples of PSHA. The first example is a simplified calculation that illustrates the basic calculational process and probability functions. The other examples represent actual applications in the WUS and EUS. These examples also illustrate how deterministic and probabilistic analyses can be used together in selecting project seismic design ground motions.

Appendix A
References

A-1. Required Publications[1]

TM 5-809-10-1
Seismic Design Guidelines for Essential Buildings

ER 1110-2-1806
Earthquake Design and Evaluation for Civil Works Projects

EM 1110-2-2400
Structural Design of Spillways and Outlet Works

A-2. Related Publications

Abrahamson 1987
Abrahamson, N. A. 1987. "Some Statistical Properties of Peak Ground Accleration (abs.)," *Seismological Research Letters*, Vol 58, pp 28-30.

Abrahamson and Silva 1997
Abrahamson, N. A., and Silva, W. J. 1997. "Empirical Response Spectral Attenuation Relations for Shallow Crustal Earthquakes," *Seismological Research Letters*, Vol 68, No. 1, pp 94-127.

Ahmad, Gazetas, and Desai 1991
Ahmad, S., Gazetas, E. S., and Desai, H. 1991. "Study of Site Response at Memphis Due to a Large New Madrid Earthquake," *Proceedings of the Second International Conference on Recent Advances in Geotechnical Earthquake Engineering and Soil Dynamics*, St. Louis, Missouri, March 11-15, 1991, University of Missouri-Rolla, pp 1259-1265.

Anderson and Quaas 1988
Anderson, J. G., and Quaas, R. 1988. "The Mexico Earthquake of September 19, 1985 -- Effect of Magnitude on the Character of Strong Ground Motion: An Example from the Guerrero, Mexico Strong Motion Network," *Earthquake Spectra*, Vol 4, No. 3, pp 635-646.

Applied Technology Council 1978
Applied Technology Council. 1978. "Tentative Provisions for the Development of Seismic Regulations for Buildings," Publication ATC 3-06, NBS Special Publication 78-8, U.S. Government Printing Office, Washington, DC.

Applied Technology Council 1984
Applied Technology Council. 1984. "Critical Aspects of Earthquake Ground Motion and Building Damage Potential," Applied Technology Council Publication ATC 10-01, Redwood City, CA, pp 105-111.

[1] References published by the Department of the Army and available through USACE Command Information Management Office Sources.

Atkinson 1984
Atkinson, G. M. 1984. "Attenuation of Strong Ground Motion in Canada from a Random Vibrations Approach," *Bulletin of the Seismological Society of America*, Vol 74, pp 2629-2653.

Atkinson and Boore 1995
Atkinson, G. M., and Boore, D. M. 1995. "Ground Motion Relations for Eastern North America," *Bulletin of the Seismological Society of America*, Vol 85, No. 1, pp 17-30.

Atkinson and Boore 1997
Atkinson, G. M., and Boore, D. M. 1997. "Some Comparisons Between Recent Ground-motion Relations," *Seismological Research Letters*, Vol 68, No. 1, pp 24-40.

Bathe and Wilson 1976
Bathe, K-J., and Wilson, E. L. 1976. "*Numerical Methods in Finite Element Analysis*," Prentice-Hall, Englewood Cliffs, NJ.

Bernreuter et al. 1989
Bernreuter, D. L., Savy, J. B., Mensing, R. W., and Chen, J. C. 1989. "Seismic Hazard Characterization of 69 Nuclear Plant Sites East of the Rocky Mountains," NUREG/CR-5250, UCID-21517, 8 volumes, U.S. Nuclear Regulatory Commission, Washington, DC.

Bolt 1988
Bolt, B. A. 1988. *Earthquakes*, 2nd ed., W. H. Freeman, New York.

Bonilla, Mark, and Lienkaemper 1984
Bonilla, M. G., Mark, R. K., and Lienkaemper, J. J. 1984. "Statistical Relations Among Earthquake Magnitude, Surface Rupture Length, and Surface Fault Displacement," *Bulletin of the Seismological Society of America*, Vol 74, pp 2379-2411.

Boore 1983
Boore, D. M. 1983. "Stochastic Simulation of High-Frequency Ground Motions Based on Seismological Models of the Radiated Spectra," *Bulletin of the Seismological Society of America*, Vol 73, pp 1865-1894.

Boore 1986
Boore, D. M. 1986. "Short-period *P*- and *S*-wave Radiation from Large Earthquakes: Implications for Spectral Scaling Relations," *Bulletin of the Seismological Society of America*, Vol 76, No. 1, pp 43-64.

Boore and Atkinson 1987
Boore, D. M., and Atkinson, G. M. 1987. "Stochastic Prediction of Ground Motion and Spectral Response Parameters at Hard-rock Sites in Eastern North America," *Bulletin of the Seismological Society of America*, Vol 77, pp 440-467.

Boore and Boatwright 1984
Boore, D. M., and Boatwright, J. A. 1984. "Average Body-wave Radiation Coefficients," *Bulletin of the Seismological Society of America*, Vol 74, pp 1615-1621.

Boore and Joyner 1991
Boore, D. M., and Joyner, W. B. 1991. "Estimation of Ground Motion at Deep-soil Sites in Eastern North America," *Bulletin of the Seismological Society of America*, Vol 81, No. 6, pp 2167-2185.

Boore, Joyner, and Fumal 1997
Boore, D. M., Joyner, W. B., and Fumal, T. E. 1997. "Equations for Estimating Horizontal Response Spectra and Peak Acceleration from Western North American Earthquakes: A Summary of Recent Work," *Seismological Research Letters,* Vol 68, No. 1, pp 128-153.

Building Seismic Safety Council 1994
Building Seismic Safety Council. 1994. "NEHRP Recommended Provisions for Seismic Regulations for New Buildings," FEMA 222A, prepared for Federal Emergency Management Agency, Washington, DC.

Campbell 1981
Campbell, K. W. 1981. "Near-source Attenuation of Peak Horizontal Acceleration," *Bulletin of the Seismological Society of America*, Vol 71, pp 2039-2070.

Campbell 1987
Campbell, K. W. 1987. "Predicting Strong Ground Motion in Utah: Assessment of Regional Earthquake Hazards and Risk along the Wasatch Front, Utah," Open-File Report 87-585, Vol 2, U.S. Geological Survey, Reston, VA, pp L1-L90.

Campbell 1990
Campbell, K. W. 1990. "Empirical Prediction of Near-source Soil and Soft Rock Ground Motion for the Diablo Canyon Power Plant Site, San Luis Obispo, California," Prepared for Lawrence Livermore National Laboratory, Livermore, CA.

Campbell 1991
Campbell, K. W. 1991. "A Random-effects Analysis of Near-source Ground Motion for the Diablo Canyon Power Plant Site, San Luis Obispo County, California," prepared by Dames and Moore, Evergreen, CO, for Lawrence Livermore National Laboratory, Livermore, CA.

Campbell 1997
Campbell, K. W. 1997. "Empirical Near-source Attenuation Relationships for Horizontal and Vertical Components of Peak Ground Acceleration, Peak Ground Velocity and Pseudo-absolute Acceleration Response Spectra," *Seismological Research Letters,* Vol 68, No. 1, pp 154-179.

Chang et al. 1990
Chang, C. -Y., Mok, C. M., Power, M. S., Tang, Y. K., Tang, H. T., and Stepp, J. C. 1990. "Equivalent Linear Versus Nonlinear Ground Response Analyses at Lotung Seismic Experiment Site," *Proceedings of the Fourth U.S. National Conference on Earthquake Engineering*, May 20-24, 1990, Palm Springs, CA, Earthquake Engineering Research Institute, El Cerrito, CA, Vol 1, pp 327-336.

Chopra 1967
Chopra, A. K. 1967. "Hydrodynamic Pressures on Dams during Earthquakes," *Journal of the Engineering Mechanics Division,* ASCE, Vol 93, No. EM6, pp 205-223.

Chopra 1981
Chopra, A. 1981. *Dynamics of Structures, A Primer*, Earthquake Engineering Research Institute, Berkeley, CA, 126 pp.

Chopra and Zhang 1991
Chopra, A. K., and Zhang, L. 1991. "Base Sliding Response of Concrete Dams to Earthquakes," Report No. UCB/EERC-91/05, Earthquake Engineering Research Center, University of California, Berkeley, CA.

Clough and Penzien 1993
Clough, R. W., and Penzien, J. 1993. *Dynamics of Structures*, 2nd ed., McGraw-Hill, New York.

Clough et al. 1985
Clough, R. W., Chang, K. T., Chen, H. Q., and Ghanaat, Y. 1985. "Dynamic Interaction Effects in Arch Dams," Report No. UCB/EERC-85/11, Earthquake Engineering Research Center, University of California, Berkeley, CA.

Cohee, Somerville, and Abrahamson 1991
Cohee, B. P., Somerville, P. G., and Abrahamson, N. A. 1991. "Simulated Ground Motions for Hypothetical M_W = 8 Earthquakes in Washington and Oregon," *Bulletin of the Seismological Society of America*, Vol 81, pp 28-56.

Coppersmith and Youngs 1986
Coppersmith, K. J., and Youngs, R. R. 1986. "Capturing Uncertainty in Probabilistic Seismic Hazard Assessments within Intraplate Environments," *Proceedings of the Third U.S. National Conference on Earthquake Engineering*, August 24-28, 1986, Charleston, SC, Earthquake Engineering Research Institute, Berkeley, CA, Vol I, pp 301-312.

Cornell 1968
Cornell, C. A. 1968. "Engineering Seismic Risk Analysis," *Bulletin of the Seismological Society of America*, Vol 58, pp 1583-1606.

Cornell and Merz 1975
Cornell, C. A., and Merz, H. A. 1975. "Seismic Risk Analysis of Boston," *Journal of the Structural Engineering Division*, ASCE, Vol 101, pp 2027-2043.

Cornell and Van Marke 1969
Cornell, C. A., and Van Marke, E. H. 1969. "The Major Influences on Seismic Risk," *Proceedings of the Third World Conference on Earthquake Engineering*, Santiago, Chile, Vol A-1, pp 69-93.

Crouse 1991
Crouse, C. B. 1991. "Ground Motion Attenuation Equations for Earthquakes on the Cascadia Subduction Zone," *Earthquake Spectra*, Vol 7, pp 201-236.

Darragh et al. 1989
Darragh, R. B., Green, R. K., Turcotte, F. Thomas. 1989. "Spectral Characteristics of Small Magnitude Earthquakes with Application to Western and Eastern North American Tectonic Environments: Surface Motions and Depth Effects," Miscellaneous Paper GL-89-16, U.S. Army Engineer Waterways Experiment Station, Vicksburg, MS.

Dasgupta and Chopra 1979
Dasgupta, G., and Chopra, A. K. 1979. "Dynamic Stiffness Matrices for Viscoelastic Half Planes," *ASCE Journal of the Engineering Mechanics Division*, Vol 105, No. EM5, pp 729-745.

Der Kiureghian and Ang 1977
Der Kiureghian, A., and Ang, A. H.-S. 1977. "A Fault-Rupture Model for Seismic Risk Analysis," *Bulletin of the Seismological Society of America*, Vol 67, No. 4, pp 1173-1194.

Dobry, Idriss, and Ng 1978
Dobry, R., Idriss, I. M., and Ng, E. 1978. "Duration Characteristics of Horizontal Components of Strong-Motion Earthquake Records," *Bulletin of the Seismological Society of America*, Vol 68, No. 5, pp 1487-1520.

Earthquake Engineering Research Institute Committee on Seismic Risk 1984
Earthquake Engineering Research Institute Committee on Seismic Risk. 1984. "Glossary of Terms for Seismic Risk Analysis," *Earthquake Spectra*, Vol 1, No. 1, pp 33-40.

Earthquake Engineering Research Institute Committee on Seismic Risk 1989
Earthquake Engineering Research Institute Committee on Seismic Risk. 1989. "The Basics of Seismic Risk Analysis," *Earthquake Spectra*, Vol 5, pp 675-702.

Ebeling 1992
Ebeling, R. M. 1992. "Introduction to the Computation of Response Spectrum for Earthquake Loading," Technical Report ITL-92-11, U.S. Army Engineer Waterways Experiment Station, Vicksburg, MS.

Ebeling and Morrison 1992
Ebeling, R. M., and Morrison, E. E., Jr. 1992. "The Seismic Design of Waterfront Retaining Structures," Technical Report ITL-92-11, U.S. Army Engineer Waterways Experiment Station, Vicksburg, MS.

Electric Power Research Institute 1987
Electric Power Research Institute. 1987. "Seismic Hazard Methodology for the Central and Eastern United States -- Volume 1, Part 1, Theory, and Part 2, Methodology," Prepared for Seismicity Owners Group under Research Projects P101-38, -45, -46, and 2256-14, EPRI Report NP-4726, Revised, February, Palo Alto, CA.

Electric Power Research Institute 1989
Electric Power Research Institute. 1989. "Methods for Estimating Maximum Earthquakes in the Central and Eastern United States - Project RP-2556-12," Draft report prepared for Seismicity Owners Group and Electric Power Research Institute by Geomatrix Consultants, San Francisco, California, and Center of Earthquake Research and Information, Memphis, Tennessee.

Electric Power Research Institute 1993
Electric Power Research Institute. 1993. "Guidelines for Determining Design Basis Ground Motions," Report TR-102293, Electric Power Research Institute, Vol 1-4, Palo Alto, CA.

Esteva 1969
Esteva, L. 1969. "Seismicity Prediction--A Brayesian Approach," *Proceedings of the Fourth World Conference on Earthquake Engineering*, Santiago, Chile, Vol 1, pp AL 172-184.

Fenves and Chopra 1986
Fenves, G. L., and Chopra, A. K. 1986. "Simplified Analysis for Earthquake Resistant Design of Concrete Gravity Dams," Report No. UCB/EERC-85/10, Earthquake Engineering Research Center, University of California, Berkeley, CA.

Fenves, Mojtahedi, and Reimer 1989
Fenves, G. L., Mojtahedi, S., and Reimer, R. B. 1989. "ADAP-88: A Computer Program for Nonlinear Earthquake Analysis of Concrete Arch Dams," Report No. UCB/EERC-89/12, Earthquake Engineering Research Center, University of California, Berkeley, CA.

Frankel et al. 1996
Frankel, A., Mueller, C., Barnhard, T., Perkins, D., Leyendecker, E., Dickman, N., Hanson, S., and Hopper, M. 1996. *National Seismic Hazard Maps,* Open-file Report 96-532, U.S. Geological Survey, Reston, VA.

Fukushima and Tanaka 1990
Fukushima, Y., and Tanaka, T. 1990. "A New Attenuation Relation for Peak Horizontal Acceleration of Strong Earthquake Ground Motion in Japan," *Bulletin of the Seismological Society of America*, Vol 80, No. 4, pp 757-783.

Geomatrix 1996
Geomatrix Consultants, Inc. 1996. "Probabilistic Seismic Hazard Assessment, Olmsted Locks and Dam Site," prepared by Geomatrix Consultants, Inc., San Francisco, CA, for U.S. Army Engineer District, Louisville, Louisville, KY.

Ghanaat 1993
Ghanaat, Y. 1993. "GDAP: Graphics-based Dam Analysis Program, User's Manual," U.S. Army Engineer Waterways Experiment Station, Vicksburg, MS.

Gomberg and Ellis 1994
Gomberg, J., and Ellis, M. 1994. "Topography and Tectonics of the Central New Madrid Seismic Zone: Results of Numerical Experiments Using a Three-Dimensional Boundary Element Program," *Journal of Geophysical Research,* Vol 99, No. 20, pp 299-310.

Goyal and Chopra 1989
Goyal, A., and Chopra, A. K. 1989. "Earthquake Analysis and Response of Intake-outlet Towers," Report No. UCB/EERC-89/04, Earthquake Engineering Research Center, University of California, Berkeley, CA.

Gutenberg and Richter 1954
Gutenberg, B., and Richter, C. F. 1954. "Seismicity of the Earth and Associated Phenomena," 2nd ed., Princeton University Press, Princeton, NJ.

Hanks and McGuire 1981
Hanks, T. C., and McGuire, R. K. 1981. "The Character of High Frequency Strong Ground Motion," *Bulletin of the Seismological Society of America,* Vol 71, pp 2071-2095.

Housner 1963
Housner, G. W. 1963. "The Behavior of Inverted Pendulum Structures during Earthquakes," *Bulletin of Seismological Society of America*, Vol 53, No. 2, pp 403-417.

Hudson 1979
Hudson, D. E. 1979. "Reading and Interpreting Strong Motion Accelerograms," Engineering Monographs on Earthquake Criteria, Structural Design, and Strong Motion Records, Vol 1, Earthquake Engineering Research Institute, Berkeley, CA.

Idriss 1991a
Idriss, I. M. 1991a. "Earthquake Ground Motions at Soft Soil Sites: Vol III," *Proceedings of the Second International Conference on Recent Advances in Geotechnical Earthquake Engineering and Soil Dynamics*, March 11-15, 1991, St. Louis, MO, Shamsher Prakesh, ed., University of Missouri-Rolla, Rolla, MO.

Idriss 1991b
Idriss, I. M. 1991b. "Selection of Earthquake Ground Motions at Rock Sites," Report Prepared for the Structures Division, Building and Fire Research Laboratory, National Institute of Standards and Technology, Department of Civil Engineering, University of California, Davis, CA.

International Committee on Large Dams 1989
International Committee on Large Dams 1989. "Selecting Seismic Parameters for Large Dams," *Guidelines*, Bulletin 72.

International Conference of Building Officials 1994 and 1997
International Conference of Building Officials. 1994 and 1997. "Uniform Building Code," Whittier, CA.

Johnston in preparation
Johnston, A. C. "Seismic Moment Assessment of Earthquakes in Stable Continental Regions: III, New Madrid 1811-1812, Charleston 1886, and Lisbon 1755," *Geophysical Journal International*, 1996.

Johnston 1996
Johnston, A. C. 1996. "Seismic Moment Assessment of Earthquakes in Stable Continental Regions—III. New Madrid 1811-1812, Charleston 1886 and Libson 1755," *Geophysical Journal International*, Vol 126, pp 314-344.

Johnston and Nava 1990
Johnston, A. C., and Nava, S. J. 1990. "Seismic-hazard Assessment in the Central United States," *Neotectonics in Earthquake Evaluation: Geological Society of America Reviews in Engineering Geology*, E. L. Krinitzsky and D. B. Slemmons, ed., Geological Society of America, Boulder, CO, Vol 8, pp 47-58.

Johnston et al. 1994
Johnston, A. C., Coppersmith, K. J., Kanter, L. R., and Cornell, C. A. 1994. "The Earthquakes of Stable Continental Regions, Volume 1: Assessment of Large Earthquake Potential," TR-102261-V1, prepared by the University of Memphis Center for Earthquake Research and Information (CERI), Memphis, and Geomatrix Consultants, Inc., San Francisco, CA, for the Electric Power Research Institute, Palo Alto, CA.

Joyner and Boore 1982
Joyner, W. B., and Boore, D. M. 1982. "Prediction of Earthquake Response Spectra," *Proceedings of the 51st Annual Convention, Structural Engineers Association of California*, Sacramento, CA, also U.S. Geological Survey Open-File Report 82-977, 16 p. Also summarized in *Earthquake Engineering and Soil Dynamics II: Recent Advances in Ground-Motion Evaluation,* proceedings of the specialty conference, June 27-30, 1988, Park City, UT, Geotechnical Special Publication No. 20, J. Lawrence Von Thun, ed., ASCE, New York, pp 359-375.

Joyner and Boore 1988
Joyner, W. B., and Boore, D. M. 1988. "Measurement, Characterization, and Prediction of Strong Ground Motion," *Earthquake Engineering and Soil Dynamics II: Recent Advances in Ground-Motion Evaluation,* proceedings of the specialty conference, June 27-30, 1988, Park City, UT, Geotechnical Special Publication No. 20, J. Lawrence Von Thun, ed., ASCE, New York, pp 359-375. pp 43-102.

Joyner and Boore 1996
Joyner, W. B., and Boore, D. M. 1996. "Empirical Methods of Ground-Motion Estimation," *Proceedings of the POLA Seismic Workshop on Seismic Engineering,* San Pedro, CA, 21-23 March 1990. Richard C. Wittcop and Geoffry R. Martin, eds., Port of Los Angeles, San Pedro, CA, pp 273-308.

Karageorgi, Darragh, and Silva 1988
Karageorgi, E., Darragh, R. B., and Silva, W. J. 1988. "Differences Between Eastern and Western North American Tectonic Environments as Evidenced from Response Spectral Shapes," *EOS*, Vol 69, p 1336.

Keefer and Bodily 1983
Keefer, D. L., and Bodily, S. E. 1983. "Three-point Approximations for Continuous Random Variables," *Management Science*, Vol 29, No. 5, pp 595-609.

Kimball 1983
Kimball, J. K. 1983. "The Use of Site Dependent Spectra," *Proceedings of the U.S. Geological Survey Workshop on Site Specific Effects of Soil and Rock on Ground Motions and Implications for Earthquake-Resistant Design*, Open-File Report 83-845, U.S. Geological Survey, Reston, VA, pp 401-422.

Krawinkler and Rahnama 1992
Krawinkler, H., and Rahnama, M. 1992. "Effects of Soft Soils on Design Spectra," *Proceedings of the 10th World Conference on Earthquake Engineering*, Madrid, Spain, 19-24 July 1992, Balkema, Rotterdam, Vol 10, pp 5841-5846.

Krinitzsky and Chang 1987
Krinitzsky, E. L., and Chang, F. K. 1987. "State-of-the-Art for Assessing Earthquake Hazards in the United States: Parameters for Specifying Intensity-Related Earthquake Ground Motions," Miscellaneous Paper S-73-1, Report 25, U.S. Army Engineer Waterways Experiment Station, Vicksburg, MS.

Krinitzsky, Chang, and Nuttli 1987
Krinitzsky, E. L., Chang, F. K., and Nuttli, O. W. 1987. "State-of-the-Art for Assessing Earthquake Hazards in the United States: Parameters for Specifying Magnitude-Related Earthquake Ground Motions," Miscellaneous Paper S-73-1, Report 26, U.S. Army Engineer Waterways Experiment Station, Vicksburg, MS.

Kulkarni, Youngs, and Coppersmith 1984
Kulkarni, R. B., Youngs, R. R., and Coppersmith, K. J. 1984. "Assessment of Confidence Intervals for Results of Seismic Hazard Analysis," *Proceedings of the Eighth World Conference on Earthquake Engineering*, San Francisco, CA, July 21-28, 1984, Vol 1, pp 263-270.

Lee and Finn 1985
Lee, K. W., and Finn, L. W. D. 1985. "DESRA-2 Computer Program," University of British Columbia, Vancouver, Canada.

Li 1990
Li, X. S. 1990. "Free-field Soil Response Under Multi-directional Earthquake Loading," Ph.D. diss., University of California, Davis.

Lilhanand and Tseng 1988
Lilhanand, K., and Tseng, W. S. 1988. "Development and Application of Realistic Earthquake Time Histories Compatible with Multiple-damping Design Spectra," *Proceedings of the Ninth World Conference on Earthquake Engineering*, Tokyo-Kyoto, Japan, August 2-9, 1988, International Association for Earthquake Engineering, Tokyo, pp 819-824.

Lysmer et al. 1981
Lysmer, J., Raissi, M., Tajirian, F., Vahdani, S., and Ostadan, F. 1981. "SASSI: A System for Analysis of Soil-Structure Interaction," Geotechnical Report No. 81-02, University of California, Berkeley.

McGuire 1974
McGuire, R. K. 1974. "Seismic Structural Response Risk Analysis, Incorporating Peak Response Regressions on Earthquake Magnitude and Distance," Research Report R74-51, Massachusetts Institute of Technology, Department of Civil Engineering, Cambridge, MA.

McGuire 1977
McGuire, R. K. 1977. "Effects of Uncertainties in Seismicity on Estimates of Seismic Hazard for the East Coast of the United States," *Bulletin of the Seismological Society of America*, Vol 67, pp 827-848.

McGuire and Shedlock 1981
McGuire, R. K., and Shedlock, K. M. 1981. "Statistical Uncertainties in Seismic Hazard Evaluations in the United States," *Bulletin of the Seismological Society of America*, Vol 71, pp 1287-1308.

McGuire, Toro, and Silva 1988
McGuire, R. K., Toro, G. R., and Silva, W. J. 1988. "Engineering Model of Earthquake Ground Motion for Eastern North America," EPRI Final Report NP-6074, prepared by Risk Engineering, Inc., for the Electric Power Research Institute, Palo Alto, CA.

Miranda 1992
Miranda, E. 1992. "Nonlinear Response Spectra for Earthquake Resistant Design," *Proceedings of the 10th World Conference on Earthquake Engineering*, Madrid, Spain, July 1992, Vol 10, pp 5835-5840.

Mitchell et al. 1991
Mitchell, B. J., Nuttli, O. W., Herrmann, R. B., and Stauder, W. 1991. "Seismotectonics of the Central United States," *Neotectonics of North America*, D. B. Slemmons, E. R. Engdahl, M. D. Zoback, and D. D. Blackwell, eds., Decade of North American Geology Project series, Geological Society of North America, Boulder, CO, pp 245-260.

Mohraz 1976
Mohraz, B. 1976. "A Study of Earthquake Response Spectra for Different Geological Conditions," *Bulletin of the Seismological Society of America*, Vol 66, No. 3, pp 915-935.

Molas and Yamazaki 1995
Molas, G. L., and Yamazaki, F. 1995. "Attenuation of Earthquake Ground Motions in Japan Including Deep Focus Events," *Bulletin of the Seismological Society of America*, Vol 71, pp 2011-2038.

National Research Council 1988
National Research Council. 1988. "Probabilistic Seismic Hazard Analysis," National Academy Press, Washington, DC.

Newmark 1965
Newmark, N. M. 1965. "Effect of Earthquakes on Dams and Embankments," *Geotechnique*, Vol 15, No. 2, pp 139-160.

Newmark and Hall 1978
Newmark, N. M., and Hall, W. J. 1978. "Development of Criteria for Seismic Review of Selected Nuclear Power Plants," Report NUREG/ CR-0098, U.S. Nuclear Regulatory Commission, Rockville, MD.

Newmark and Hall 1982
Newmark, N. M., and Hall, W. J. 1982. "Earthquake Spectra and Design," Engineering Monographs on Earthquake Criteria, Structural Design, and Strong Motion Records, Vol 3, Earthquake Engineering Research Institute, University of California, Berkeley, CA.

Newmark and Rosenblueth 1971
Newmark, N. M., and Rosenblueth, E. 1971. *Fundamentals of Earthquake Engineering*, Prentice-Hall, Englewood Cliffs, NJ.

Pacific Gas and Electric Company 1988
Pacific Gas and Electric Company. 1988. "Final Report of the Diablo Canyon Long-term Seismic Program," Docket Nos. 50-275 and 50-323. U.S. Nuclear Regulatory Commission, Rockville, MD.

Paulay 1986
Paulay, T. M. 1986. "The Design of Ductile Reinforced Concrete Structural Walls for Earthquake Resistance," *Earthquake Spectra*, Vol 2, No. 4, pp 783-823.

Power 1994
Power, M. S. 1994. "Implications of Developing Knowledge of Earthquake Ground Motions to Building Codes," *Proceedings of the 1994 Fall Seminar on the Developing Art of Seismic Engineering*, Structural Engineers Association of Northern California, San Francisco.

Russ 1982
Russ, D. P. 1982. Style and Significance of Surface Deformation in the Vicinity of New Madrid, Missouri," *Investigations of the New Madrid, Missouri, Earthquake Region*, Geological Survey Professional Paper 1236-H, F. A. McKeown and L. C. Paksier, eds., U.S. Geological Survey, Washington, DC, pp 95-114.

Sadigh, Egan, and Youngs 1986
Sadigh, K., Egan, J. A., and Youngs, R. R. 1986. "Specification of Ground Motion for Seismic Design of Long Period Structures," *Earthquake Notes*, Vol 57, No. 1, p 13. Relationships are tabulated in *Earthquake Engineering and Soil Dynamics II: Recent Advances in Ground-Motion Evaluation*, proceedings of the specialty conference, June 27-30, 1988, Park City, UT, Geotechnical Special Publication No. 20, J. Lawrence Von Thun, ed., ASCE, New York.

Sadigh et al. 1993
Sadigh, K., Chang, C. -Y., Abrahamson, N. A., Chiou, S. J., and Power, M. S. 1993. "Specification of Long-period Ground Motions: Updated Attenuation Relationships for Rock Site Conditions and Adjustment Factors for Near-fault Effects," *Proceedings of ATC-17-1 Seminar on Seismic Isolation, Passive Energy Dissipation, and Active Control*; *Vol 1: Seismic Isolation Systems*, San Francisco, CA, March 11-12, 1993, Applied Technology Council, Redwood City, CA, pp 59-70.

Sadigh et al. 1997
Sadigh, K., Chang, C.-Y., Egan, J. A., Makdisi, F. I., and Youngs, R. R. 1997. "Attenuation Relationships for Shallow Crustal Earthquakes Based on California Strong Motion Data," *Seismological Research Letters*, Vol 68, No. 1, pp 180-189.

Schnabel, Seed, and Lysmer 1972
Schnabel, P. B., Seed, H. B., and Lysmer, J. 1972. "SHAKE -- A Computer Program for Earthquake Response Analysis of Horizontally Layered Sites," Report No. EERC 72-12, Earthquake Engineering Research Center, University of California, Berkeley, CA.

Schwartz 1988
Schwartz, D. P. 1988. "Geology and Seismic Hazards -- Moving into the 1990's," *Earthquake Engineering and Soil Dynamics II: Recent Advances in Ground-Motion Evaluation*, proceedings of the specialty conference, June 27-30, 1988, Park City, UT, Geotechnical Special Publication No. 20, J. Lawrence Von Thun, ed., ASCE, New York.

Schwartz and Coppersmith 1984
Schwartz, D. P., and Coppersmith, K. J. 1984. "Fault Behavior and Characteristic Earthquakes from the Wasatch and San Andreas Faults," *Journal of Geophysical Research*, Vol 89, pp 5681-5698.

Schwartz and Coppersmith 1986
Schwartz, D. P., and Coppersmith, K. J. 1986. "Seismic Hazards -- New Trends in Analysis Using Geologic Data," *Active Tectonics*, National Academy Press, Washington, DC, pp 215-230.

Seed and Idriss 1969
Seed, H. B., and Idriss, I. M. 1969. "Influence of Soil Conditions on Ground Motions during Earthquakes," *Journal of the Soil Mechanics and Foundation Division, ASCE*, Vol 95, No. SM1, pp 99-137.

Seed and Idriss 1970
Seed, H. B., and Idriss, I. M. 1970. "Soil Moduli and Damping Factors for Dynamic Response Analyses," Report No. EERC-70-10, Earthquake Engineering Research Center, University of California, Berkeley, CA.

Seed and Schnabel 1980
Seed, H. B., and Schnabel, P. B. 1980. "Ground Motions and Soil Liquefaction during Earthquakes," Engineering Monographs on Earthquake Criteria, Structural Design, and Strong Motion Records, Vol 5, Earthquake Engineering Research Institute, Berkeley, CA.

Seed and Sun 1989
Seed, H. B., and Sun, J. 1989. "Implications of Site Effects in the Mexico City Earthquake of September 19, 1985 for Earthquake-resistant Design Criteria in the San Francisco Bay Area of California," Report No. UCB/EERC-89/03, Earthquake Engineering Research Center, University of California, Berkeley, CA.

Seed, Ugas, and Lysmer 1976
Seed, H. B., Ugas, C., and Lysmer, J. 1976. "Site Dependent Spectra for Earthquake-Resistant Design," *Bulletin of the Seismological Society of America*, Vol 66, No. 1, pp 221-244.

Silva 1989
Silva, W. 1989. "Site Dependent Specification of Strong Ground Motion," *Dynamic Soil Properties and Site Characterization*, Proceedings of the Workshop sponsored by the National Science Foundation and the Electric Power Research Institute, Palo Alto, CA, pp 6-1 thru 6-80.

Silva 1997
Silva, W. J. 1997. "Characteristics of Vertical Strong Ground Motions for Applications to Engineering Design," *Proceedings of the FHWA/NCEER Workshop on the National Representation of Seismic Ground Motion for New and Existing Highway Facilities*, Burlingame, CA, September 22, 1997, Ian Friedland, Maurice S. Power, and Ronald L. Mayes, ed., National Center for Earthquake Engineering Research, State University of New York at Buffalo, pp 205-252.

Silva and Green 1989
Silva, W. J., and Green, R. K. 1989. "Magnitude and Distance Scaling of Response Spectral Shapes for Rock Sites with Applications to North American Tectonic Environment," *Earthquake Spectra*, Vol 5, No. 3, pp 591-624.

Silva and Lee 1987
Silva, W. J., and Lee, K. 1987. "State-of-the-Art for Assessing Earthquake Hazards in the United States: WES RASCAL Code for Synthesizing Earthquake Ground Motions," Miscellaneous Paper S-73-1, Report 24, U.S. Army Engineer Waterways Experiment Station, Vicksburg, MS.

Silva et al. 1989
Silva, W. J., Darragh, R. B., Green, R. K., and Turcotte, F. T. 1989. "Estimated Ground Motions for a New Madrid Event," Miscellaneous Paper GL-89-17, U.S. Army Engineer Waterways Experiment Station, Vicksburg, MS.

Slemmons 1982
Slemmons, D. B. 1982. "Determination of Design Earthquake Magnitudes for Microzonation." *Proceedings of the Third International Earthquake Microzonation, Conference*, Seattle, WA, June 28-July 1, 1982, Mehmet Sherif, ed., U.S. National Science Foundation, Washington, DC, Vol 1, pp 119-130.

Somerville 1997
Somerville, P. G. 1997. "The Characteristics and Quantification of Near Fault Ground Motion," *Proceedings of the NCEER Workshop on National Representation of Seismic Ground Motion for New and Existing Highway Facilities*, San Francisco, CA, May 29-30, 1997, National Center for Earthquake Engineering Research, Buffalo, NY, pp 293-318.

Somerville and Graves 1993
Somerville, P., and Graves, R. 1993. "Conditions That Give Rise to Unusually Large Long Period Ground Motions," *Proceedings of ATC-17-1 Seminar on Seismic Isolation, Passive Energy Dissipation, and Active Control; Vol 1: Seismic Isolation Systems*, San Francisco, CA, March 11-12, 1993. Applied Technology Council, Redwood City, CA, pp 83-99.

Somerville et al. 1997
Somerville, P. G., Smith, N. F., Graves, R. W., and Abrahamson, N. A. 1997. "Modification of Empirical Strong Ground Motion Attenuation Relations to Include the Amplitude and Duration Effects of Rupture Directivity," *Seismological Research Letters*, Vol 68, No. 1, pp 199-222.

Stepp 1972
Stepp, J. C. 1972. "Analysis of Completeness of the Earthquake Sample in the Puget Sound Area and Its Effect on Statistical Estimates of Earthquake Hazard," *International Conference on Microzonation for Safer Construction, Research, and Application*, Seattle, WA, National Science Foundation, Vol 2, pp 897-910.

Structural Engineers Association of California 1996
Structural Engineers Association of California. 1996. "Recommended Lateral Force Requirements and Commentary," Sacramento, CA.

Sykora, Wahl, and Wallace 1992
Sykora, D. W., Wahl, R. E., and Wallace, D. C. 1992. "USACE Geotechnical Earthquake Engineering Software: WESHAKE for Personal Computers (Version 1.0)," IR GL-92-4, Report 1, U.S. Army Engineer Waterways Experiment Station, Vicksburg, MS.

Toro, Abrahamson, and Schneider 1997
Toro, G. R., Abrahamson, N. A., and Schneider, J. F. 1997. "Model of Strong Ground Motions from Earthquakes in Central and Eastern North America: Best Estimates and Uncertainties," *Seismological Research Letters*, Vol 68, No. 1, pp 41-57.

U.S. Army Engineer District, Louisville 1992
U.S. Army Engineer District, Louisville. 1992. "Olmsted Locks Feature Design Memorandum," Design Memorandum No. 7, Louisville, KY.

U.S. Nuclear Regulatory Commission 1990
U.S. Nuclear Regulatory Commission. 1990. "Standard Review Plan for the Review of Safety Analysis Reports for Nuclear Power Plants," Report NUREG-0800, Rev. 2, Office of Nuclear Reactor Regulation, Rockville, MD.

U.S. Geological Survey 1996
U.S. Geological Survey. 1996. "National Seismic Hazard Maps: Documentation June 1996," Open-File Report 96-532, Reston, VA.

Wass and Hartmann 1984
Wass, G., and Hartmann, H. G. 1984. "Seismic Analysis of Pile Foundations Including Pile-soil-pile Interaction," *Proceedings of the Eighth World Conference on Earthquake Engineering*, San Francisco, CA, July 21-28, 1984, Vol V, pp 55-62.

Weichert 1980
Weichert, D. H. 1980. "Estimation of the Earthquake Recurrence Parameters for Unequal Observation Periods for Different Magnitudes," *Bulletin of the Seismological Society of America*, Vol 70, No. 4, pp 1337-1346.

Wells and Coppersmith 1994
Wells, D. L., and Coppersmith, K. J. (1994). "Earthquake Source Parameters: Updated Empirical Relationships among Magnitude, Rupture Length, Rupture Area, and Surface Displacement," *Bulletin of the Seismological Society of America*, Vol 84, No. 4, pp 974-1002.

Wesnousky et al. 1983
Wesnousky, S., Scholz, C. H., Shinazaki, K., and Matsuda, T. 1983. "Earthquake Frequency Distribution and Mechanics of Faulting," *Journal of Geophysical Research*, Vol 88, pp 9331-9340.

Westergaard 1933
Westergaard, H. M. 1933. "Water Pressures on Dams During Earthquakes," *Transactions, American Society of Civil Engineers*, Vol 98, pp 418-433.

Wilson, Der Kiureghian, and Bayo 1981
Wilson, E. L., Der Kiureghian, A., and Bayo, E. P. 1981. "Short Communication: A Replacement for the SRSS Method in Seismic Analysis," *Journal of Earthquake Engineering and Structural Dynamics*, Vol 9, pp 187-194.

Working Group on California Earthquake Probabilities 1990
Working Group on California Earthquake Probabilities. 1990. "Probabilities of Large Earthquakes in the San Francisco Bay Region, California," U.S. Geological Survey Circular 1053, U.S. Geological Survey, Denver, CO.

Wyss 1979
Wyss, M. 1979. "Estimating Maximum Expectable Magnitude of Earthquakes from Fault Dimensions," *Geology*, Vol 7, pp 336-340.

Youngs and Coppersmith 1985a
Youngs, R. R., and Coppersmith, K. J. 1985a. "Development of a Fault-specific Recurrence Model," *Earthquake Notes* (abs.), Vol 56, No. 1, pp 16.

Youngs and Coppersmith 1985b
Youngs, R. R., and Coppersmith, K. J. 1985b. "Implications of Fault Slip Rates and Earthquake Recurrence Models to Probabilistic Seismic Hazard Estimates," *Bulletin of the Seismological Society of America*, Vol 75, pp 939-964.

Youngs, Day, and Stevens 1988
Youngs, R. R., Day, S. M., and Stevens, J. B. 1988. "Near Field Motions on Rock for Large Subduction Zone Earthquakes," *Earthquake Engineering and Soil Dynamics II: Recent Advances in Ground-Motion Evaluation*, proceedings of the specialty conference, June 27-30, 1988, Park City, UT, Geotechnical Special Publication No. 20, J. Lawrence Von Thun, ed., ASCE, New York, pp 445-462.

Youngs, Swan, and Power 1988
Youngs, R. R., Swan, F. H., and Power, M. S. 1988. "Use of Detailed Geologic Data in Regional Probabilistic Seismic Hazard Analysis -- An Example from the Wasatch Front, Utah," *Earthquake Engineering and Soil Dynamics II: Recent Advances in Ground-Motion Evaluation*, proceedings of the specialty conference, June 27-30, 1988, Park City, UT, Geotechnical Special Publication No. 20, J. Lawrence Von Thun, ed., ASCE, New York, pp 156-172. Permission for use was granted by ASCE.

Youngs et al. 1985
Youngs, R. R., Coppersmith, K. J., Power, M. S., and Swan, F. H. 1985. "Seismic Hazard Assessment of the Hanford Region, Eastern Washington State," *Proceedings of the DOE Natural Hazards Phenomena Hazards Mitigation Conference*, October 7-11, 1985, Las Vegas, NV, pp 169-176.

Youngs et al. 1987
Youngs, R. R., Swan, F. H., Power, M. S., Schwartz, D. P., and Green, R. K. 1987. "Probabilistic Analysis of Earthquake Ground Shaking Hazard along the Wasatch Front, Utah," *Assessment of Regional Earthquake Hazards and Risk Along the Wasatch Front, Utah, U.S.*, Open-File Report 87-585, U.S. Geological Survey, Vol II, pp M-1 thru M-110.

Youngs et al. 1993a
Youngs, R. R., Chiou, S. -J., Silva, W. J., and Humphrey, J. R. 1993a. "Strong Ground Motion Attenuation Relationships for Subduction Zone Earthquakes Based on Empirical Data and Numerical Modeling" (abstract), *Seismological Research Letters*, Vol 64, p 18.

Youngs et al. 1993b
Youngs, R. R., Coppersmith, K. J., Taylor, C. L., Power, M. S., Di Silvestro, L. A., Angell, M. M., Hall, N. T., Wesling, J. R., and Mualchin, L. 1993b. "A Comprehensive Seismic Hazard Model for the San Francisco Bay Region." *Proceedings of the Second Conference on Earthquake Hazards in the Eastern San Francisco Bay Area*, Hayward, CA, March 25-29, 1992. Glenn Borchardt et al., ed., Special Publication 113, California Division of Mines and Geology, Sacramento, CA, pp 431-441.

Youngs et al. 1997
Youngs, R. R., Chiou, S.-J. Silva, W. J., and Humphrey, J. R. 1997. "Strong Ground Motion Attenuation Relationships for Subduction Zone Earthquakes," *Seismological Research Letters*, Vol 68, No. 1, pp 58-73.

Appendix B
Illustration of Newmark-Hall Approach to Developing Design Response Spectra

B-1. Introduction

Newmark and Hall (1982) describe their approach for developing design response spectra using peak ground motion parameters (peak ground acceleration (PGA), peak ground velocity (PGV), and peak ground displacement (PGD)) multiplied by the appropriate spectral amplification factors. For ease of reference, summarized herein are the amplification factors developed by Newmark and Hall (1978, 1982) and the use of these factors to develop elastic response spectra. As illustrated by Newmark and Hall (1982), in general, it can be shown that the response of a simple damped oscillator to a dynamic motion of its base can be represented graphically in a simple fashion by a logarithmic plot as shown in Figure B-1.

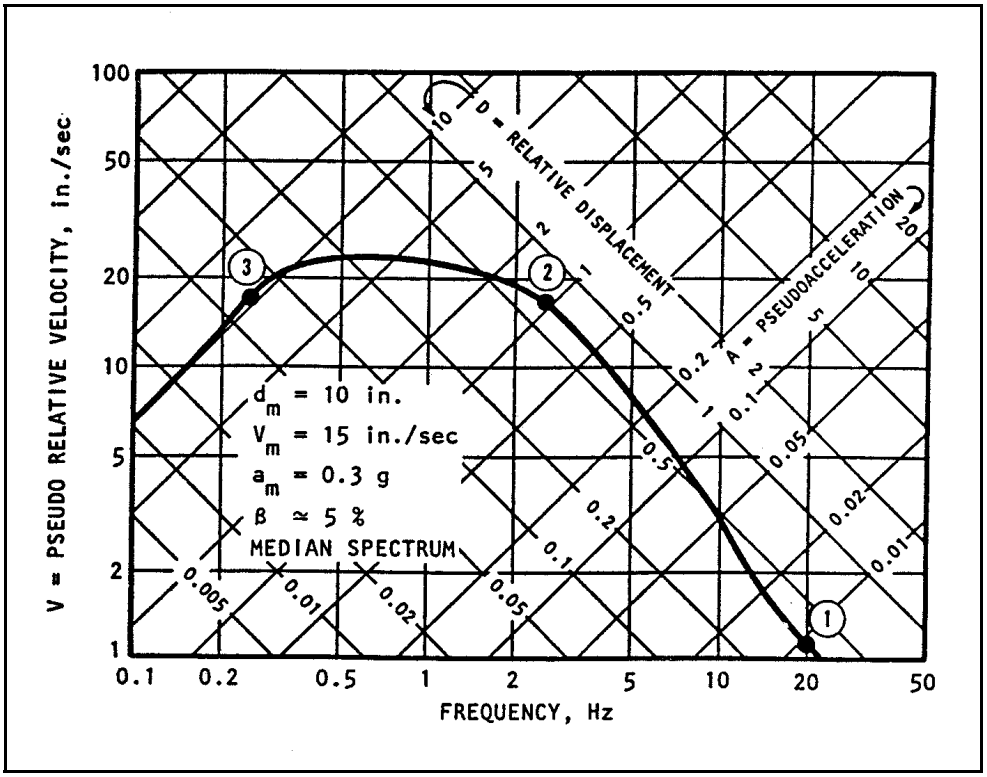

Figure B-1. Typical response spectrum for earthquake motions (Newmark and Hall 1982)

In this figure, the plot uses four logarithmic scales to show the following three response quantities:

D = maximum relative displacement between the mass of the oscillator and its base

V = maximum pseudo-relative velocity = ωD

A = maximum pseudo-acceleration of the mass of the oscillator = $\omega^2 D$

B-2. Response Curve

In these relations, ω is the circular natural frequency of the oscillator, or $\omega = 2\pi f$ where f is frequency in cycles per second (cps) or Hertz (Hz). The peak ground motions for the earthquake motion for which the oscillator response in Figure B-1 is drawn in approximate form are PGD = 10 in., PGV = 15 in. per sec, and PGA = 0.3 g, where g is the acceleration of gravity. The response curve shown is a smooth curve rather than the actual jagged curve that one normally obtains from a calculation for an earthquake accelerogram, and is given for a damping ratio β of about 5 percent of critical. The symbols 1, 2, and 3 on the curve denote the response of different oscillators, No. 1 having a frequency of 20 Hz, No. 2 of 2.5 Hz, and No. 3 of 0.25 Hz. The advantage of using the tripartite logarithmic plot, with frequency also plotted logarithmically, is that one curve can be drawn to represent the three quantities *D, V,* and *A.* The tripartite logarithmic representation is possible only for quantities such as *D, V,* and *A* that are simply related by powers of ω. As noted by Hudson (1979), for earthquake-like excitations, it can be shown that the pseudo-relative velocity can be assumed equivalent to the maximum relative velocity and the pseudo-acceleration equivalent to the maximum acceleration over most of the usual frequency and damping range, with the acceleration equivalence being more accurate than the velocity equivalence.

B-3. Elastic Design Spectrum

A simplified spectrum is shown in Figure B-2, plotted on a logarithmic tripartite graph; note that the various regions of the spectrum are smoothed to straight line portions. On the same graph are shown dotted lines that are drawn at the level of the maximum (peak) ground motion values, and the figure therefore indicates the amplifications of maximum (peak) ground motions for the various parts of the spectrum. It should be noted that the Newmark-Hall approach illustrated in Figure B-2 requires that the values of peak

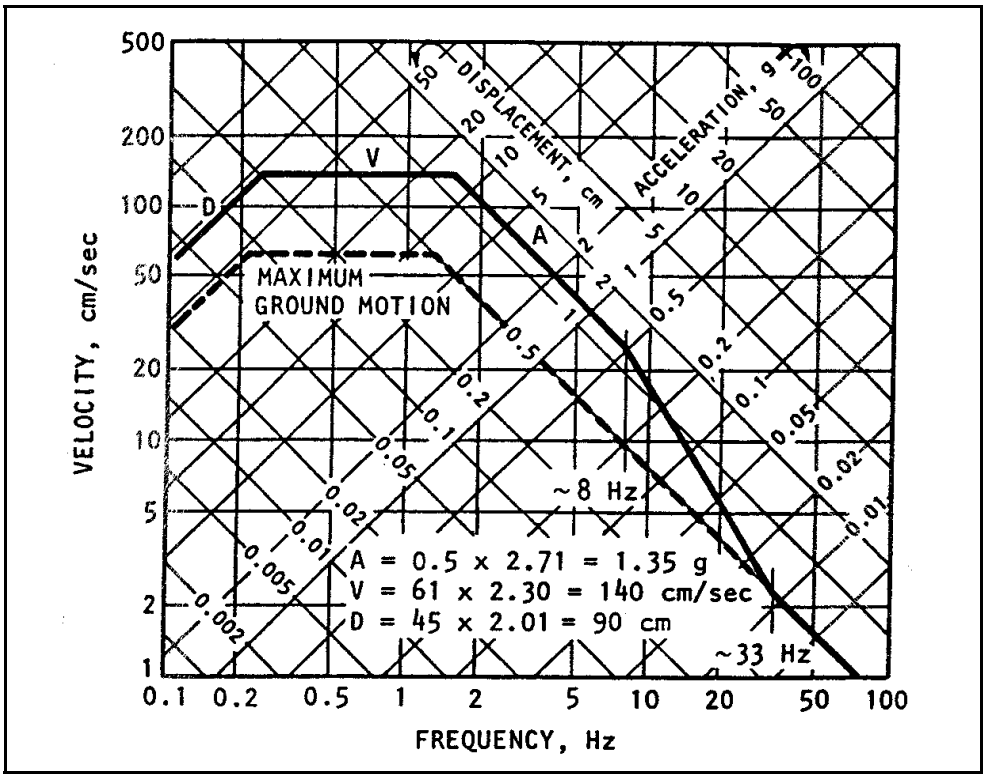

Figure B-2. Elastic design spectrum horizontal motion (0.5 g maximum acceleration, 5 percent damping, one sigma cumulative probability) (Newmark and Hall 1982)

ground motion parameters (PGA, PGV, and PGD) be estimated before the response spectrum can be constructed. Using appropriate ground motion data and relationships, these values can be estimated at the site given the earthquake magnitude, source-to-site distance, and local soil conditions. However, lacking other information, Newmark and Hall (1982) recommend that for competent soil conditions a V/A ratio of 122 cm/sec/g be used, and for rock a V/A ratio of about 91 cm/sec/g be used. Also, to ensure that the spectrum represents an adequate band (frequency) width to accommodate a possible range of earthquakes, Newmark and Hall (1982) recommend that AD/V^2 be taken equal to about 6.0 (in the above *A*, *V*, and *D* are PGA, PGV, and PGD, respectively). Using these V/A and AD/V^2 values, the corresponding D/A values of 90 cm/g and 51 cm/g are computed for competent soil conditions and rock, respectively. The smooth elastic design spectrum shown in Figure B-2 is an 84th-percentile spectrum developed for a site located on competent soil conditions with an estimated PGA value of 0.5 g. In this example, a V/A value of 122 cm/sec/g and a D/A value of 90 cm/g are used. Using these values the PGV and PGD values corresponding to PGA = 0.5 g are 61 cm/sec and 45 cm. Newmark and Hall (1978) provided values of amplification factors for the different parts of the spectrum; these spectrum amplification factors are shown in Table B-1 for various damping ratios and for two levels of probability (50th and 84th percentiles) considering the distribution to be lognormal. Using the 84th-percentile spectrum amplification factors of 2.71, 2.30, and 2.01 associated with the acceleration, velocity, and displacement regions of the spectrum for 5 percent damping (Table B-1), the following response spectrum bounds are computed:

$A = 0.5 \times 2.71 = 1.35$ g

$V = 61 \times 2.30 = 140$ cm/sec

$D = 45 \times 2.01 = 90$ cm

The resulting elastic response spectrum is shown in Figure B-2. As noted in this figure, Newmark and Hall (1982) connect the amplified acceleration *A* at 8 Hz to the PGA at 33 Hz to complete the high-frequency portion of the spectrum. However, Newmark and Hall (1982) do not specify at what frequency the amplified displacement *D* should be connected to the PGD line.

Table B-1
Spectrum Amplification Factors for Horizontal Elastic Response (Newmark and Hall 1982)

Damping	One Sigma (84.1%)			Median (50%)		
% Critical	A	V	D	A	V	D
0.5	5.10	3.84	3.04	3.68	2.59	2.01
1	4.38	3.38	2.73	3.21	2.31	1.82
2	3.66	2.92	2.42	2.74	2.03	1.63
3	3.24	2.64	2.24	2.46	1.86	1.52
5	2.71	2.30	2.01	2.12	1.65	1.39
7	2.36	2.08	1.85	1.89	1.51	1.29
10	1.99	1.84	1.69	1.64	1.37	1.20
20	1.26	1.37	1.38	1.17	1.08	1.01

Appendix C
Development of Site-Specific Response Spectra Based on Statistical Analysis of Strong-Motion Recordings

C-1. Description of the Approach

The general approach used for this method is described by Kimball (1983) and in the U.S. Nuclear Regulatory Commission's Standard Review Plan (USNRC 1990). This method consists of conducting statistical analysis of a suite of strong motion recordings within a distance range and from earthquakes having magnitudes similar to the design earthquake. Before the statistical analysis is conducted, these recordings are first adjusted or modified for differences in magnitude, distance, style of faulting, site conditions, and other factors (e.g., topographic effects) between the site-specific conditions and the conditions for the recordings. Typically, records are selected from sites having subsurface conditions similar to those of the project, in which case no modification is needed for differences in site conditions. The approach consists of the following steps:

a. Selecting recordings. Select a suite of recordings from earthquakes having magnitudes and within a distance range similar to the design earthquake.

b. Modification to recordings. Adjust or modify peak ground acceleration and response spectral values for differences in magnitude, distance, style of faulting, and other factors between the site-specific conditions and the conditions for the recordings. These modifications are made using attenuation relationships for peak ground acceleration and response spectral values.

c. Statistical analysis. Conduct statistical analysis of the adjusted/modified response spectra of the recordings to obtain site-specific response spectra.

C-2. Example

This example illustrates the use of statistical analysis of strong motion recordings to develop site-specific response spectra representative of recordings on rock or rocklike material for a strike-slip earthquake of moment magnitude 6.5 at a closest source-to-site distance of 18 km. A total of six rock recordings (12 horizontal components) obtained during shallow-crustal earthquakes of moment magnitude 6.5 ± 0.25 and recorded in the distance range 15 to 25 km were selected. These records are listed in Table C-1 in terms of the earthquake name, date, type of faulting, magnitude, distance, the component directions, and the peak acceleration value for each record. In this database, four records were from thrust earthquakes and two records were from strike-slip earthquakes. Before the statistical analysis of these near-source records was conducted, they were scaled/adjusted, if necessary, to be compatible with conditions at the site; i.e., they were adjusted to a moment magnitude of 6.5, a source-to-site distance of 18 km, and strike-slip style of faulting. Described below are the various scaling factors used to modify the records for distance, magnitude, and style of faulting.

a. Scaling factors for distance and magnitude. The rock attenuation relationships of Sadigh, Egan, and Youngs (1986) were selected for scaling peak ground acceleration and response spectral values. The relationships for strike-slip faulting are summarized in Table C-2. Using the attenuation relationships given in Table C-2 for each record listed in Table C-1, scaling factors were derived for peak ground acceleration (PGA) and response spectral ordinates relative to a moment magnitude M_W of 6.5 and a source-to-site distance R of 18 km. For example, the scaling factors for PGA for the San Fernando

Table C-1
Database for Statistical Analysis for Shallow Crustal Earthquake (M_W 6.5, R = 18 km)

Earthquake	Date	RUPT	M_W	M_L	STAN	CLD	COMP	PGA
San Fernando, CA	2/9/71	Thrust	6.6	6.4	126	24.2	S69E	0.200
							S21W	0.159
					127	23.5	N21E	0.147
							N69W	0.131
					128	20.3	N21E	0.374
							N69W	0.288
					141	17.4	S00W	0.188
							S00W	0.180
Imperial Valley (M)	10/15/79	Strike Slip	6.5	6.6	6604	23.5	N57W	0.157
							S33E	0.166
Morgan Hill	4/24/84	Strike Slip	6.2	6.2	47379	16.2	N40W	0.100
							S50W	0.073

Note: RUPT = type of faulting
M_W = moment magnitude
M_L = local magnitude
STAN = station number
CLD = closest distance (km)
COMP = component
PGA = peak ground acceleration (g)

earthquake (M_W = 6.6) record at Station 126 (R = 24.2 km) and for the Morgan Hill earthquake (M_W = 6.2) record at Station 47379 (R = 16.2 km) were obtained as follows:

(1) For San Fernando earthquake record at Station 126:

$$\text{PGA scaling factor} = \frac{\text{PGA } (M_W \text{ 6.5, R = 18 km})}{\text{PGA } (M_W \text{ 6.6, R = 24.2 km})}$$

$$= \frac{0.191 \text{ g}}{0.147 \text{ g}} = 1.30$$

(2) For Morgan Hill earthquake record at Station 47379:

$$\text{PGA scaling factor} = \frac{\text{PGA } (M_W \text{ 6.5, R = 18 km})}{\text{PGA } (M_W \text{ 6.2, R = 16.2 km})}$$

$$= \frac{0.191 \text{ g}}{0.173 \text{ g}} = 1.10$$

Scaling factors for PGA for other records listed in Table C-1 were obtained in the same manner. Similarly, the attenuation relationships for response spectral velocity given in Table C-2 were used to derive spectrum scaling factors for various periods for each record.

Table C-2
Values of Coefficients for the Selected Attenuation Relationship for Shallow Crustal Events, Horizontal Peak Ground Acceleration, and Pseudo-Relative Spectral Velocities (Rock Relationships by Sadigh, Egan, and Youngs 1986)

Ground Motion Parameter *Y*	Period sec	Coefficient C_1	C_2	C_3	C_4	σ_Y
PGA	---	-1.406	0	1.353[a] 0.579[b]	0.406[a] 0.537[b]	1.26 - 0.14*M*[a] 0.35[b]
PSRV	0.1	2.059	0.007	1.353[a] 0.579[b]	0.406[a] 0.537[b]	1.332 - 0.148*M*[a] 0.37[b]
PSRV	0.2	2.961	-0.008	1.353[a] 0.579[b]	0.406[a] 0.537[b]	1.453 - 0.162*M*[a] 0.40[b]
PSRV	0.3	3.303	-0.018	1.353[a] 0.579[b]	0.406[a] 0.537[b]	1.486 - 0.164*M*[a] 0.42[b]
PSRV	0.5	3.564	-0.036	1.353[a] 0.579[b]	0.406[a] 0.537[b]	1.584 - 0.176*M*[a] 0.44[b]
PSRV	1.0	3.674	-0.065	1.353[a] 0.579[b]	0.406[a] 0.537[b]	1.62 - 0.18*M*[a] 0.45[b]
PSRV	2.0	3.601	-0.100	1.353[a] 0.579[b]	0.406[a] 0.537[b]	1.62 - 0.18*M*[a] 0.45[b]
PSRV	4.0	3.259	-0.150	1.353[a] 0.579[b]	0.406[a] 0.537[b]	1.62 - 0.18*M*[a] 0.45[b]

Note: Coefficients C_1 through C_4 for use in the relationship:
$\ln Y = C_1 + 1.1M + C_2 (8.5 - M)^{2.5} - 2.05 \ln (R + C_3 \exp C_4 M)$ where M is moment magnitude, and R is closest distance to rupture surface in km.
σ_Y = standard error of estimate of the relationship (the standard error in ln Y).
PGA = horizontal peak ground acceleration, g's.
PSRV = pseudo-relative spectral velocity (5% damping), cm/sec.

[a] Magnitude < 6.5
[b] Magnitude ≥ 6.5

b. Scaling factors for style of faulting. Quantification of the effect of style of faulting on PGA was based on published studies, analysis of soil and rock data sets, and numerical modeling results (Table C-3). On the basis of these analyses, a factor of 0.833 (or 1/1.2) was selected to scale recordings from a thrust faulting mechanism to a strike-slip faulting mechanism.

c. Results. The response spectra for each record in Table C-1 were adjusted (on a relative basis) to a target moment magnitude of 6.5 and a target distance of 18 km using appropriate magnitude and distance scaling relationships (i.e., using the selected attenuation relationships in Table C-2). Also, the response spectra of the four recordings from thrust earthquakes were adjusted (using a factor of 0.833) to a strike-slip style of faulting mechanism. Subsequently, a statistical analysis of this adjusted response spectral data set was performed on the logarithm of spectral pseudo-relative velocity (PSRV). The results of the analysis are shown in Figure C-1 in terms of the median (50th percentile) and median plus one standard deviation (84th percentile) of the fitted log-normal distribution for a damping value of 5 percent. It is noted that before such spectra are designated as design spectra, it would be appropriate to smooth the spectral peaks and valleys.

Table C-3
Effect of Style of Faulting on Peak Ground Acceleration

Empirical Relationships	Ratio of PGA for Thrust Faulting to PGA for Strike-Slip Faulting
Campbell (1981)	1.17 - 1.28
Campbell (1987)	1.38 - 1.40
Campbell (1990)	1.24
Joyner and Boore (1996)	1.25
Sadigh, Egan, and Youngs (1986)	1.20
Long Term Seismic Program (Pacific Gas and Electric Company (PG&E) 1988)	1.22 - 1.27
Numerical Simulations	
Boore and Boatwright (1984)	1.14 - 1.28
Long Term Seismic Program (PG&E 1988)	1.16
Selected for the Example Study	1.2

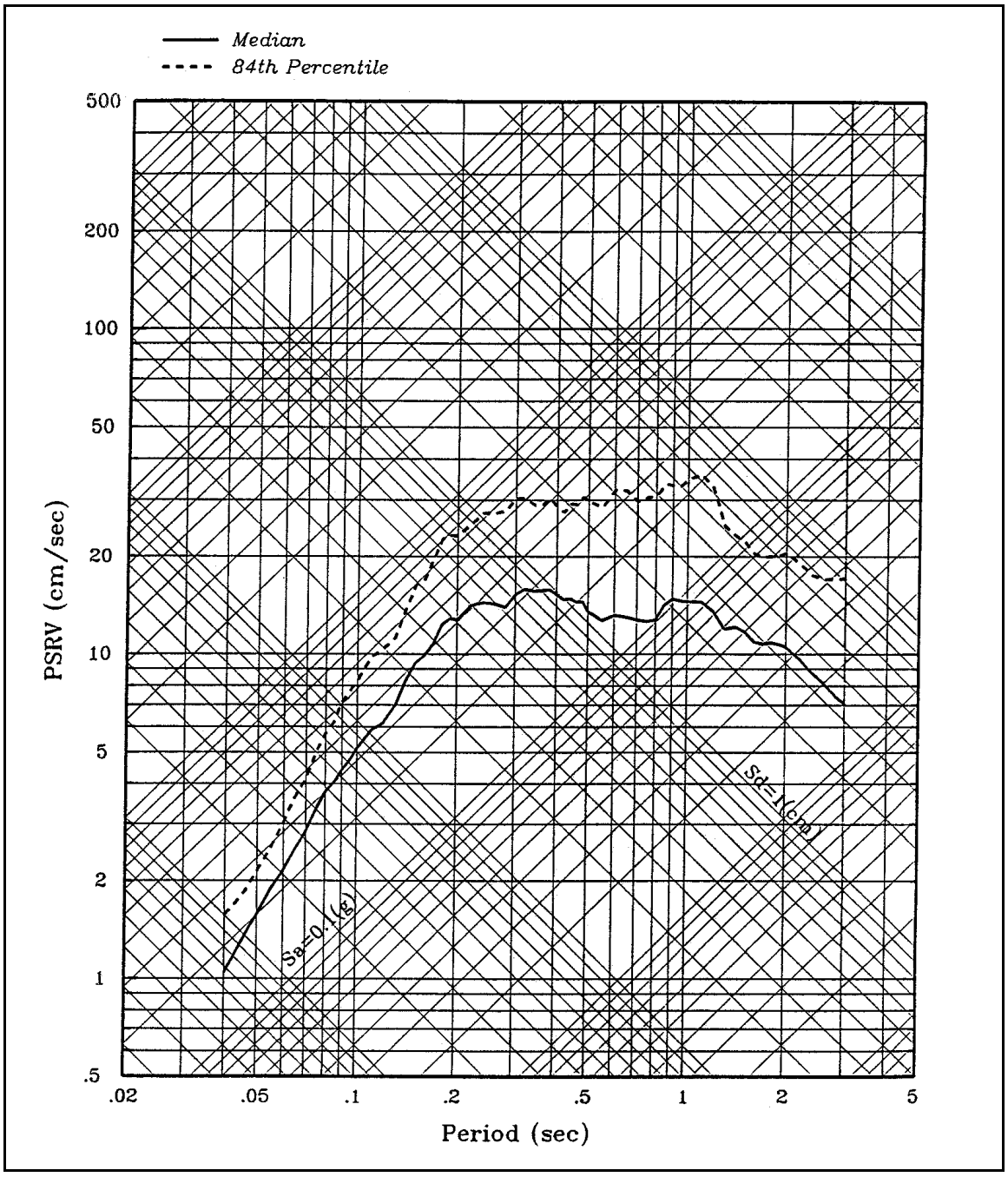

Figure C-1. Median and 84th percentile spectra (5 percent damping) for a magnitude 6.5 strike-slip earthquake at 18 km based on statistics of adjusted rock recordings

Appendix D
Development of Site-Specific Response Spectra Based on Random Earthquake Analysis

D-1. Random Earthquake Analysis

A "random earthquake" analysis is performed when it is desired to estimate the response spectrum at the site due to a randomly located ("floating") earthquake occurring within the vicinity of the site when its location cannot be ascribed to a specific geologic structure at a specific distance from the site. This type of analysis had its origin in estimating ground motions at nuclear power plant sites in the eastern United States, and it has been used for other facilities and locations as well. The most common procedure used is to conduct a statistical analysis of response spectra of available near-source recordings (typically within a source-to-site distance of 25 km) from earthquakes within a magnitude band centered on the target magnitude (typically plus or minus one-half magnitude unit). A random earthquake analysis can also be performed using response spectra attenuation relationships appropriate for the site conditions and tectonic environment where the site is located. It should be noted that in many cases sufficient recordings may not be available to conduct a random earthquake analysis using statistical analysis of response spectra; in these cases a random earthquake analysis can be carried out using only appropriate attenuation relationships. It may be desirable to conduct the random earthquake analysis using both the statistical analysis procedure and the procedure using attenuation relationships. The following sections illustrate the use of the statistical procedure and the attenuation relationships in conducting a random earthquake analysis.

D-2. Statistical Analysis of Recorded Strong Motion Data

a. As mentioned previously, when the design earthquake is specified as a random event occurring in the site vicinity, the available near-source recordings from earthquakes with magnitudes close to the target magnitude are analyzed statistically to obtain estimates of the site-specific spectra. In this example, the site-specific ground motions for a random shallow crustal earthquake of moment magnitude 6.0 were evaluated by conducting a statistical analysis of response spectra computed from accelerograms recorded during earthquakes of magnitude M 6.0 ± 0.5 at source-to-site distances R of approximately 25 km or less. Only recordings from stations located on rock or rocklike material (shear wave velocity ≥ 2,500 fps) were used. The records available for this analysis are listed in Table D-1 in terms of the earthquake name, date, type of faulting, magnitude, station number, closest source-to-site distance, the component directions, and the peak acceleration value for each accelerogram. A total of 30 records (60 horizontal components) were selected from earthquakes in the magnitude range of 5.5 to 6.5. A scattergram showing the magnitude-distance distribution of the records used in the analysis is shown in Figure D-1. The mean closest source-to-site distance of the recordings is 13.7 km. If an earthquake is assumed to occur randomly with a uniform distribution within a 25-km-radius circle about the site, then the mean distance should be 16.7 km. The probability of an event occurring within a specific distance band is equal to the ratio of the area within the distance band to the total area in the 25-km-radius circle. These probabilities are compared in Table D-2 with percentages of the data set lying in various distance bands.

b. As can be seen, the distribution of data is not the same as that expected for a random event within a circle. To adjust the distribution, a weighted statistical analysis was performed with the spectra in each distance band assigned a weight such that their contribution to the total is equal to the probability of a random event occurring in the appropriate distance band. The statistical analysis of this weighted

Table D-1
Database for Statistical Analysis for Shallow Crustal Random Earthquake (M 5.5 - 6.5, R ≤ 25 km, Rock Site Recordings (60 Records Total)

Earthquake	Date	RUPT	M_w	ML	STAN	CLD	COMP	PGA
Parkfield, CA	6/27/66	StrikeSlip	6.1	5.6	1438	9.9	N65W	0.282
Parkfield, CA	6/27/66	StrikeSlip	6.1	5.6	1438	9.9	S25W	0.411
Koyna, India	12/10/67	StrikeSlip	6.3	6.3	9001	3.0	LONG	0.631
Koyna, India	12/10/67	StrikeSlip	6.3	6.3	9001	3.0	TRAN	0.490
Oroville, CA (M)	8/1/75	Normal	5.9	5.7	1051	9.5	N53W	0.103
Oroville, CA (M)	8/1/75	Normal	5.9	5.7	1051	9.5	N37E	0.108
Friuli Sequence	9/11/76	Thrust	5.5	5.5	8022	15.5	NORT	0.042
Friuli Sequence	9/11/76	Thrust	5.5	5.5	8022	15.5	EAST	0.071
Friuli Sequence	9/11/76	Thrust	5.9	5.9	8022	14.5	NORT	0.091
Friuli Sequence	9/11/76	Thrust	5.9	5.9	8022	14.5	EAST	0.093
Friuli Sequence	9/15/76	Thrust	6.1	6.1	8022	9.0	NORT	0.069
Friuli Sequence	9/15/76	Thrust	6.1	6.1	8022	9.0	EAST	0.123
Coyote Lake, CA	8/6/79	StrikeSlip	5.7	5.7	1445	3.2	N70E	0.230
Coyote Lake, CA	8/6/79	StrikeSlip	5.7	5.7	1445	3.2	N20W	0.160
Coyote Lake, CA	8/6/79	StrikeSlip	5.7	5.7	1408	9.3	S40E	0.130
Coyote Lake, CA	8/6/79	StrikeSlip	5.7	5.7	1408	9.3	N50E	0.100
Coyote Lake, CA	8/6/79	StrikeSlip	5.7	5.7	1413	3.1	S40E	0.340
Coyote Lake, CA	8/6/79	StrikeSlip	5.7	5.7	1413	3.1	N50E	0.420
Imperial Valley (M)	10/15/79	StrikeSlip	6.5	6.6	286	26.0	S45E	0.210
Imperial Valley (M)	10/15/79	StrikeSlip	6.5	6.6	286	26.0	N45E	0.120
Imperial Valley (M)	10/15/79	StrikeSlip	6.5	6.6	6604	23.5	N57W	0.157
Imperial Valley (M)	10/15/79	StrikeSlip	6.5	6.6	6604	23.5	S33E	0.166
Mammoth Lakes - A	5/25/80	StrikeSlip	6.2	6.1	54214	15.5	090	0.079
Mammoth Lakes - A	5/25/80	StrikeSlip	6.2	6.1	54214	15.5	000	0.125
Mammoth Lakes - A	5/25/80	StrikeSlip	6.2	6.1	54214	15.5	090	0.068
Mammoth Lakes - A	5/25/80	StrikeSlip	6.2	6.1	54214	15.5	000	0.109
Mammoth Lakes - C	5/25/80	StrikeSlip	6.0	6.1	54214	19.7	090	0.075
Mammoth Lakes - C	5/25/80	StrikeSlip	6.0	6.1	54214	19.7	000	0.088

Note:

RUPT = Type of Faulting
M_w = Moment Magnitude
ML = Local Magnitude
STAN = Station No.
CLD = Closest Distance (km)
COMP = Component
PGA = Peak Ground Acceleration (g)

(Continued)

Table D-1 (Concluded)

Earthquake	Date	RUPT	M_w	ML	STAN	CLD	COMP	PGA
Mammoth Lakes - C	5/25/80	StrikeSlip	6.0	6.1	54214	19.7	090	0.060
Mammoth Lakes - C	5/25/80	StrikeSlip	6.0	6.1	54214	19.7	000	0.112
Mammoth Lakes C01	5/25/80	StrikeSlip	5.7	5.7	54214	14.4	090	0.063
Mammoth Lakes C01	5/25/80	StrikeSlip	5.7	5.7	54214	14.4	000	0.099
Mammoth Lakes C01	5/25/80	StrikeSlip	5.7	5.7	54214	14.4	090	0.043
Mammoth Lakes C01	5/25/80	StrikeSlip	5.7	5.7	54214	14.4	000	0.083
Mammoth Lakes - D	5/27/80	StrikeSlip	6.0	6.2	54214	20.0	090	0.207
Mammoth Lakes - D	5/27/80	StrikeSlip	6.0	6.2	54214	20.0	000	0.208
Mammoth Lakes - D	5/27/80	StrikeSlip	6.0	6.2	54214	20.0	090	0.180
Mammoth Lakes - D	5/27/80	StrikeSlip	6.0	6.2	54214	20.0	000	0.219
Mammoth Lakes - D	5/27/80	StrikeSlip	6.0	6.2	54424	24.5	160	0.119
Mammoth Lakes - D	5/27/80	StrikeSlip	6.0	6.2	54424	24.5	070	0.093
Mexicali Valley, MX	6/9/80	StrikeSlip	6.4	6.4	6604	8.5	N45E	0.611
Mexicali Valley, MX	6/9/80	StrikeSlip	6.4	6.4	6604	8.5	S45E	0.603
Coalinga, CA AS12	07/21/83	Thrust	5.9	6.0	67	9.5	N00E	0.960
Coalinga, CA AS12	07/21/83	Thrust	5.9	6.0	67	9.5	N90W	0.838
Coalinga, CA AS12	07/21/83	Thrust	5.9	6.0	46	15.3	N90E	0.116
Coalinga, CA AS12	07/21/83	Thrust	5.9	6.0	46	15.3	N00E	0.136
Coalinga, CA AS12	07/21/83	Thrust	5.9	6.0	65	11.3	N00E	0.219
Coalinga, CA AS12	07/21/83	Thrust	5.9	6.0	65	11.3	N90W	0.218
Coalinga, CA AS12	07/21/83	Thrust	5.9	6.0	61	12.4	N00E	0.231
Coalinga, CA AS12	07/21/83	Thrust	5.9	6.0	61	12.4	N90W	0.375
Coalinga, CA AS12	07/21/83	Thrust	5.9	6.0	65	11.3	N00E	0.194
Coalinga, CA AS12	07/21/83	Thrust	5.9	6.0	65	11.3	N90W	0.219
Morgan Hill, CA	04/24/84	StrikeSlip	6.2	6.2	57217	0.1	N75W	1.304
Morgan Hill, CA	04/24/84	StrikeSlip	6.2	6.2	57217	0.1	S15W	0.707
Morgan Hill, CA	04/24/84	StrikeSlip	6.2	6.2	57383	11.8	N90E	0.293
Morgan Hill, CA	04/24/84	StrikeSlip	6.2	6.2	57383	11.8	N00E	0.228
Morgan Hill, CA	04/24/84	StrikeSlip	6.2	6.2	47379	16.2	N40W	0.100
Morgan Hill, CA	04/24/84	StrikeSlip	6.2	6.2	47379	16.2	S50W	0.073
North Palm Springs	7/8/86	StrikeSlip	5.9	5.9	12206	25.8	N90E	0.119
North Palm Springs	7/8/86	StrikeSlip	5.9	5.9	12206	25.8	N00E	0.145

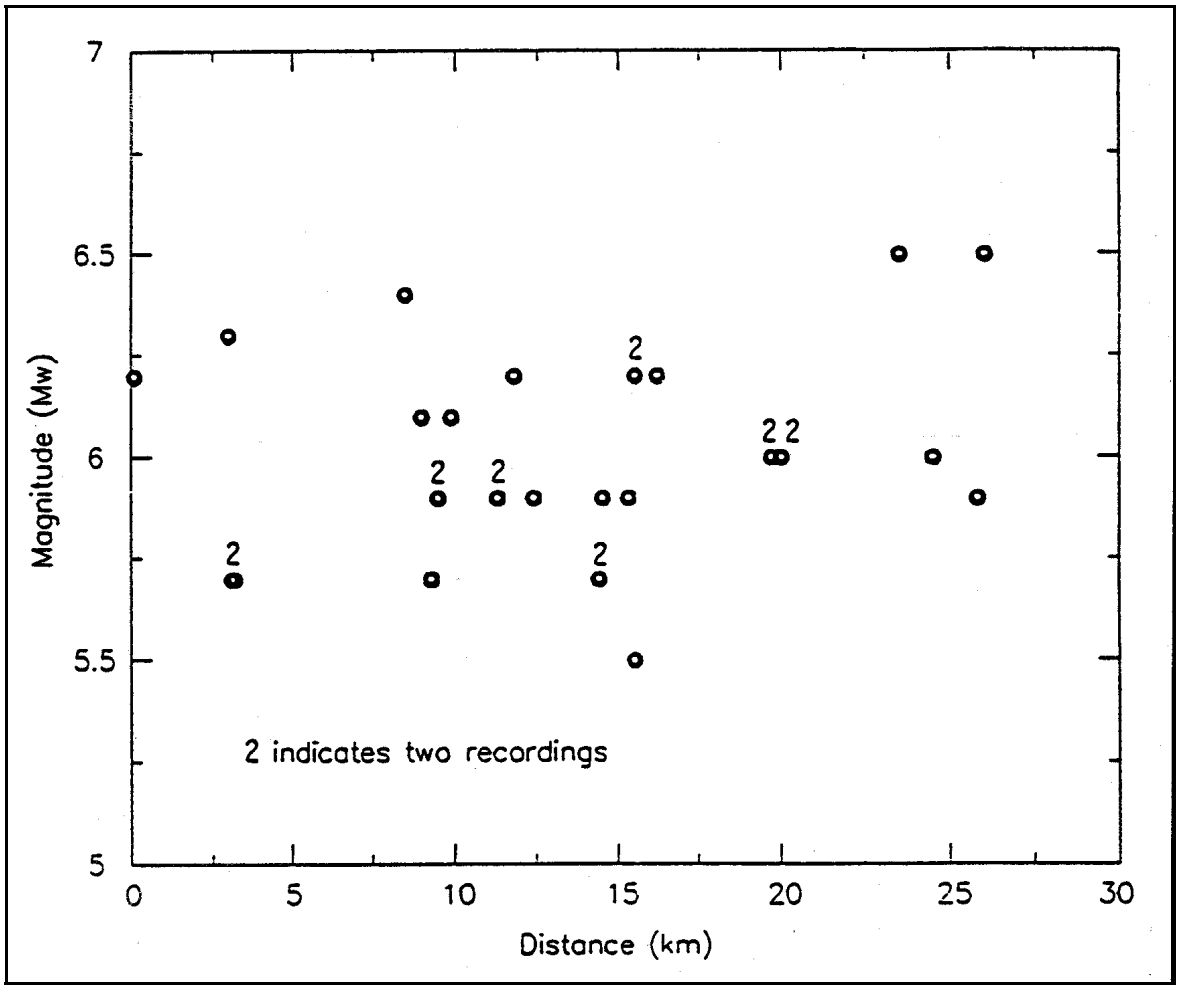

Figure D-1. Scattergram of recordings used in the example analysis

Table D-2
Probability of an Event Occurring in a Distance Band Versus Percentage of Data Set in Distance Band

Distance Range, km	Probability of a Random Event in Distance Band	Fraction of Data Set in Distance Band
0 - 5	0.04	0.133
5 - 10	0.12	0.200
10 - 15	0.20	0.233
15 - 20	0.28	0.233
20 - 25	0.36	0.200

data set was performed on the logarithm of spectral pseudo-relative velocity (PSRV). Several studies (e.g., Esteva 1969; McGuire 1974; Campbell 1981; Abrahamson 1987) have shown that the variability in recorded ground motions is best modeled by a lognormal distribution. The results of the analysis are shown in Figure D-2 in terms of the median (50th percentile) and median plus one standard deviation (84th percentile) of the fitted lognormal distribution for a damping value of 5 percent.

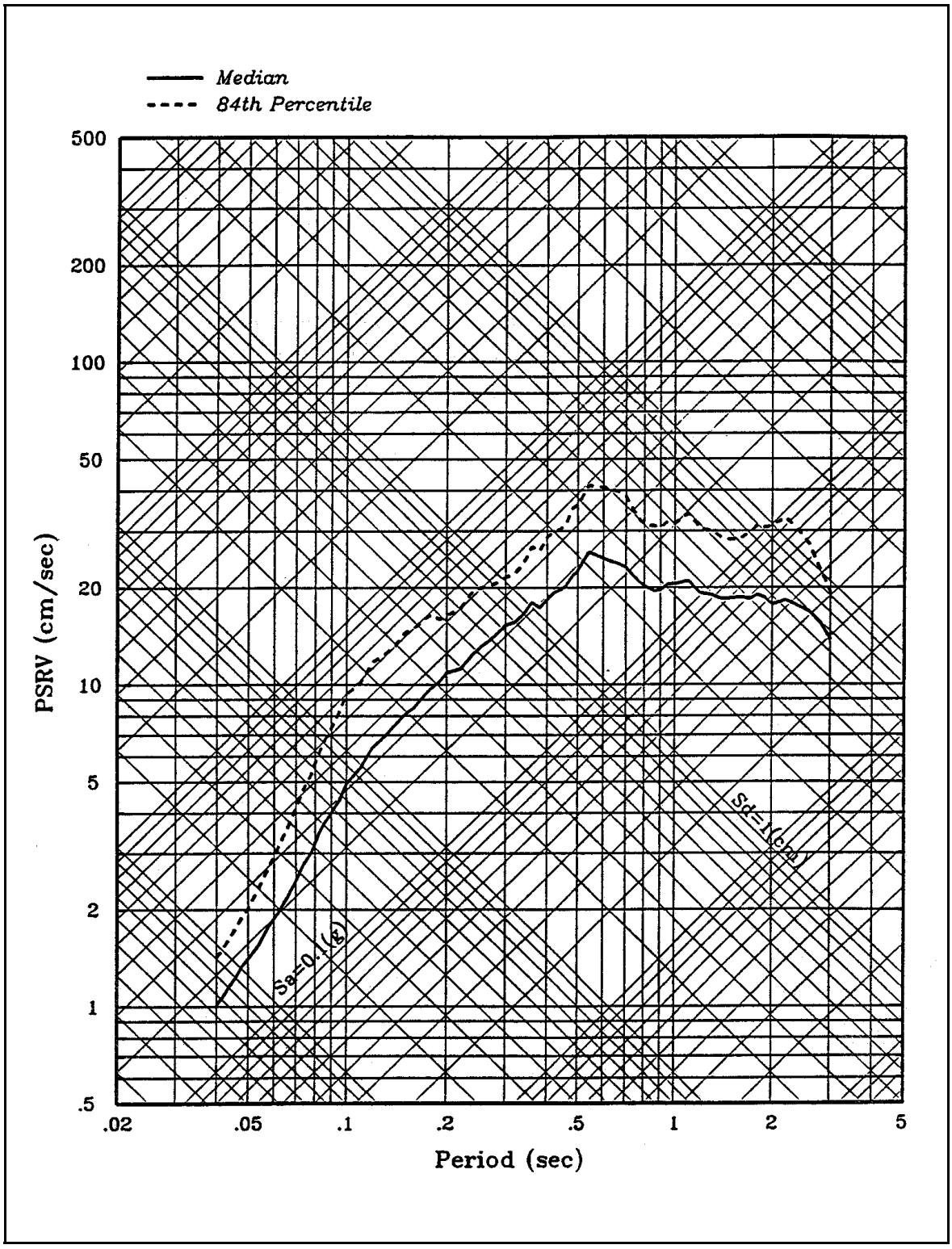

Figure D-2. Horizontal response spectra (5 percent damping) from statistical analysis of selected rock recordings, shallow crustal random earthquake (M6 at R ≤ 25 km)

D-3. Estimates of Site-Specific Spectra Using Attenuation Relationships

a. As mentioned in paragraph D-2, attenuation relationships can be used to estimate the median and 84th-percentile ground motions for an event occurring randomly within a specified distance from the site. In this approach, the mean log ground motion level, E [ln (Y)], is given by

$$E\ [\ln\ (Y)] = \int_M \int_R f(M) \bullet f(R) \bullet E\ [\ln\ (Y) \mid m,r]\ dr\ dm \qquad \text{(D-1)}$$

where

$f(M)$ = probability density function for the event magnitude

$f(R)$ = probability density function for the distance to a random event

E [ln (Y) $\mid$ m,r] = mean log ground motion level given by the attenuation relationship for a specific magnitude m and distance r

The 84th-percentile ground motion level is found by solving iteratively for the value, y, that satisfies the equation

$$\int_M \int_R f(M) \bullet f(R) \bullet P(Y>y \mid m,r) dr\ dm = 0.8416 \qquad \text{(D-2)}$$

where $P(Y>y \mid m,r)$ is given by the cumulative normal probability function assuming the ground motions are lognormally distributed about the mean log value specified by the attenuation relationship.

b. This approach can be viewed as the use of an attenuation relationship to simulate a very large artificial data set with the distance distribution of earthquake magnitudes and source-to-site distances, and then performing a statistical analysis of that data set. In this case, because the simulated data will have the desired distance distribution, weighting functions are not necessary.

c. This approach is illustrated for a rock site in the eastern United States located within a large seismic source zone where no active faults were identified. The site is the same as for Example 5 in Appendix G. The probability distribution for the earthquake magnitude of the maximum credible earthquake (MCE) in the source zone is (probabilities in parentheses): m_b 5.5 (0.06), m_b 6 (0.47), m_b 6.5 (0.27), m_b 7 (0.15), m_b 7.5 (0.05) (mean value m_b 6.3, where m_b is body wave magnitude). The MCE was assumed to occur randomly within a 25-km-radius circle around the site. The length of fault rupture associated with an MCE of a given magnitude was incorporated into the development of the distance distribution. This procedure produces a smaller average distance to a random event within the circle than does a point source assumption. The attenuation relationships for peak ground acceleration and response spectral accelerations of rock motions of Electric Power Research Institute (1993) (later published as Toro, Abrahamson, and Schneider (1997), Tables 3-1 and 3-3 of this manual) were used. These relationships are applicable to rock sites in the eastern United States. The relationships are characterized by increased high-frequency ground motions compared with ground motions at western United States rock sites (see paragraph 3-4 of this manual). As described in Example 5 in Appendix G, an adjustment to these relationships was made to account for somewhat softer rock at the site than the hard rock applicable to the attenuation relationships. The median response spectrum for MCE ground motions at the site resulting from the analysis is shown in Figure D-3.

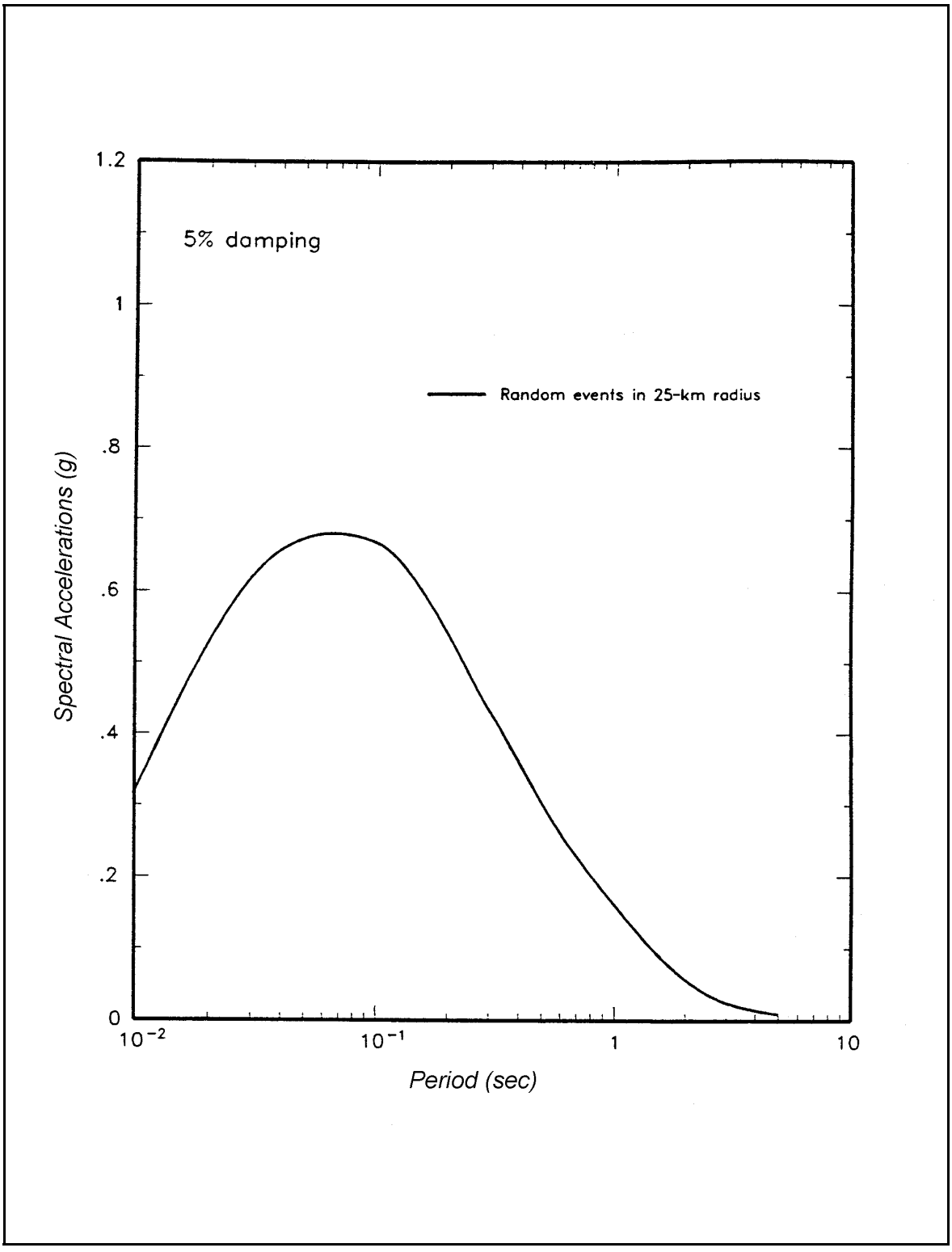

Figure D-3. Horizontal site response spectrum for MCE in seismic source zone Iapetan Rifted Margin in vicinity of site

Appendix E
Ground Response Analysis to Develop Site-Specific Response Spectra at Soil Sites

E-1. Steps in Ground Response Analysis

This appendix describes one-dimensional ground response analyses, which are often used to modify earthquake motions in bedrock to account for the effects of a soil profile at a site. Steps involved in ground response analyses to develop site-specific response spectra at a soil site are briefly summarized below and are illustrated by an example.

a. Characterization of site conditions. Based on results of field and laboratory investigation programs, one or more idealized soil profiles are developed for the site. Site characterization includes development of dynamic soil properties (e.g., shear modulus and soil damping and their variations with shearing strain) for each soil layer present at the site.

b. Selection of rock motions. Appropriate rock motions (either natural or synthetic acceleration time-histories) are selected or developed to represent the design rock motion for the site. If natural time-histories are used, a suite of time-histories that have ground motion characteristics (e.g., peak ground motion parameters, response spectral content, and duration of strong shaking) generally similar to characteristics estimated for the design rock motions are selected. The response spectra for the selected rock motions should, in aggregate, approximately fit or reasonably envelop the design rock spectrum developed for the site. Natural time-histories may be scaled by a factor to improve the match to the design rock spectrum. If synthetic time-histories (i.e., recorded time-histories modified to achieve a match to a smooth response spectrum) are used, their spectra should approximately fit the design rock spectrum. The duration of shaking should also be reasonable. It is desirable that more than one synthetic time-history be used. Preferably, rock motions are assigned at a hypothetical rock outcrop at the site, rather than directly at the base of the soil profile. This is because the knowledge of rock motions is based on recordings at rock outcrops; and unless the rock is rigid, the motions at the base of the soil profile will differ from those of the outcrop. (The differences increase as the ratio of shear wave velocity of rock to shear wave velocity of soil decreases.) Some computer codes allow the rock motion to be assigned as an outcropping motion.

c. Ground response analyses and development of ground surface response spectra. Using the rock time-histories as input motions, ground response analyses are conducted for the modeled soil profile(s) to compute ground motions at the ground surface. Nonlinear soil response is approximated by either equivalent linear analysis methods (e.g., SHAKE (Schnabel, Seed, and Lysmer 1972), or WESHAKE (Sykora, Wahl, and Wallace 1992)) or nonlinear analysis methods (e.g., DESRA (Lee and Finn 1985) or SUMDES (Li 1990)). Parametric analyses should be made to incorporate uncertainties in dynamic soil properties. Analyses are generally made for best-estimate (average), upper-bound, and lower-bound soil properties. Response spectra of the ground surface motions are calculated for the various analyses made. These response spectra can then be statistically analyzed and/or interpreted in some manner to develop design response spectra of surface motions. The time-histories obtained from the site response analyses can be used as representative time-histories of surface motions. Because the response spectra of the input rock time-histories may not closely match the rock design response spectrum (particularly when natural time-histories are used), it may be desirable to obtain “site amplification ratios” from the ground response analyses rather than using the response spectra of calculated surface motions directly. Site amplification ratios are ratios of the response spectra of the ground surface motions computed from the

ground response analyses divided by the response spectra of the corresponding input rock motions. Statistical analyses can be made on the amplification ratios or some other method used to obtain design amplification ratios. The estimated response spectrum at the ground surface is then obtained by multiplying the site amplification ratios by the design rock response spectrum over the entire period range. A design response spectrum is then developed by further smoothing the estimated ground surface response spectrum as required. The time-histories from the ground response analyses can be used directly to represent ground surface motions, or synthetic time-histories can be developed to match the design ground surface response spectrum.

E-2. Example Ground Response Analysis

The procedure described in paragraph E-1 for development of site-specific response spectra at the ground surface of a soil site is illustrated by the example described below. Based on results of field and laboratory investigation programs, the site was idealized by the soil profile shown in Figure E-1. Variations of shear modulus (expressed as the ratio of shear modulus G to the maximum shear modulus G_{max} at a very low strain of 0.0001 percent) and damping ratio with shear strain for clays and for sand were selected as shown in Figures E-2 and E-3, respectively. Three sets of natural time-histories (two components for each set) were selected to represent the design rock motions. Ground response analyses including parametric variations in soil properties were performed. A comparison of response spectra of the computed ground surface motion and the input rock motion for a single analysis is shown in Figure E-4. Typical site amplification ratios computed for average soil properties for three sets of rock motions are shown in Figure E-5. Based on these results, an estimate of site amplification ratios was selected and used to multiply the design rock response spectrum to develop an estimate of the ground surface response spectrum. This spectrum was then smoothed to develop the design response spectrum. The resulting design soil response spectrum is compared with the design rock response spectrum in Figure E-6, which plots the spectral pseudo-relative velocity (PSRV) versus the period.

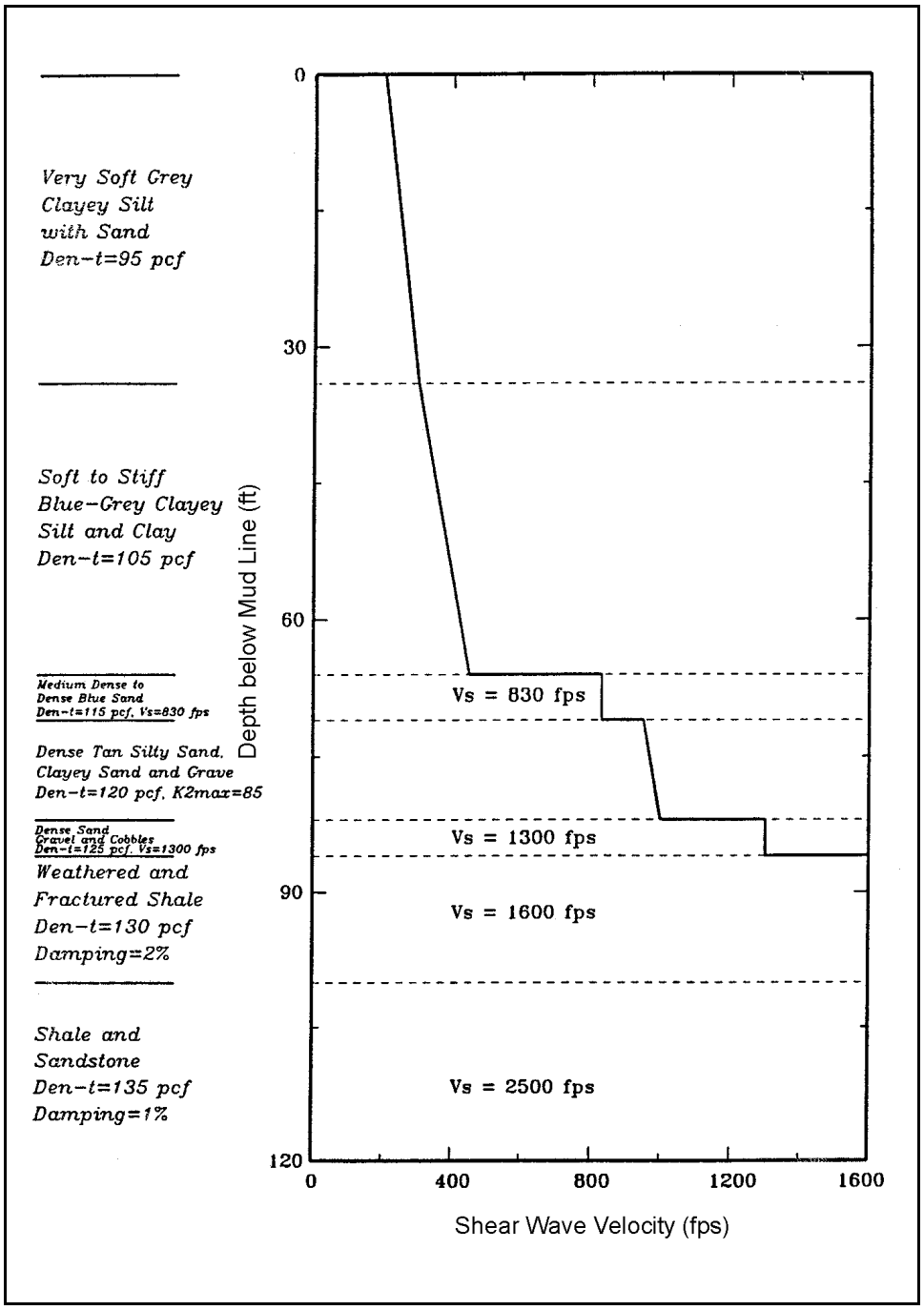

Figure E-1. Estimated shear wave velocity. Note: Den-t = total density; Vs = shear wave velocity; $K2_{max}$ = shear modulus coefficient (1 pcf = 16.02 kg/m^3; 1 fps = 0.305 m/sec)

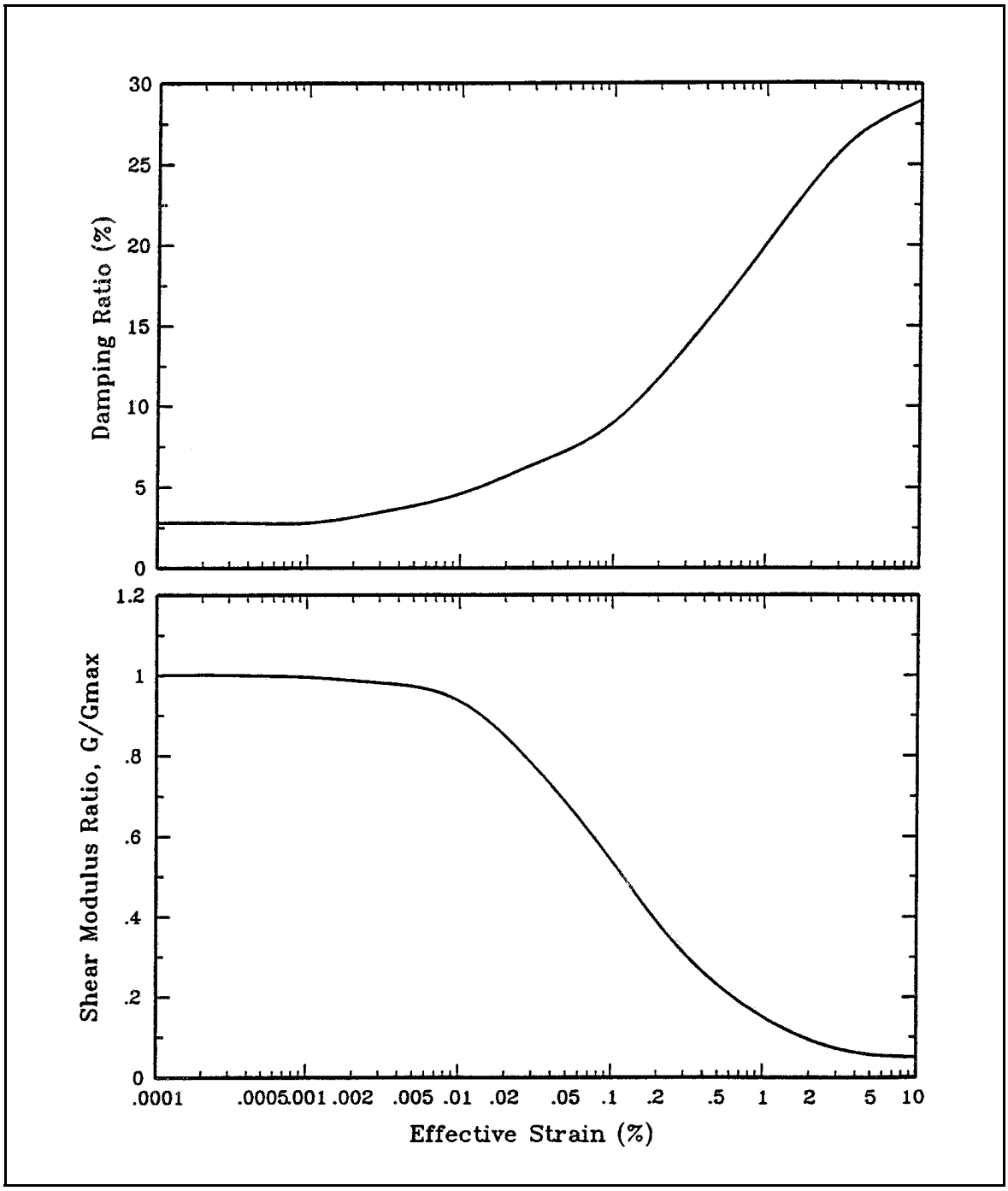

Figure E-2. Variation of shear modulus and damping ratio with shear strain for clays (Seed and Sun 1989, courtesy of Earthquake Engineering Research Center, University of California at Berkeley)

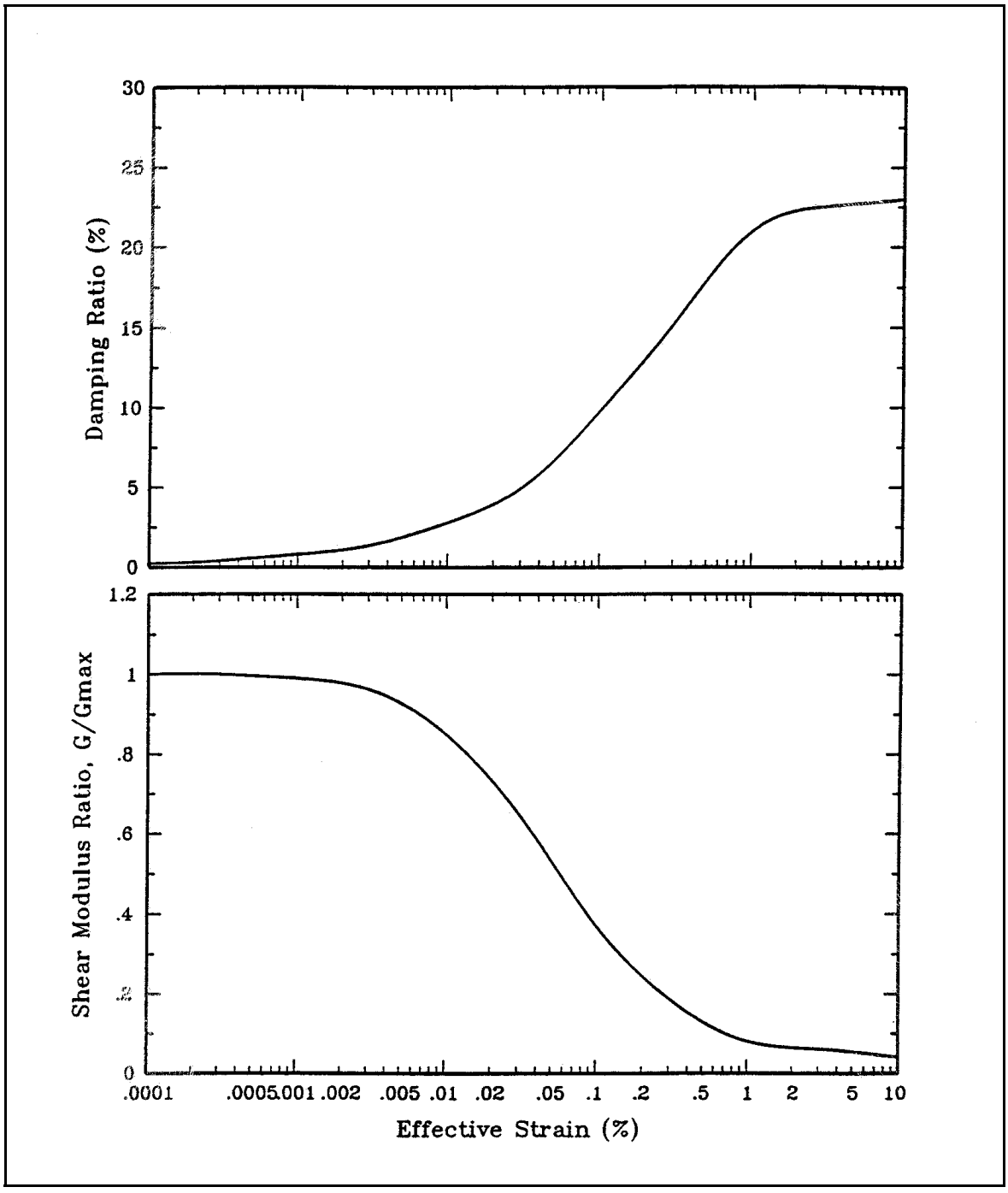

Figure E-3. Variation of shear modulus and damping ratio with shear strain for sand (Seed and Idriss 1970, courtesy of Earthquake Engineering Research Center, University of California at Berkeley)

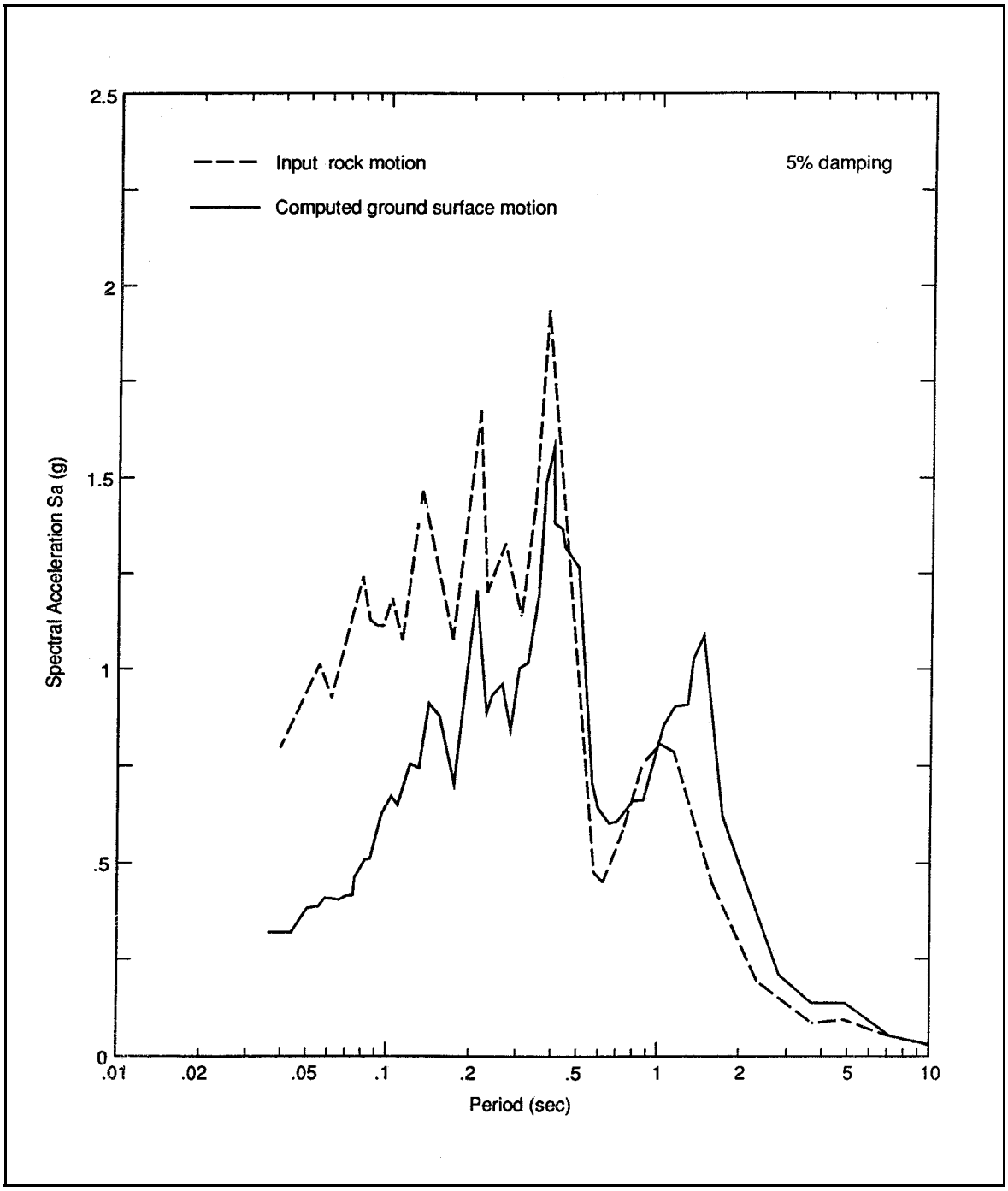

Figure E-4. Comparison of response spectra of computed ground surface motion with input rock motion, average soil properties

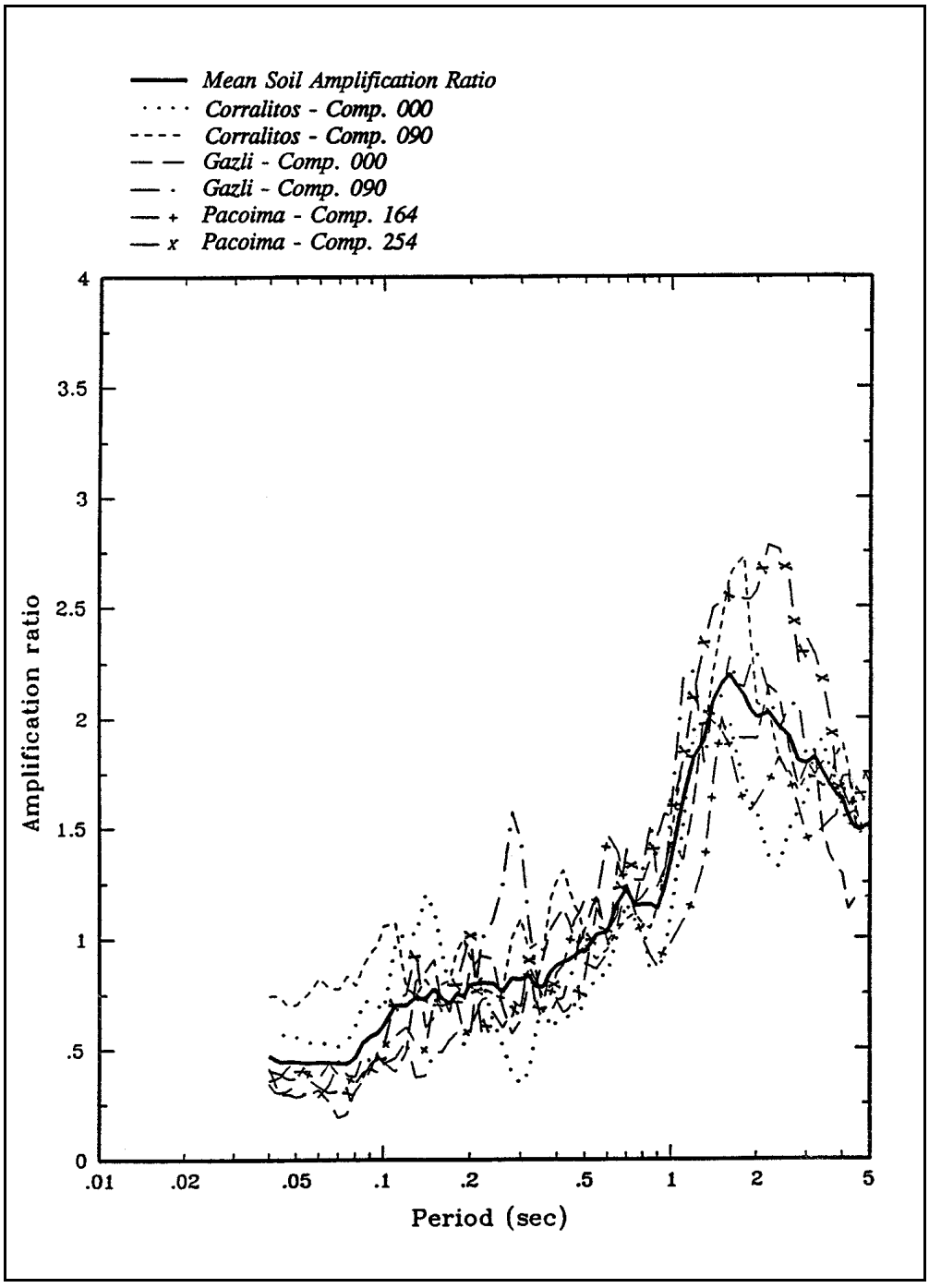

Figure E-5. Soil amplification ratios, average soil properties

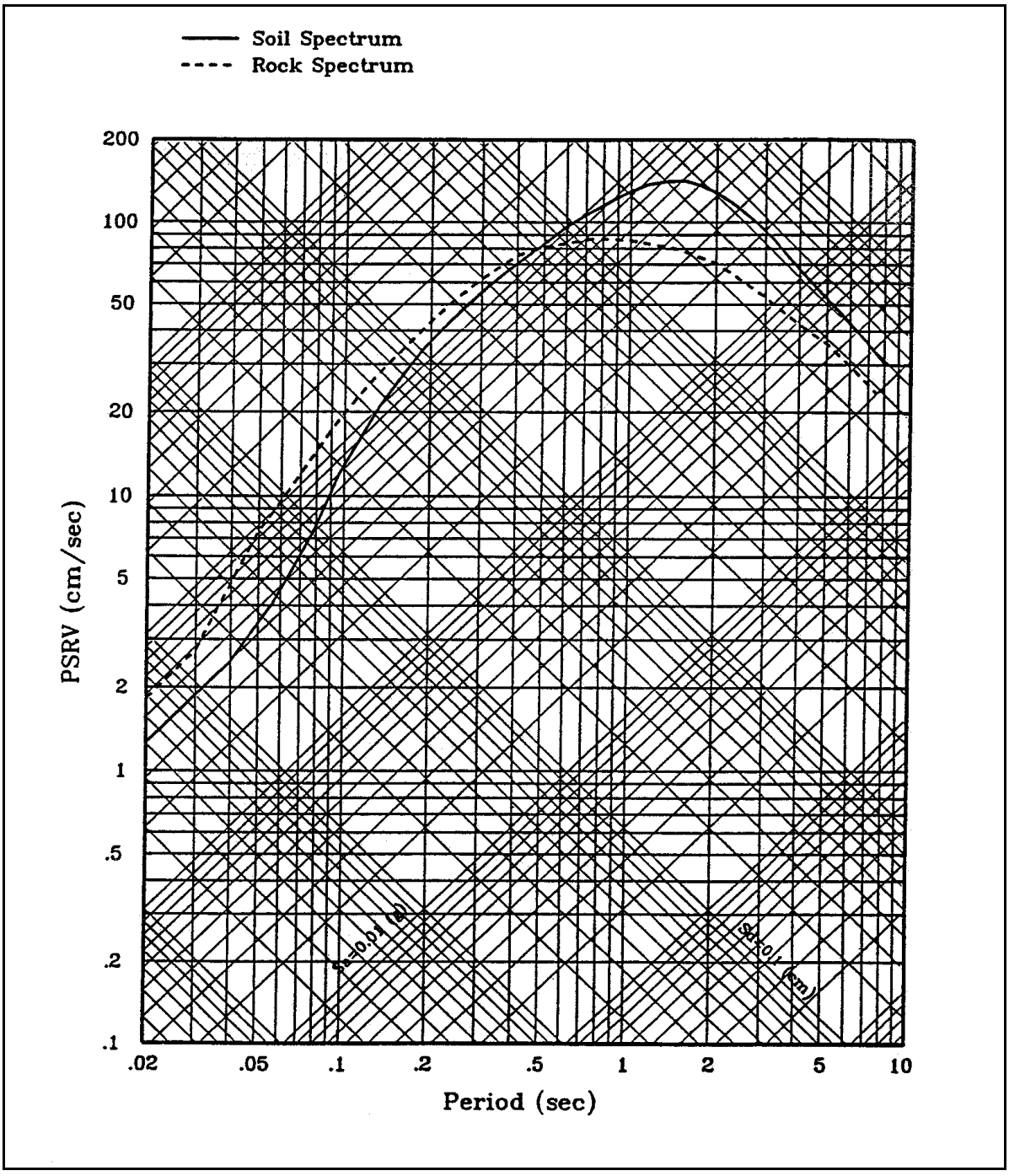

Figure E-6. Median smooth soil spectrum (5 percent damped)

Appendix F
Use of Logic Trees in Probabilistic Seismic Hazard Analysis

F-1. Logic Trees in Probabilistic Seismic Hazard

a. Introduction. The assessment of seismic hazards, whether on a deterministic or a probabilistic basis, must address uncertainties caused by an incomplete understanding of the mechanisms that control the complex process of earthquake generation and seismic wave propagation. Because of this uncertainty, seismic hazards must be assessed using assumptions about what constraints the available information provides on the location, size, and likelihood of occurrence of future earthquakes and their effects on a site. These uncertainties can be dealt with by a variety of approaches, ranging from simple engineering judgment to formal probabilistic treatment. Formal probabilistic treatment of uncertainty has the advantages of quantifying judgments that are always made in any assessment of seismic hazard and providing a framework for assessing the impact of new data or knowledge on an assessment.

b. Logic trees. Logic trees provide a convenient form for formal and quantitative treatment of uncertainty. The use of logic trees in probabilistic seismic hazard analysis has a long history, ranging from weighting of a few alternative assumptions (Cornell and Merz 1975; McGuire 1977; McGuire and Shedlock 1981) to full uncertainty treatment for all of the inputs to a probabilistic seismic hazard assessment (Kulkarni, Youngs, and Coppersmith 1984; Coppersmith and Youngs 1986; Electric Power Research Institute 1987; National Research Council 1988). Logic tree analysis consists of specifying a sequence of assessments that must be made in order to perform an analysis and then addressing the uncertainties in each of these assessments in a sequential manner. Thus, it provides a convenient approach for breaking a large, complex assessment into a sequence of smaller, simpler components that can be more easily addressed.

c. Structure. The general structure of a logic tree is shown in Figure F-1a. The logic tree is composed of a series of nodes and branches. Each node represents an assessment of a state of nature or an input parameter value that must be made to perform the analysis. Each branch leading from the node represents one possible discrete alternative for the state of nature or parameter value being addressed. If the variable in question is continuous, it can be discretized at a suitable increment. The branches at each node are intended to represent mutually exclusive and collectively exhaustive states of the input parameter. In practice, a sufficient number of branches are placed at a given node to adequately represent the uncertainty in the parameter estimation, as discussed in paragraph F-2.

F-2. Probabilities

a. Assigning probabilities. Probabilities that represent the relative likelihood or degree of belief that the branch represents the correct value or state of the input parameter are assigned to each branch. These probabilities are assessed conditionally on the assumption that all the branches leading to that node represent the true state of the preceding parameters. Because they are conditional probabilities for an assumed mutually exclusive and collectively exhaustive set of values, the sum of the conditional probabilities at each node is unity. The probabilities are usually based on subjective judgments because the available data are often too limited to allow for statistical analysis, and because scientific judgment is needed to weigh alternative interpretations of the available data. The logic tree approach simplifies these subjective assessments because the uncertainty in a single parameter is considered individually with all other parameters leading up to that parameter assessment assumed to be known with certainty. Thus, the nodes of the logic tree are sequenced to provide for the conditional aspects or dependencies among the

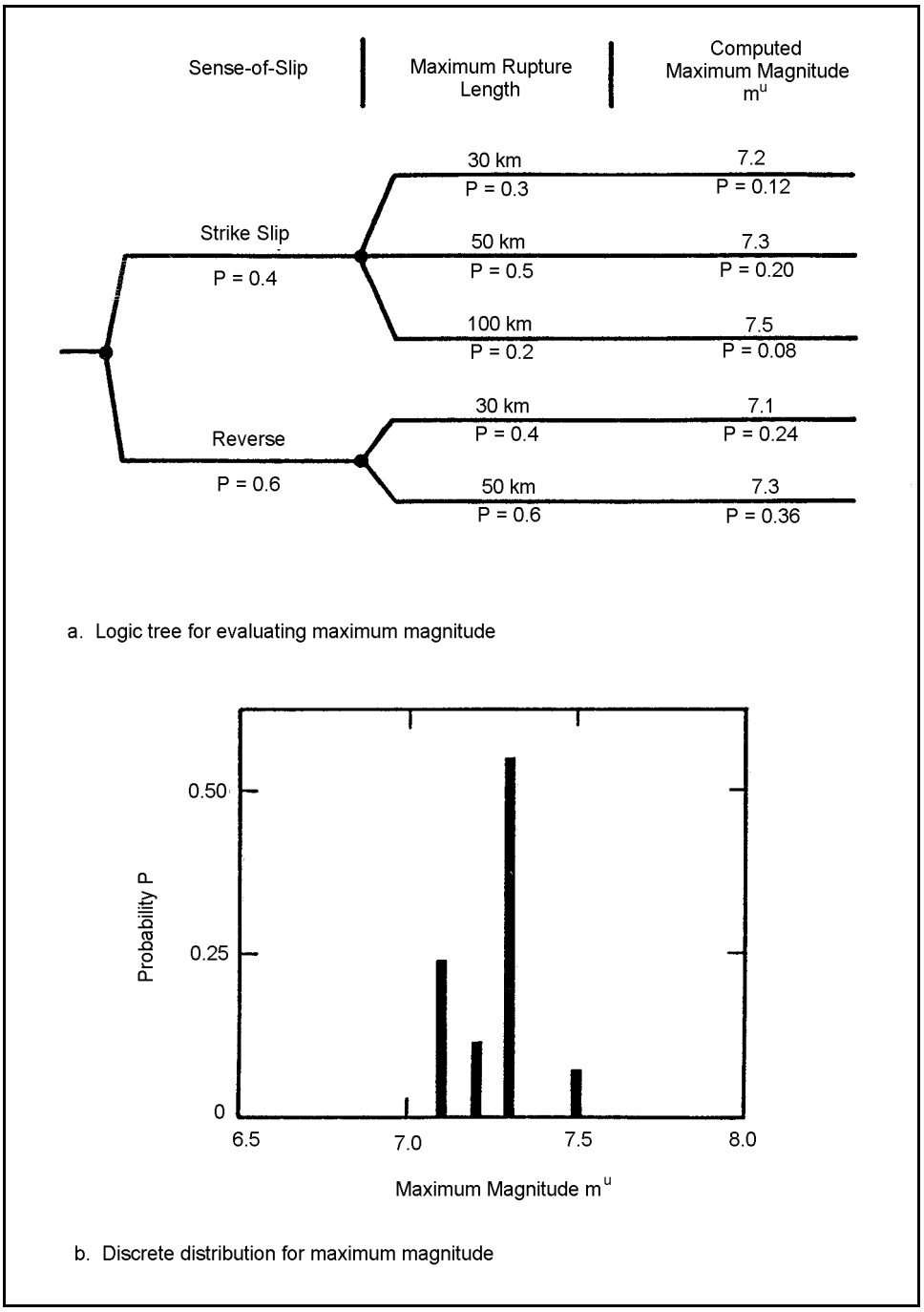

Figure F-1. Example logic tree for evaluating maximum magnitude

parameters and to provide a logical progression of assumptions from the general to the specific in defining the input parameters for an evaluation. In most cases, the probabilities assigned to the branches at a node are in units of tenths, unless there is a basis for more fine-scale resolution.

b. Types of probability assessments. Usually these weights represent one of two types of probability assessments.

(1) In the first, a range or distribution of parameter values is represented by the logic tree branches for that parameter and their associated weights. For example, the slip rate on a fault is usually uncertain because of uncertainties in the amount of displacement of a particular geologic unit across the fault and the age of the unit. The resulting slip rate is usually represented by a preferred value and a range of higher and lower values, similar to a normal or lognormal statistical distribution. This type of distribution can be represented by three (or more) branches of a logic tree. For example, Keefer and Bodily (1983) have shown that a normal distribution can be reliably represented by three values: the central estimate (with a weight of 0.6) and a higher and lower value (each with weights of 0.2) that represent the 5th and 95th percentiles (about plus or minus two standard deviations). Although a large number of branches for an individual assessment can be included on a logic tree, usually the results are not sensitive to having more than about three branches at any one node in a logic tree with many nodes.

(2) A second type of probability assessment to which logic trees are suited is in indicating a relative preference for or degree of belief in alternative hypotheses. For example, the sense of slip on a fault may be uncertain; two possible alternatives might be strike-slip or reverse-slip. Based on the pertinent data, a relative preference for these alternatives can be expressed by the logic tree weights. A strong preference is usually represented by weights such as 0.9 and 0.1 for the two alternatives. If there is no preference for either hypothesis, they are assigned equal weights (0.5 and 0.5 for two hypotheses). Increasing weights from 0.5 to 0.9 reflect an increasing preference for the alternative. Although the logic tree weights are ultimately subjective judgments based on available information, it is important to document the data and interpretations that led to the assessment of parameter values and to assignment of weights. The example logic tree shown in Figure F-1a might be used to represent the uncertainty in assessing the maximum magnitude for a fault on the basis of a relationship between maximum rupture length per event and earthquake magnitude (e.g., Slemmons 1982). In order to assess the maximum magnitude, two pieces of information are required: the sense of slip *S* of the fault and the maximum rupture length in any one event *RL*. The logic tree thus contains two levels of nodes, one for each parameter. In the example, the particular values that might be assigned to the maximum rupture length are dependent on the assumed sense of slip (strike-slip earthquakes may tend to produce greater rupture lengths than reverse earthquakes) and are thus more easily assessed given knowledge of the sense of slip. Consequently, the node for maximum rupture length per event is located after the node for sense of slip. The assigned weights reflect a slight preference for reverse faulting.

c. Maximum rupture length. The next level of assessment in the example addresses maximum rupture length for a maximum event. A range of possible values is considered for both assumptions about the sense of slip. The probability that 30 km is the correct maximum rupture length per event is assessed conditionally depending on which sense of slip is assumed to be correct. That is, the probability of a 30-km rupture length given strike-slip faulting, $P(RL=30 \mid S=strike\ slip)$, is a separate assessment from $P(RL=30 \mid S=reverse)$, and the two probabilities do not have to be equal. Similar assessments are made for the other branches at each node. In the example there is a preference for longer rupture lengths for strike-slip faulting than for reverse faulting represented by both the parameter values considered and the assessment of relative likelihoods. The logic tree shown in Figure F-1a defines a discrete distribution for the maximum magnitude computed using the relationship developed by Slemmons (1982). The resulting distribution is shown in Figure F-1b. The probability that the maximum magnitude, $m^u(S,RL)$, will take on any particular value $m^u(s_i, rl_j)$ is equal to the joint probability of the set of parameters s_i and rl_j being the true parameter values.

$$P[m^u(s_i, rl_j)] = P(S = s_i) \cdot P(RL = rl_j \mid s_i) \qquad \text{(F-1)}$$

The expected or mean value of $m^u(S,RL)$ given the uncertainty in the input parameters S and RL is given by:

$$E[m^u\ (S,RL)] = \sum_i \sum_j m^u\ (s_i,rl_j) \cdot P(S = s_i) \cdot P(RL = rl_j | s_i) \quad \text{(F-2)}$$

and the variance in $m^u(S,RL)$ is given by:

$$VAR[m^u\ (S,RL)] = \sum_i \sum_j \left\{\left[(m^u(s_i,rl_j)\right] - E[m^u\ (S,RL)]\right\}^2 \cdot P(S = s_i) \cdot P(RL = rl_j | s_i) \quad \text{(F-3)}$$

In analyses with larger logic trees the results can be ordered to allow computation of various percentiles of the discrete distribution formed by the logic tree. (An example of a discrete distribution formed by a small logic tree is given in Example 1 of Appendix G.) Figure F-2 displays a partial logic tree representing a seismic hazard model developed for analysis of the seismic hazard at a site in the North Sea. The logic tree is laid out to provide a logical progression from general aspects/hypotheses regarding the characteristics of seismicity and seismic wave propagation in the region to specific input parameters for individual sources. The rationale for developing the various levels of the logic tree is discussed in paragraph F-3. The bases for selecting the parameter values and assigning relative weights are presented in Coppersmith and Youngs (1986).

F-3. Nodes

The first node of the logic tree represents the uncertainty in selecting the appropriate strong ground motion attenuation relationship. Attenuation was placed first in the tree because it is felt that a single relationship (whichever relationship may be "correct") is applicable to all earthquake sources in the region. The second node of the logic tree represents the uncertainty in identifying what structures and processes are giving rise to earthquakes in the region. The fault model assumes the activity is occurring on reactivated normal faults that have been mapped using high-resolution seismic refraction and reflection surveys. The source zone model assumes that the sources of earthquakes are unknown except for their general extent as imaged by the historical seismicity. The next node applies to the fault source model only and addresses the question of differences in the rate of activity of the identified faults defined on the basis of differences in the age and amount of recent slip. The following nodes address the uncertainty in specifying the depth distribution of earthquake activity, the details of seismic zonation in the North Sea region, alternative constraints on earthquake recurrence parameters (*b*-value), and the appropriate relationship between earthquake magnitude and rupture size. All the levels of the logic tree to this point are assumed to apply universally to all sources. The logic tree is now expanded into subtrees to address parameters that vary independently from source to source. These include the sense of slip on individual sources, the dip of fault planes, and individual source maximum magnitudes. Each end branch of the logic tree shown in Figure F-2 defines a particular characterization of the seismic sources and ground motion attenuation in the region for which the rate of exceedance of ground motions at the site can be computed. The likelihood that this computation is the "correct" hazard at the site is given by the product of all the conditional probabilities along the path through the logic tree. The end branches thus define a discrete distribution for $v(z)$ (see Section III, Chapter 3).

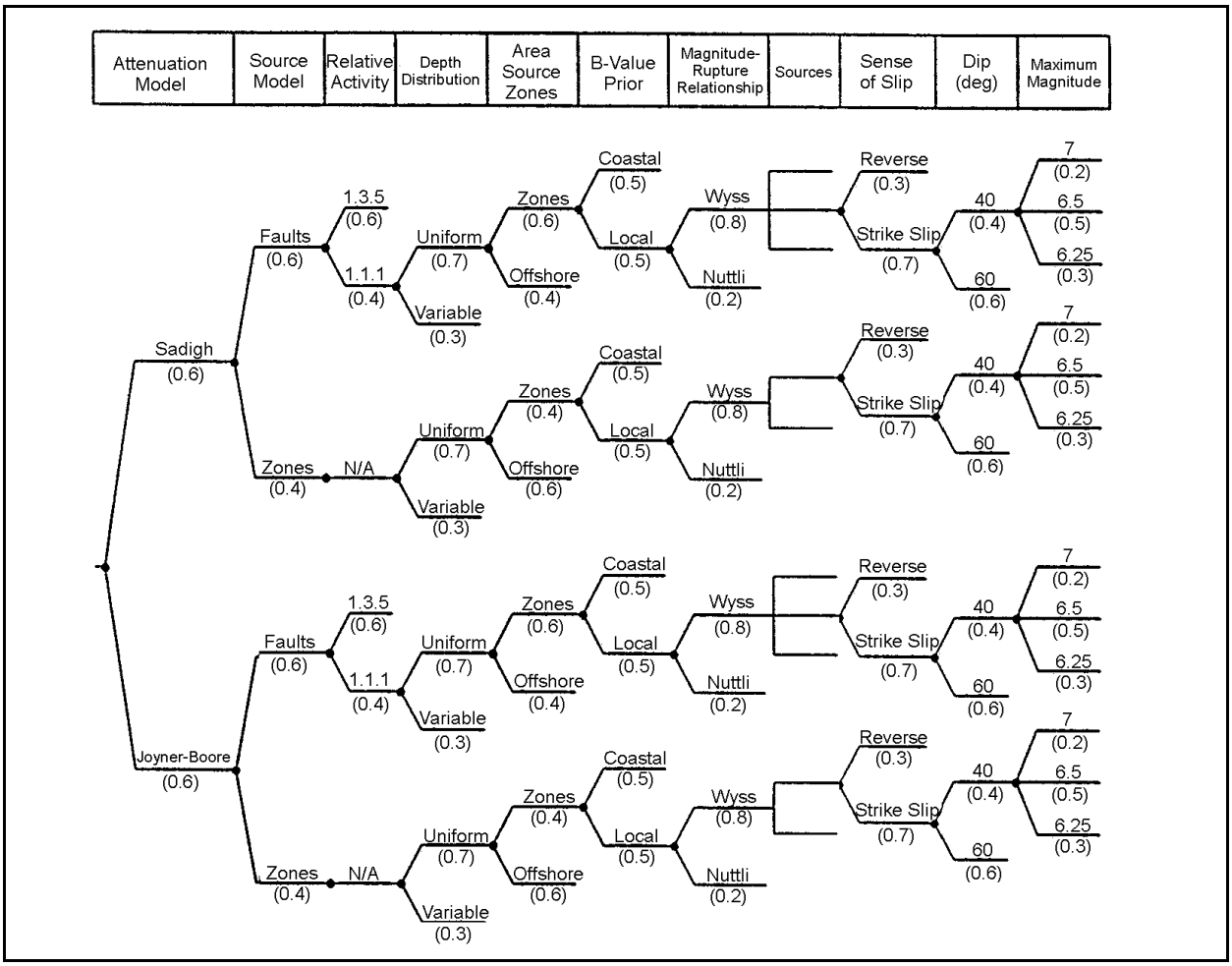

Figure F-2. Seismic hazard model logic tree for North Sea site

Appendix G
Examples of Probabilistic Seismic Hazard Analysis

Section I
Example 1
Simplified Calculation of Probabilistic Seismic Hazard

G1-1. Introduction

a. This example presents a simplified seismic hazard analysis illustrating the steps involved in computing the frequency of exceedance of a peak ground acceleration of 0.2 g at a site, $\nu(0.2)$. The frequency of exceedance is computed using the equation

$$\nu(z) = \sum_N \left[\sum_M \lambda(m_i) \cdot \sum_R P(R = r_j \mid m_i) \cdot P(Z > z \mid m_i, r_j) \right]_n \quad \text{(G1-1)}$$

The calculation involves the following steps:

(1) Computing the frequency of occurrence of events of magnitude m_i on source n, $(\lambda(m_i))$.

(2) Calculating the probability distribution for distances from the site to events of magnitude m_i on source n, $(P(R = r_j \mid m_i))$.

(3) For each source-to-site distance, computing the probability that an event of magnitude m_i will exceed the specified ground motion level z, $(P(Z > z \mid m_i, r_j))$.

The total rate of exceedance is then obtained by summing over all distances for a given event magnitude, and then over all event magnitudes.

The example calculation presented in this section is performed using the input parameters for the two seismic sources defined in Figure G1-1.

G1-2. Computation of Event Rates, $\lambda(m_i)$

a. The first step is the computation of the rate of occurrence of events of magnitude m_i, $\lambda(m_i)$. These are obtained by discretizing the cumulative recurrence relationship at a specified discretization step size, Δm. The cumulative earthquake recurrence relationship is given by the truncated exponential form of the Gutenberg and Richter recurrence law

$$N(M > m) = \alpha(m^0) \cdot \frac{10^{-b(m-m^0)} - 10^{-b(m^u-m^0)}}{1.0 - 10^{-b(m^u-m^0)}} \quad \text{(G1-2)}$$

where

m^0 = lower bound magnitude of interest to the calculation

m^u = maximum magnitude event that can occur on the source

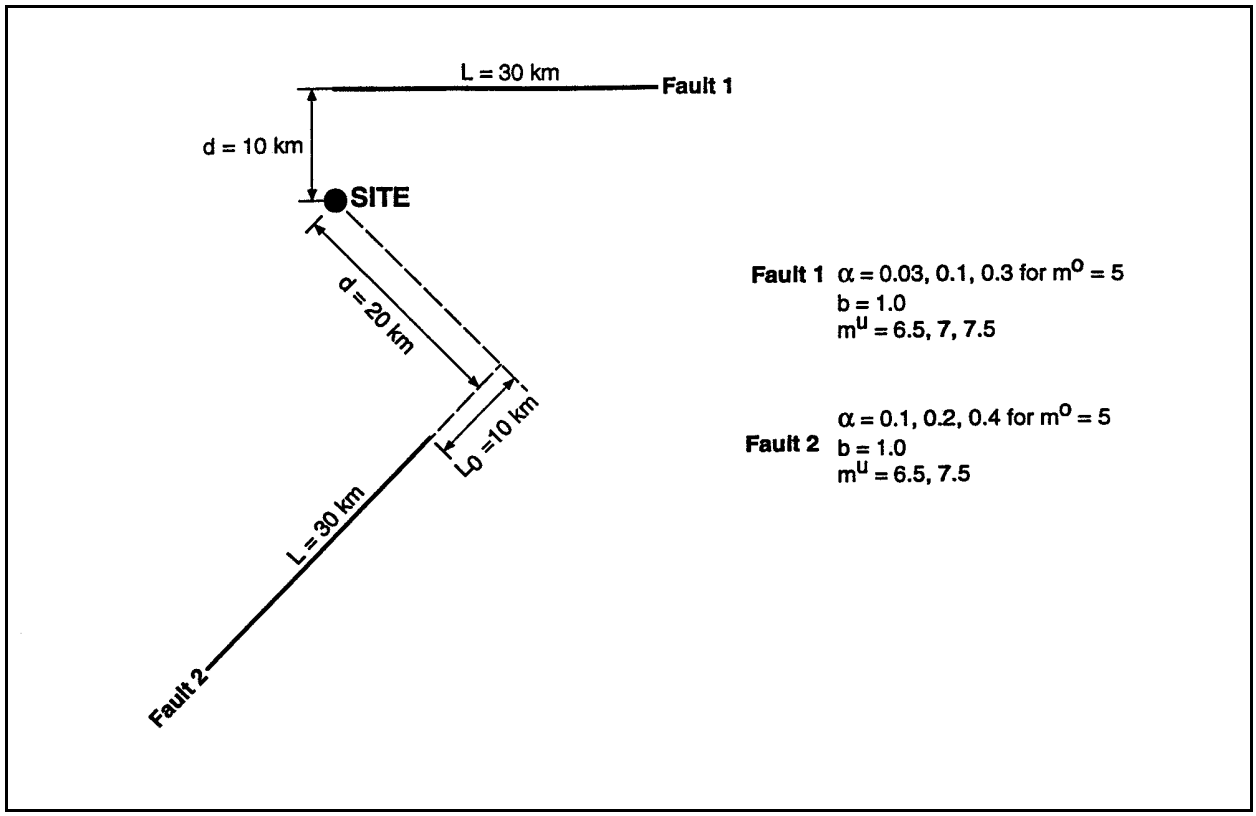

Figure G1-1. Example problem

b = slope or b-value of the recurrence curve

$\alpha(m^0)$ = frequency of occurrence of events of magnitude m^0 and larger

b. The computation of the event rate is given by the expression

$$\lambda(m_i) = N(m > m_i - \Delta m/2) - N(m > m_i + \Delta m/2) \quad \text{(G1-3)}$$

Using a discretization step, Δm = 0.5, gives $\lambda(m_i)$ for Fault 1 using the following parameters (see Figure G1-1):

m^0 = 5.0, $\alpha(m^0)$ = 0.1, b = 1.0, m^u = 6.5, 7.0, 7.5.

c. The calculation procedure is illustrated in Figure G1-2 for the specific case of computing λ(m = 5.5) given $\alpha(m^0)$ = 0.1, b = 1.0, and m^u = 6.5. Using Equation G1-2, the computed cumulative number of events of magnitude greater than $m - \Delta m/2 = 5.25$ is 0.0548 and the cumulative number of events of magnitude greater than $m + \Delta m/2 = 5.75$ is 0.0151. Using Equation G1-3, $\lambda(m = 5.5) = 0.0548 - 0.0151 = 0.0397$. This calculation is repeated for all of the events that are considered for a given maximum magnitude. These calculations are tabulated in Table G1-1 for the three maximum magnitude values.

d. The earthquake recurrence rates for $\alpha(m^0)$ = 0.03 and 0.3 are equal to 0.3 and 3.0 times the values in Table G1-1. Similarly, $\lambda(m_i)$ for Fault 2 is obtained using the following parameters (Figure G1-1):

m^0 = 5.0, $\alpha(m^0)$ = 0.2, b = 1.0, m^u = 6.5, 7.5 (Table G1-2).

Table G1-1
Earthquake Recurrence Frequencies for Fault 1

	$m^u = 6.5$			$m^u = 7$			$m^u = 7.5$		
m_i	$N(m > m_i - \Delta m/2)$	$N(m > m_i + \Delta m/2)$	$\lambda(m_i)$	$N(m > m_i - \Delta m/2)$	$N(m > m_i + \Delta m/2)$	$\lambda(m_i)$	$N(m > m_i - \Delta m/2)$	$N(m > m_i + \Delta m/2)$	$\lambda(m_i)$
5	0.10000	0.05480	0.04520	0.10000	0.05579	0.04421	0.10000	0.05610	0.04390
5.5	0.05480	0.01510	0.03971	0.05579	0.01695	0.03884	0.05610	0.01752	0.03857
6	0.01510	0.00254	0.01256	0.01695	0.00467	0.01228	0.01752	0.00532	0.01220
6.5	0.00254	0.00000	0.00254	0.00467	0.00079	0.00388	0.00532	0.00147	0.00386
7				0.00079	0.00000	0.00079	0.00147	0.00025	0.00122
7.5							0.00025	0.00000	0.00025

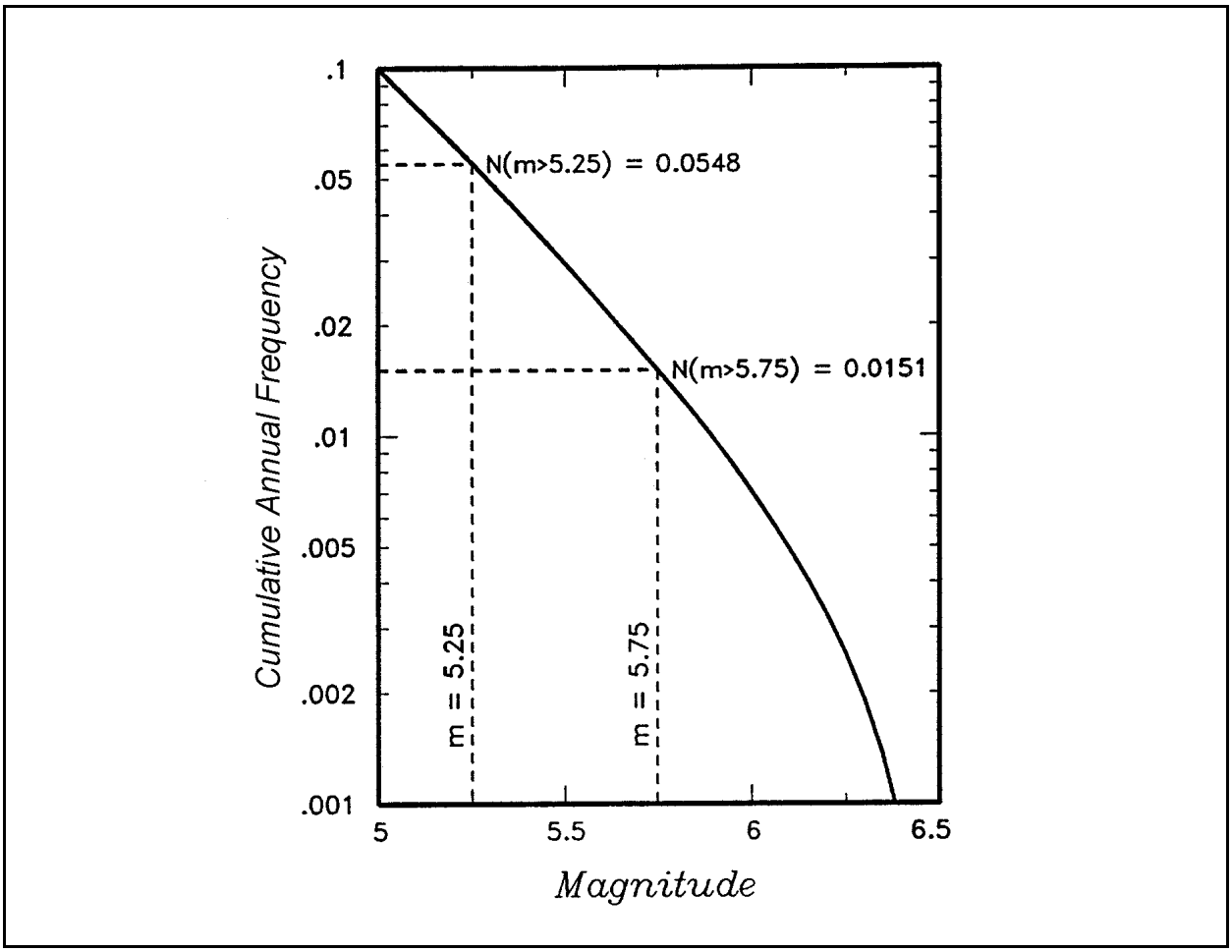

Figure G1-2. Example recurrence rate calculation

Table G1-2
Earthquake Recurrence Frequencies for Fault 2

	$m^u = 6.5$			$m^u = 7.5$		
m_i	$N(m > m_i - \Delta m/2)$	$N(m > m_i + \Delta m/2)$	$\lambda(m_i)$	$N(m > m_i - \Delta m/2)$	$N(m > m_i + \Delta m/2)$	$\lambda(m_i)$
5	0.20000	0.10961	0.09039	0.20000	0.11219	0.08781
5.5	0.10961	0.03020	0.07941	0.11219	0.03504	0.07715
6	0.03020	0.00508	0.02511	0.03504	0.01065	0.02440
6.5	0.00508	0.00000	0.00508	0.01065	0.00293	0.00771
7				0.00293	0.00049	0.00244
7.5				0.00049	0.00000	0.00049

The earthquake occurrence rates for $\alpha(m^0)$ = 0.1 and 0.4 are obtained by multiplying the rates in Table G1-2 by 0.5 and 2.0.

G1-3. Computation of the Conditional Probability Distribution for Source-to-Site Distance

a. The probability distribution for distance from the site to earthquake rupture on the source is computed conditionally on the earthquake magnitude because it is affected by the rupture size of the earthquake rupture.

b. Der Kiureghian and Ang (1977) give the following expression for the cumulative probability distribution to a linear rupture segment uniformly distributed along a linear fault

$$P(R < r) = 0 \qquad \text{for } R < (d^2 + L_0^2)^{1/2}$$

$$P(R < r) = \frac{(r^2 - d^2)^{1/2} - L_0}{L - X(m_i)} \qquad \text{for } (d^2 + L_0^2)^{1/2} \le R < \left\{d^2 + [L + L_0 - X(m_i)]^2\right\}^{1/2} \quad \text{(G1-4)}$$

$$P(R < r) = 1 \qquad \text{for } R > \left\{d^2 + [L + L_0 - X(m_i)]^2\right\}^{1/2}$$

where $X(m_i)$ = rupture length, km, for magnitude m_i given by the equation $X(m_i)$ = MIN [exp (-4.654 + 1.189m_i), fault length]. The MIN function is used to confine the rupture to the fault length. Occasionally, the expected length of rupture, given a magnitude, will exceed the fault length for maximum magnitude estimated by techniques other than rupture length.

c. The conditional distance probability function $P(R = r_j \mid m_i)$ is obtained by discretizing the cumulative distance probability relationship using a suitable step size.

d. Using a discretization step Δr = 5.0 km and the fault geometries shown in Figure G1-1, the discrete distance distributions are obtained for the two faults. The calculation procedure is illustrated in Figure G1-3 for the specific case of computing P(r = 15) given d = 10 km, L_0 = 0, L = 30 km, and $X(m = 5)$ = 3.64 km for Fault 1. Using Equation G1-4, the cumulative probability that $R < 15 - \Delta r/2$ = 12.5 km is 0.2845 and the cumulative probability that $R < 15 + \Delta r/2$ = 17.5 km is 0.5447. The difference between these two cumulative probabilities is the probability that R = 15 km, and is 0.5447 - 0.2845 = 0.2602. This calculation is repeated for all of the distances that are possible for the fault. These calculations are tabulated in Table G1-3 for the two faults.

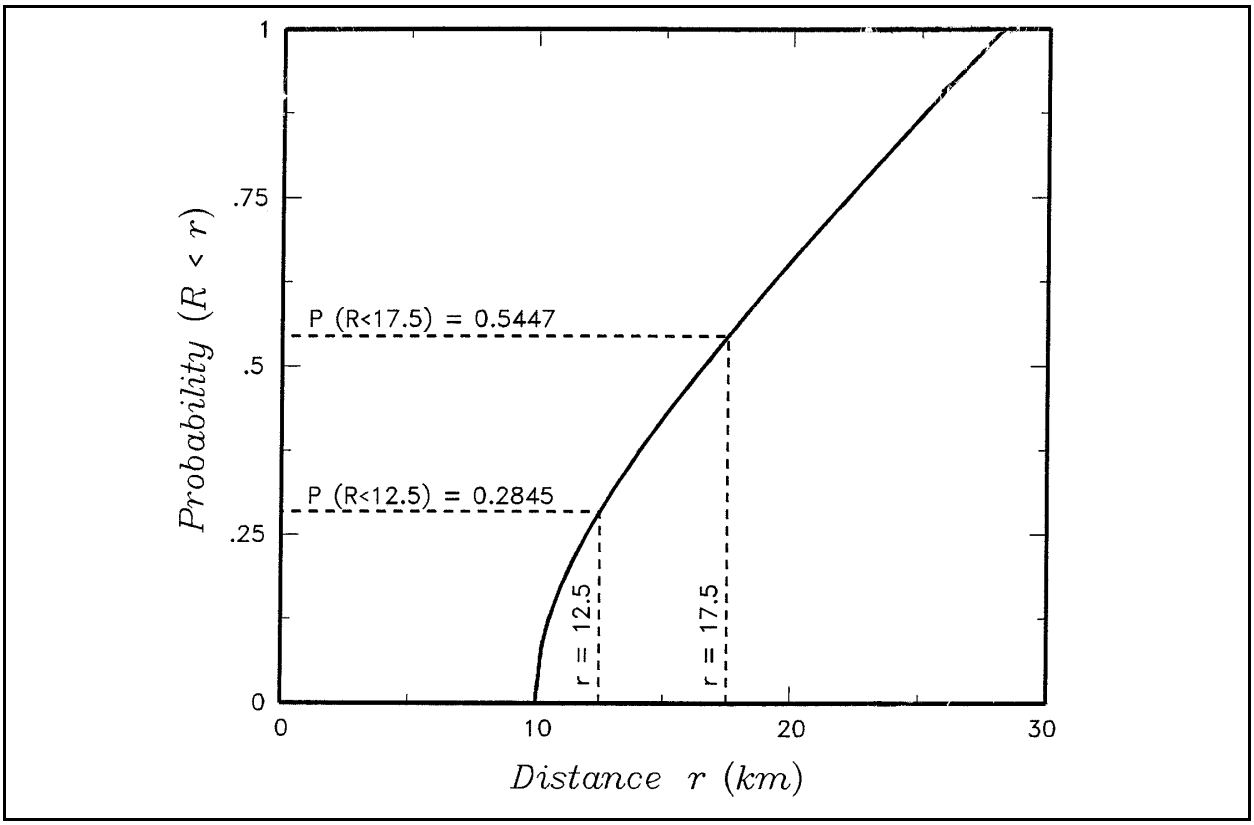

Figure G1-3. Example distance probability calculation

G1-4. Computation of Attenuation Conditional Probability of Exceedance

a. The attenuation conditional probability distribution $P(Z > z \mid m_i, r_j)$ is computed using a lognormal distribution

$$P(Z > z \mid m_i, r_j) = 1.0 - F' \left\{ \frac{\ln(z) - E[\ln(Z)]}{S[\ln(Z)]} \right\} \tag{G1-5}$$

where E [ln (Z)] is the mean log ground motion level given by the attenuation relationship. For this example, the ground motion attenuation relationship for peak acceleration is given by the relationship of Sadigh, Egan, and Youngs (1986):

$$\begin{aligned} E[\ln(Z)] &= -2.611 + 1.1 \cdot m_i - 1.750 \cdot \ln\left(r_j + 0.8217 \cdot e^{0.4814 \cdot m_i}\right) \quad for\ m \le 6.5 \\ E[\ln(Z)] &= -2.611 + 1.1 \cdot m_i - 1.75 \cdot \ln\left(r_j + 0.3157 \cdot e^{0.6286 \cdot m_i}\right) \quad for\ m > 6.5 \end{aligned} \tag{G1-6}$$

where r_j is in km and Z is in g, and S [ln (Z)] is the standard error of the log ground motion level given by the relationship

$$\begin{aligned} S[\ln(Z)] &= 1.26 - 0.14 \cdot m_i \quad for\ m \le 6.5 \\ S[\ln(Z)] &= 0.35 \quad for\ m > 6.5 \end{aligned} \tag{G1-7}$$

Table G1-3
Discrete Distance Distributions for Faults 1 and 2

m_i	$X(m_i)$	r_j	$P(R < r_j + \Delta r/2 \mid m_i)$	$P(R = r_j \mid m_i)$
For Fault 1: d = 10 km, L_0 = 0 km, and L = 30 km				
5	3.64	5	0.0000	0.0000
		10	0.2845	0.2845
		15	0.5447	0.2603
		20	0.7645	0.2198
		25	0.9717	0.2072
		30	1.0000	0.0283
5.5	6.59	5	0.0000	0.0000
		10	0.3204	0.3204
		15	0.6135	0.2931
		20	0.8610	0.2475
		25	1.0000	0.1390
		30	1.0000	0.0000
6	11.94	5	0.0000	0.0000
		10	0.4153	0.4153
		15	0.7953	0.3799
		20	1.0000	0.2047
		25	1.0000	0.0000
		30	1.0000	0.0000
6.5	21.64	5	0.0000	0.0000
		10	0.8970	0.8970
		15	1.0000	0.1030
		20	1.0000	0.0000
		25	1.0000	0.0000
		30	1.0000	0.0000
7	30.00	5	0.0000	0.0000
		10	1.0000	1.0000
		15	1.0000	0.0000
		20	1.0000	0.0000
		25	1.0000	0.0000
		30	1.0000	0.0000
7.5	30.00	5	0.0000	0.0000
		10	1.0000	1.0000
		15	1.0000	0.0000
		20	1.0000	0.0000
		25	1.0000	0.0000
		30	1.0000	0.0000
For Fault 2: d = 20 km, L_0 = 10 km, and L = 30 km				
5	3.64	15	0.0000	0.0000
		20	0.0117	0.0117
		25	0.3366	0.3249

(Continued)

Table G1-3 (Concluded)

m_i	$X(m_i)$	r_j	$P(R < r_j + \Delta r/2 \mid m_i)$	$P(R = r_j \mid m_i)$
		For Fault 2: d = 20 km, L_0 = 10 km, and L = 30 km		
5 (Cont.)	3.64	30	0.5924	0.2558
		35	0.8239	0.2315
		40	1.0000	0.1761
5.5	6.59	15	0.0000	0.0000
		20	0.0131	0.0131
		25	0.3791	0.3659
		30	0.6671	0.2880
		35	0.9279	0.2607
		40	1.0000	0.0721
6	11.94	15	0.0000	0.0000
		20	0.0170	0.0170
		25	0.4914	0.4744
		30	0.8648	0.3734
		35	1.0000	0.1352
		40	1.0000	0.0000
6.5	21.64	15	0.0000	0.0000
		20	0.0368	0.0368
		25	1.0000	0.9632
		30	1.0000	0.0000
		35	1.0000	0.0000
		40	1.0000	0.0000
7	30.00	15	0.0000	0.0000
		20	1.0000	1.0000
		25	1.0000	0.0000
		30	1.0000	0.0000
		35	1.0000	0.0000
		40	1.0000	0.0000
7.5	30.00	15	0.0000	0.0000
		20	1.0000	1.0000
		25	1.0000	0.0000
		30	1.0000	0.0000
		35	1.0000	0.0000
		40	1.0000	0.0000

The distribution is truncated at the 3σ level so that $F'()$ represents the cumulative of a truncated normal distribution

$$F'(U) = \frac{F(U) - F(-3)}{1.0 - 2 \cdot F(-3)} \tag{G1-8}$$

where $F(U)$ is the standard cumulative normal distribution, $U = \{\ln(z) - E[\ln(Z)]\}/S[\ln(Z)]$, and $F(-3)$ is 0.00135. A table of standard normal cumulative probability values is provided in Table G1-4.

Table G1-4
Cumulative Probabilities for Unit Normal Variable

U	*F(U)*	*U*	*F(U)*	*U*	*F(U)*	*U*	*F(U)*	*U*	*F(U)*
-4.00	0.000032	-3.99	0.000033	-3.98	0.000034	-3.97	0.000036	-3.96	0.000037
-3.95	0.000039	-3.94	0.000041	-3.93	0.000042	-3.92	0.000044	-3.91	0.000046
-3.90	0.000048	-3.89	0.000050	-3.88	0.000052	-3.87	0.000054	-3.86	0.000057
-3.85	0.000059	-3.84	0.000062	-3.83	0.000064	-3.82	0.000067	-3.81	0.000069
-3.80	0.000072	-3.79	0.000075	-3.78	0.000078	-3.77	0.000082	-3.76	0.000085
-3.75	0.000088	-3.74	0.000092	-3.73	0.000096	-3.72	0.000100	-3.71	0.000104
-3.70	0.000108	-3.69	0.000112	-3.68	0.000117	-3.67	0.000121	-3.66	0.000126
-3.65	0.000131	-3.64	0.000136	-3.63	0.000142	-3.62	0.000147	-3.61	0.000153
-3.60	0.000159	-3.59	0.000165	-3.58	0.000172	-3.57	0.000178	-3.56	0.000185
-3.55	0.000193	-3.54	0.000200	-3.53	0.000208	-3.52	0.000216	-3.51	0.000224
-3.50	0.000233	-3.49	0.000242	-3.48	0.000251	-3.47	0.000260	-3.46	0.000270
-3.45	0.000280	-3.44	0.000291	-3.43	0.000302	-3.42	0.000313	-3.41	0.000325
-3.40	0.000337	-3.39	0.000349	-3.38	0.000362	-3.37	0.000376	-3.36	0.000390
-3.35	0.000404	-3.34	0.000419	-3.33	0.000434	-3.32	0.000450	-3.31	0.000466
-3.30	0.000483	-3.29	0.000501	-3.28	0.000519	-3.27	0.000538	-3.26	0.000557
-3.25	0.000577	-3.24	0.000598	-3.23	0.000619	-3.22	0.000641	-3.21	0.000664
-3.20	0.000687	-3.19	0.000711	-3.18	0.000736	-3.17	0.000762	-3.16	0.000789
-3.15	0.000816	-3.14	0.000845	-3.13	0.000874	-3.12	0.000904	-3.11	0.000935
-3.10	0.000968	-3.09	0.001001	-3.08	0.001035	-3.07	0.001070	-3.06	0.001107
-3.05	0.001144	-3.04	0.001183	-3.03	0.001223	-3.02	0.001264	-3.01	0.001306
-3.00	0.001350	-2.99	0.001395	-2.98	0.001441	-2.97	0.001489	-2.96	0.001538
-2.95	0.001589	-2.94	0.001641	-2.93	0.001695	-2.92	0.001750	-2.91	0.001807
-2.90	0.001866	-2.89	0.001926	-2.88	0.001988	-2.87	0.002052	-2.86	0.002118
-2.85	0.002186	-2.84	0.002256	-2.83	0.002327	-2.82	0.002401	-2.81	0.002477
-2.80	0.002555	-2.79	0.002635	-2.78	0.002718	-2.77	0.002803	-2.76	0.002890
-2.75	0.002980	-2.74	0.003072	-2.73	0.003167	-2.72	0.003264	-2.71	0.003364
-2.70	0.003467	-2.69	0.003573	-2.68	0.003681	-2.67	0.003793	-2.66	0.003907
-2.65	0.004025	-2.64	0.004145	-2.63	0.004269	-2.62	0.004396	-2.61	0.004527
-2.60	0.004661	-2.59	0.004799	-2.58	0.004940	-2.57	0.005085	-2.56	0.005234
-2.55	0.005386	-2.54	0.005543	-2.53	0.005703	-2.52	0.005868	-2.51	0.006037
-2.50	0.006210	-2.49	0.006387	-2.48	0.006569	-2.47	0.006756	-2.46	0.006947
-2.45	0.007143	-2.44	0.007344	-2.43	0.007549	-2.42	0.007760	-2.41	0.007976
-2.40	0.008198	-2.39	0.008424	-2.38	0.008656	-2.37	0.008894	-2.36	0.009137
-2.35	0.009387	-2.34	0.009642	-2.33	0.009903	-2.32	0.010170	-2.31	0.010444
-2.30	0.010724	-2.29	0.011011	-2.28	0.011304	-2.27	0.011604	-2.26	0.011911
-2.25	0.012224	-2.24	0.012545	-2.23	0.012874	-2.22	0.013209	-2.21	0.013553
-2.20	0.013903	-2.19	0.014262	-2.18	0.014629	-2.17	0.015003	-2.16	0.015386
-2.15	0.015778	-2.14	0.016177	-2.13	0.016586	-2.12	0.017003	-2.11	0.017429
-2.10	0.017864	-2.09	0.018309	-2.08	0.018763	-2.07	0.019226	-2.06	0.019699
-2.05	0.020182	-2.04	0.020675	-2.03	0.021178	-2.02	0.021692	-2.01	0.022216
-2.00	0.022750	-1.99	0.023295	-1.98	0.023852	-1.97	0.024419	-1.96	0.024998

Table G1-4 (Continued)

U	*F(U)*	*U*	*F(U)*	*U*	*F(U)*	*U*	*F(U)*	*U*	*F(U)*
-1.95	0.025588	-1.94	0.026190	-1.93	0.026803	-1.92	0.027429	-1.91	0.028067
-1.90	0.028717	-1.89	0.029379	-1.88	0.030054	-1.87	0.030742	-1.86	0.031443
-1.85	0.032157	-1.84	0.032884	-1.83	0.033625	-1.82	0.034380	-1.81	0.035148
-1.80	0.035930	-1.79	0.036727	-1.78	0.037538	-1.77	0.038364	-1.76	0.039204
-1.75	0.040059	-1.74	0.040930	-1.73	0.041815	-1.72	0.042716	-1.71	0.043633
-1.70	0.044565	-1.69	0.045514	-1.68	0.046479	-1.67	0.047460	-1.66	0.048457
-1.65	0.049471	-1.64	0.050503	-1.63	0.051551	-1.62	0.052616	-1.61	0.053699
-1.60	0.054799	-1.59	0.055917	-1.58	0.057053	-1.57	0.058208	-1.56	0.059380
-1.55	0.060571	-1.54	0.061780	-1.53	0.063008	-1.52	0.064255	-1.51	0.065522
-1.50	0.066807	-1.49	0.068112	-1.48	0.069437	-1.47	0.070781	-1.46	0.072145
-1.45	0.073529	-1.44	0.074934	-1.43	0.076359	-1.42	0.077804	-1.41	0.079270
-1.40	0.080757	-1.39	0.082264	-1.38	0.083793	-1.37	0.085343	-1.36	0.086915
-1.35	0.088508	-1.34	0.090123	-1.33	0.091759	-1.32	0.093418	-1.31	0.095098
-1.30	0.096800	-1.29	0.098525	-1.28	0.100273	-1.27	0.102042	-1.26	0.103835
-1.25	0.105650	-1.24	0.107488	-1.23	0.109349	-1.22	0.111232	-1.21	0.113139
-1.20	0.115070	-1.19	0.117023	-1.18	0.119000	-1.17	0.121000	-1.16	0.123024
-1.15	0.125072	-1.14	0.127143	-1.13	0.129238	-1.12	0.131357	-1.11	0.133500
-1.10	0.135666	-1.09	0.137857	-1.08	0.140071	-1.07	0.142310	-1.06	0.144572
-1.05	0.146859	-1.04	0.149170	-1.03	0.151505	-1.02	0.153864	-1.01	0.156248
-1.00	0.158655	-0.99	0.161087	-0.98	0.163543	-0.97	0.166023	-0.96	0.168528
-0.95	0.171056	-0.94	0.173609	-0.93	0.176186	-0.92	0.178786	-0.91	0.181411
-0.90	0.184060	-0.89	0.186733	-0.88	0.189430	-0.87	0.192150	-0.86	0.194895
-0.85	0.197663	-0.84	0.200454	-0.83	0.203269	-0.82	0.206108	-0.81	0.208970
-0.80	0.211855	-0.79	0.214764	-0.78	0.217695	-0.77	0.220650	-0.76	0.223627
-0.75	0.226627	-0.74	0.229650	-0.73	0.232695	-0.72	0.235762	-0.71	0.238852
-0.70	0.241964	-0.69	0.245097	-0.68	0.248252	-0.67	0.251429	-0.66	0.254627
-0.65	0.257846	-0.64	0.261086	-0.63	0.264347	-0.62	0.267629	-0.61	0.270931
-0.60	0.274253	-0.59	0.277595	-0.58	0.280957	-0.57	0.284339	-0.56	0.287740
-0.55	0.291160	-0.54	0.294599	-0.53	0.298056	-0.52	0.301532	-0.51	0.305026
-0.50	0.308538	-0.49	0.312067	-0.48	0.315614	-0.47	0.319178	-0.46	0.322758
-0.45	0.326355	-0.44	0.329969	-0.43	0.333598	-0.42	0.337243	-0.41	0.340903
-0.40	0.344578	-0.39	0.348268	-0.38	0.351973	-0.37	0.355691	-0.36	0.359424
-0.35	0.363169	-0.34	0.366928	-0.33	0.370700	-0.32	0.374484	-0.31	0.378280
-0.30	0.382089	-0.29	0.385908	-0.28	0.389739	-0.27	0.393580	-0.26	0.397432
-0.25	0.401294	-0.24	0.405165	-0.23	0.409046	-0.22	0.412936	-0.21	0.416834
-0.20	0.420740	-0.19	0.424655	-0.18	0.428576	-0.17	0.432505	-0.16	0.436441
-0.15	0.440382	-0.14	0.444330	-0.13	0.448283	-0.12	0.452242	-0.11	0.456205
-0.10	0.460172	-0.09	0.464144	-0.08	0.468119	-0.07	0.472097	-0.06	0.476078
-0.05	0.480061	-0.04	0.484047	-0.03	0.488034	-0.02	0.492022	-0.01	0.496011
0.00	0.500000	0.01	0.503989	0.02	0.507978	0.03	0.511966	0.04	0.515953
0.05	0.519939	0.06	0.523922	0.07	0.527903	0.08	0.531881	0.09	0.535856

(Sheet 2 of 4)

Table G1-4 (Continued)

U	*F(U)*	*U*	*F(U)*	*U*	*F(U)*	*U*	*F(U)*	*U*	*F(U)*
0.10	0.539828	0.11	0.543795	0.12	0.547758	0.13	0.551717	0.14	0.555670
0.15	0.559618	0.16	0.563559	0.17	0.567495	0.18	0.571424	0.19	0.575345
0.20	0.579260	0.21	0.583166	0.22	0.587064	0.23	0.590954	0.24	0.594835
0.25	0.598706	0.26	0.602568	0.27	0.606420	0.28	0.610261	0.29	0.614092
0.30	0.617911	0.31	0.621720	0.32	0.625516	0.33	0.629300	0.34	0.633072
0.35	0.636831	0.36	0.640576	0.37	0.644309	0.38	0.648027	0.39	0.651732
0.40	0.655422	0.41	0.659097	0.42	0.662757	0.43	0.666402	0.44	0.670031
0.45	0.673645	0.46	0.677242	0.47	0.680822	0.48	0.684386	0.49	0.687933
0.50	0.691462	0.51	0.694974	0.52	0.698468	0.53	0.701944	0.54	0.705401
0.55	0.708840	0.56	0.712260	0.57	0.715661	0.58	0.719043	0.59	0.722405
0.60	0.725747	0.61	0.729069	0.62	0.732371	0.63	0.735653	0.64	0.738914
0.65	0.742154	0.66	0.745373	0.67	0.748571	0.68	0.751748	0.69	0.754903
0.70	0.758036	0.71	0.761148	0.72	0.764238	0.73	0.767305	0.74	0.770350
0.75	0.773373	0.76	0.776373	0.77	0.779350	0.78	0.782305	0.79	0.785236
0.80	0.788145	0.81	0.791030	0.82	0.793892	0.83	0.796731	0.84	0.799546
0.85	0.802337	0.86	0.805106	0.87	0.807850	0.88	0.810570	0.89	0.813267
0.90	0.815940	0.91	0.818589	0.92	0.821214	0.93	0.823814	0.94	0.826391
0.95	0.828944	0.96	0.831472	0.97	0.833977	0.98	0.836457	0.99	0.838913
1.00	0.841345	1.01	0.843752	1.02	0.846136	1.03	0.848495	1.04	0.850830
1.05	0.853141	1.06	0.855428	1.07	0.857690	1.08	0.859929	1.09	0.862143
1.10	0.864334	1.11	0.866500	1.12	0.868643	1.13	0.870762	1.14	0.872857
1.15	0.874928	1.16	0.876976	1.17	0.879000	1.18	0.881000	1.19	0.882977
1.20	0.884930	1.21	0.886861	1.22	0.888768	1.23	0.890651	1.24	0.892512
1.25	0.894350	1.26	0.896165	1.27	0.897958	1.28	0.899727	1.29	0.901475
1.30	0.903199	1.31	0.904902	1.32	0.906582	1.33	0.908241	1.34	0.909877
1.35	0.911492	1.36	0.913085	1.37	0.914657	1.38	0.916207	1.39	0.917736
1.40	0.919243	1.41	0.920730	1.42	0.922196	1.43	0.923642	1.44	0.925066
1.45	0.926471	1.46	0.927855	1.47	0.929219	1.48	0.930563	1.49	0.931888
1.50	0.933193	1.51	0.934478	1.52	0.935745	1.53	0.936992	1.54	0.938220
1.55	0.939429	1.56	0.940620	1.57	0.941792	1.58	0.942947	1.59	0.944083
1.60	0.945201	1.61	0.946301	1.62	0.947384	1.63	0.948449	1.64	0.949497
1.65	0.950529	1.66	0.951543	1.67	0.952540	1.68	0.953521	1.69	0.954486
1.70	0.955435	1.71	0.956367	1.72	0.957284	1.73	0.958185	1.74	0.959071
1.75	0.959941	1.76	0.960796	1.77	0.961636	1.78	0.962462	1.79	0.963273
1.80	0.964070	1.81	0.964852	1.82	0.965621	1.83	0.966375	1.84	0.967116
1.85	0.967843	1.86	0.968557	1.87	0.969258	1.88	0.969946	1.89	0.970621
1.90	0.971283	1.91	0.971933	1.92	0.972571	1.93	0.973197	1.94	0.973810
1.95	0.974412	1.96	0.975002	1.97	0.975581	1.98	0.976148	1.99	0.976705
2.00	0.977250	2.01	0.977784	2.02	0.978308	2.03	0.978822	2.04	0.979325
2.05	0.979818	2.06	0.980301	2.07	0.980774	2.08	0.981237	2.09	0.981691
2.10	0.982136	2.11	0.982571	2.12	0.982997	2.13	0.983414	2.14	0.983823
2.15	0.984222	2.16	0.984614	2.17	0.984997	2.18	0.985371	2.19	0.985738

Table G1-4 (Concluded)

U	*F(U)*	*U*	*F(U)*	*U*	*F(U)*	*U*	*F(U)*	*U*	*F(U)*
2.20	0.986097	2.21	0.986447	2.22	0.986791	2.23	0.987126	2.24	0.987455
2.25	0.987776	2.26	0.988089	2.27	0.988396	2.28	0.988696	2.29	0.988989
2.30	0.989276	2.31	0.989556	2.32	0.989830	2.33	0.990097	2.34	0.990358
2.35	0.990613	2.36	0.990863	2.37	0.991106	2.38	0.991344	2.39	0.991576
2.40	0.991802	2.41	0.992024	2.42	0.992240	2.43	0.992451	2.44	0.992656
2.45	0.992857	2.46	0.993053	2.47	0.993244	2.48	0.993431	2.49	0.993613
2.50	0.993790	2.51	0.993963	2.52	0.994132	2.53	0.994297	2.54	0.994457
2.55	0.994614	2.56	0.994766	2.57	0.994915	2.58	0.995060	2.59	0.995201
2.60	0.995339	2.61	0.995473	2.62	0.995604	2.63	0.995731	2.64	0.995855
2.65	0.995975	2.66	0.996093	2.67	0.996207	2.68	0.996319	2.69	0.996427
2.70	0.996533	2.71	0.996636	2.72	0.996736	2.73	0.996833	2.74	0.996928
2.75	0.997020	2.76	0.997110	2.77	0.997197	2.78	0.997282	2.79	0.997365
2.80	0.997445	2.81	0.997523	2.82	0.997599	2.83	0.997673	2.84	0.997744
2.85	0.997814	2.86	0.997882	2.87	0.997948	2.88	0.998012	2.89	0.998074
2.90	0.998134	2.91	0.998193	2.92	0.998250	2.93	0.998305	2.94	0.998359
2.95	0.998411	2.96	0.998462	2.97	0.998511	2.98	0.998559	2.99	0.998605
3.00	0.998650	3.01	0.998694	3.02	0.998736	3.03	0.998777	3.04	0.998817
3.05	0.998856	3.06	0.998893	3.07	0.998930	3.08	0.998965	3.09	0.998999
3.10	0.999032	3.11	0.999065	3.12	0.999096	3.13	0.999126	3.14	0.999155
3.15	0.999184	3.16	0.999211	3.17	0.999238	3.18	0.999264	3.19	0.999289
3.20	0.999313	3.21	0.999336	3.22	0.999359	3.23	0.999381	3.24	0.999402
3.25	0.999423	3.26	0.999443	3.27	0.999462	3.28	0.999481	3.29	0.999499
3.30	0.999517	3.31	0.999534	3.32	0.999550	3.33	0.999566	3.34	0.999581
3.35	0.999596	3.36	0.999610	3.37	0.999624	3.38	0.999638	3.39	0.999651
3.40	0.999663	3.41	0.999675	3.42	0.999687	3.43	0.999698	3.44	0.999709
3.45	0.999720	3.46	0.999730	3.47	0.999740	3.48	0.999749	3.49	0.999758
3.50	0.999767	3.51	0.999776	3.52	0.999784	3.53	0.999792	3.54	0.999800
3.55	0.999807	3.56	0.999815	3.57	0.999821	3.58	0.999828	3.59	0.999835
3.60	0.999841	3.61	0.999847	3.62	0.999853	3.63	0.999858	3.64	0.999864
3.65	0.999869	3.66	0.999874	3.67	0.999879	3.68	0.999883	3.69	0.999888
3.70	0.999892	3.71	0.999896	3.72	0.999900	3.73	0.999904	3.74	0.999908
3.75	0.999912	3.76	0.999915	3.77	0.999918	3.78	0.999922	3.79	0.999925
3.80	0.999928	3.81	0.999931	3.82	0.999933	3.83	0.999936	3.84	0.999938
3.85	0.999941	3.86	0.999943	3.87	0.999946	3.88	0.999948	3.89	0.999950
3.90	0.999952	3.91	0.999954	3.92	0.999956	3.93	0.999958	3.94	0.999959
3.95	0.999961	3.96	0.999963	3.97	0.999964	3.98	0.999966	3.99	0.999967
4.00	0.999968								

(Sheet 4 of 4)

b. For ground motion level z = 0.2 g, ln (z) = -1.6094. Considering a magnitude 5 earthquake occurring at a distance of 10 km from the site, the median ground motions that this event will produce, from Equation G1-6, is 0.103 g, and the standard error of ln (z), from Equation G1-7, is 0.56. The probability that this event will produce a peak acceleration in excess of 0.2 g is computed using

Equation G1-8. The normalized deviate, U, is computed by [ln (0.2) - ln (0.103)]/0.56 = 1.188. The probability that ground motions produced by this event will be less than or equal to 0.2 g, assuming a truncated lognormal distribution, is F' (1.188) = [F(1.188) - F(-3)]/[1 - 2F(-3)] = [0.88258 - 0.00135]/[1 - 0.0027] = 0.88369. Therefore, the probability of exceeding 0.2 g is 1 - 0.88369 = 0.11631. The computed values of $P(Z > z \mid m_i, r_j)$ are tabulated in Table G1-5 for the range of magnitudes and distances considered.

Table G1-5
Conditional Probabilities of Exceeding 0.2 g

m_i	r_j	E [ln (Z)]	S [ln (Z)]	U	$P(Z > z \mid m_i, r_j)$
5	10	-2.275	0.56	1.188	0.11631
	15	-2.681	0.56	1.914	0.02652
	20	-3.011	0.56	2.503	0.00482
	25	-3.288	0.56	2.998	0.000001
	30	-3.528	0.56	3.425	0
5.5	10	-1.939	0.49	0.672	0.25025
	15	-2.303	0.49	1.415	0.07738
	20	-2.604	0.49	2.03	0.01987
	25	-2.861	0.49	2.555	0.00397
	30	-3.085	0.49	3.012	0
6	10	-1.627	0.42	0.042	0.48304
	15	-1.949	0.42	0.809	0.20853
	20	-2.221	0.42	1.456	0.07156
	25	-2.456	0.42	2.016	0.02062
	30	-2.663	0.42	2.509	0.00471
6.5	10	-1.341	0.35	-0.768	0.77954
	15	-1.621	0.35	0.033	0.48689
	20	-1.862	0.35	0.723	0.23415
	25	-2.075	0.35	1.329	0.09078
	30	-2.264	0.35	1.87	0.02948
7	10	-1.168	0.35	-1.26	0.89723
	15	-1.398	0.35	-0.605	0.72799
	20	-1.6	0.35	-0.026	0.51032
	25	-1.782	0.35	0.493	0.31045
	30	-1.947	0.35	0.963	0.16682
7.5	10	-1.031	0.35	-1.652	0.95200
	15	-1.215	0.35	-1.128	0.87135
	20	-1.381	0.35	-0.653	0.74392
	25	-1.532	0.35	-0.22	0.58731
	30	-1.672	0.35	0.179	0.42886

G1-5. Computation of Frequency of Exceedance

a. Computation of $\nu(0.2)$ from Equation G1-1 is performed by multiplying the values of $\lambda(m_i)$ by the probability of a specific distance, $P(R = r_j \mid m_i)$, and the conditional probability of ground motion exceedance for the specified magnitude and distance, $P(Z > z \mid m_i, r_j)$, then summing over all distances and magnitudes. For example, the frequency of magnitude 5 events on Fault 1, $\lambda(m = 5)$, is given in

Table G1-1 (for m^u = 6.5) as 0.04520. From Table G1-3, the probability that a magnitude 5 earthquake on Fault 1 will occur at 10 km from the site is 0.2845. From Table G1-5, the probability that a magnitude 5 earthquake at a distance of 10 km will produce a peak acceleration in excess of 0.2 g is 0.11631. Thus the frequency of those magnitude 5 earthquakes occurring on Fault 1 at 10 km from the site that contribute to the hazard of exceeding 0.2 g is $\nu(0.2) = 0.04520 \times 0.2845 \times 0.11631 = 0.00150$. Table G1-6 summarizes the calculations for $\nu(0.2)$ for the two faults for one earthquake recurrence rate.

b. In the same manner that the event rates for $\alpha(m^0)$ = 0.03 and 0.3 for Fault 1 were simple multiples of the event rates for $\alpha(m^0)$ = 0.1, the values of $\nu(0.2)$ for Fault 1 for $\alpha(m^0)$ = 0.03 and 0.3 are obtained by multiplying the values of $\nu(0.2)$ for $\alpha(m^0)$ = 0.1 listed in Table G1-6 by 0.3 and 3, respectively. The values of $\nu(0.2)$ for Fault 2 for $\alpha(m^0)$ = 0.1 and 0.4 are obtained by multiplying the values of $\nu(0.2)$ for $\alpha(m^0)$ = 0.2 listed in Table G1-6 by 0.5 and 2, respectively.

G1-6. Logic Tree Analysis

a. The example problem in Figure G1-1 contains alternative values for the frequency of earthquake occurrence on each of the faults $\alpha(m^0)$ and maximum magnitude m^u. These alternative values are represented in logic trees shown in Figure G1-4. The probabilities assigned to each of the branches on the logic trees represent subjective assessments of the relative credibility of each of the parameters. The logic trees shown in the figure are abbreviated, in that they do not show all of the branches possible, but only those branches corresponding to the computations listed in Table G1-6. Table G1-7 lists the exceedance frequencies for all of the branches of the logic trees. Note the maximum magnitude distributions shown on the logic trees are repeated for each value of activity rate $\alpha(m^0)$.

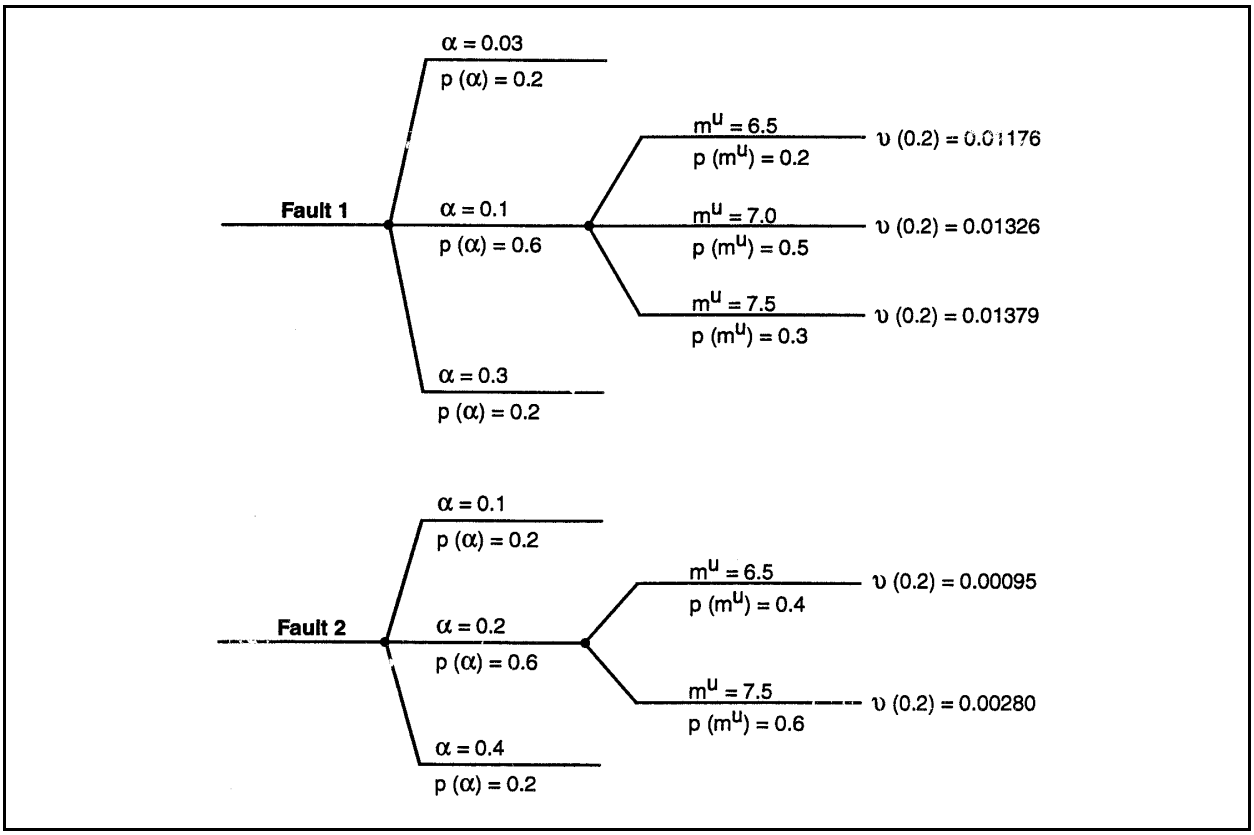

Figure G1-4. Logic trees

Table G1-6
Computation of Frequency of Exceeding 0.2 g, $\nu(0.2)$

	$m^u = 6.5$					$m^u = 7$					$m^u = 7.5$				
m_i	$\lambda(m_i)$	r_i	$P(r_i)$	$P(Z > 0.2)$	$\nu(0.2)$	$\lambda(m_i)$	r_i	$P(r_i)$	$P(Z > 0.2)$	$\nu(0.2)$	$\lambda(m_i)$	r_i	$P(r_i)$	$P(Z > 0.2)$	$\nu(0.2)$
For Fault 1 and $\alpha(m^0) = 0.1$															
5	0.04520	10	0.2845	0.11631	0.00150	0.04421	10	0.2845	0.11631	0.00146	0.04391	10	0.2845	0.11631	0.00145
		15	0.2603	0.02652	0.00031		15	0.2603	0.02652	0.00031		15	0.2603	0.02652	0.00030
		20	0.2198	0.00482	0.00005		20	0.2198	0.00482	0.00005		20	0.2198	0.00482	0.00005
		25	0.2072	0.00001	0.00000		25	0.2072	0.00001	0.00000		25	0.2072	0.00001	0.00000
		30	0.0283	0	0.00000		30	0.0283	0	0.00000		30	0.0283	0	0.00000
5.5	0.03971	10	0.3204	0.25025	0.00318	0.03884	10	0.3204	0.25025	0.00311	0.03857	10	0.3204	0.25025	0.00309
		15	0.2931	0.07738	0.00090		15	0.2931	0.07738	0.00088		15	0.2931	0.07738	0.00087
		20	0.2475	0.01987	0.00020		20	0.2475	0.01987	0.00019		20	0.2475	0.01987	0.00019
		25	0.1390	0.00397	0.00002		25	0.1390	0.00397	0.00002		25	0.1390	0.00397	0.00002
		30	0.0000	0	0.00000		30	0.0000	0	0.00000		30	0.0000	0	0.00000
6	0.01256	10	0.4153	0.48304	0.00252	0.01228	10	0.4153	0.48304	0.00246	0.01220	10	0.4153	0.48304	0.00245
		15	0.3799	0.20853	0.00099		15	0.3799	0.20853	0.00097		15	0.3799	0.20853	0.00097
		20	0.2047	0.07156	0.00018		20	0.2047	0.07156	0.00018		20	0.2047	0.07156	0.00018
		25	0.0000	0.02062	0.00000		25	0.0000	0.02062	0.00000		25	0.0000	0.02062	0.00000
6.5	0.00254	10	0.8970	0.77954	0.00178	0.00388	10	0.8970	0.77954	0.00272	0.00386	10	0.8970	0.77954	0.00270
		15	0.1030	0.48689	0.00013		15	0.1030	0.48689	0.00019		15	0.1030	0.48689	0.00019
		20	0.0000	0.23415	0.00000		20	0.0000	0.23415	0.00000		20	0.0000	0.23415	0.00000
7						0.000786	10	1.0000	0.89723	0.00071	0.00122	10	1.0000	0.89723	0.00109
							15	0.0000	0.72799	0.00000		15	0.0000	0.72799	0.00000
7.5											0.00025	10	1.0000	0.95200	0.00024
												15	0.0000	0.87135	0.00000
				Σ = 0.01176						Σ = 0.01326					Σ = 0.01379
For Fault 2 and $\alpha(m^0) = 0.2$															
5	0.09039	20	0.0117	0.00482	0.00001	--	--	--	--	--	0.08781	20	0.0117	0.00482	0.00000
		25	0.3249	0.00001	0.00000	--	--	--	--	--		25	0.3249	0.00001	0.00000
		30	0.2558	0	0.00000	--	--	--	--	--		30	0.2558	0	0.00000
		35	0.2315	0	0.00000	--	--	--	--	--		35	0.2315	0	0.00000
		40	0.1761	0	0.00000	--	--	--	--	--		40	0.1761	0	0.00000
5.5	0.07941	20	0.0131	0.01987	0.00002	--	--	--	--	--	0.07715	20	0.0131	0.01987	0.00002
		25	0.3659	0.00397	0.00012	--	--	--	--	--		25	0.3659	0.00397	0.00011
		30	0.2880	0	0.00000	--	--	--	--	--		30	0.2880	0	0.00000
		35	0.2607	0	0.00000	--	--	--	--	--		35	0.2607	0	0.00000
		40	0.0721	0	0.00000	--	--	--	--	--		40	0.0721	0	0.00000
6	0.02511	20	0.0170	0.07156	0.00003	--	--	--	--	--	0.02440	20	0.0170	0.07156	0.00003
		25	0.4744	0.02062	0.00025	--	--	--	--	--		25	0.4744	0.02062	0.00024
		30	0.3734	0.00471	0.00004	--	--	--	--	--		30	0.3734	0.00471	0.00004
		35	0.1352	0.00024	0.00000	--	--	--	--	--		35	0.1352	0.00024	0.00000
		40	0.0000	0	0.00000	--	--	--	--	--		40	0.0000	0	0.00000
6.5	0.00508	20	0.0368	0.23415	0.00004	--	--	--	--	--	0.00772	20	0.0368	0.23415	0.00007
		25	0.9632	0.09078	0.00044	--	--	--	--	--		25	0.9632	0.09078	0.00067
		30	0.0000	0.02948	0.00000	--	--	--	--	--		30	0.0000	0.02948	0.00000
7						--	--	--	--	--	0.00244	20	1.0000	0.51032	0.00124
						--	--	--	--	--		25	0.0000	0.31045	0.00000
7.5						--	--	--	--	--	0.00050	20	1.0000	0.74392	0.00037
						--	--	--	--	--		25	0.0000	0.58731	0.00000
				Σ = 0.000951											Σ = 0.002803

Table G1-7
Frequencies of Exceeding 0.2 g, $\nu(0.2)$, for Faults 1 and 2 Computed for Parameters Shown in Figure G1-4.

$\alpha(m^o)$	$P(\alpha)$	m^u	$P(m^u)$	$\nu(0.2)$	$P(\nu)$
			Fault 1		
0.03	0.2	6.5	0.2	0.00353	0.04
0.03	0.2	7.0	0.5	0.00398	0.10
0.03	0.2	7.5	0.3	0.00414	0.06
0.10	0.6	6.5	0.2	0.01176	0.12
0.10	0.6	7.0	0.5	0.01326	0.30
0.10	0.6	7.5	0.3	0.01379	0.18
0.30	0.2	6.5	0.2	0.03528	0.04
0.30	0.2	7.0	0.5	0.03978	0.10
0.30	0.2	7.5	0.3	0.04138	0.06
					$\Sigma P(\nu) = 1.00$
			Fault 2		
0.1	0.2	6.5	0.4	0.00048	0.08
0.1	0.2	7.5	0.6	0.00140	0.12
0.2	0.6	6.5	0.4	0.00095	0.24
0.2	0.6	7.5	0.6	0.00280	0.36
0.4	0.2	6.5	0.4	0.00190	0.08
0.4	0.2	7.5	0.6	0.00560	0.12
					$\Sigma P(\nu) = 1.00$

b. The mean exceedance frequency for Fault 1 is computed as follows:

$$E[\nu(0.2)]_{Fault\,1} = \sum_k P\left[\nu(0.2)_k\right] \cdot \nu_k(0.2) = 0.0165 \quad \text{(G1-9)}$$

c. The mean exceedance frequency for Fault 2 is

$$E[\nu(0.2)]_{Fault\,2} = \sum_k P\left[\nu(0.2)_k\right] \cdot \nu_k(0.2) = 0.0023 \quad \text{(G1-10)}$$

d. The total hazard is found by summing the contributions from the two faults:

$$E[\nu(0.2)] = \sum_n E[\nu(0.2)]_n = 0.0188 \quad \text{(G1-11)}$$

The distribution in the computed hazard is found by computing the sum of all possible combinations of the end branches of the two logic trees. That is

$$\nu(0.2)_{ij} = \nu(0.2)_i + \nu(0.2)_j \quad \text{(G1-12)}$$

$$P[\nu(0.2)_{ij}] = P[\nu(0.2)_i] \cdot P[\nu(0.2)_j] \quad \text{(G1-13)}$$

where $\nu(0.2)_i$ refers to hazard from Fault 1 and $\nu(0.2)_j$ refers to hazard from Fault 2.

e. Computing the 54 combinations of possible hazard values and ordering the result in increasing exceedance frequency gives the discrete distribution for the exceedance frequency from the two faults listed in Table G1-8. Various percentiles of the distribution are listed in the right column. The resulting distribution is plotted in Figure G1-5.

Table G1-8
Distribution for Exceedance Frequency

$\nu(0.2)$	$P[\nu(0.2)]$	$\Sigma P[\nu(0.2)]$	
0.00401	0.00320	0.00320	
0.00446	0.00800	0.01120	
0.00448	0.00960	0.02080	
0.00462	0.00480	0.02560	
0.00493	0.02400	0.04960	
0.00493	0.00480	0.05440	5th percentile
0.00509	0.01440	0.06880	
0.00538	0.01200	0.08080	
0.00543	0.00320	0.08400	
0.00554	0.00720	0.09120	
0.00588	0.00800	0.09920	
0.00604	0.00480	0.10400	
0.00633	0.01440	0.11840	
0.00678	0.03600	0.15440	15th percentile
0.00694	0.02160	0.17600	
0.00913	0.00480	0.18080	
0.00958	0.01200	0.19280	
0.00974	0.00720	0.20000	
0.01224	0.00960	0.20960	
0.01271	0.02880	0.23840	
0.01316	0.01440	0.25280	
0.01366	0.00960	0.26240	
0.01374	0.02400	0.28640	
0.01421	0.07200	0.35840	
0.01427	0.01440	0.37280	
0.01456	0.04320	0.41600	
0.01466	0.03600	0.45200	
0.01474	0.04320	0.49520	
0.01516	0.02400	0.51920	50th percentile
0.01519	0.02160	0.54080	
0.01569	0.01440	0.55520	
0.01606	0.10800	0.66320	
0.01659	0.06480	0.72800	
0.01736	0.01440	0.74240	
0.01886	0.03600	0.77840	

(Continued)

Table G1-8 (Concluded)

$\nu(0.2)$	$P[\nu(0.2)]$	$\Sigma P[\nu(0.2)]$	
0.01939	0.02160	0.80000	
0.03576	0.00320	0.80320	
0.03623	0.00960	0.81280	
0.03668	0.00480	0.81760	
0.03718	0.00320	0.82080	
0.03808	0.01440	0.83520	
0.04026	0.00800	0.84320	
0.04073	0.02400	0.86720	85th percentile
0.04088	0.00480	0.87200	
0.04118	0.01200	0.88400	
0.04168	0.00800	0.89200	
0.04186	0.00480	0.89680	
0.04233	0.01440	0.91120	
0.04258	0.03600	0.94720	
0.04278	0.00720	0.95440	95th percentile
0.04328	0.00480	0.95920	
0.04418	0.02160	0.98080	
0.04538	0.01200	0.99280	
0.04698	0.00720	1.00000	

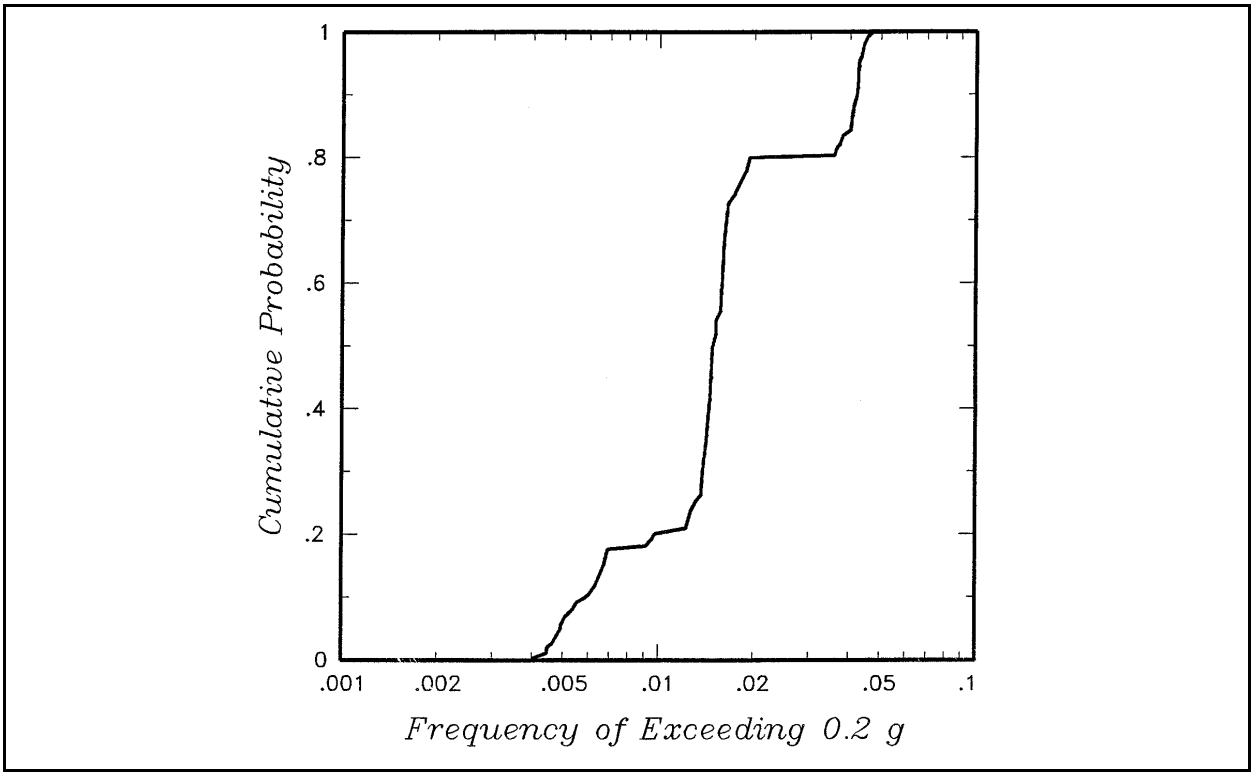

Figure G1-5. Exceedance frequency probability distribution

Section II
Example 2
Probabilistic Seismic Hazard Analysis for Rock Site in San Francisco Bay Area

G2-1. Introduction

The site location is shown in Figure G2-1 relative to the locations of active faults in the San Francisco Bay area. For this site, equal hazard response spectra of rock motions were developed and compared with deterministic response spectra for maximum credible earthquakes.

G2-2. Seismic Source Characterization

The site is located approximately 21 km east of the San Andreas fault and 7 km west of the Hayward fault, as shown in Figure G2-1. The seismic sources, including discrete faults and area sources, are shown in Figure G2-2. The corridors shown around the faults are for analyzing the seismicity that is likely associated with the faults. For each fault, cumulative earthquake recurrence based on seismicity was plotted and compared with earthquake recurrence based on geologic slip rate data for the fault. For the slip-rate-based recurrence assessments, two magnitude distribution models were initially used: exponential model and characteristic model. Comparisons of recurrence estimated for each model with seismicity were made. Examples of these comparisons for the San Andreas fault and Hayward fault are shown in Figures G2-3 and G2-4, respectively. These comparisons and comparisons for other faults indicate that the characteristic magnitude distribution used in conjuction with fault slip rate data provided recurrence characterizations in good agreement with seismicity data. On the other hand, the exponential magnitude distribution used with fault slip rate data resulted in recurrence rates that exceeded the rates from seismicity data. From these comparisons and comparisons for the other faults, it was concluded that the fault-specific recurrence was appropriately modeled using the characteristic magnitude distribution model. This model was used for all the fault-specific sources. Recurrence on the area sources was modeled using both the exponential magnitude distribution and seismicity data and both the exponential and characteristic magnitude distributions and tectonic data on plate convergence rates in the San Francisco Bay area. For the entire central bay area, a comparison was made between the recurrence predicted by the adopted recurrence models and the observed seismicity. This comparison is shown in Figure G2-5. The faults contribute much more to the regional recurrence than do the area sources. Because the fault recurrence is modeled using geologic slip-rate data, the comparison in Figure G2-5 indicates good agreement between seismicity and geologic data in defining the regional rate of earthquake activity. Figure G2-6 illustrates the generic logic tree for seismic source characterization used for the probabilistic seismic hazard analysis (PSHA). As shown, alternative hypotheses and parameter values were incorporated for segmentation, maximum rupture length (influencing maximum earthquake magnitude), maximum magnitude estimate correlations, recurrence approach (alternatives of using seismicity data and tectonic convergence rate data for source zones), recurrence rates and b-values, and magnitude distribution model for recurrence assessments (characteristic for faults and characteristic and exponential for area sources).

G2-3. Ground Motion Attenuation Characterization

Three different sets of rock ground motion attenuation relationships for response spectral acceleration at different periods of vibration (5 percent damping) as well as for peak acceleration were utilized. Median values for these relationships (for magnitudes 5, 6, and 7) are illustrated in Figure G2-7 for peak acceleration and spectral acceleration at two periods of vibration. Each set of these relationships also has its associated model of uncertainty (dispersion) around the median curves. The dispersion relationships for the preferred attenuation model (designated Caltrans 1991 in Figure G2-7) are summarized in Table G2-1.

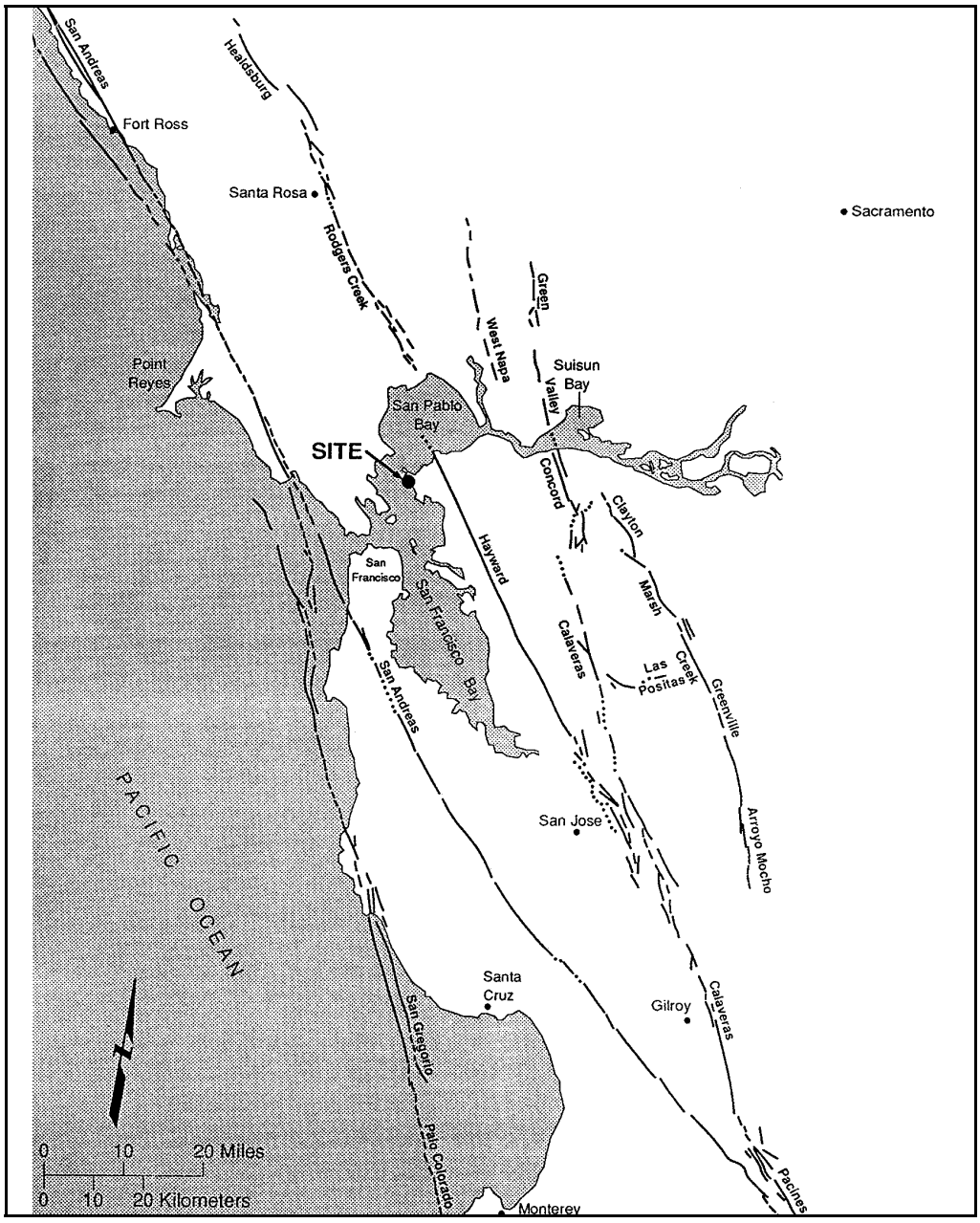

Figure G2-1. Regional active fault map

(The attenuation model designated Caltrans 1991 is the relationship of Sadigh et al. 1993.) This model predicts increasing dispersion for decreasing magnitude and increasing period of vibration, based on analysis of ground motion data. The three sets of attenuation relationships form three additional branches that are added to the logic tree in Figure G2-6.

G2-4. PSHA Results

Typical results of the PSHA are illustrated in Figure G2-8 in terms of the hazard curves obtained for peak acceleration and response spectral acceleration at two periods of vibration. The distribution about the

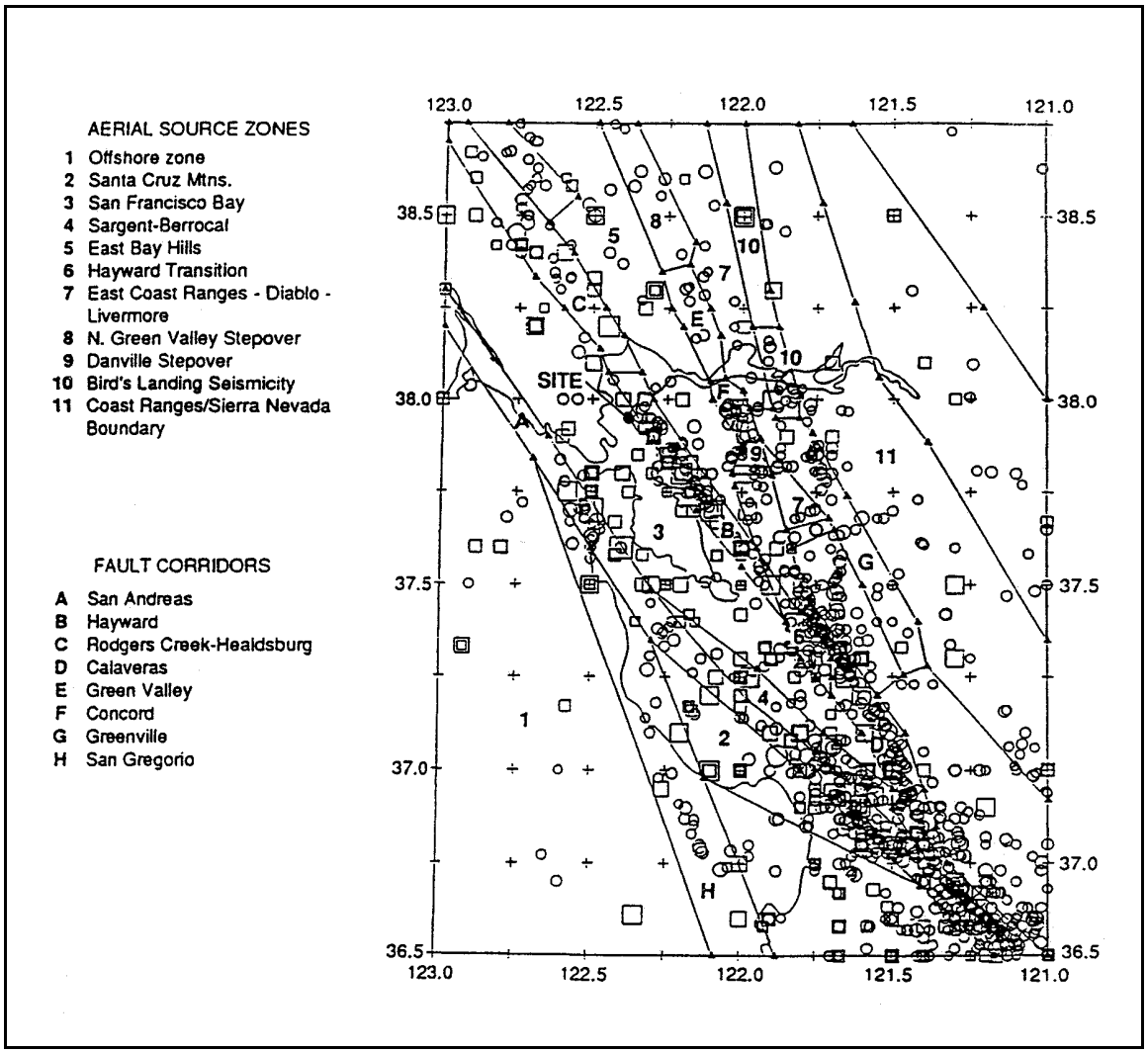

Figure G2-2. Map of the San Francisco Bay area showing independent earthquakes, fault corridors, and areal source zones. Fault corridors define the area within which seismicity is assumed to be related to fault-specific sources

mean hazard curves represents the uncertainty in seismic source characterization and ground motion attenuation characterization modeled in the logic tree. Figure G2-9 shows the contributions of different seismic sources to the hazard (sources are shown in Figures G2-1 and G2-2). As shown, the Hayward fault, which is closest to the site, dominates the hazard for peak ground acceleration (PGA) and response spectral values at low periods of vibration, but the San Andreas fault contribution increases with increasing vibrational period (reflecting the potential for larger magnitude earthquakes on the San Andreas fault than on the Hayward fault and the relatively greater influence of magnitude on long-period motions than on short-period motions). Magnitude contributions to the mean hazard curves are illustrated in Figure G2-10. The contributions of higher magnitudes increase both with increasing period of vibration and with increasing return period (RP). Analyses of two of the components of the seismic hazard model that contribute to the uncertainty in the hazard curves are illustrated in Figures G2-11 and G2-12. From Figure G2-11, it can be seen that much of the uncertainty in the hazard curves is associated with uncertainties as to the appropriate attenuation relationship. By comparison, Figure G2-12 indicates that the uncertainty associated with different models of fault segmentation for the San Andreas fault is

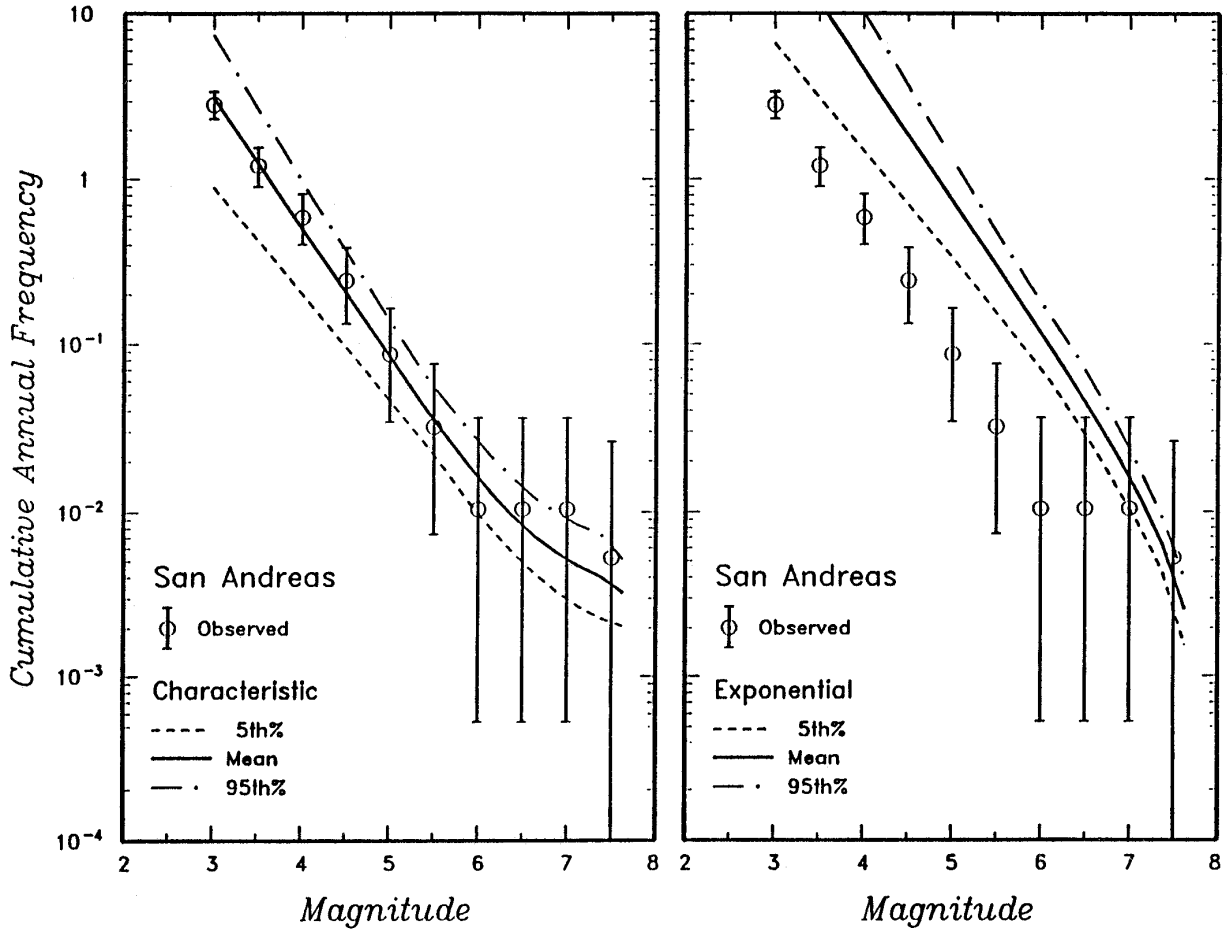

Figure G2-3. Comparison of recurrence rates developed from independent seismicity and from fault slip rates for the San Andreas fault. Predicted recurrence rates are shown for the characteristic earthquake and exponential magnitude distribution models

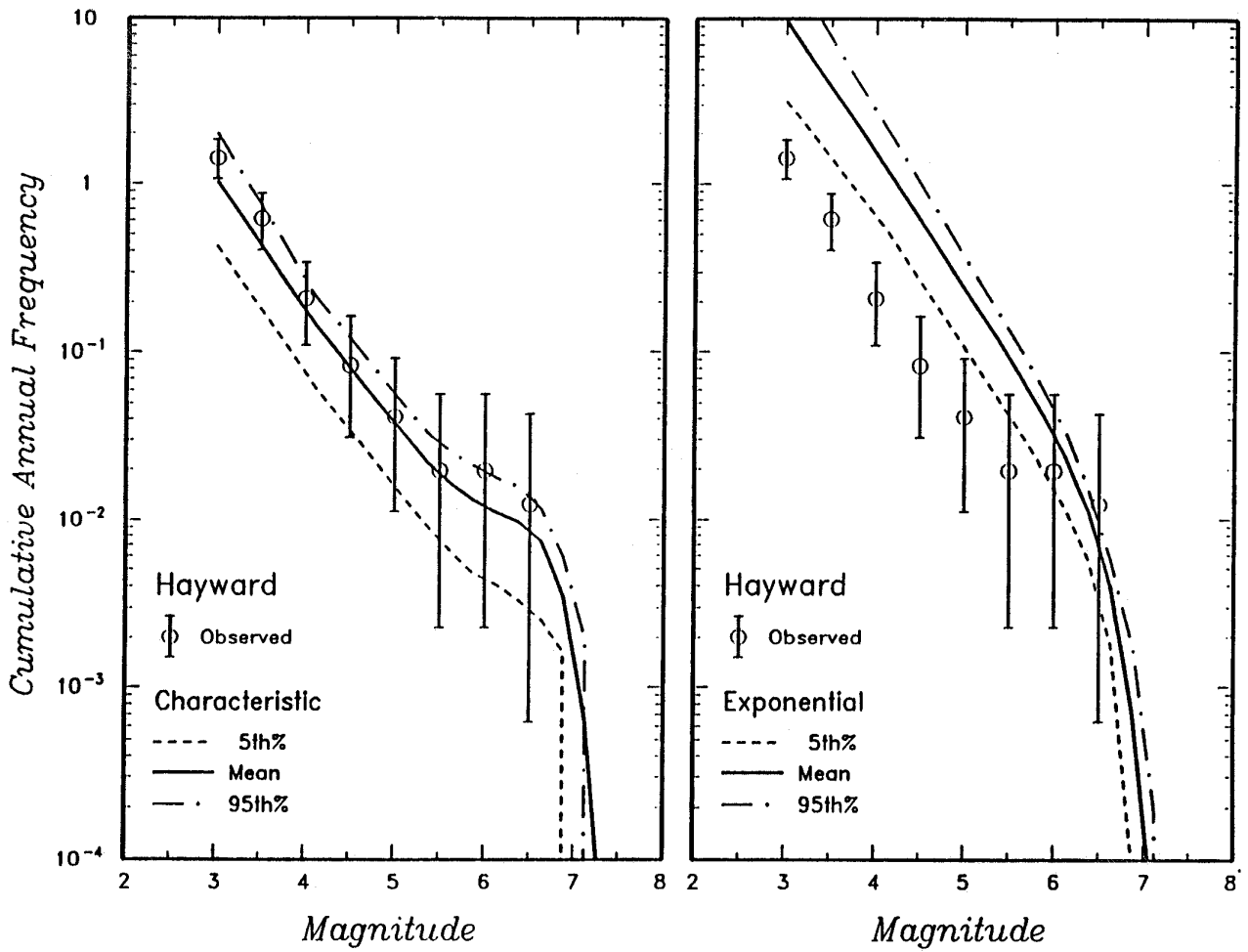

Figure G2-4. Comparison of recurrence rates developed from independent seismicity and from fault slip rates for the Hayward fault. Predicted recurrence rates are shown for the characteristic earthquake and exponential magnitude distribution models

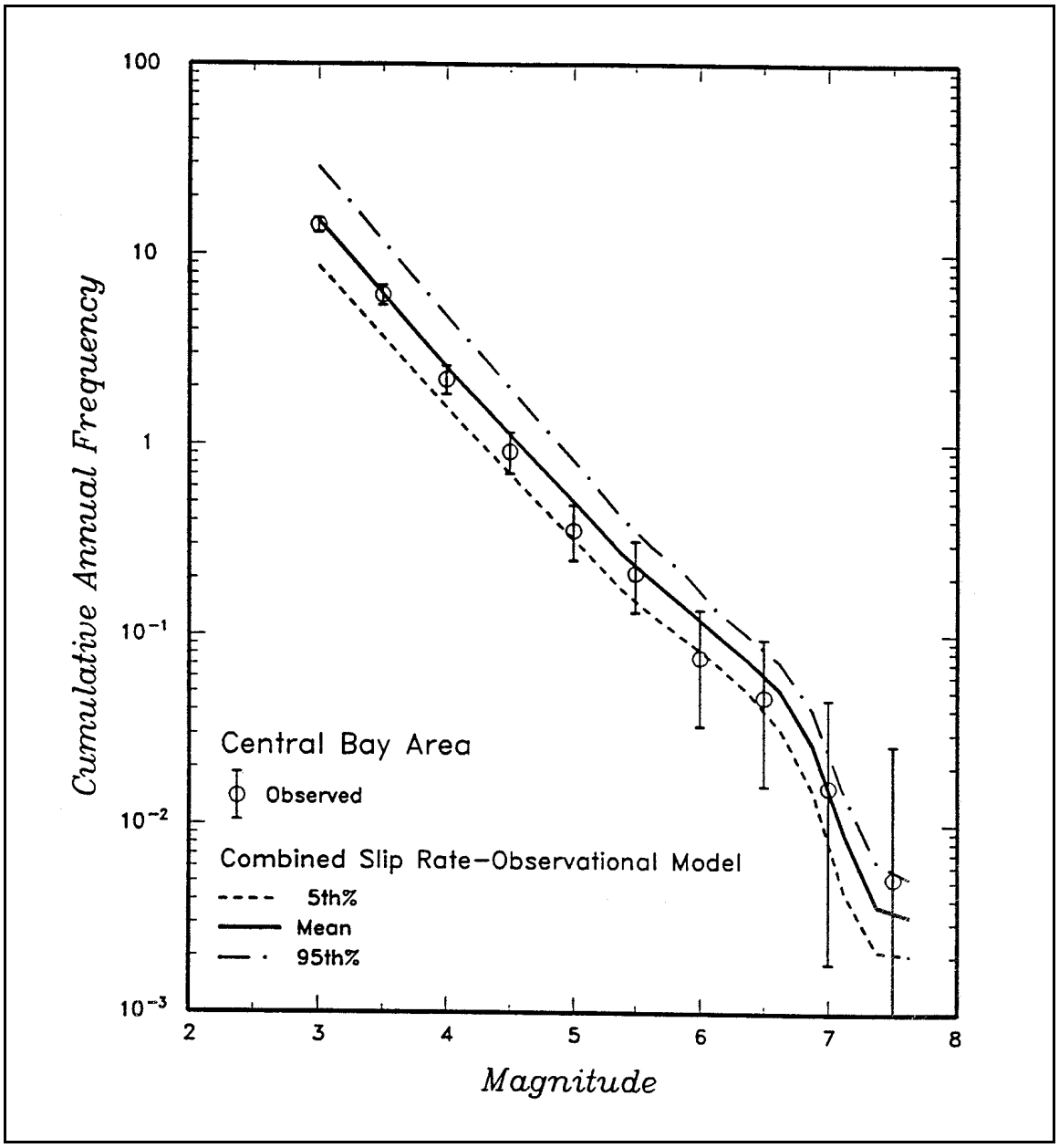

Figure G2-5. Comparison of modeled recurrence and seismicity for the central bay area

relatively small, particularly at lower frequencies of exceedance. Equal hazard response spectra (expressed in the form of tripartite plots) constructed from the mean hazard results are shown in Figure G2-13 for return periods varying from 100 to 2,000 years.

G2-5. Comparison of Probabilistic and Deterministic Results

Deterministic response spectra estimates for the site were also developed for maximum credible earthquakes (MCEs) on the San Andreas fault (MCE of moment magnitude M_w 8) and the Hayward fault (MCE of M_w 7.25), assumed to occur on the portion of the faults closest to the site. Both median and 84th percentile response spectra were developed using the preferred set of attenuation relationships. In

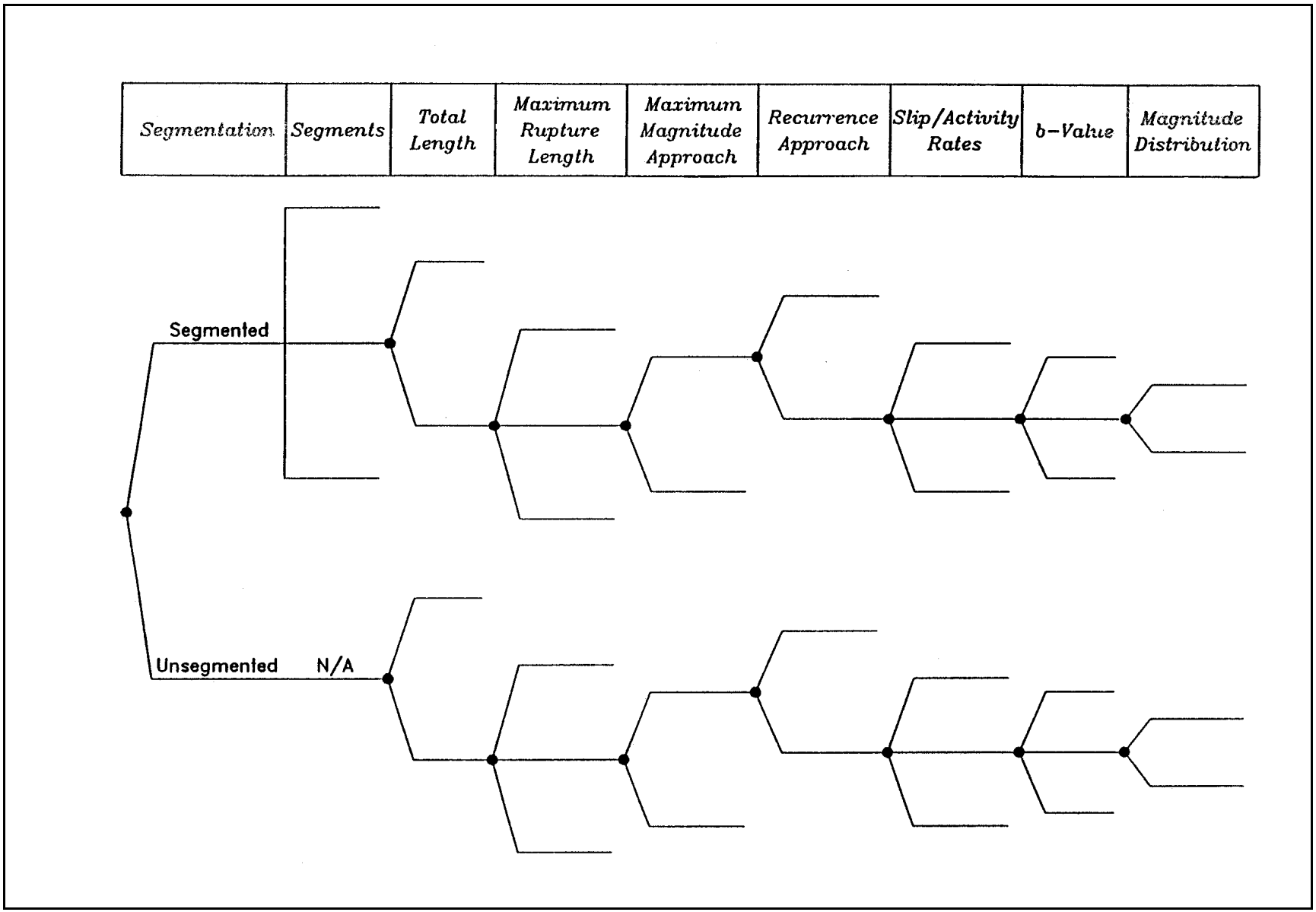

Figure G2-6. Generic logic tree used in this study to characterize seismic sources for PSHA

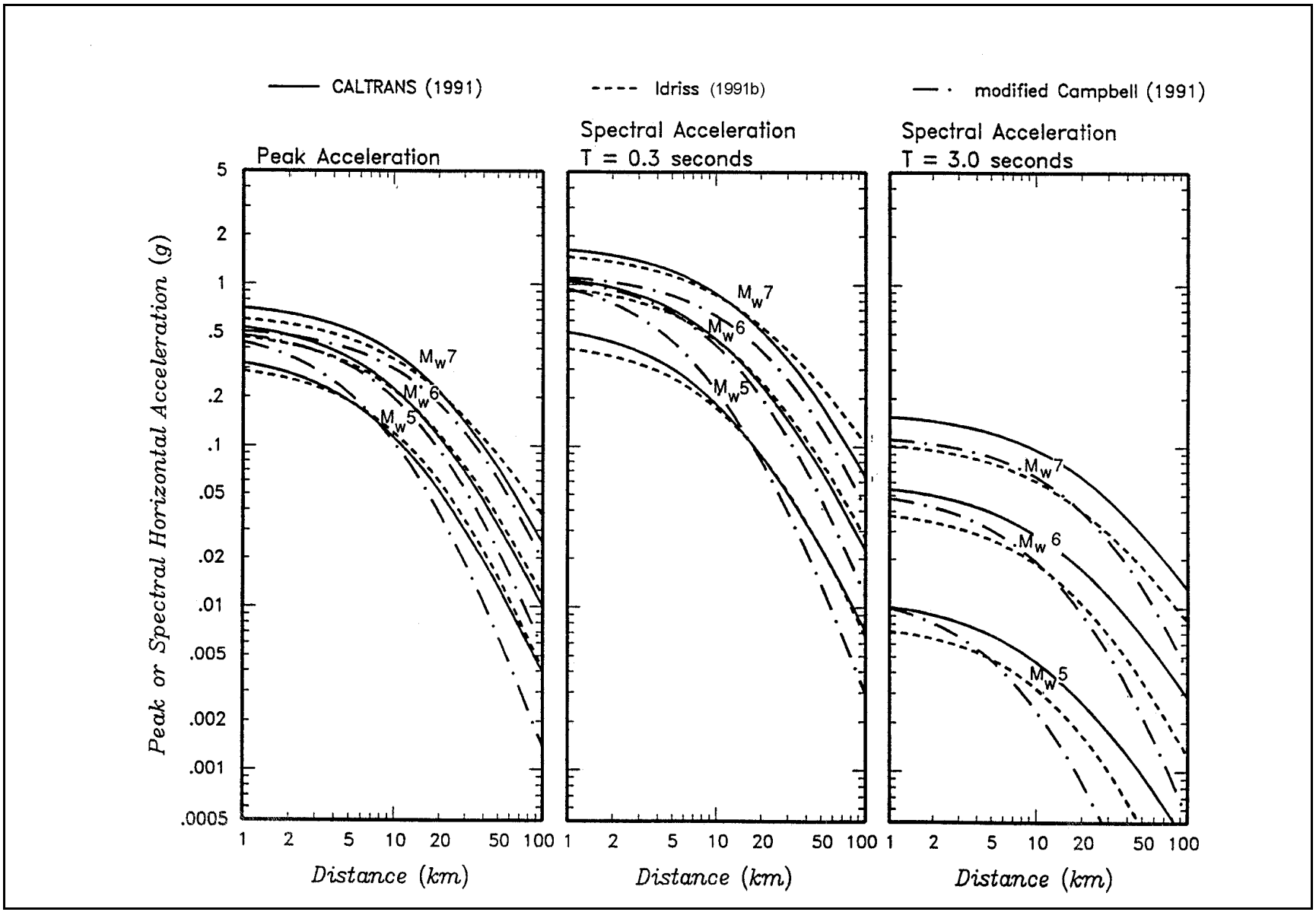

Figure G2-7. Ground motion attenuation relationships

Table G2-1
Dispersion Relationships for Horizontal Rock Motion

Ground Motion Parameter	Period (sec)	Sigma (*ln y*)
Peak ground acceleration (g)	--	1.39 - 0.14*M; 0.38 for M > = 7.25
Response spectra acceleration (g)	0.05	1.39 - 0.14*M; 0.38 for M > = 7.25
	0.07	1.40 - 0.14*M; 0.39 for M > = 7.25
	0.09	1.40 - 0.14*M; 0.39 for M > = 7.25
	0.10	1.41 - 0.14*M; 0.40 for M > = 7.25
	0.12	1.41 - 0.14*M; 0.40 for M > = 7.25
	0.14	1.42 - 0.14*M; 0.41 for M > = 7.25
	0.15	1.42 - 0.14*M; 0.41 for M > = 7.25
	0.17	1.42 - 0.14*M; 0.41 for M > = 7.25
	0.20	1.43 - 0.14*M; 0.42 for M > = 7.25
	0.24	1.44 - 0.14*M; 0.43 for M > = 7.25
	0.30	1.45 - 0.14*M; 0.44 for M > = 7.25
	0.40	1.48 - 0.14*M; 0.47 for M > = 7.25
	0.50	1.50 - 0.14*M; 0.49 for M > = 7.25
	0.75	1.52 - 0.14*M; 0.51 for M > = 7.25
	1.00	1.53 - 0.14*M; 0.52 for M > = 7.25
	> 1.00	1.53 - 0.14*M; 0.52 for M > = 7.25

Note: Sigma (ln y) is the standard deviation of the natural logarithm of the respective ground motion parameter *y*. *M* is earthquake moment magnitude.

Figure G2-14, the deterministic spectra are compared with the equal hazard spectra. It may be noted that in terms of response spectral amplitudes, the Hayward MCE 84th percentile governs over the San Andreas MCE except at periods greater than about 3 sec, and the Hayward MCE spectrum is approximately at the level of the 1000- to 2000-year return period equal hazard spectrum through the period range. Because it was desired for this site to establish an MCE as a design earthquake and to have a return period of about 1000 to 2000 years associated with the design ground motions, it was decided to select the 84th percentile spectrum for the Hayward MCE as the design response spectrum.

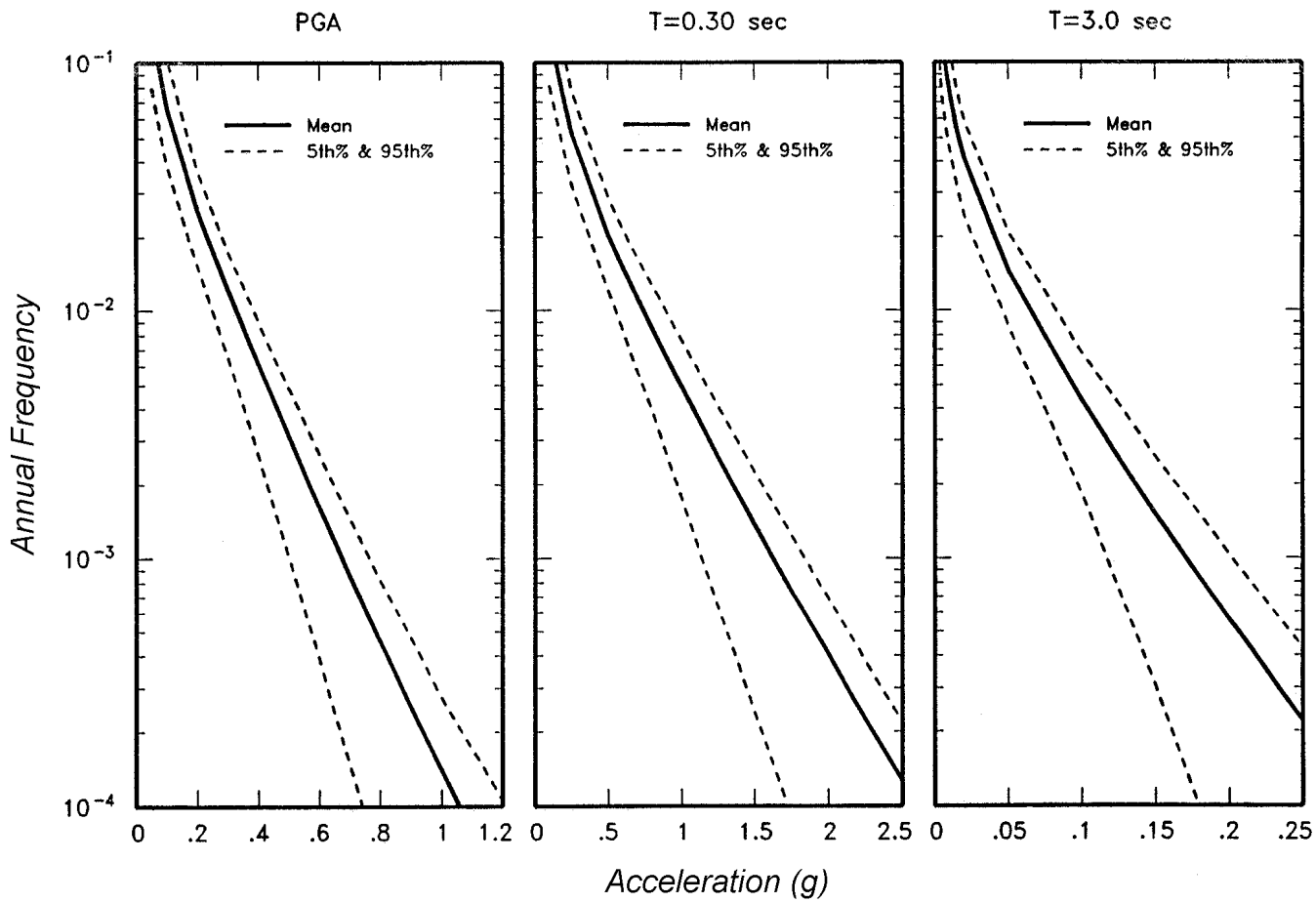

Figure G2-8. Mean, 5th, and 95th percentile hazard curves for the site for peak acceleration and 5 percent-damped spectral accelerations at periods of 0.3 and 3.0 sec

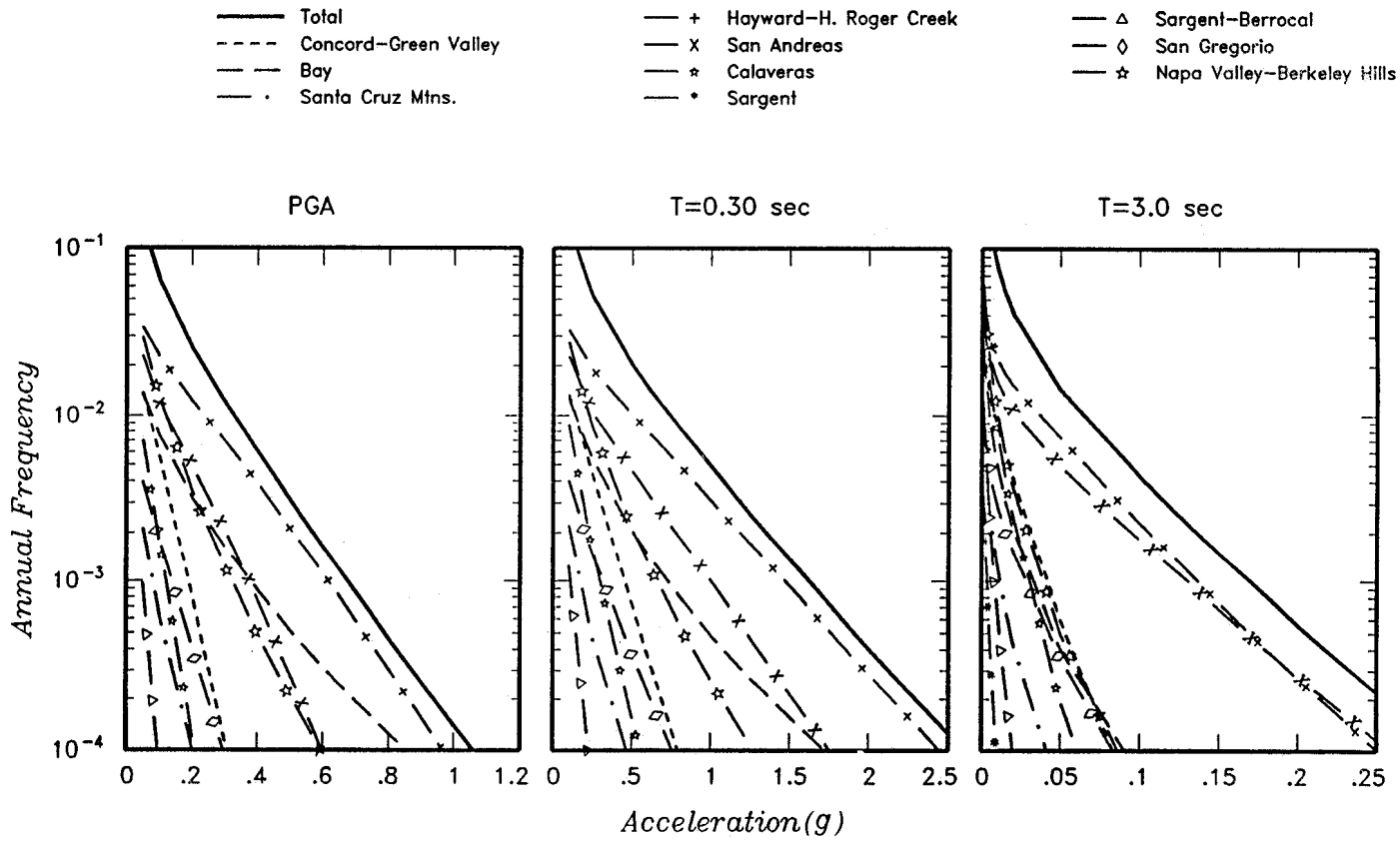

Figure G2-9. Contributions of various sources to mean hazard at the site. Shown are results for peak acceleration and 5 percent-damped spectral accelerations at periods of 0.3 and 3.0 sec

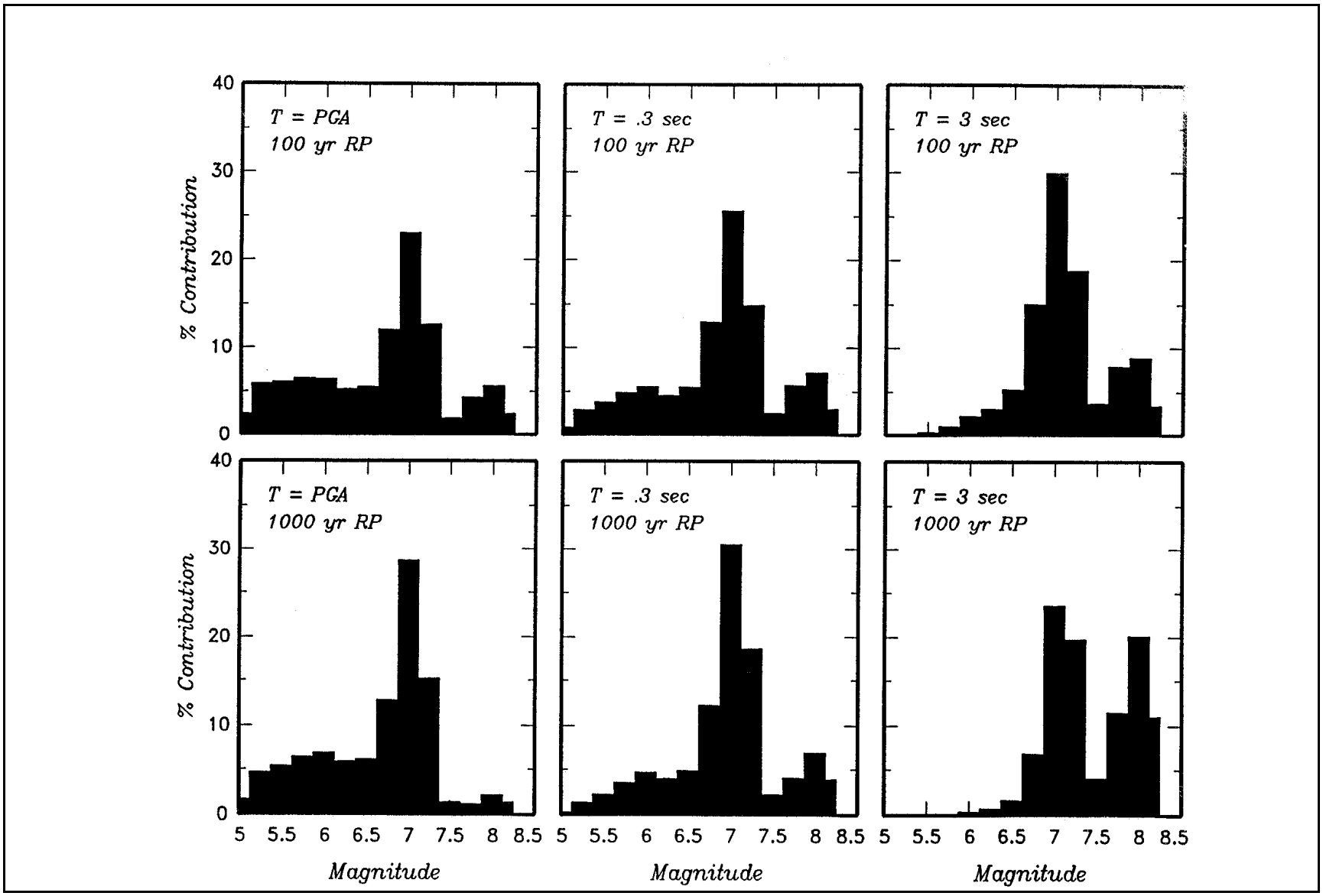

Figure G2-10. Contributions of events in various magnitude intervals to the mean hazard at the site. Shown are results for peak acceleration and 5 percent-damped spectral accelerations at periods of 0.3 and 3.0 sec

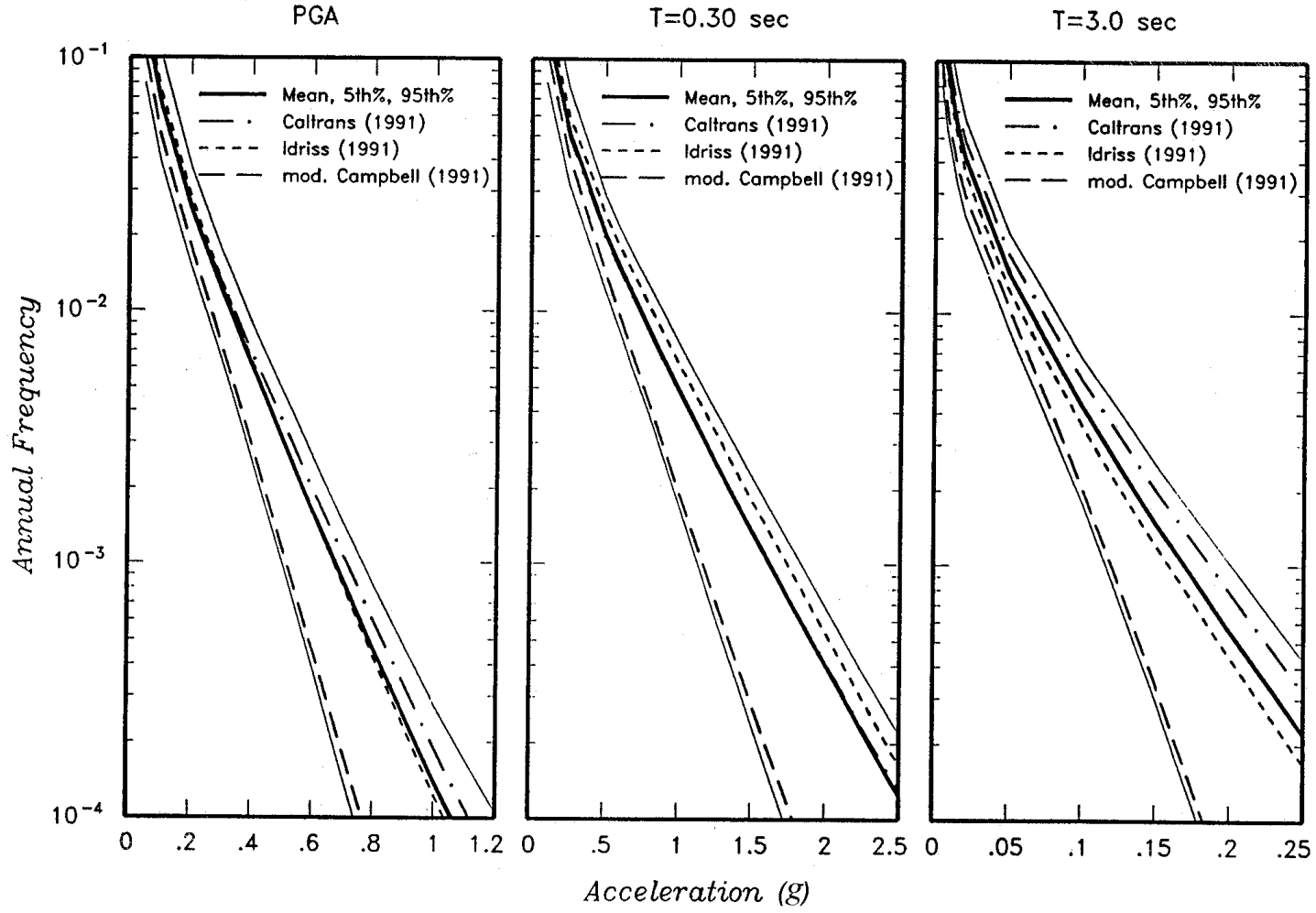

Figure G2-11. Sensitivity of mean hazard at the site to the choice of attenuation model. Shown are results for peak acceleration and 5 percent-damped spectral accelerations at periods of 0.3 and 3.0 sec

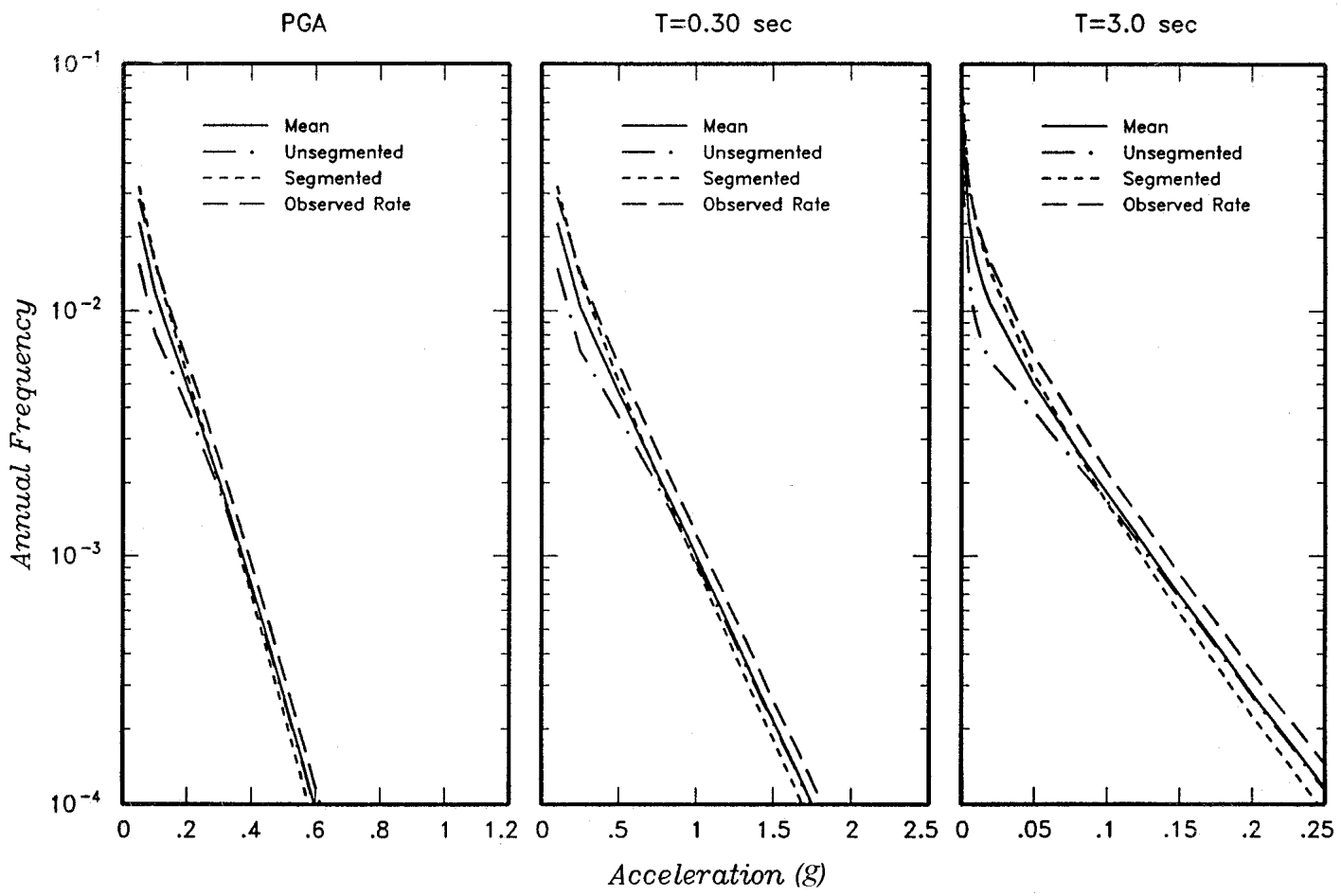

Figure G2-12. Sensitivity of mean hazard at the site to the choice of segmentation model for the San Andreas fault. Shown are results for peak acceleration and 5 percent-damped spectral accelerations at periods of 0.3 and 3.0 sec

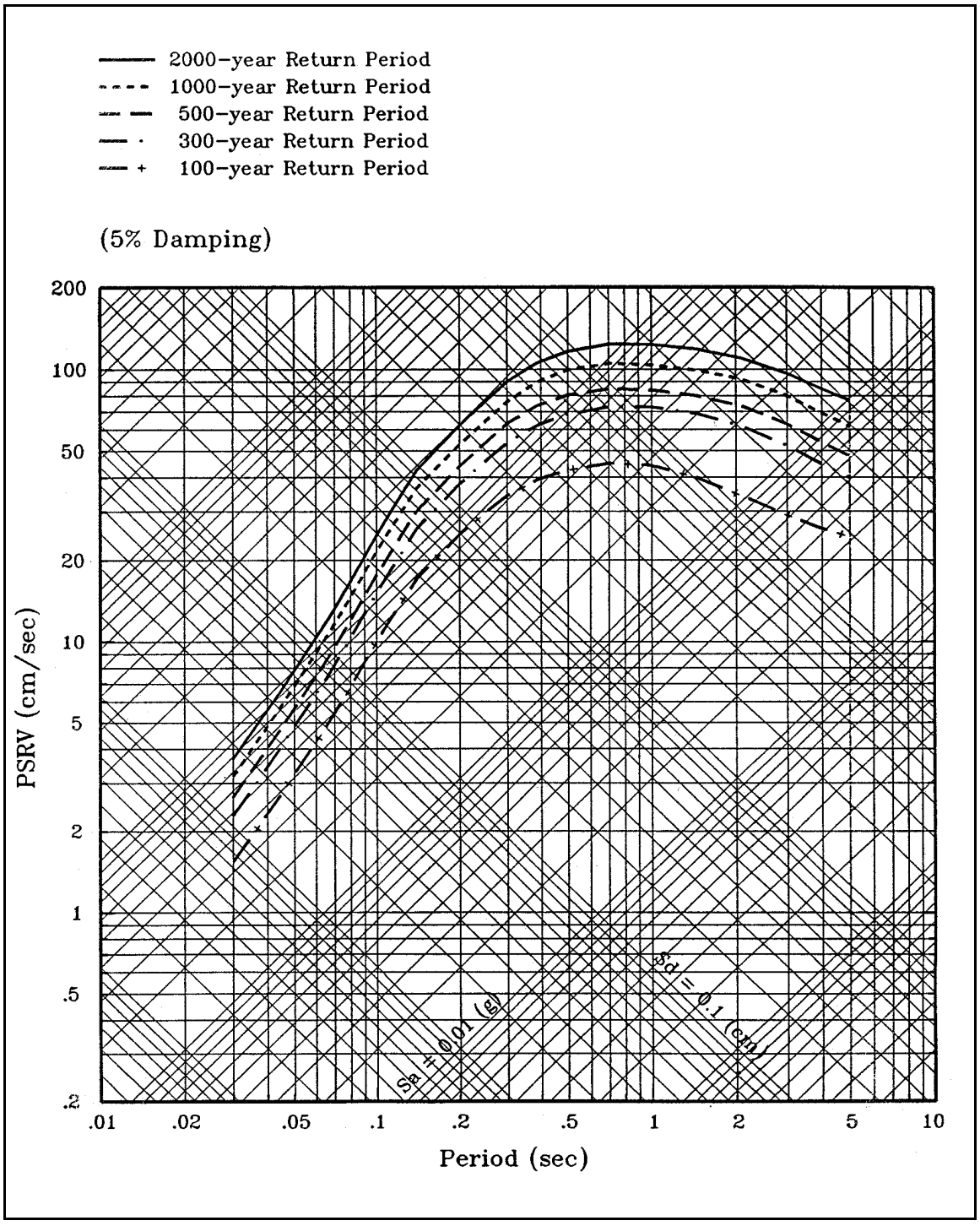

Figure G2-13. Equal-hazard pseudo-relative velocity (PSRV) response spectra for the site (5 percent damping)

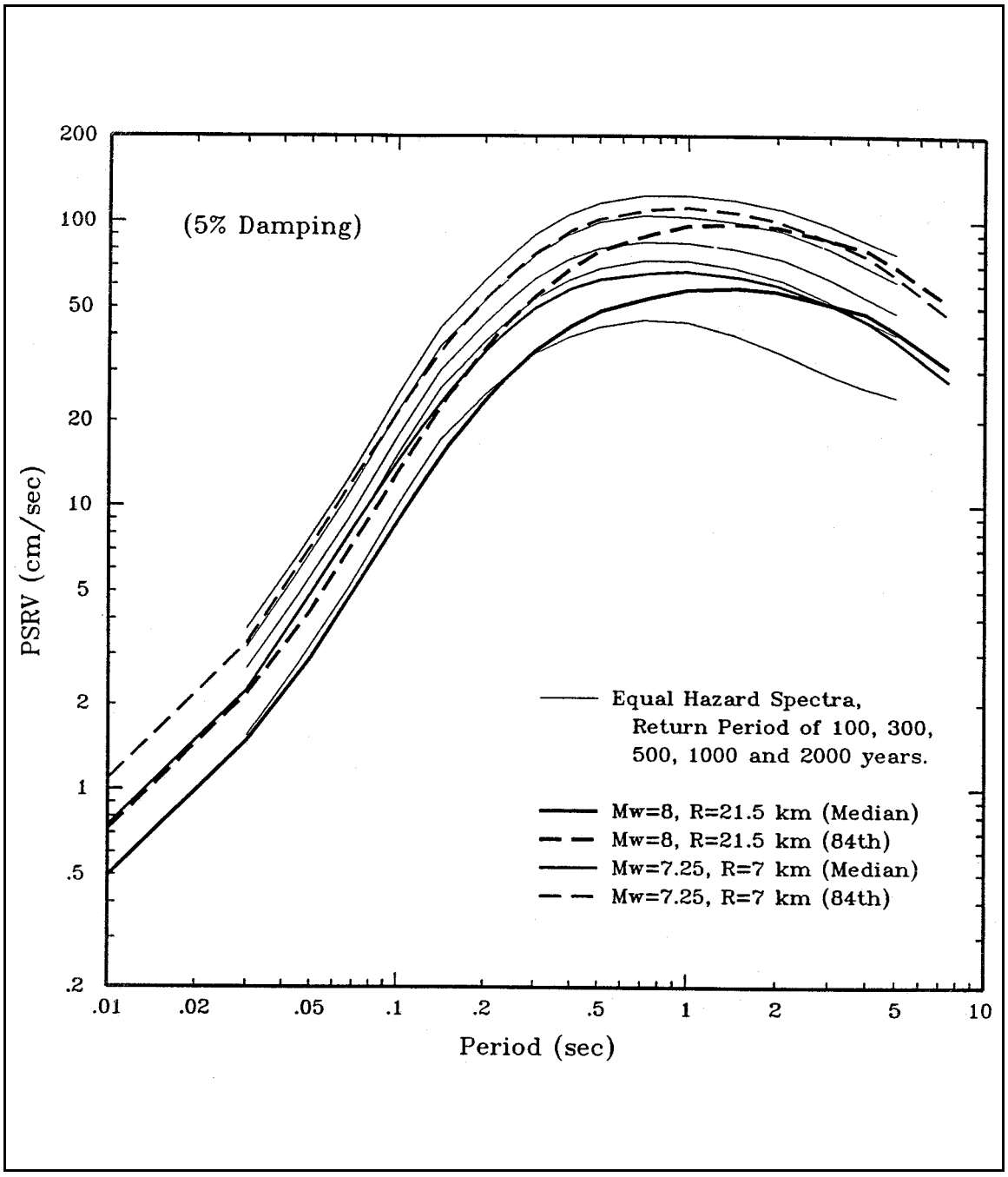

Figure G2-14. Comparison of the deterministic response spectra with equal hazard spectra for the site

Section III
Example 3
Soil Site in Arkansas

G3-1. Introduction

The site location, shown in Figure G3-1, is in southeast Arkansas near the Mississippi River. For this site, equal hazard response spectra of top-of-soil ground motions were developed and compared with deterministic response spectra for maximum credible earthquakes (MCE).

G3-2. Seismic Source Characterization

The seismic source zones identified for the study are shown in Figure G3-1 along with seismicity epicenters. These zones were developed as a synthesis of results presented in two comprehensive studies of seismic hazard in the eastern United States by the Electric Power Research Institute (EPRI) (1987) and the Lawrence Livermore National Laboratory (Bernreuter et al. 1989), as well as subsequent generalized evaluations by Johnston and Nava (1990) and Mitchell et al. (1991). The site is located in the Ouachita fold belt seismic zone, a region of low seismicity. North of and close to the site is the low-seismicity Southern Reelfoot rift seismic zone, while farther north (180 km from the site) is the relatively high seismicity New Madrid seismic zone, which was the source of the 1811-1812 New Madrid earthquake sequence. On the basis of analysis of historical seismicity, earthquake recurrence relationships were developed for the various seismic source zones. The historical seismicity for the New Madrid seismic zone is shown in Figure G3-2 along with a fitted recurrence curve having an exponential magnitude distribution. Also shown in Figure G3-2 is the inferred recurrence of large-magnitude earthquakes from paleoseismic data. Since the evidence from paleoseismic data is somewhat equivocal, two recurrence relationships were used for the New Madrid seismic zone. One consisted of the exponential model fitted to the seismicity and extrapolated to the maximum magnitude (m_b approximately 7.5) for this source zone; the other consisted of a characteristic magnitude model that fits the moderate-magnitude seismicity data yet also fits the paleoseismic data for the occurrence of large earthquakes. The two recurrence relationships used are shown by the upper and lower curves in Figure G3-3. An exponential magnitude distribution fitting historical seismicity was used to model recurrence for the other seismic source zones. Seismicity rates for the Ouachita fold belt source zone are illustrated in Figure G3-4. The modeling of uncertainty in the seismic source characterization is shown in the logic tree in Figure G3-5. For all sources, two methods, equally weighted, were used to analyze completeness in the seismicity catalog. Figure G3-5 elaborates on the modeling of the Ouachita fold belt seismic source. As shown, it was modeled as both a single zone (the entire source) and two zones roughly separated by the Mississippi River, since the region to the east appears to have lower seismicity than the region to the west (Figure G3-4). These models were given equal weight. To account for uncertainty in maximum magnitude, two values were used, weighted as shown. The wide range in modeled recurrence rates and b-values reflects the limited amount of seismicity data.

G3-3. Ground Motion Attenuation Characterization

a. Ground motion attenuation relationships were selected to estimate peak ground acceleration and response spectral values at the ground surface at the site, which is a deep-soil site. Two sets of relationships were selected. The first set was that developed by Boore and Joyner (1991) for deep-soil-site ground motions in the eastern United States. The second set consisted of a modification of the Boore and Joyner (1991) relationships. The modified attenuation relationships were developed by conducting

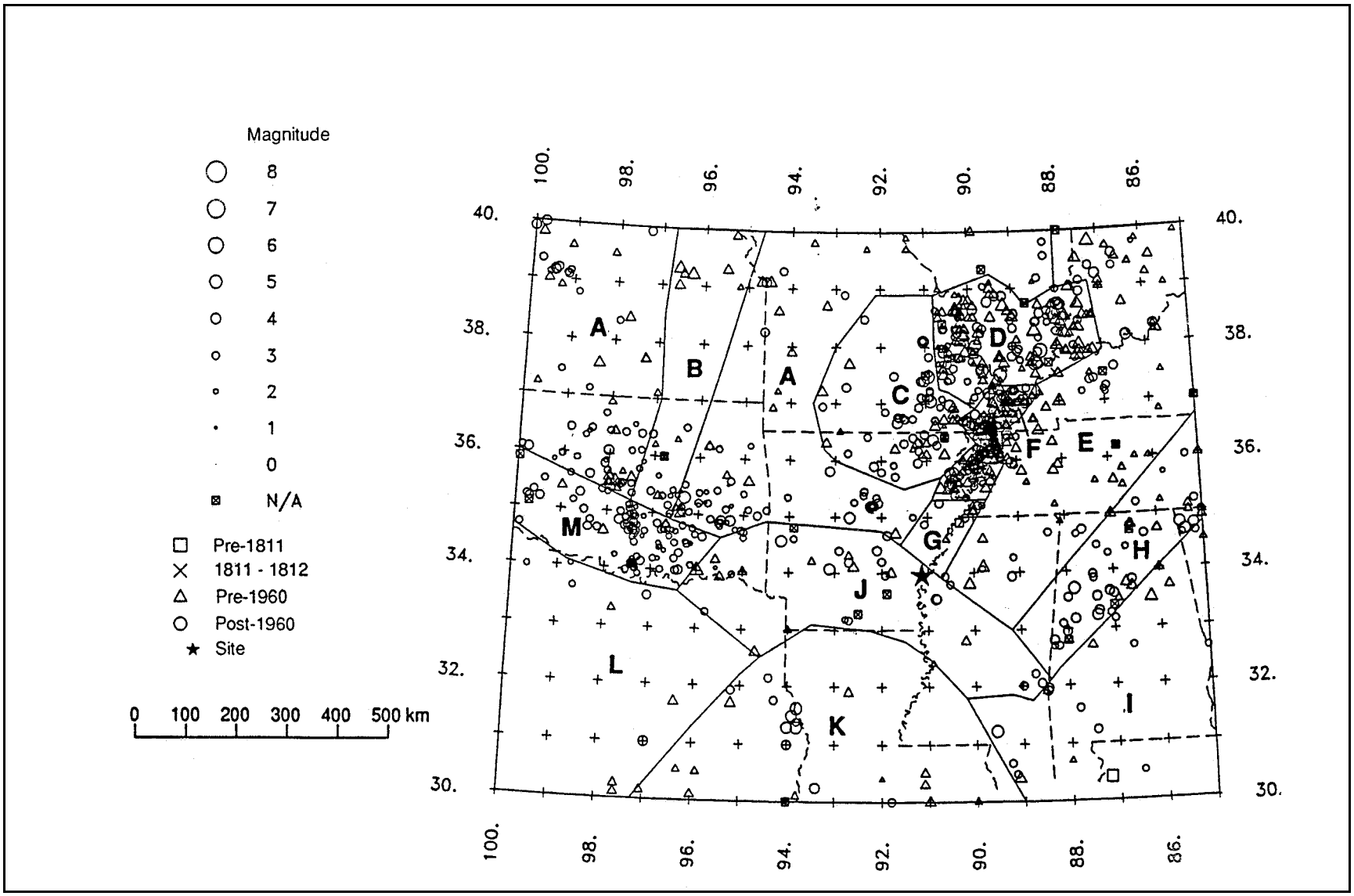

Figure G3-1. Historical seismicity and seismic source zones for the south-central United States. A - Great Plains, B - Nemaha ridge, C - Ozark uplift, D - St. Louis-Wabash, E - South-central, F - New Madrid seismic zone/Reelfoot rift complex, G - Southern Reelfoot rift, H - New York-Alabama lineament, I - Eastern Piedmont/Mesozoic basins, J - Ouachita fold belt, K - Southern Gulf Coast, L - New Mexico-Texas, M - Oklahoma aulacogen

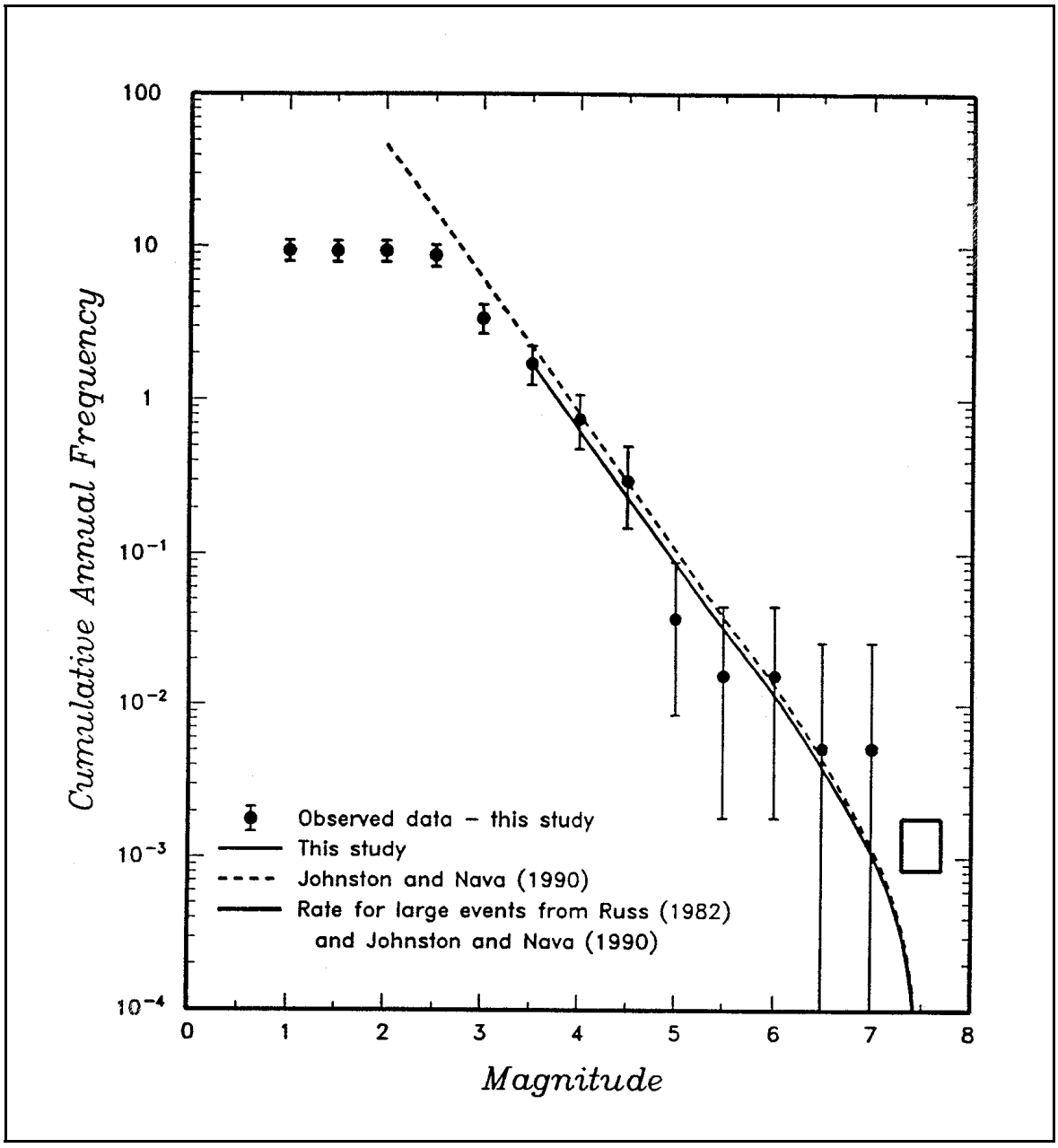

Figure G3-2. Earthquake recurrence relationships for New Madrid source zone. Box at lower right is inferred rate for large-magnitude events from paleoseismic data

site-specific theoretical (numerical) modeling of seismic wave propagation and site response using the Band-Limited White Noise/Random Vibration Theory (BLWN/RVT) approach for estimating rock motions combined with a local equivalent-linear site response analysis. The method is described by Silva and Lee (1987), Silva (1989), and Silva et al. (1989). The soil profile and crustal structure for the site vicinity were modeled for this analysis.

b. The two sets of attenuation relationships are shown in Figure G3-6 for peak ground acceleration and response spectral accelerations at two periods of vibration. These two sets of attenuation relationships, equally weighted, comprise additional branches on the logic tree shown in Figure G3-5.

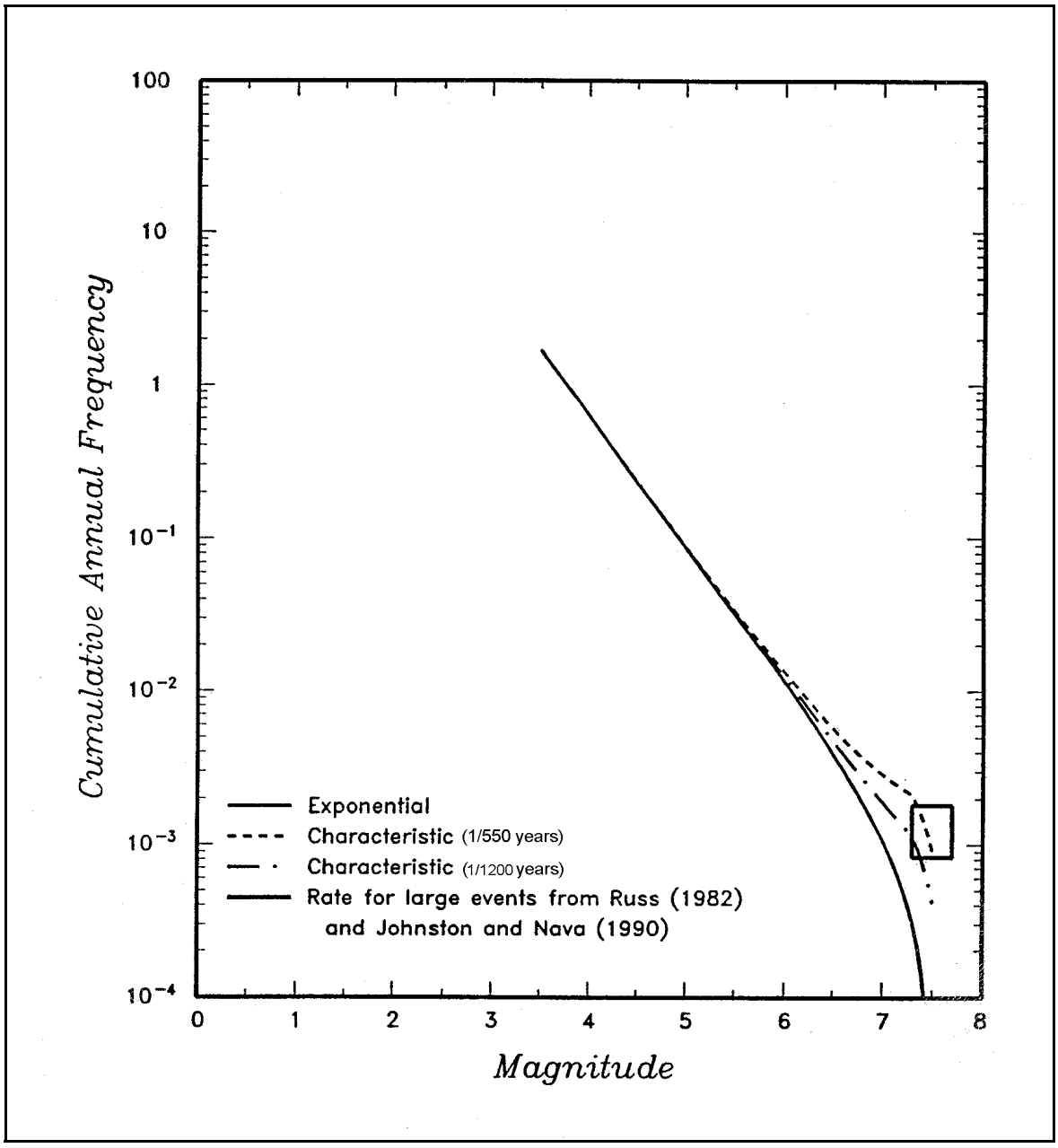

Figure G3-3. Recurrence relationships used to model New Madrid seismicity

G3-4. PSHA Results

Hazard curves obtained from the analysis for peak ground acceleration and response spectral accelerations for three periods of vibration are shown in Figure G3-7. The bands around the mean curves reflect the uncertainty in input parameters as incorporated in the logic tree. Contributions of different seismic sources to the hazard are shown in Figure G3-8. The hazard is dominated by the New Madrid seismic zone because its rate of earthquake occurrence is much higher than the other seismic zones. From the hazard curve results for a number of periods of vibration, equal hazard response spectra were constructed. These response spectra are shown in Figure G3-9 for return periods varying from 100 to 5000 years.

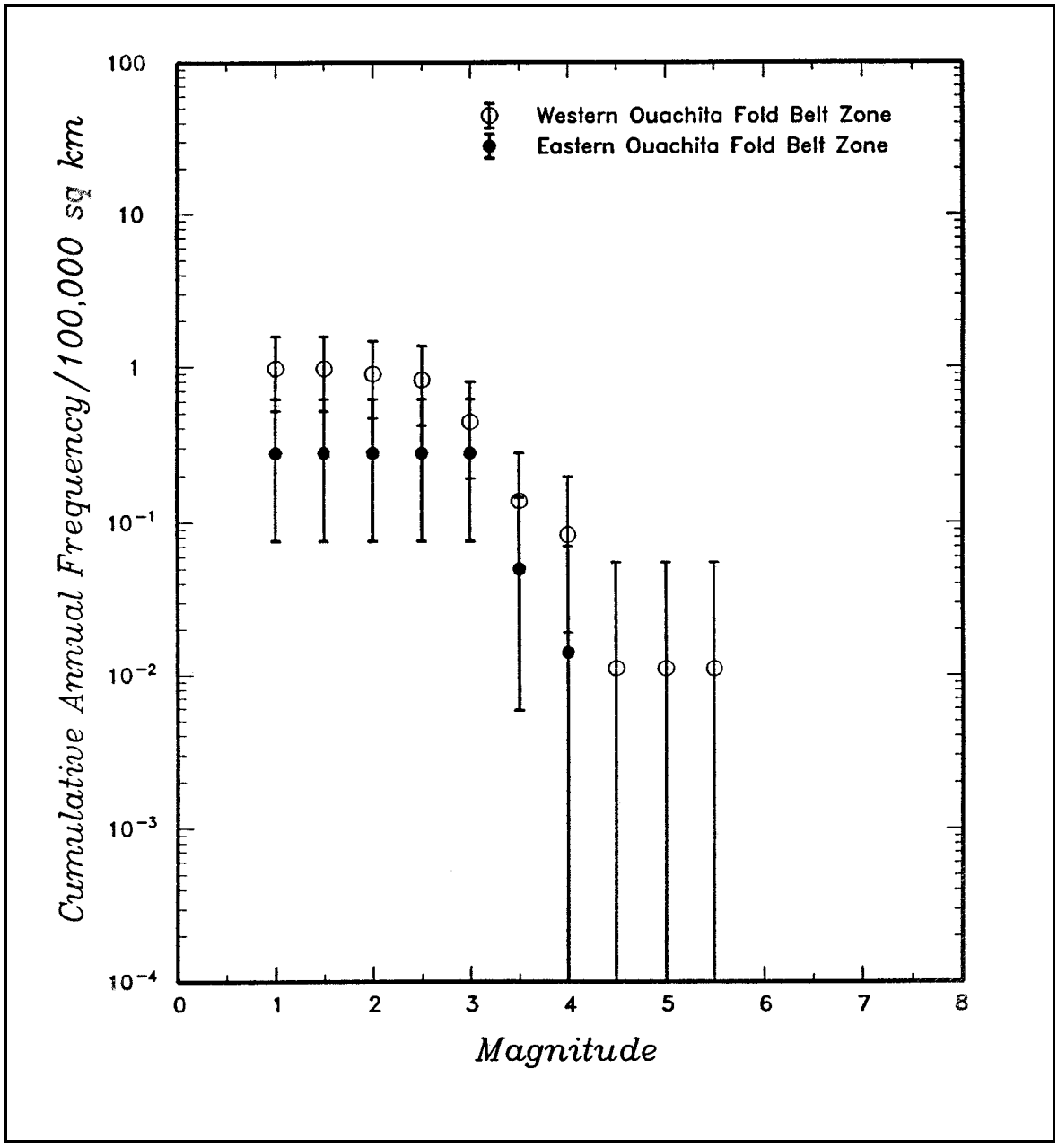

Figure G3-4. Cumulative earthquake frequencies for the western and eastern portions of the Ouachita fold belt source zone

G3-5. Comparison of Deterministic and Probabilistic Results

a. The equal hazard response spectra are compared in Figure G3-10 with deterministic estimates of response spectra for an MCE (magnitude m_b 7.5) occurring on the New Madrid seismic zone at the closest approach to the site (180 km). As shown, the median and mean spectra for the MCE are associated with return periods generally in the range of 1000 to 5000 years, whereas the 84th percentile spectrum for the MCE is associated with a return period greater than 5000 years. The equal hazard spectra were also compared with spectra deterministically estimated for the Ouachita fold belt seismic

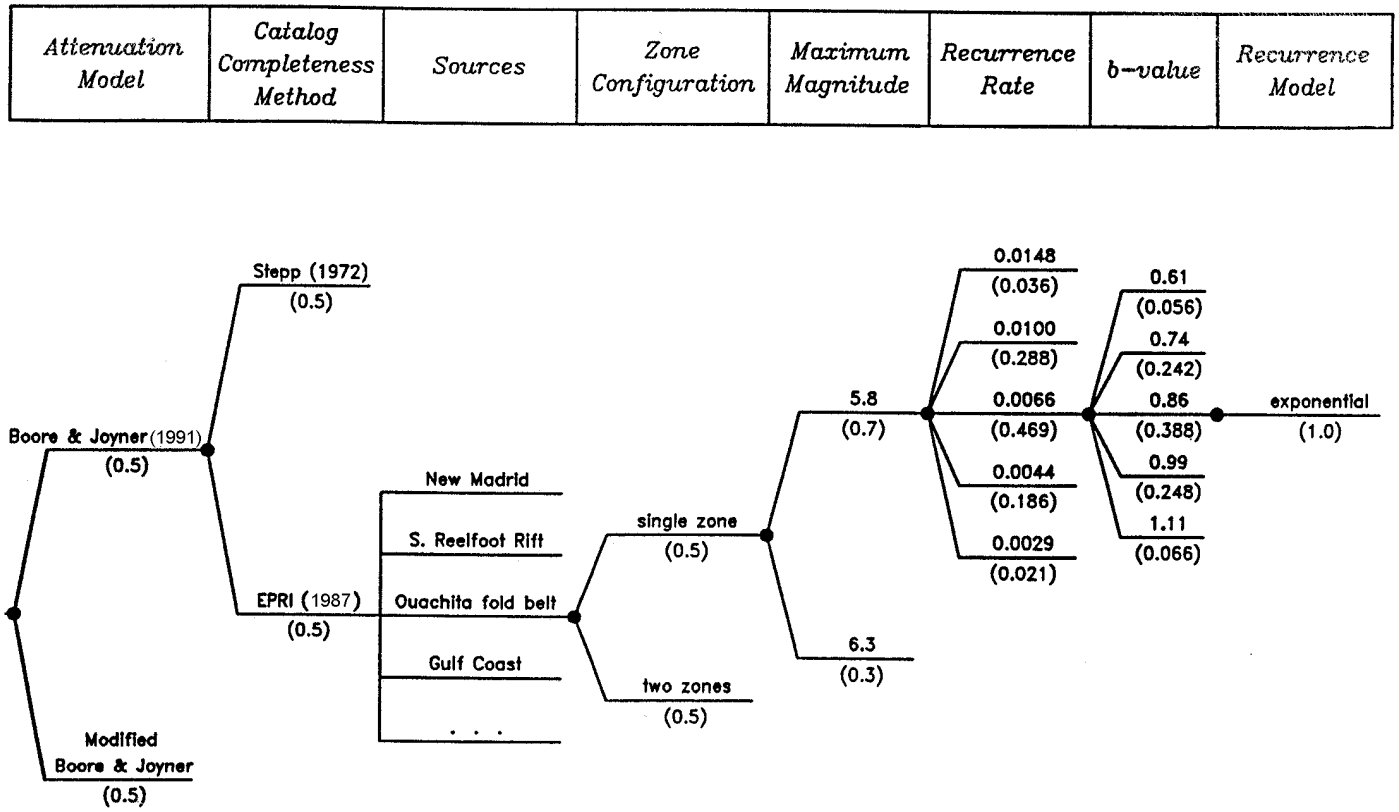

Figure G3-5. Logic tree used to model input parameter uncertainty for probabilistic seismic hazard analysis

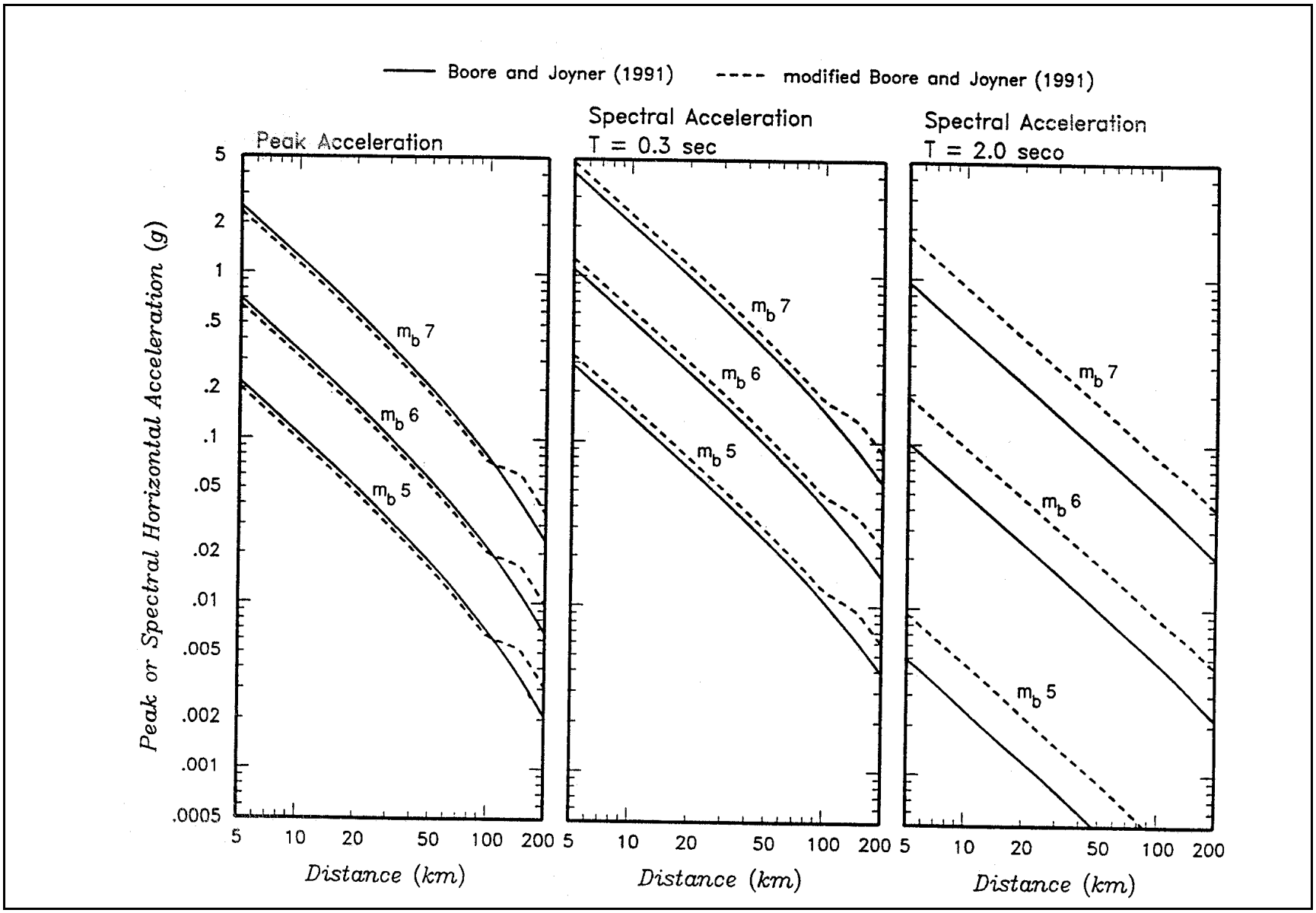

Figure G3-6. Attenuation relationships

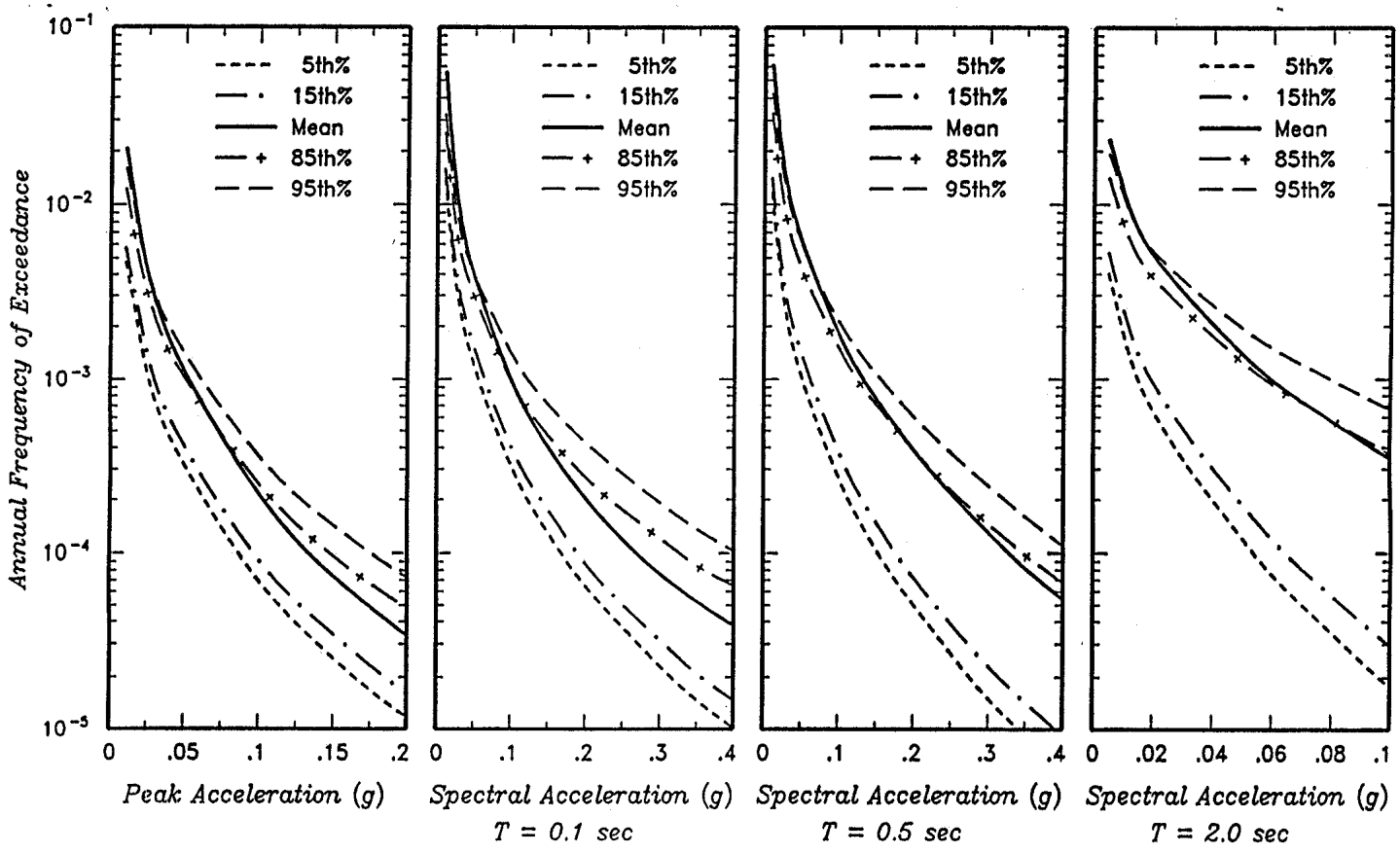

Figure G3-7. Computed hazard curves for peak acceleration and 5 percent-damped spectral accelerations at periods of 0.1, 0.5, and 2.0 sec. Shown are the mean hazard curves and the 5th, 15th, 85th, and 95th percentile hazard curves developed from the distributions of the input parameters

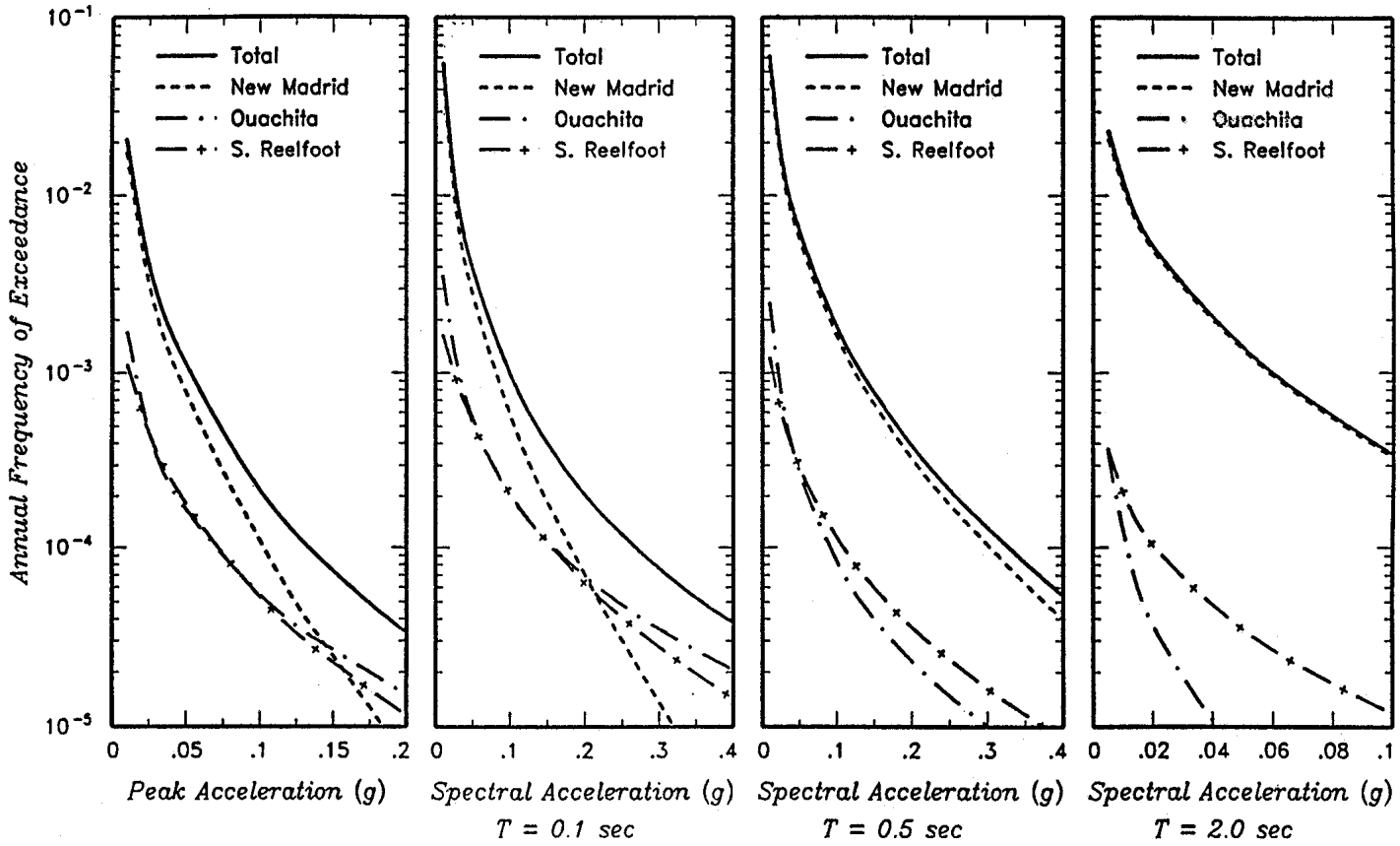

Figure G3-8. Contributions of the main seismic sources to the total mean hazard

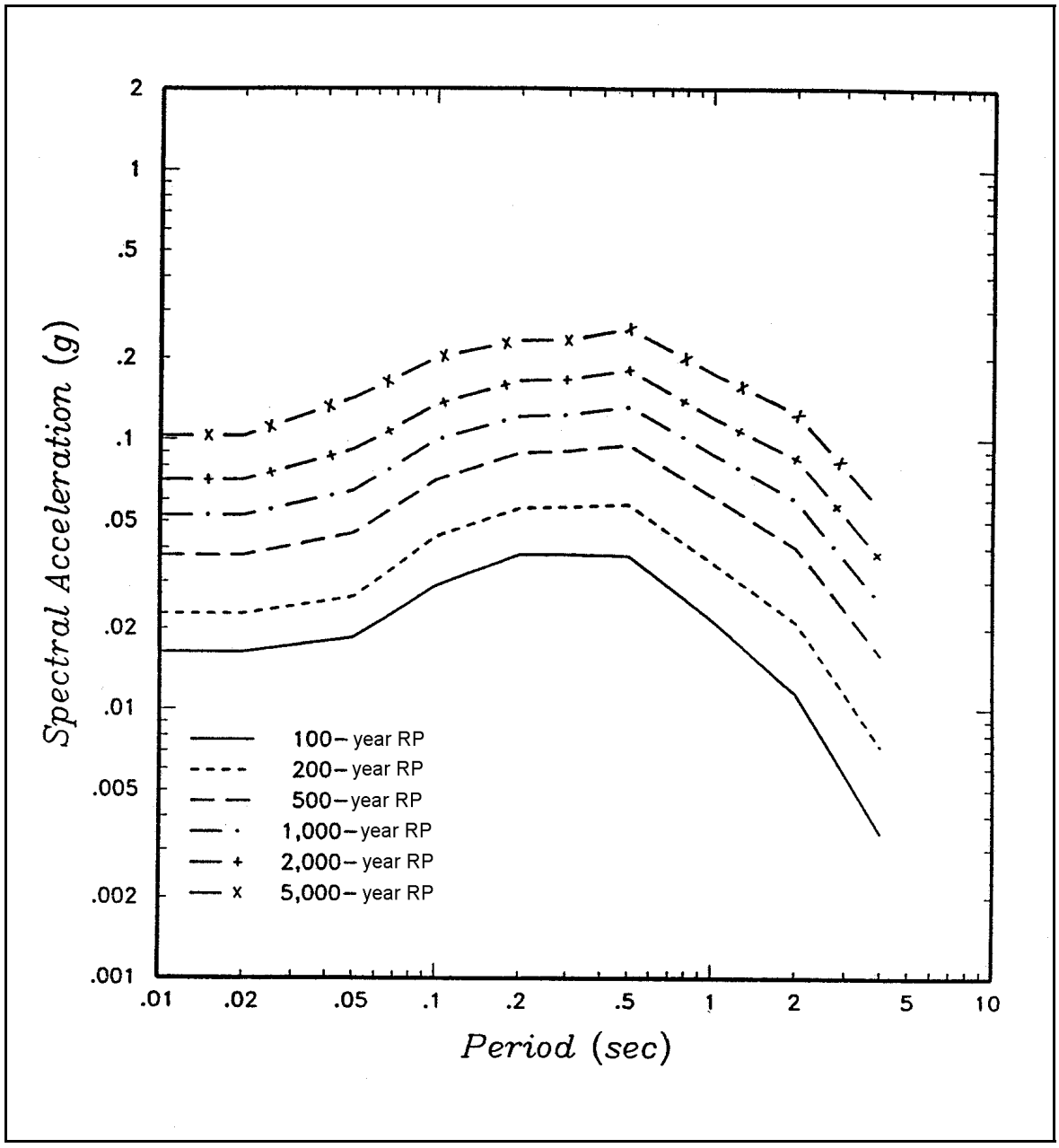

Figure G3-9. Equal-hazard spectra (5 percent damping) for return periods of 100, 200, 500, 1000, 2000, and 5000 years

zone (MCE m_b 5.8) and Reelfoot rift seismic zone (MCE m_b 6.8). In the case of the Ouachita fold belt, a source-to-site distance of 15 km was assumed, which provides an estimate consistent with a statistical random earthquake analysis for a 25-km radius around the site (see Appendix D for description of random earthquake analysis methodology). In the case of the Reelfoot rift seismic zone, the earthquake was assumed to occur at the closest approach of the zone to the site (20 km). The deterministic versus probabilistic comparisons for these two sources are shown in Figures G3-11 and G3-12. For the Ouachita fold belt, ground motions corresponding to the mean estimate were selected. As shown in Figure G3-11, at periods of vibration less than 0.7 sec, these ground motions have a return period longer than 5000 years. For the Reelfoot rift seismic zone, it was assessed that the deterministic event was

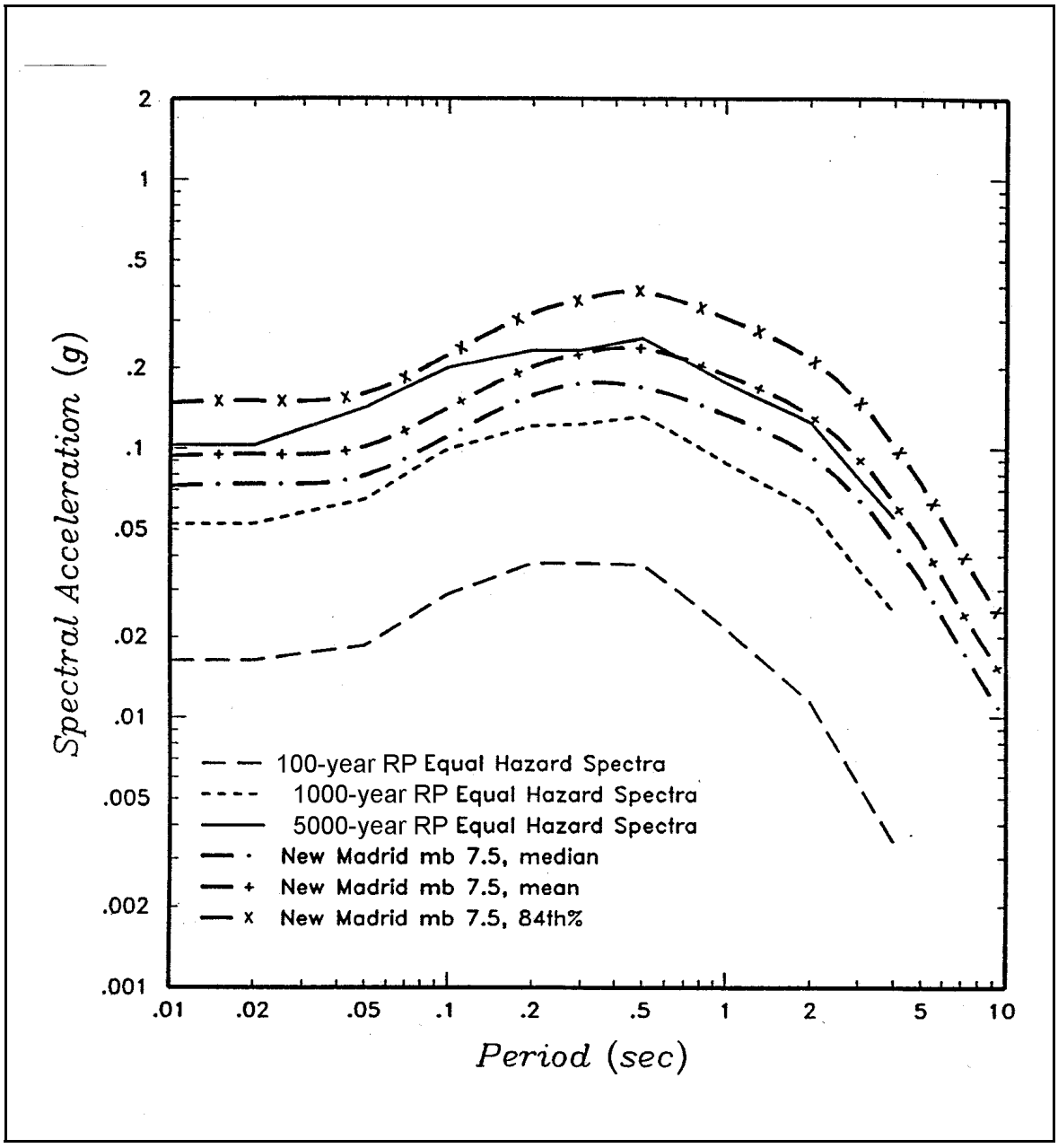

Figure G3-10. Comparison of deterministic ground motion spectra for the New Madrid seismic zone with the equal-hazard spectra from Figure G3-9 (5 percent damping)

sufficiently unlikely (ground motions in Figure G3-12 have return periods much longer than 5000 years) that it would be overly conservative to include this event as an MCE.

b. For this project, the following four design response spectra were selected from the probabilistic and deterministic results:

(1) Operating basis earthquake (OBE), having a 50 percent chance of exceedance in 100 years (corresponding return period of 144 years), which is defined by an equal hazard response spectrum for a 144-year return period.

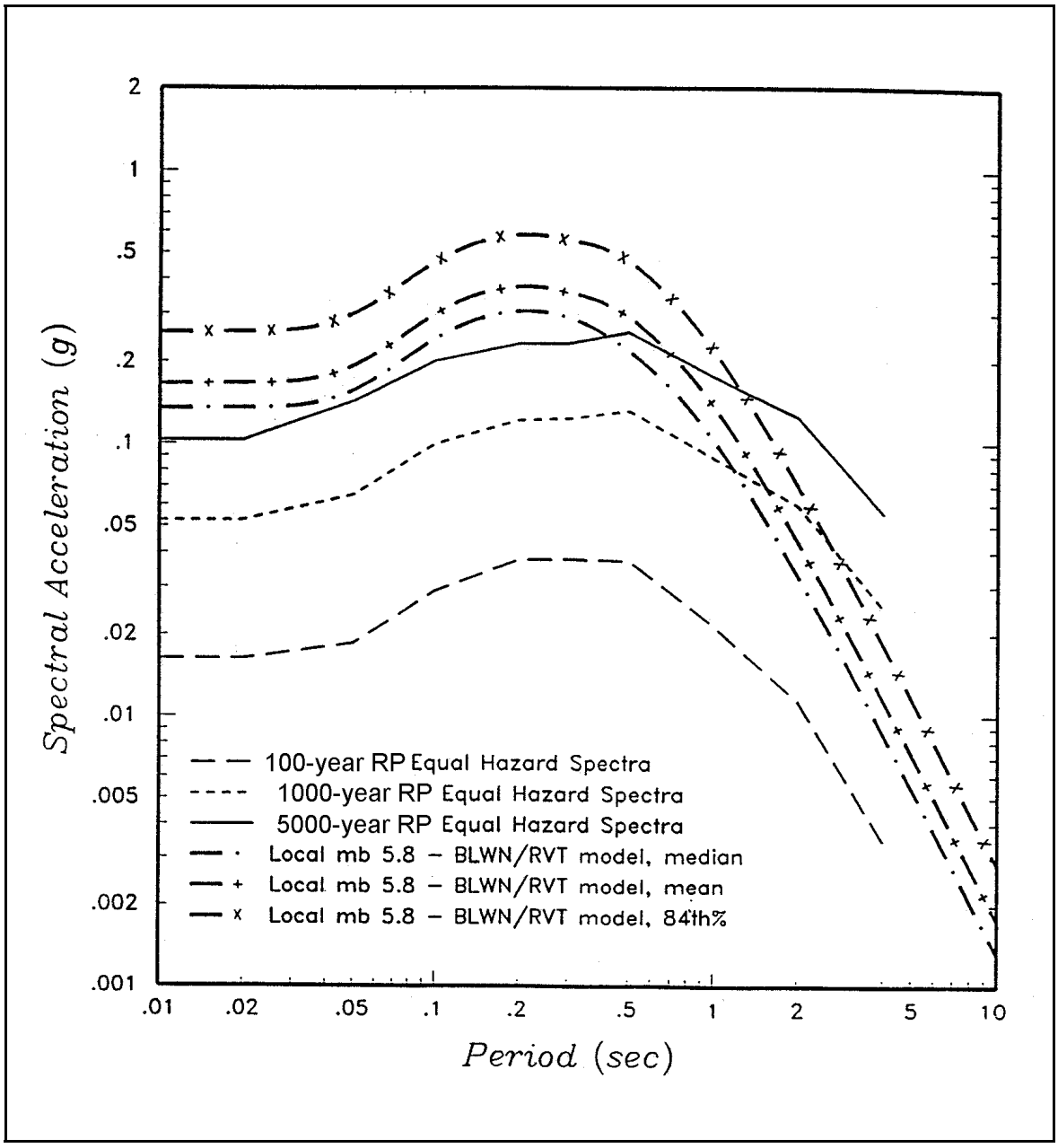

Figure G3-11. Comparison of deterministic ground motion spectra for the Ouachita fold belt source zone with the equal-hazard spectra from Figure G3-9 (5 percent damping)

(2) MDE having a 10 percent probability of exceedance in 100 years (corresponding return period of 950 years), which is defined by an equal hazard response spectrum for a 950-year return period.

(3) Maximum design earthquake (MDE) taken as the MCE on the New Madrid seismic zone at the closest approach to the site, defined by a mean response spectrum for the MCE as described in *a* above.

(4) MDE taken as the MCE on the Ouachita fold belt seismic zone at a 15-km distance from the site, defined by a mean response spectrum for the MCE as described in *a* above.

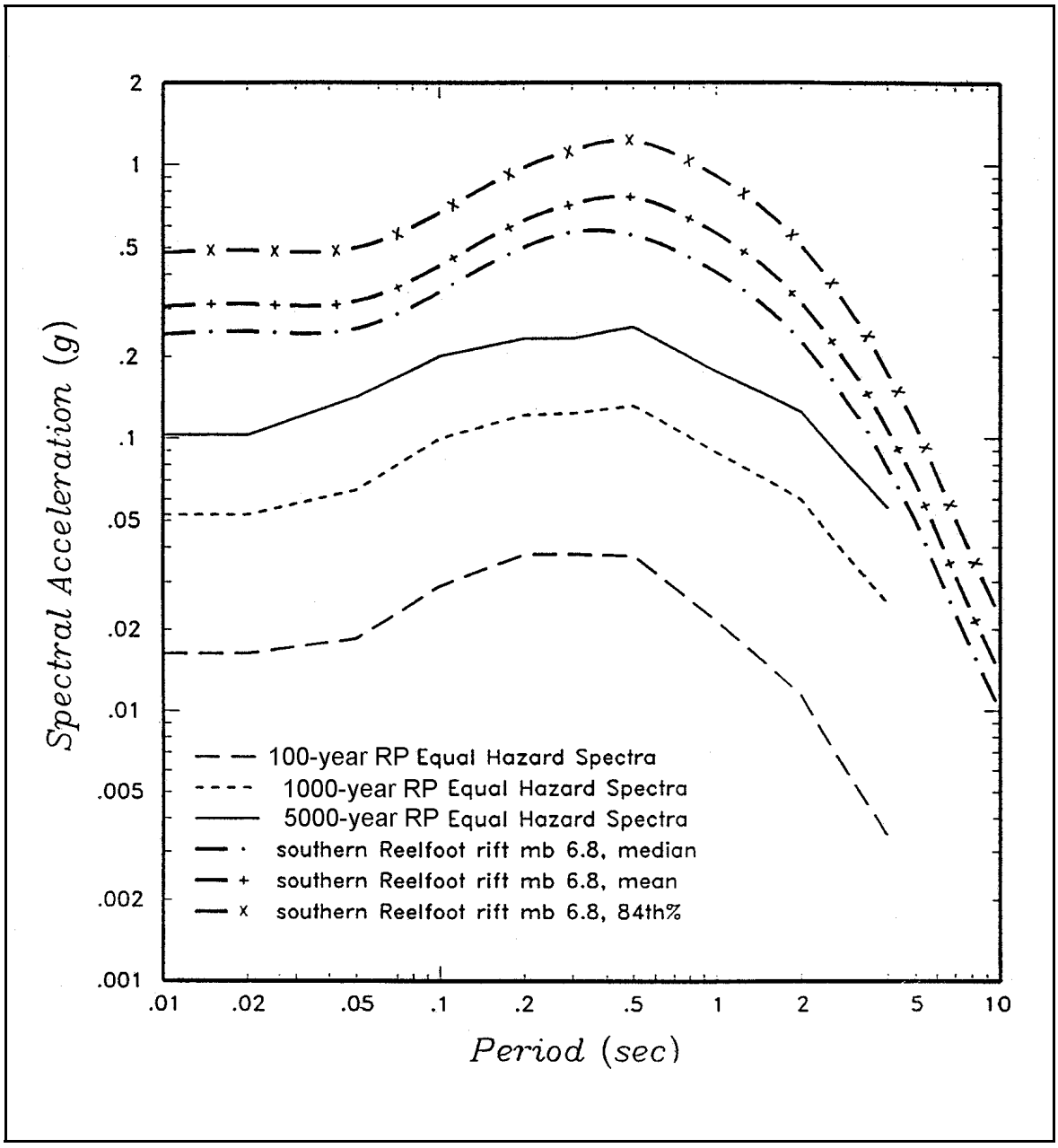

Figure G3-12. Comparison of deterministic ground motion spectra for the southern Reelfoot rift source zone with the equal-hazard spectra from Figure G3-9 (5 percent damping)

The OBE and MDE response spectra are shown in Figures G3-13 and G3-14, respectively. Figure G3-14 also compares the MDE with the spectra obtained using the effective PGA mapped for the site region and the spectral shapes defined in ATC 3-06 (Applied Technology Council 1978) or by the National Earthquake Hazards Reduction Program provisions (Building Seismic Safety Council 1994).

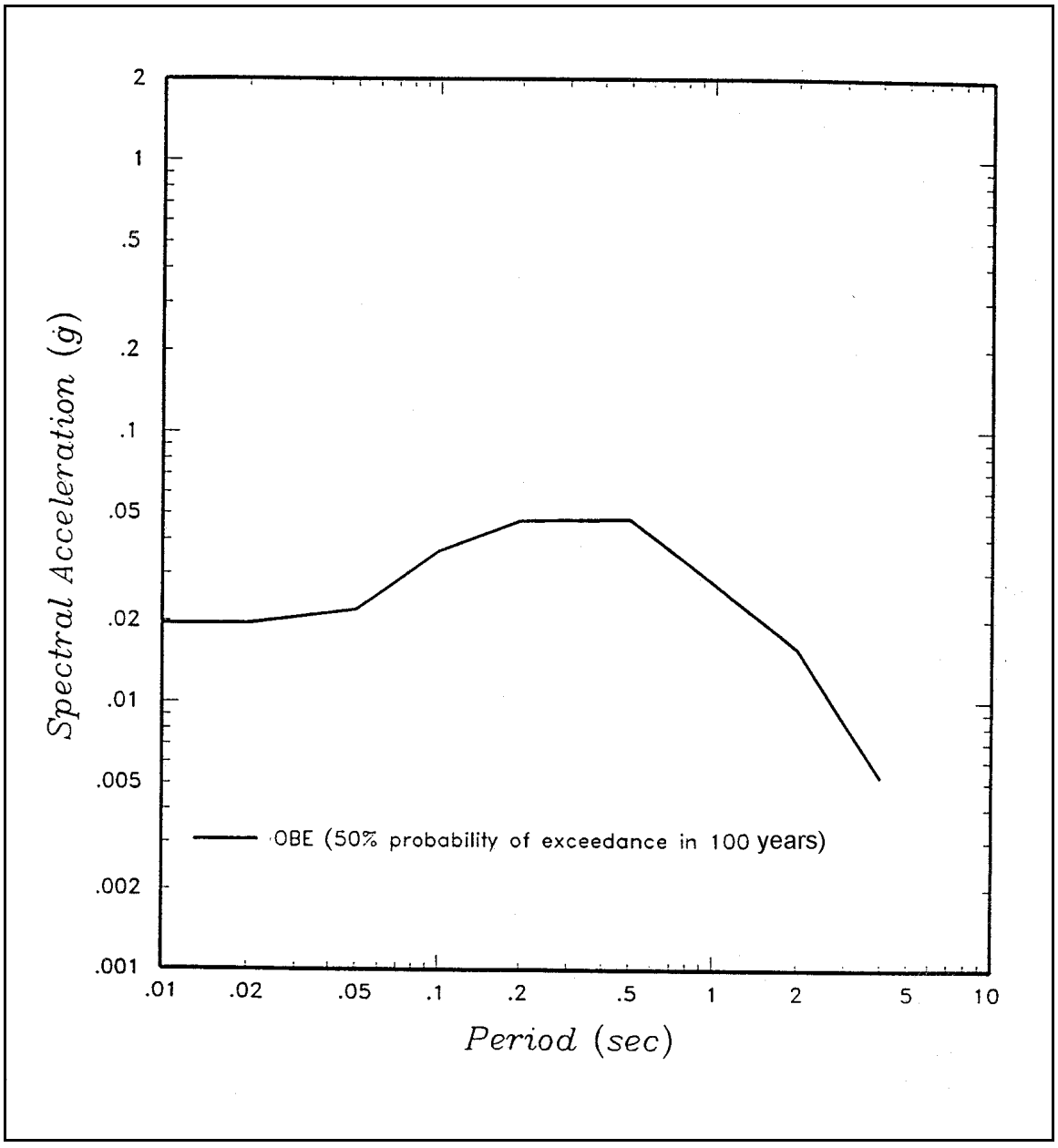

Figure G3-13. OBE spectrum (5 percent damping)

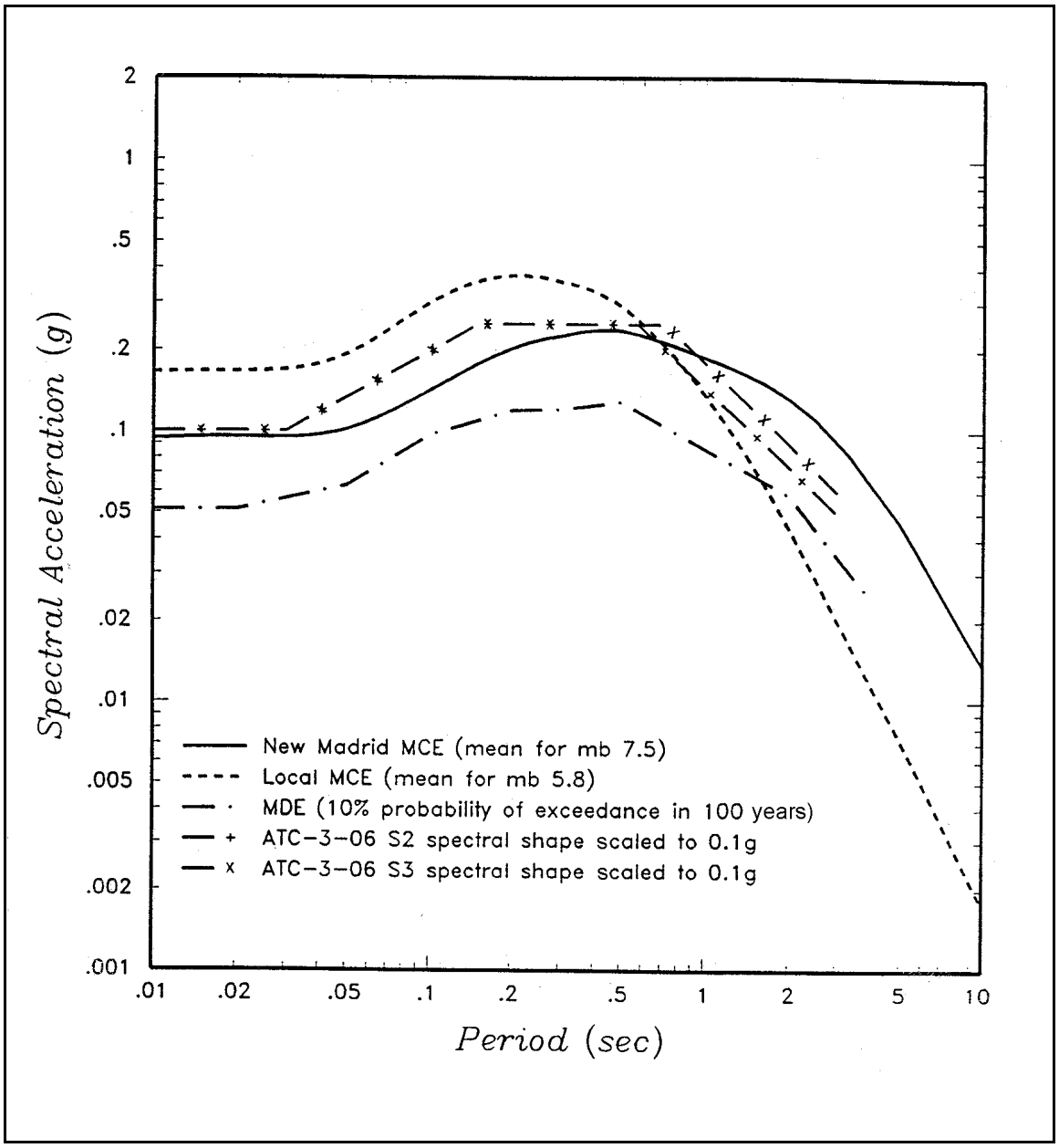

Figure G3-14. MDE spectra (5 percent damping)

Section IV
Example 4
Rock Site in Illinois

G4-1. Introduction

The site location, shown in Figure G4-1, is in southern Illinois on the Ohio River. For this site, equal-hazard response spectra of rock motions were developed for the MDE and OBE. The equal-hazard spectra are compared with deterministic response spectra for the MCE.

G4-2. Seismic Source Characterization

The dominant source zone for this site is the Iapetan Continental Rifts source zone (ICR), which represents an interconnected system of partially developed and failed continental rifts that lie within the midcontinent region of the United States. This zone includes the New Madrid source zone (NSZ), where the large 1811 and 1812 earthquakes occurred. The extent of ICR is shown by the heavy line in Figure G4-1 along with source zones outside ICR and the historical seismicity. Modeling of earthquake recurrence within the dominant ICR can be summarized as follows:

a. The recurrence rate for large (1811-1812 type) earthquakes in NSZ is modeled based on paleoseismic evidence. As shown in Figure G4-2, the paleoseismic-determined rate of these earthquakes exceeds the rate of large earthquakes predicted from the historical seismicity.

b. The recurrence rate for smaller earthquakes in ICR is determined by the historical seismicity. Two basic models are used within a logic tree framework for defining subzones for characterizing recurrence within ICR: a seismicity-based model (given a weight of 0.25) and a geology-based model (given a weight of 0.75). The seismicity-based model divides ICR into cells of one-half degree latitude and longitude and calculates recurrence rates based on the historical seismicity in the cell. Different degrees of smoothing of seismicity rates and b-values among adjacent cells are accomplished using the methodology developed by EPRI (1987). In the geology-based model, Zone ICR is divided into subzones as indicated in Figure G4-1. Different combinations of subzones are defined in a logic tree approach. The possible combinations are controlled in part by the presence or absence of four possible tectonic boundaries within the ICR (Figure G4-1) and the assessed likelihood that these features represent fundamental boundaries that control the distribution, rate, and maximum magnitudes of seismicity. The logic tree for weights assigned to these boundaries is shown in Figure G4-3. Thirty alternative subzonations (not shown herein) of ICR result from the logic tree of Figure G4-3. Within each subzone of each alternative, seismicity rates are determined based on the seismicity within the subzone and assuming the rate is uniform within the subzone.

Probabilistic distributions of maximum earthquake magnitudes are also part of the source model logic tree. These probabilistic distributions were determined using the methodology developed by EPRI (Johnston et al. 1994). This methodology used worldwide databases to assess maximum earthquake magnitudes in stable continental regions (like the eastern United States) where active faults have not been identified and therefore maximum magnitude cannot be estimated on the basis of fault dimensions (as is done in the western United States). However, for the New Madrid zone, maximum earthquake magnitudes were estimated on the basis of both estimated rupture models by Johnston (1996) and Gomberg and Ellis (1994) and correlations of magnitude with rupture dimensions; and estimates of magnitudes of the 1811-1812 earthquakes by Johnston (1996).

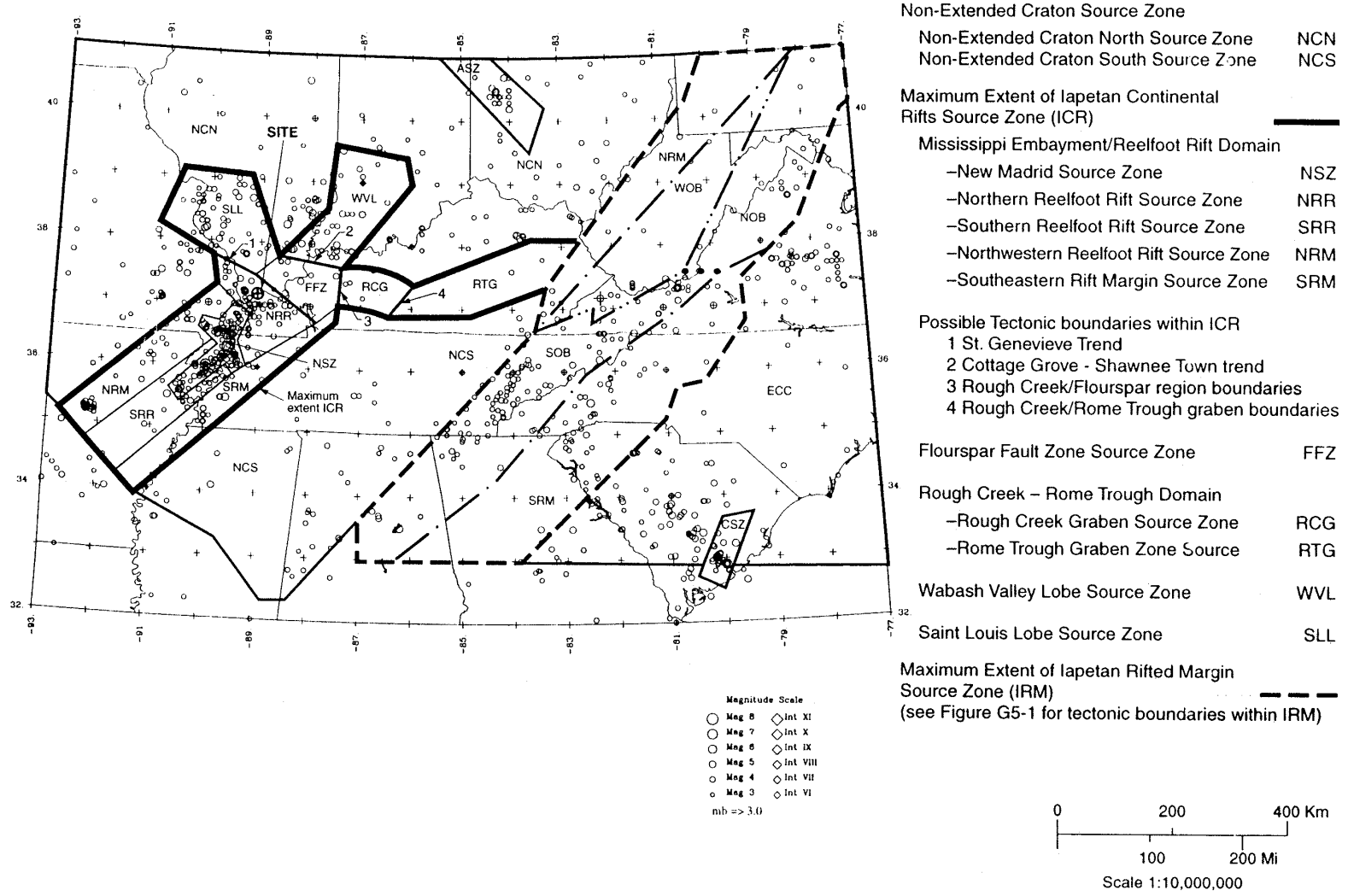

Figure G4-1. Seismic source zonation model of central and southeastern United States, rock site in Illinois

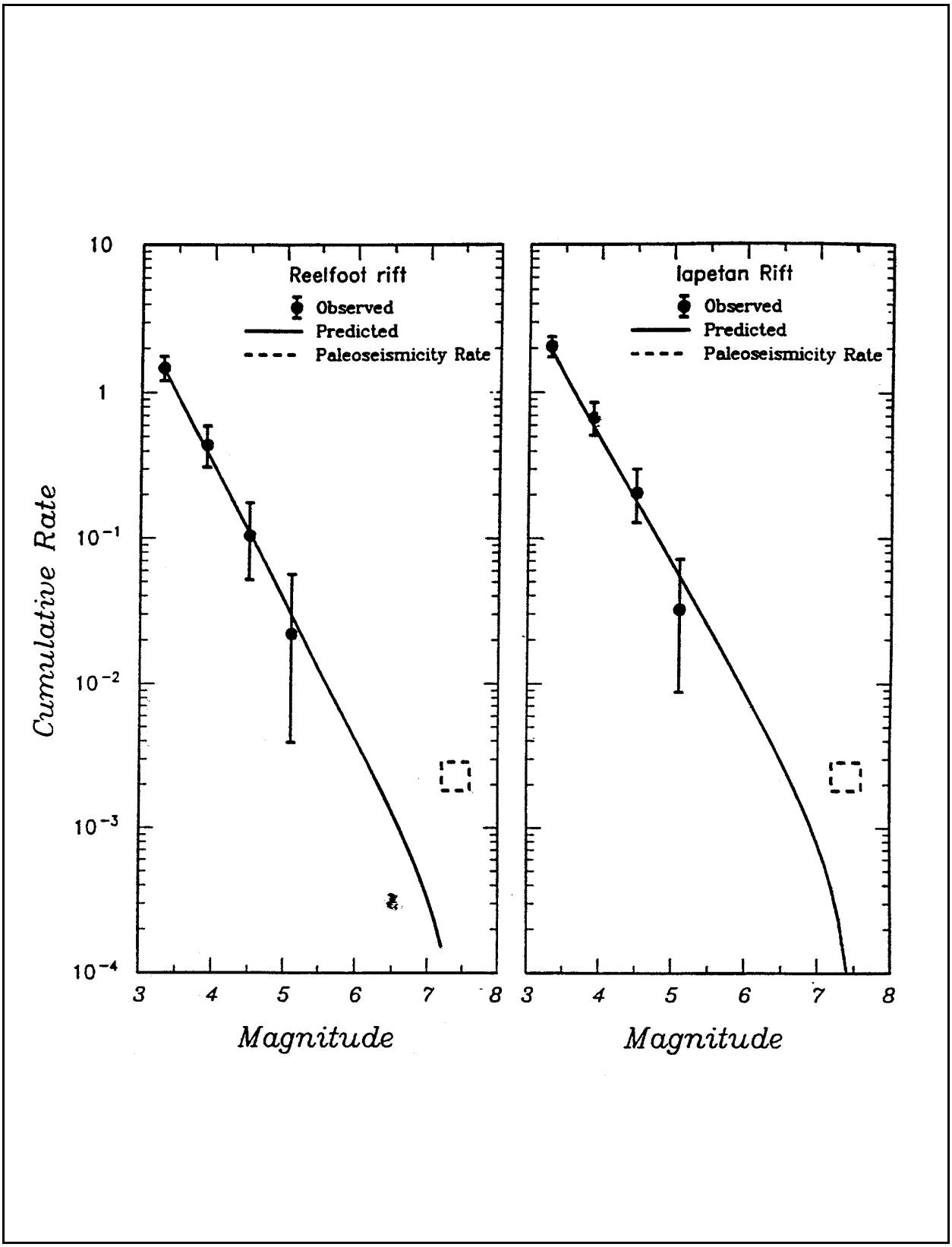

Figure G4-2. Comparison of historical and paleoseismic recurrence estimates for the Reelfoot Rift and Iapetan Rift siesmic zone

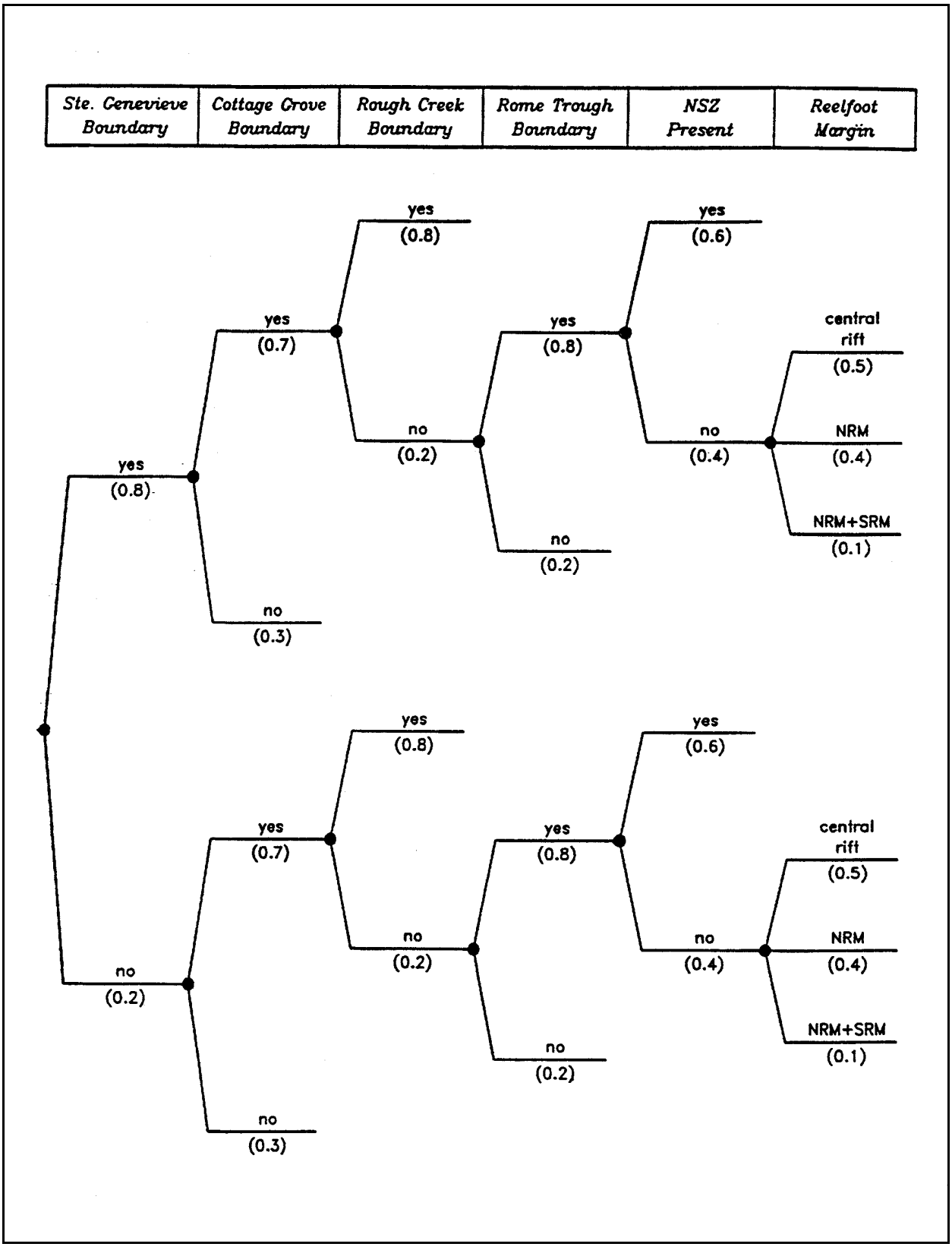

Figure G4-3. Logic tree showing relative weights assigned to boundaries separating potential subzones of the Iapetan Rift seismic zone

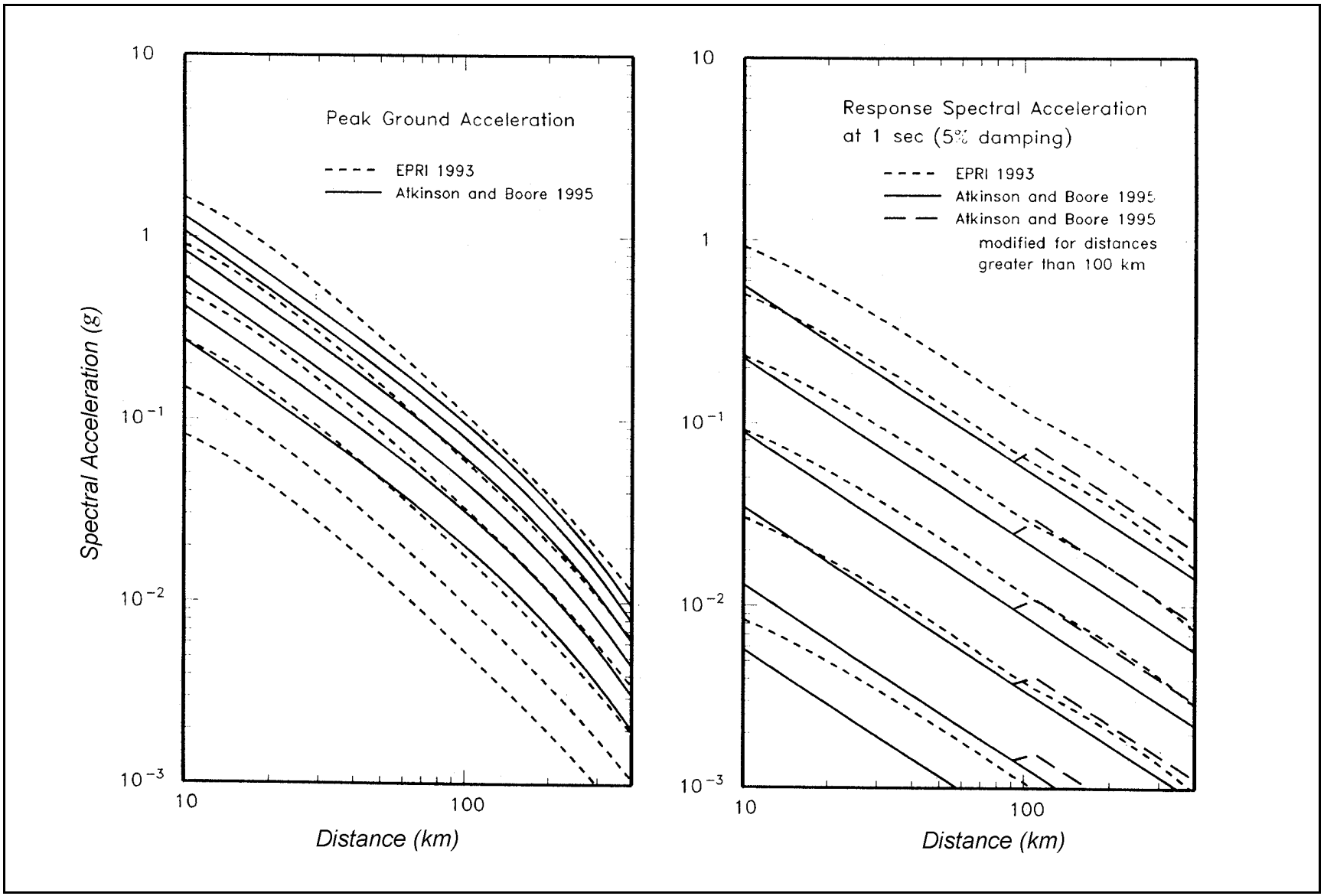

Figure G4-4. Attenuation curves of Atkinson and Boore (1995) and EPRI (1993) for peak ground acceleration and response spectral acceleration at 1.0-sec period. Note: Lowest curve for each relationship is for m_b 5.0; highest curve, for m_b 7.5

G4-3. Ground Motion Attenuation Characterization

a. It was desired to estimate ground motions on rock at the site. Two attenuation relationships applicable to hard rock in the eastern United States for horizontal peak ground acceleration and response spectral accelerations of ground motions at different periods of vibration were used. The relationships are those of EPRI (1993) (later published as Toro, Abrahamson, and Schneider 1997, see Tables 3-1 and 3-3, main text) and Atkinson and Boore (1995) (later published as Atkinson and Boore 1997, see Tables 3-1 and 3-3, main text).

b. The relationship for response spectral acceleration of EPRI extends to periods as long as 1 sec, and that of Atkinson and Boore extends to a period of 2 sec. The EPRI relationship was extrapolated to a period of 2 sec. This was accomplished by extrapolating the coefficients of the attenuation relationship and examining the reasonableness of the resulting spectral prediction. The smooth quadratic form of the relationship of Atkinson and Boore (1995) underestimates their simulations of longer period ground motions at distances beyond 100 km. Therefore, their relationships were modified at periods greater than 0.5 sec to result in ground motion estimates closer to the simulation results.

c. Plots of the attenuation relationships of EPRI (1993) and Atkinson and Boore (1995) for peak ground acceleration and response spectral accelerations at 1.0 sec are presented in Figure G4-4. The modifications to the 1-sec motion at distances greater than 100 km can be seen in the figure. The plots in Figure G4-4 clearly indicate the distinctive differences between the two eastern United States attenuation relationships: the Atkinson and Boore (1995) relationships result in higher spectral values than those of EPRI (1993) for peak ground acceleration and for short-period response spectral accelerations (less than about 0.2-sec period), but lower values than those of EPRI (1993) at longer periods.

d. In the hazard analysis, the relationship of EPRI (1993) was given a higher weight (0.67) than that of Atkinson and Boore (1995) (0.33). The reason for this judgment was that the EPRI (1993) relationship resulted from an EPRI study that involved input from a number of ground motion experts and thus could be viewed as having achieved a certain degree of consensus regarding the model. The practical effect of higher weighting on the EPRI (1993) model is to increase longer period ground motions and reduce short-period ground motions.

G4-4. PSHA Results

Hazard curves obtained from the analysis for peak ground acceleration and response spectral acceleration at two periods of vibration are shown in Figure G4-5. The uncertainty bands around the mean curves, reflecting the alternative seismic source models and attenuation relationships incorporated into the logic tree, are shown in the figure. The contributions to the hazard are almost entirely from Zone ICR. Figure G4-6 shows contributions within ICR from large New Madrid Zone earthquakes with rates defined by paleoseismic data (dashed-dotted line) and smaller earthquakes defined by seismicity (dashed line). It can be seen that the smaller earthquakes dominate hazard at higher frequencies (probabilities) of exceedance and the larger, 1811-1812-type earthquakes dominate at lower frequencies (probabilities) of exceedance. Figure G4-7 compares the hazard obtained from geology-based and seismicity-based models. It can be seen that, for this site, the two modeling approaches lead to almost identical results. Equal-hazard response spectra obtained from the mean hazard results for all the periods of vibration analyzed are shown in Figure G4-8 for return periods varying from 144 to 10,000 years.

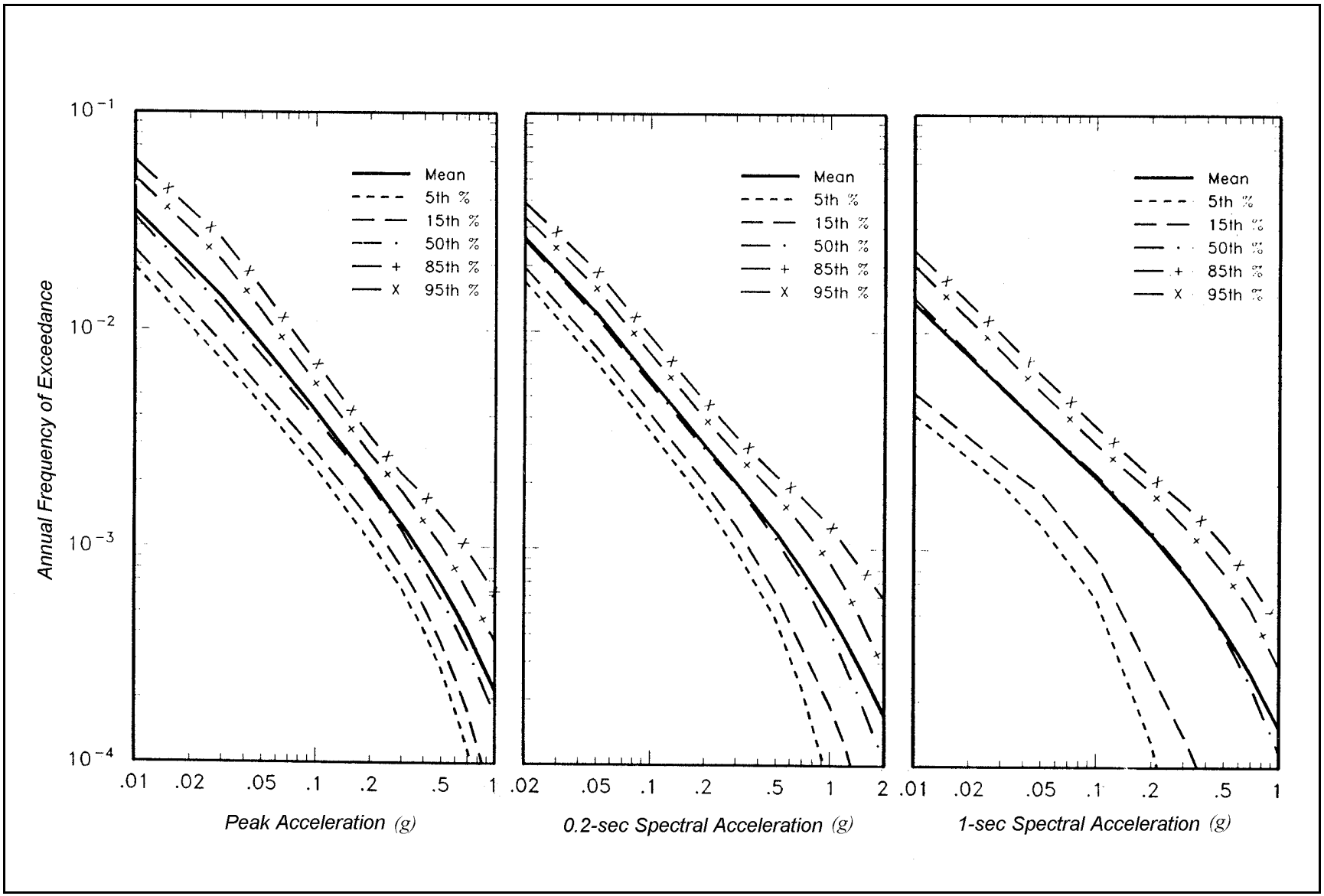

Figure G4-5. Computed hazard for peak ground acceleration and response spectral accelerations at 0.2- and 1.0-sec periods (5 percent damping total hazard curves)

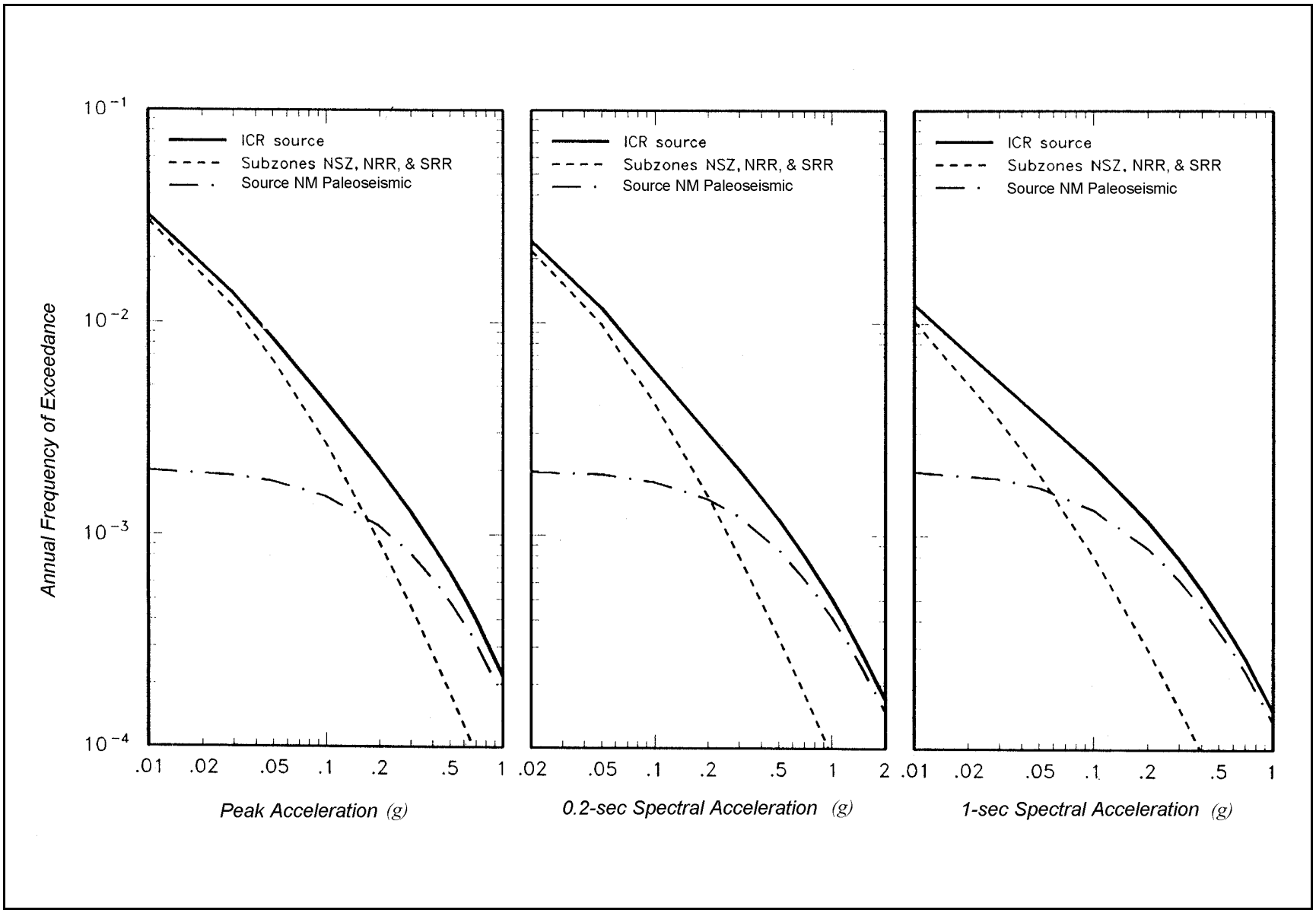

Figure G4-6. Contributions of components of the ICR source to the hazard at 5 percent damping

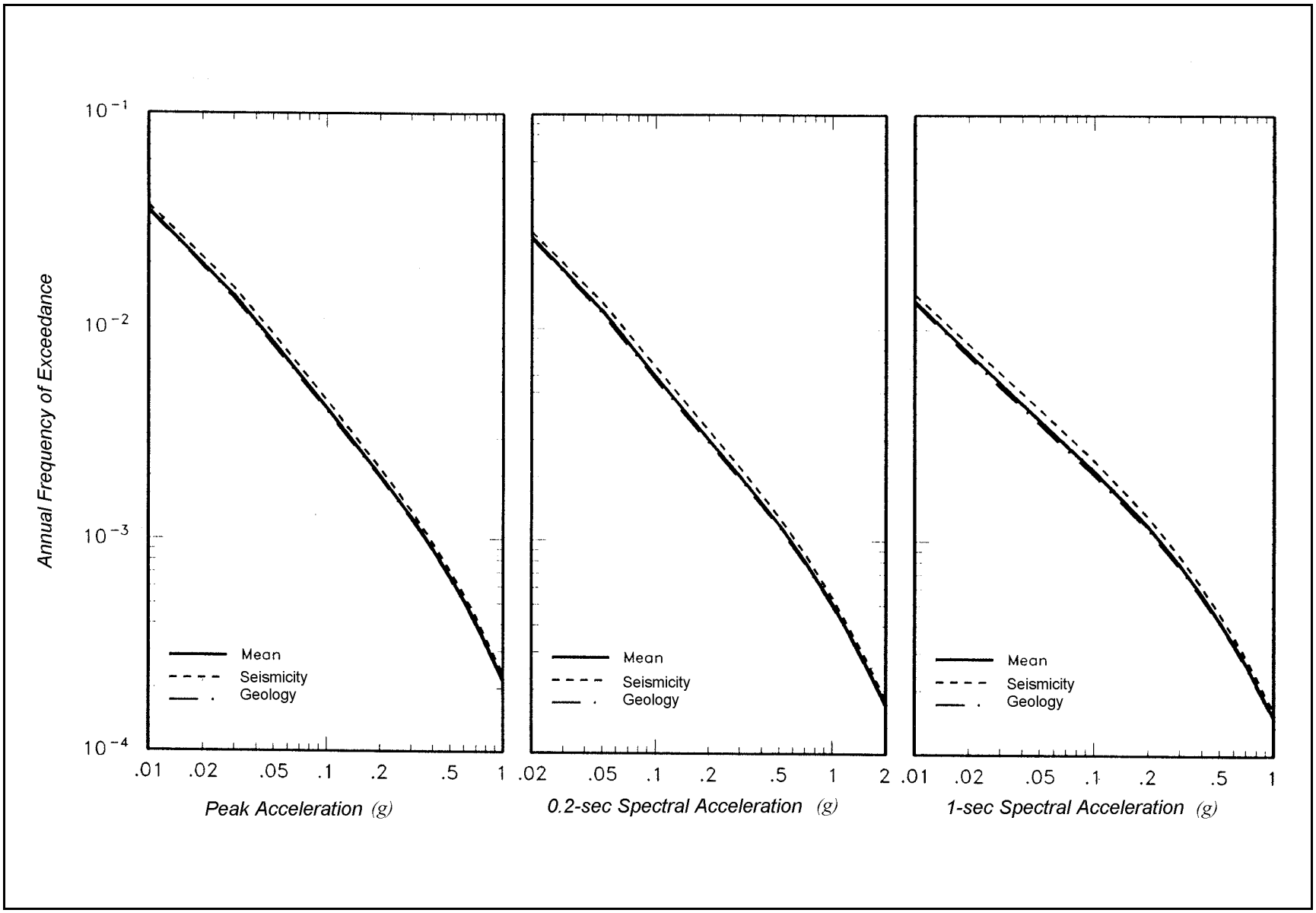

Figure G4-7. Comparisons of hazard from the geology- and seismicity-based models at 5 percent damping

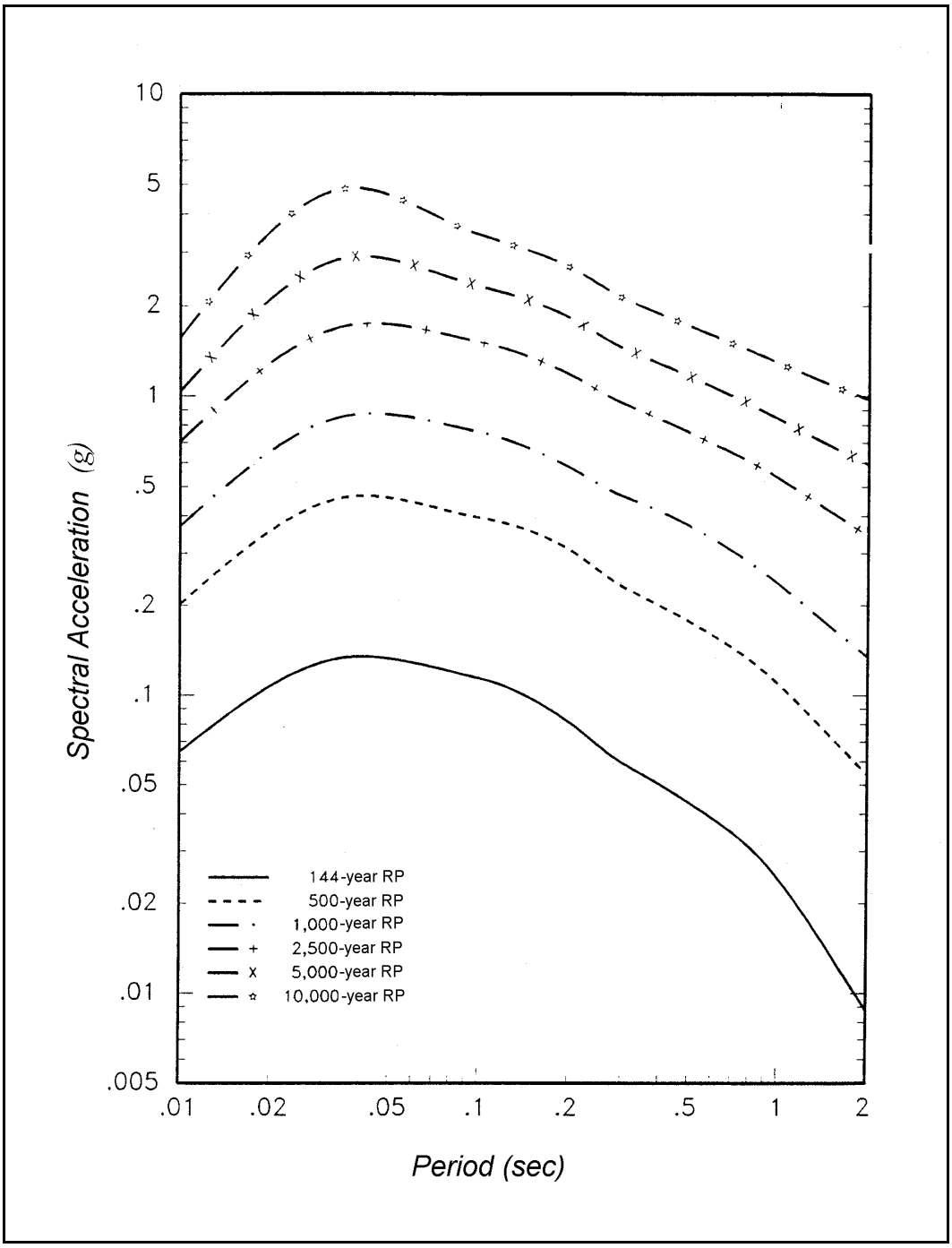

Figure G4-8. Equal-hazard response spectra (5 percent damping)

G4-5. Comparison of Deterministic and Probabilistic Results

a. The probabilistic equal-hazard spectra of rock motions at this site were compared with deterministic spectra of rock motions at the site for an MCE occurring on the closest approach of the New Madrid source. The maximum event assigned to this source ranged from m_b 7.0 to 8.0 with a mean value of m_b 7.5. The closest approach of this source to the site is 30 km. Deterministic response spectra for the

New Madrid source were computed using the attenuation models selected for the PSHA and the distribution of maximum magnitudes developed for the New Madrid source. Figure G4-9 compares median (50^{th} percentile) and 84^{th} percentile deterministic response spectra for this event with the equal-hazard spectra presented in Figure G4-8. The median deterministic spectrum corresponds to ground motions with a return period between 1000 and 2500 years, and the 84^{th} percentile deterministic spectrum corresponds to ground motions with a return period of about 5000 years.

b. For this project, the equal-hazard response spectrum with a 144-year return period (50 percent probability of exceedance in 100 years) was selected as the OBE ground motion. The MDE ground motion was selected as the equal-hazard response spectrum having a 1000-year return period (approximate 10 percent probability of exceedance in 100 years).

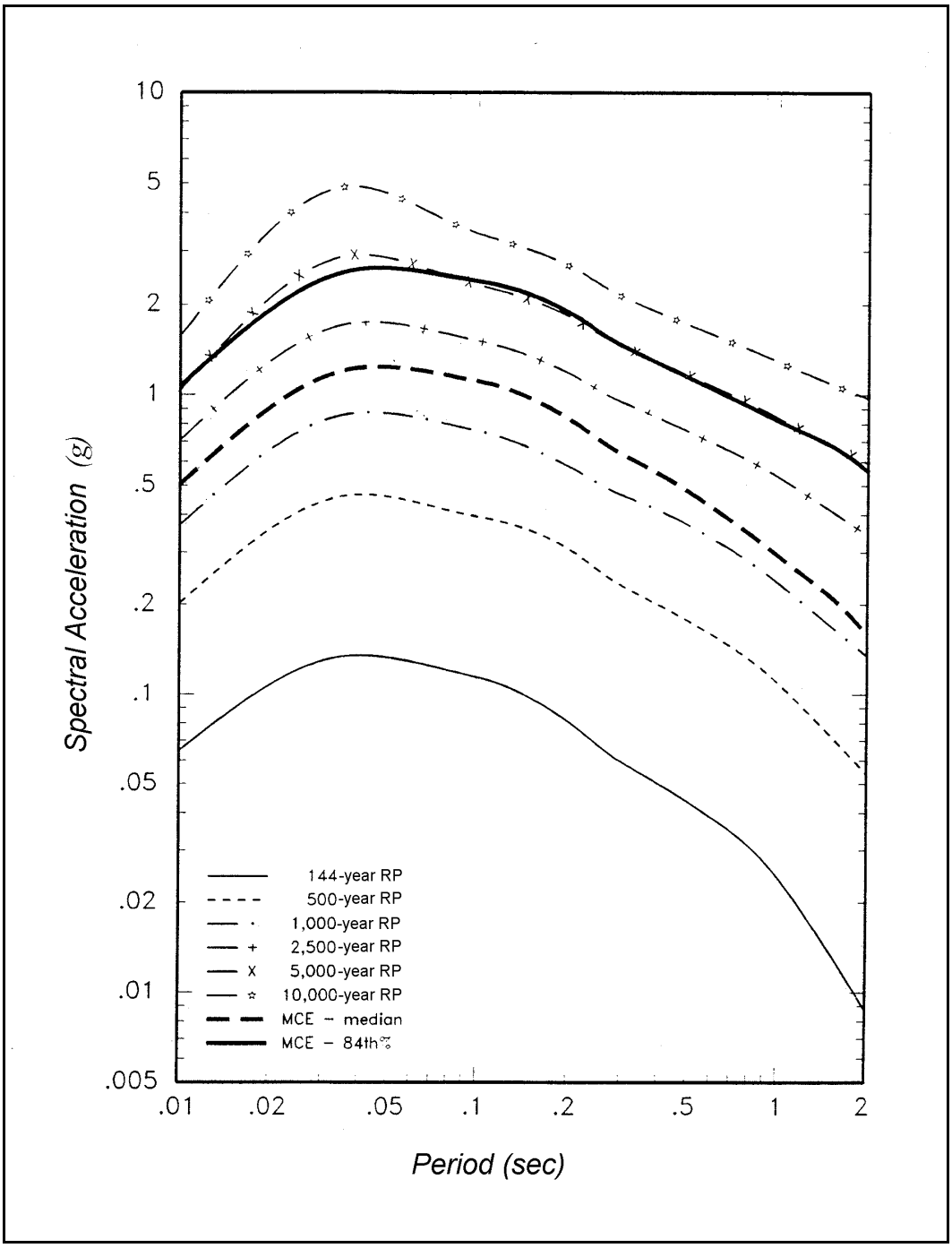

Figure G4-9. Comparison of equal-hazard and deterministic response spectra (5 percent damping)

Section V
Example 5
Rock Site in West Virginia

G5-1. Introduction

The site is located in south-central West Virginia (Figure G5-1). For this site, equal-hazard response spectra were developed for the MDE and OBE. The equal-hazard spectra are compared with the deterministic response spectrum for the MCE.

G5-2. Seismic Source Characterization

a. The site is in an area of low seismicity (Figure G5-1). Two source zones dominate the seismic hazard at the site: the ICR, which is described in Example G4; and the Iapetan Rifted Margin source zone (IRM), in which the site is located (Figure G5-1). The IRM is defined by the known or inferred presence of large normal faults formed along the passive margin of the late Proterozoic to early Paleozoic Iapetus Ocean. Compressional reactivation of favorably oriented Iapetan faults has been suggested as the causal mechanism for several seismically active regions in eastern North America. The extent of the IRM is shown by the heavy black line in Figure G5-1. Source zones outside IRM and ICR are also shown in the figure.

b. Modeling of earthquake recurrence rates within source zone ICR is described in Example G4. A similar approach to recurrence modeling was taken for source zone IRM, except that paleoseismic data are not available to supplement seismicity data for IRM.

c. As was done for ICR, two basic models were used within a logic tree framework to define subzones for characterizing recurrence within IRM: a seismicity-based model (given a weight of 0.25) and a geology-based model (given a weight 0.75). The seismicity-based model divides IRM into cells of one-half degree latitude and longitude and calculates recurrence rates based on the historical seismicity in the cell. Different degrees of smoothing of seismicity rates and b-values among adjacent cells are accomplished using the methodology developed by EPRI (1987). In the geology-based model, Zone IRM is divided into subzones as indicated in Figure G5-1. Different combinations of subzones are defined in a logic tree approach. The possible combinations are controlled by the presence or absence of three possible tectonic boundaries within IRM (Figure G5-1) and the assessed likelihood that these features represent fundamental boundaries that control the distribution, rate, and maximum magnitudes of seismicity. The logic tree for weights assigned to these boundaries is shown in Figure G5-2. Five alternative subzonations (not shown herein) of IRM result from the logic tree of Figure G5-2. Within each subzone of each alternative, seismicity rates are determined based on the seismicity within the subzone and assuming the rate is uniform within the subzone.

d. Probabilistic distributions of maximum earthquake magnitudes are also part of the source model logic tree. These probabilistic distributions were determined using the methodology developed by EPRI (Johnston et al. 1994). As discussed in paragraph G4-2, this methodology used worldwide databases to assess maximum earthquake magnitudes in stable continental regions (like the eastern United States) where active faults have not been identified and therefore maximum magnitudes cannot be estimated on the basis of fault dimensions (as is done in the western United States).

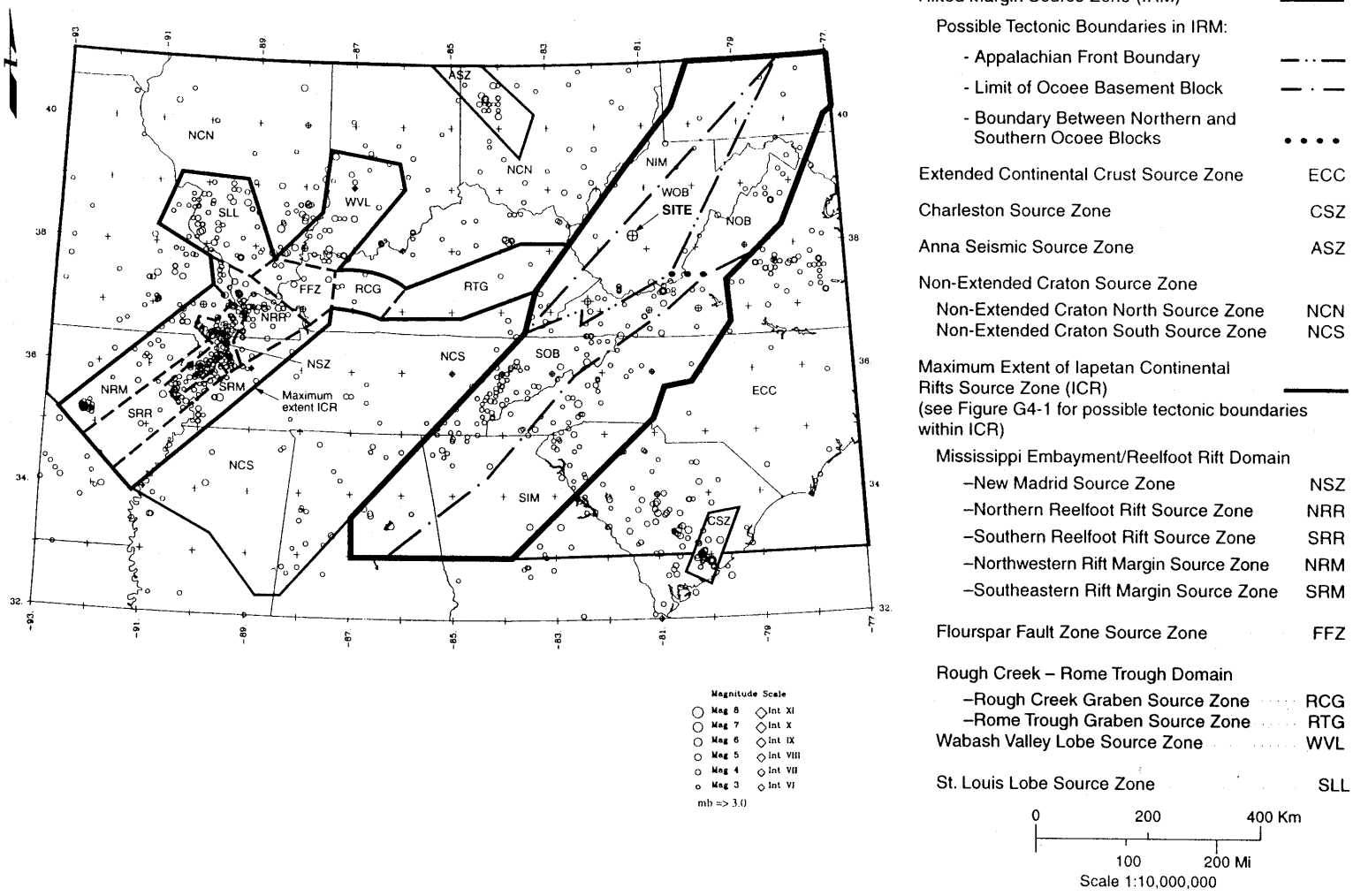

Figure G5-1. Seismic source zonation model of central and southeastern United States, rock site in West Virginia

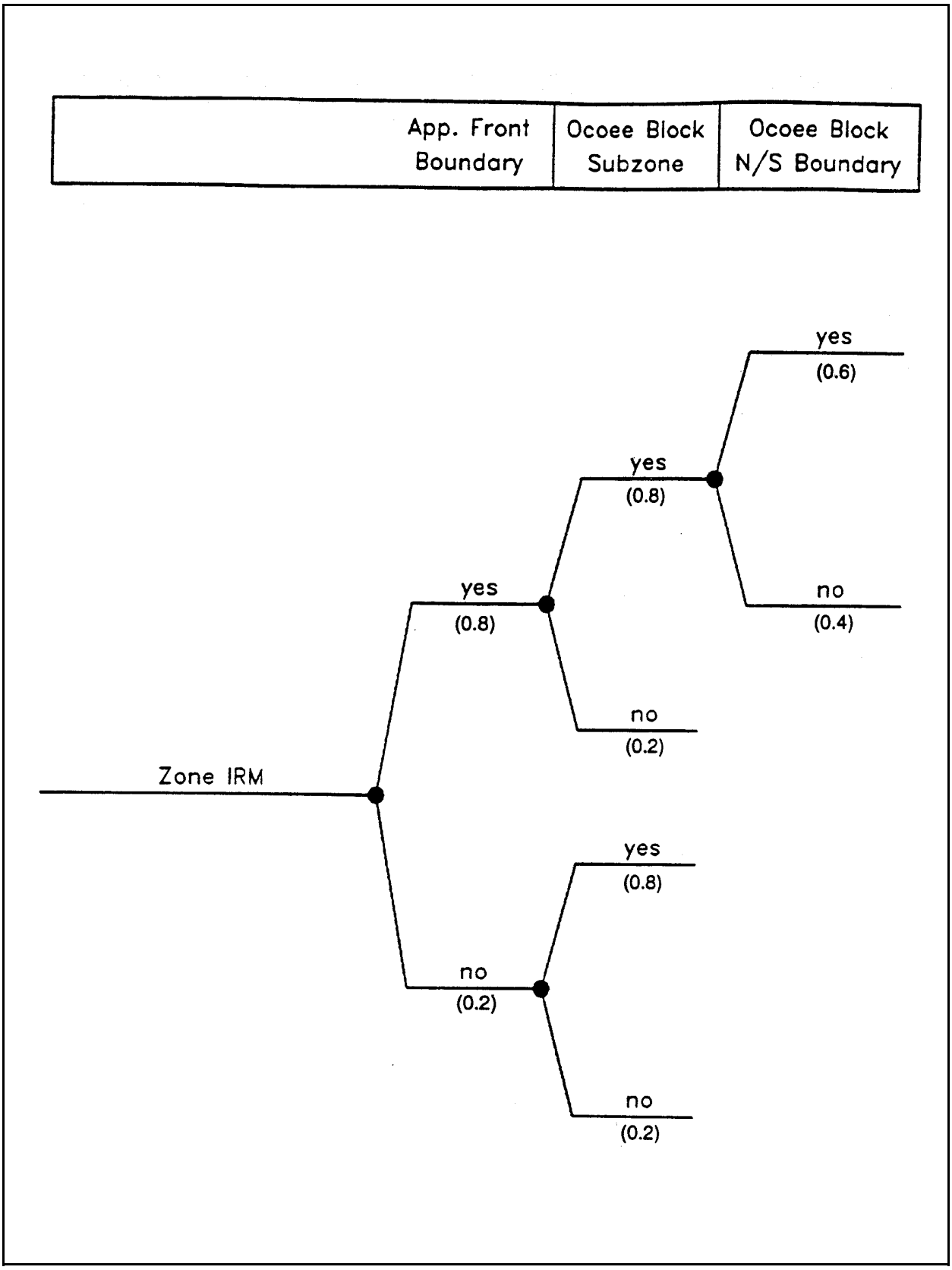

Figure G5-2. Seismic source model logic tree for Zone IRM

G5-3. Ground Motion Attenuation Characterization

It was desired to estimate ground motions on rock at the site. Two attenuation relationships applicable to hard rock in the eastern United States for horizontal peak ground acceleration and response spectral acceleration of ground motions at different periods of vibration were used. These relationships are the same as those used for Example G4, including the relative weighting given to the relationships. The relationships are described in Section G4-3 and illustrated in Figure G4-4. An adjustment to these relationships was made to account for somewhat softer rock at the site than the hard rock applicable to the attenuation relationships. The adjustment was made by analyzing the rock crustal structure using the stochastic ground motion model of Boore (1983, 1986). The adjustments were a maximum spectral amplification of 1.2 times at periods greater than 0.1 sec, a maximum spectral deamplification of 0.8 time at periods less than 0.1 sec, and 1.0 at zero period (taken to be 0.01-sec period).

G5-4. PSHA Results

a. Hazard curves obtained from the analysis for peak ground acceleration and response spectral acceleration at two periods of vibration are shown in Figure G5-3. The uncertainty bands around the mean curves, reflecting the alternative seismic source models and attenuation relationships incorporated into the logic tree, are shown in the figure. The contributions to the hazard from different source zones for peak ground acceleration, spectral acceleration at 0.3 sec, and spectral acceleration at 1.0 sec are shown in Figure G5-4. As can be seen, for peak ground acceleration, source zone IRM dominates the hazard. With increasing period of vibration, source zone ICR contributes relatively more to the hazard and is the dominant contributor at a period of 1.0 sec. Earthquake magnitude and distance contributions to the hazard for peak ground acceleration and 1.0-sec response spectral acceleration for a return period of 1000 years are shown in Figure G5-5. For peak ground acceleration, most of the hazard comes from m_b 5 to 6 earthquakes occurring within 200 km of the site (within IRM). However, for 1.0-sec spectral acceleration, the hazard is dominated by m_b 7 to 8 earthquakes occurring at distances greater than 200 km (in the New Madrid zone). Similar to the results for Example G4, the geology-based and seismicity-based models for zone IRM give practically identical results (this result will not necessarily be obtained at other sites, however).

b. Equal-hazard response spectra obtained from the hazard results for all the periods of vibration analyzed are shown in Figure G5-6 for mean hazard results and in G5-7 for the 95th percentile of the hazard distribution (Figure G5-3). The equal-hazard spectra are relatively flat because of the long-period contribution to the hazard by source zone ICR.

G5-5. Comparison of Deterministic and Probabilistic Results

a. The probabilistic equal-hazard spectra of rock motions at the site were compared with the median deterministic spectrum of rock motions at the site for an MCE occurring within zone IRM in which the site is located. The deterministic response spectrum was determined from a statistical random earthquake analysis for the occurrence of an MCE within a radius of 25 km from the site. The distribution for the earthquake magnitude of the MCE that was developed for the PSHA was used for this analysis. The mean value of maximum magnitude from this distribution was m_b 6.3. The random earthquake analysis carried out for the site is described in paragraph D-3. Figures G5-8 and G5-9, respectively, compare the deterministic MCE response spectrum with the mean and 95th percentile equal hazard spectra. These comparisons indicate that the deterministic MCE ground motions correspond to ground motions with very long return period for periods of vibration equal to or less than about 1 sec. At periods increasingly longer than 1 sec, the return period associated with the MCE spectrum progressively decreases. This

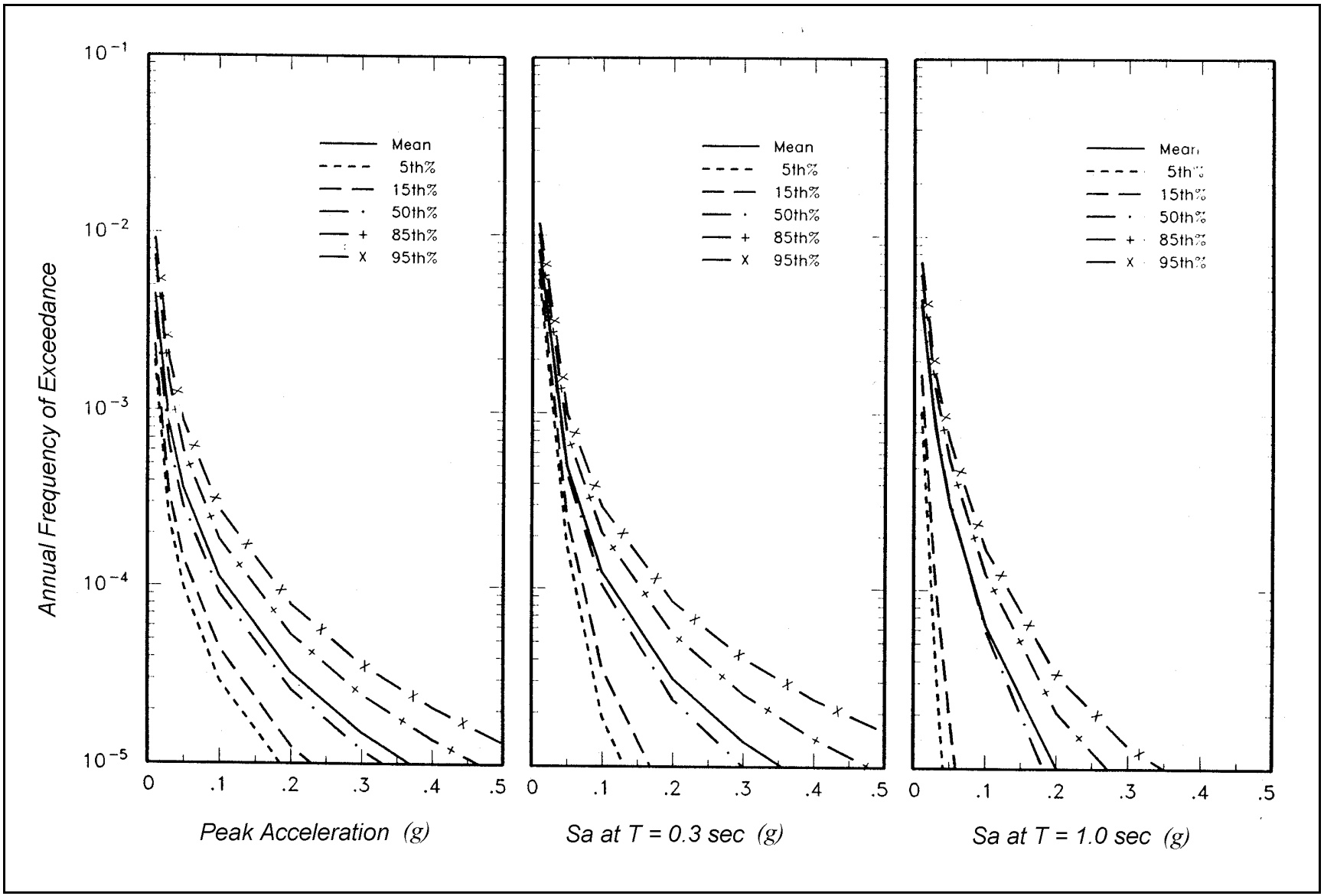

Figure G5-3. Computed rock hazard curves for peak ground acceleration and response spectral acceleration at periods of 0.3 and 1 sec and 5 percent damping

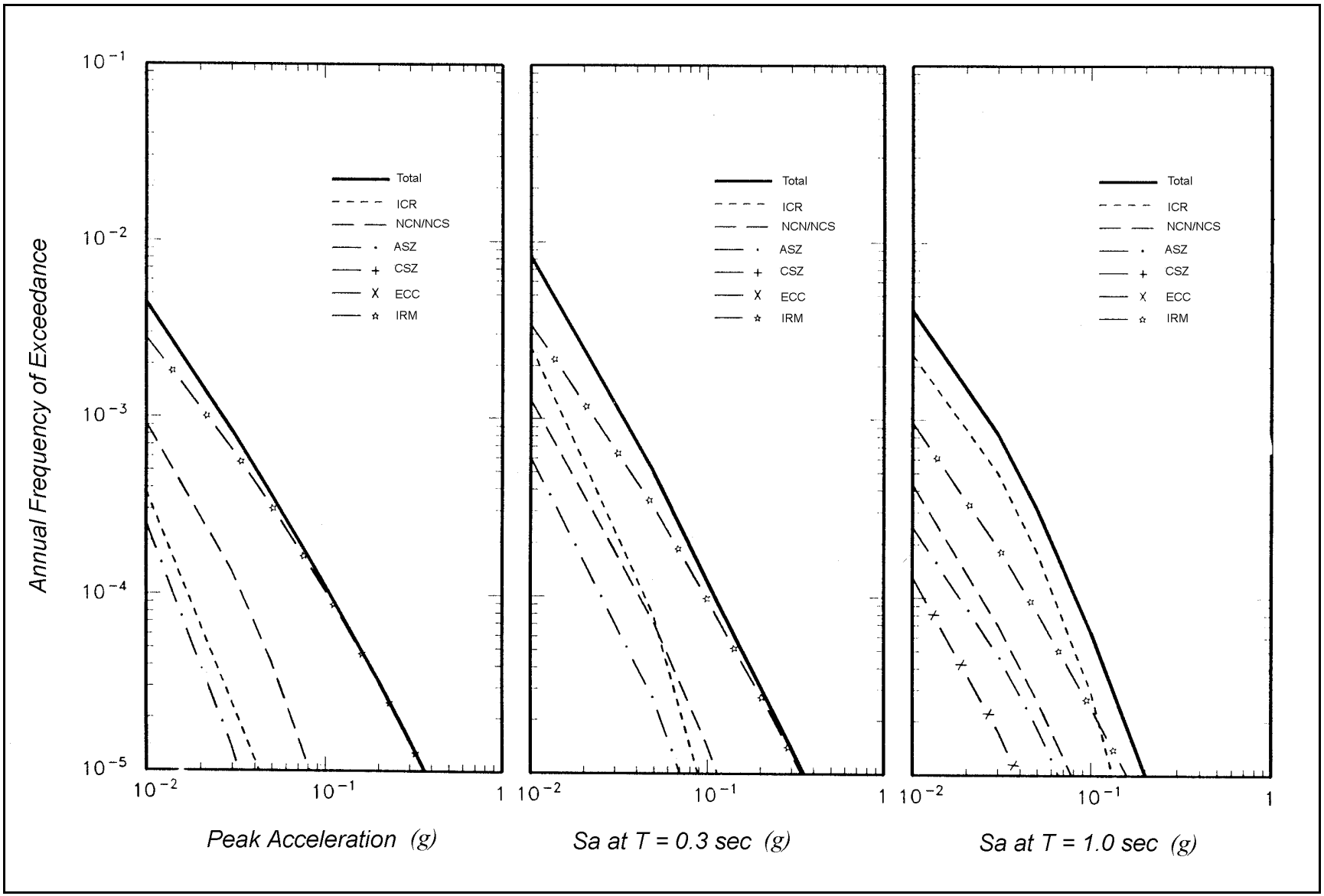

Figure G5-4. Source contributions to hazard for peak ground acceleration and spectral accelerations at periods of 0.3 and 1 sec, rock hazard curves at 5 percent damping

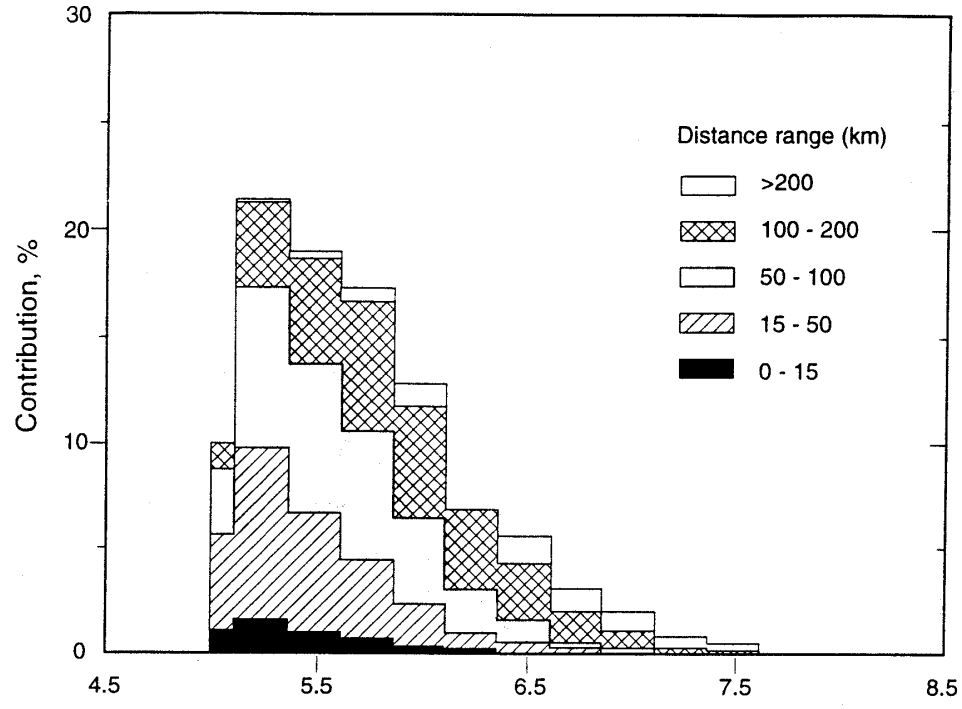

a. Peak ground acceleration

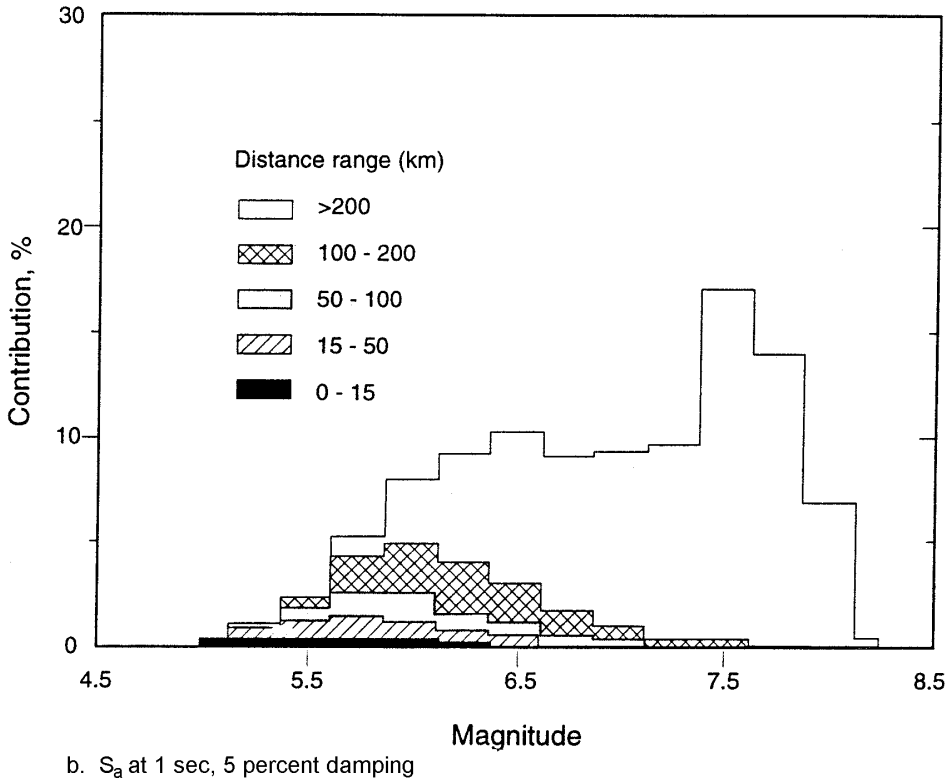

b. S_a at 1 sec, 5 percent damping

Figure G5-5. Magnitude and distance contributions to hazard for peak ground acceleration and response spectral acceleration at 1.0 sec for 1000-year return period

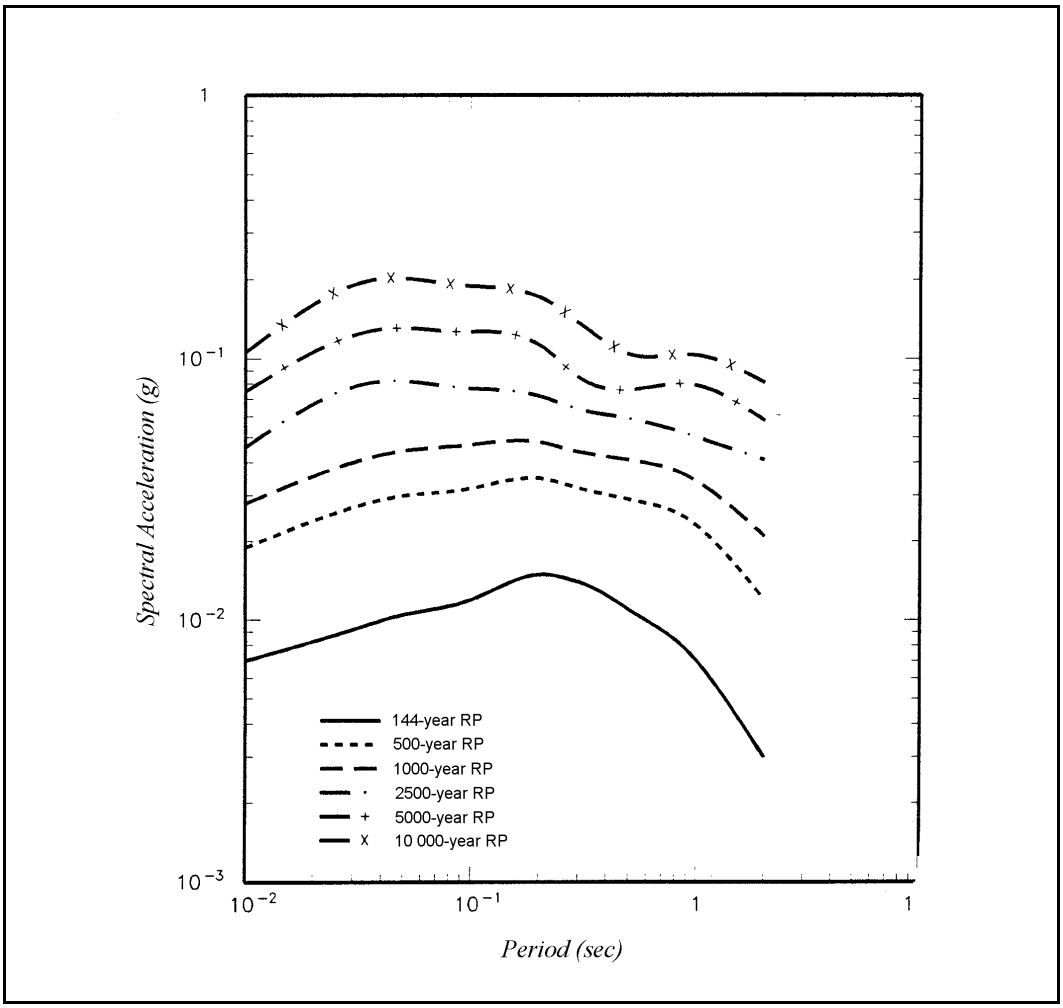

Figure G5-6. Equal-hazard response spectra, mean curves, 5 percent damping

reflects the influence of source zone ICR at long periods in the equal hazard spectrum, whereas the MCE is for the local source zone IRM.

b. The probabilistic seismic ground motion hazard at this site is quite low, reflecting the low historic seismicity in the site region. At the same time, there is considerable uncertainty in the hazard (reflecting scientific uncertainties in modeling seismic sources and ground motion attenuation), which is illustrated by the uncertainty band in hazard estimates (5^{th} to 95^{th} percentile) in Figure G5-3. Because of the low hazard and the uncertainty, the project team decided to adopt the 95^{th} percentile, rather than the mean, estimates of the equal-hazard spectra as a basis for design. The equal-hazard response spectrum with a 144-year return period (50 percent probability of exceedance in 100 years) was selected as the OBE ground motion. The MDE ground motion was selected as the equal hazard response spectrum having a 1000-year return period (approximate 10 percent probability of exceedance in 100 years).

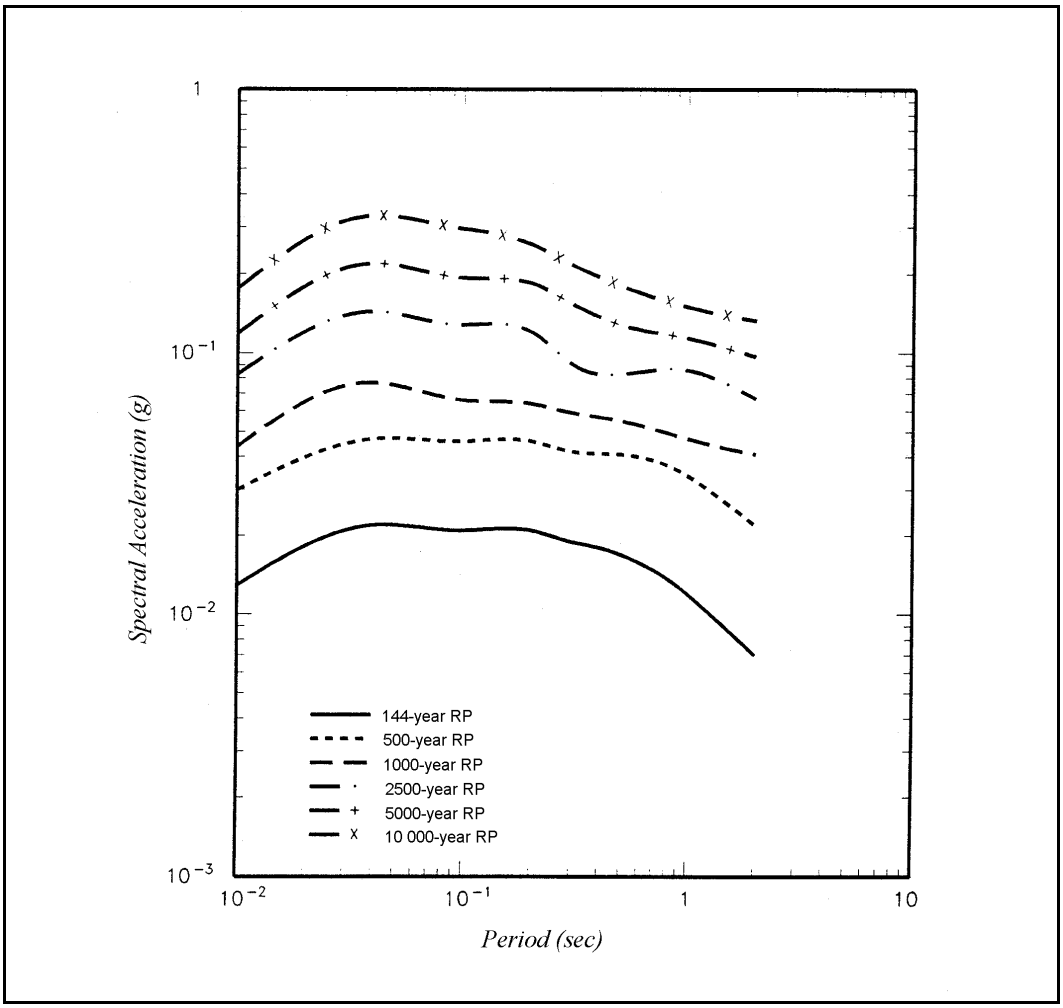

Figure G5-7. Equal-hazard response spectra, 95th percentile curves, 5 percent damping

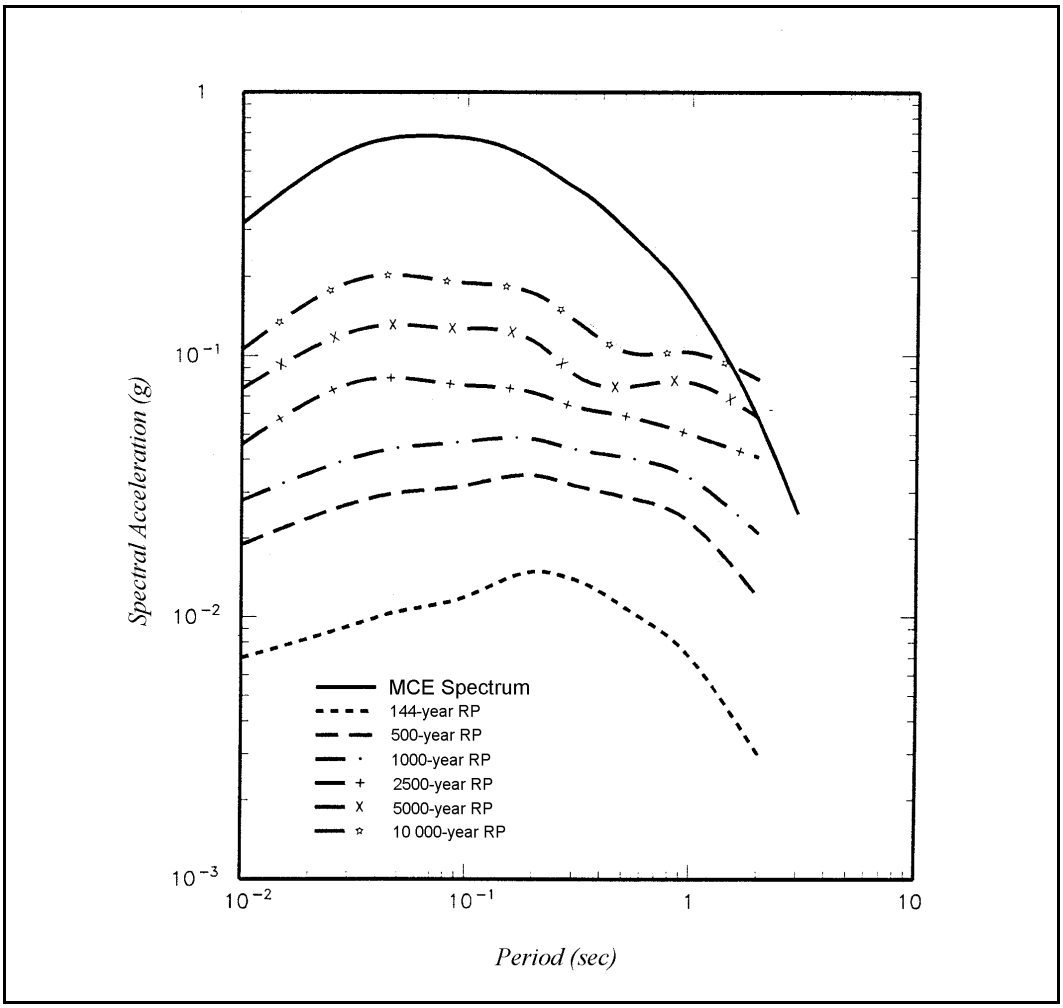

Figure G5-8. Comparison of MCE response spectrum with mean equal hazard response spectra, 5 percent damping

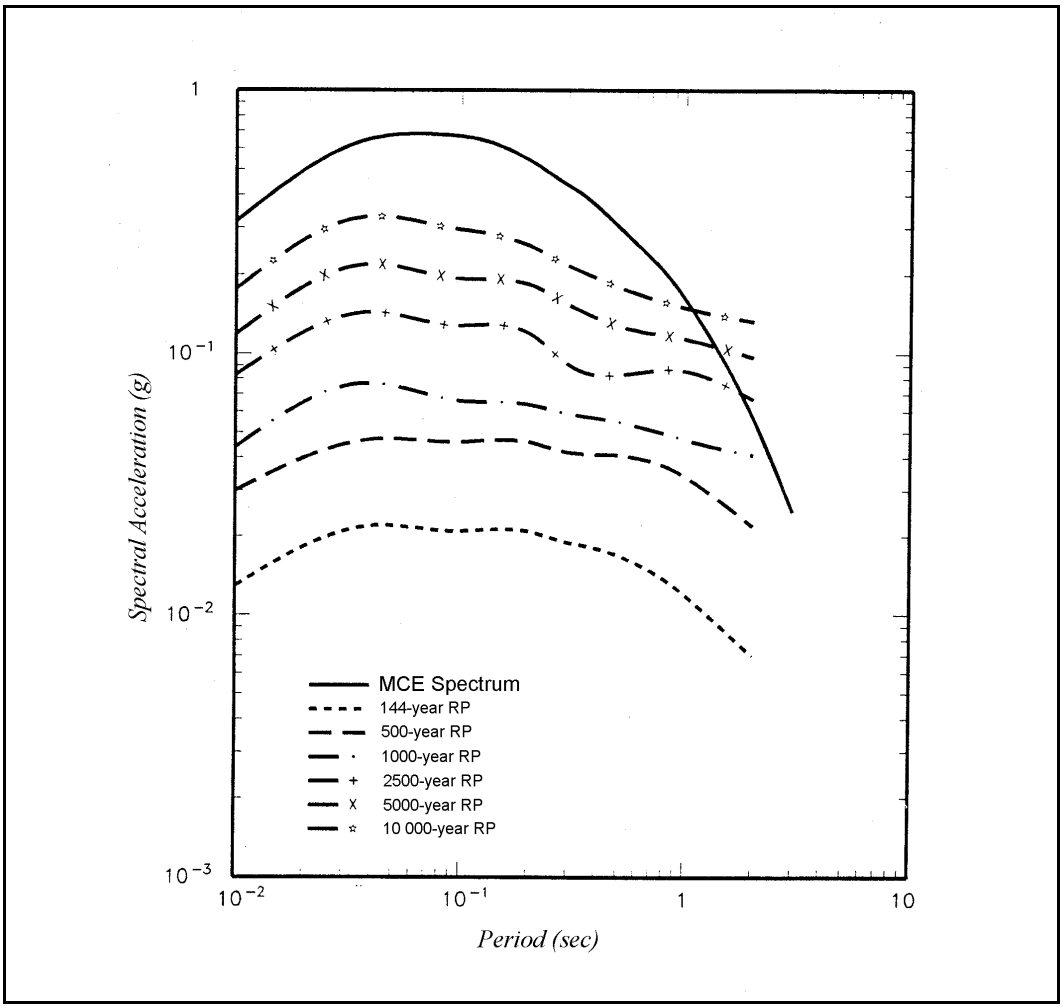

Figure G5-9. Comparison of MCE response spectrum with 95th percentile equal hazard response spectra, 5 percent damping

Appendix H
Response-Spectrum Modal Analysis of a Free-standing Intake Tower

H-1. Introduction

a. The example problem presented in this appendix illustrates the response spectrum modal analysis (RSMA) procedures applied to the earthquake response computation of a free-standing intake tower. The purpose of this example is to demonstrate the structural modeling and the process of computing earthquake demands for a free-standing intake tower due to site-specific and standard response spectra.

b. The structural modeling including the added hydrodynamic masses of the surrounding and contained water is described. The natural periods and mode shapes are determined with and without the effect of shear deformation considered, and then used to compute tower displacements, shears, and moments induced by a standard and a site-specific ground motion. The seismic responses are computed separately for excitation along each horizontal axis of the tower and then combined to obtain the total response for combined excitation along both axes.

c. See paragraph H-7 for a conversion chart.

H-2. Description of Example Tower

The example intake tower is shown in Figure H-1, where H_s is the structure height, H_o is the depth of outside water, and H_i is the depth of inside water. It is 60.96 m high with a rectangular cross section whose dimensions and wall thickness vary along the height of the tower (paragraph H-5*a*). The tower is built on a rock foundation, and the normal water pool is at elevation (el) 1016.81 m.

H-3. Earthquake Ground Motion

The earthquake ground motions for the example problem consist of a site-specific and a standard response spectrum developed for a rock site in the San Francisco Bay area. The site-specific ground motion is the equal hazard response spectrum with a return period of 1000 years developed in Appendix G (Example 2). The peak ground acceleration for the site-specific ground motion is 0.7 g, representing a rock site 21 km east of the San Andreas Fault and 7 km west of the Hayward Fault, as shown in Figure G2-1. The standard response spectrum is based on the 1994 National Earthquake Hazards Reduction Program spectral acceleration maps (Building Seismic Safety Council 1994) and was developed in accord with CECW-ET memorandum, Earthquake Design Guidance for Structures, dated 30 October 1996. The estimated effective peak ground acceleration for the standard ground motion is 0.6756 g. The standard and site-specific response spectra are shown in Figure H-2.

H-4. Method of Analysis

The example tower is analyzed using the response spectrum modal superposition method described in paragraph 2-8. The analyses are carried out using the computer program SAP-IV, but spreadsheet calculations are also provided to illustrate the analysis procedures. Slender towers with cross-section dimensions 10 times less than the height of the structure can adequately be represented solely by the flexural deformations of the tower. However, the effects of shear deformations on vibration frequencies

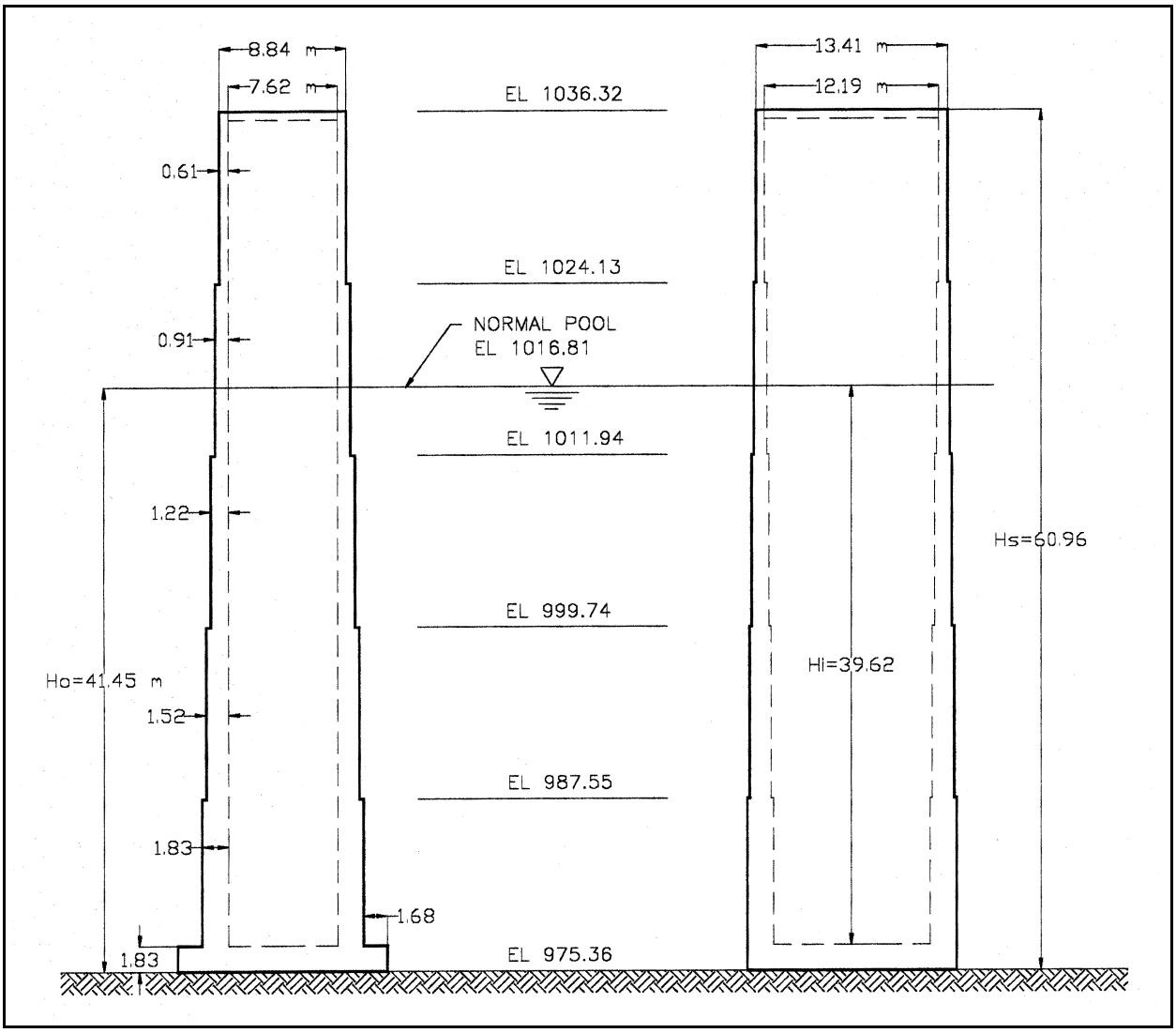

Figure H-1. Geometry of example intake tower

and section forces, especially for higher modes, are significant when the cross-section dimensions exceed 1/10 of the tower height. In this example, the computer analyses are used to demonstrate the effects of shear deformations as well as the number of vibration modes that should be included in the response analysis of the tower. The spreadsheet calculations, on the other hand, are employed to illustrate the steps involved in the customary two-mode approximation method of tower analysis.

H-5. Structural Model

The example tower was idealized as a series of beam elements with the mass of tower lumped at the element nodal points. The idealized models for excitation along the transverse and longitudinal axes of the structure are shown in Figures H-3 and H-4, respectively. The two models are similar, except for the stiffness properties and the added mass of water, which depend on direction of the excitation. At each cross-section discontinuity, a nodal point was introduced to generate beam elements having uniform

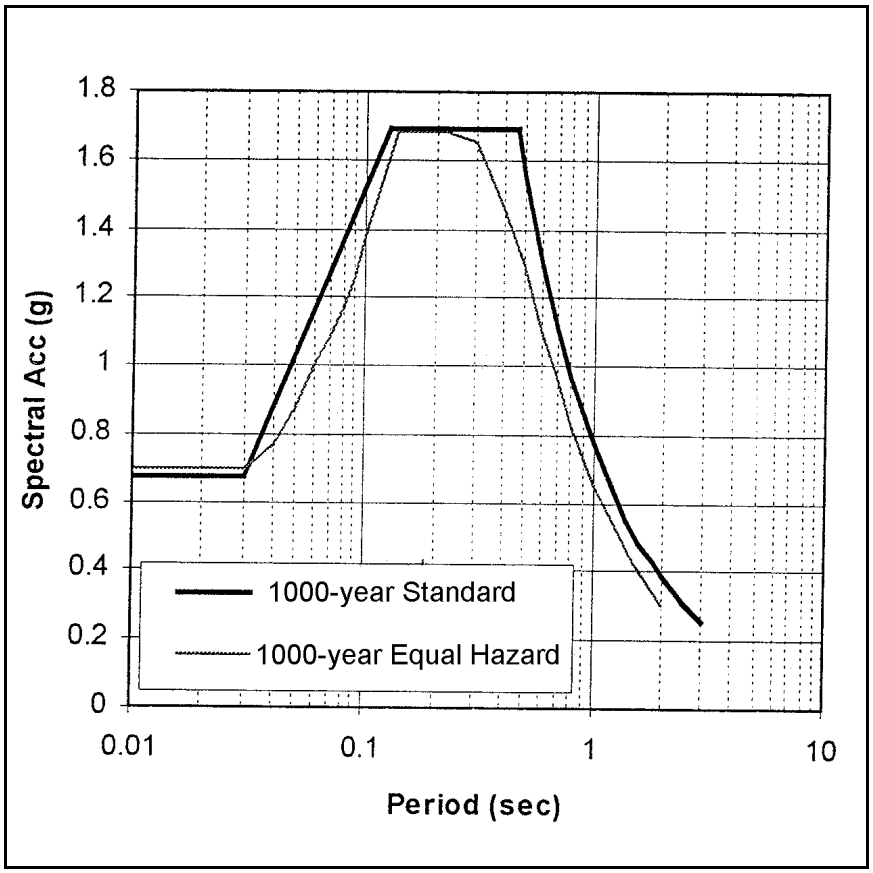

Figure H-2. Site-specific and standard response spectra for rock site in San Francisco Bay area

cross-section properties. In addition, midpoint nodes and a node at the water pool elevation were also provided for greater accuracy. Except for Node 1, which is fixed, all other nodes include one translation and one rotational degree of freedom. Each model, therefore, consists of 12 beam elements and 13 nodal points with a total of 24 degrees of freedom. The hydrodynamic interaction effects of the outside and inside water are approximated by the equivalent added hydrodynamic masses described in *b* below. The computed added masses of water are then combined with the mass of the structure in the earthquake response analysis of the tower.

a. Structural mass and section parameters. In the computer analysis, the element stiffness properties and lumped masses are computed from the cross-section area, mass, and moments of inertia. The cross-section properties at each level of discontinuity are computed using the dimensions provided in Figure H-1. In the following calculations A_{sx} and A_{sy} are the shear area associated with shear forces in x- and y-directions, respectively. They are needed as input parameters, if the effects of shear deformations are to be considered in the analysis. I_{xx} is the larger moment of inertia for bending in the longitudinal direction, and I_{yy} is the smaller component corresponding to bending in the transverse direction. The structure mass m_0 is given in terms of mass/unit length. The calculations are shown in the following diagrams and the results are summarized in Table H-1.

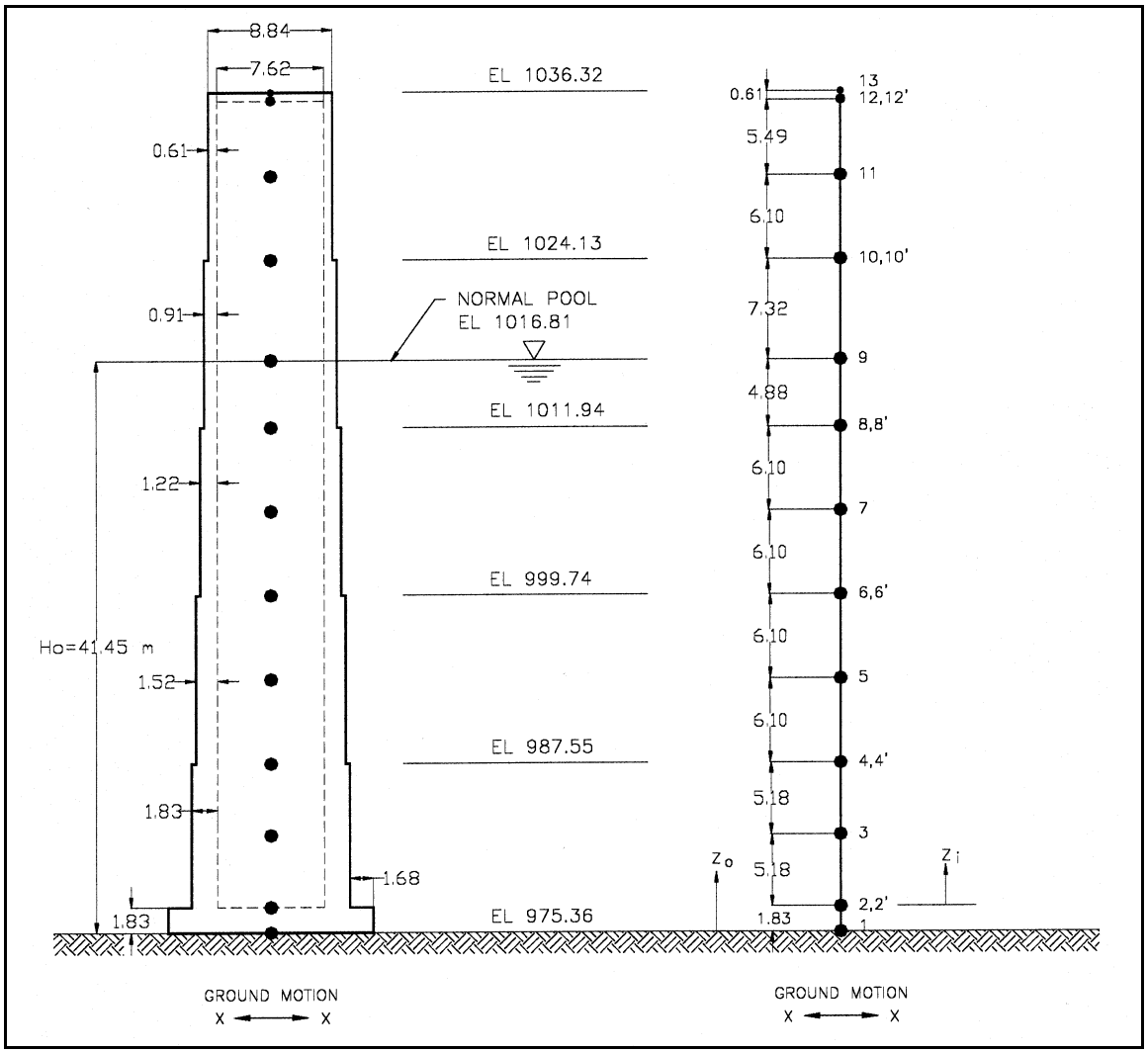

Figure H-3. Structural idealization for excitation along transverse axis (x-axis)

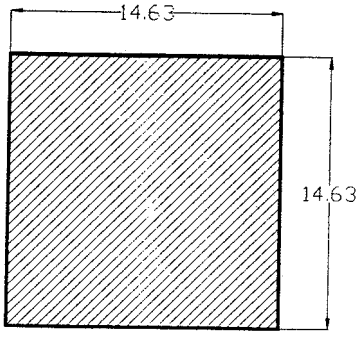

$$El\ 975.36 - 977.19$$

$$A = 14.63(14.63) = 214.04 \quad m^2$$

$$A_{xx} = A_{sy} = 142.69 \quad m^2$$

$$m_o = \frac{214.04(0.024)}{9.81} = 0.524 \quad MN - \sec^2/m^2$$

$$I_{xx} = I_{yy} = \frac{14.63(14.63)^3}{12} = 3{,}817.65 \quad m^4$$

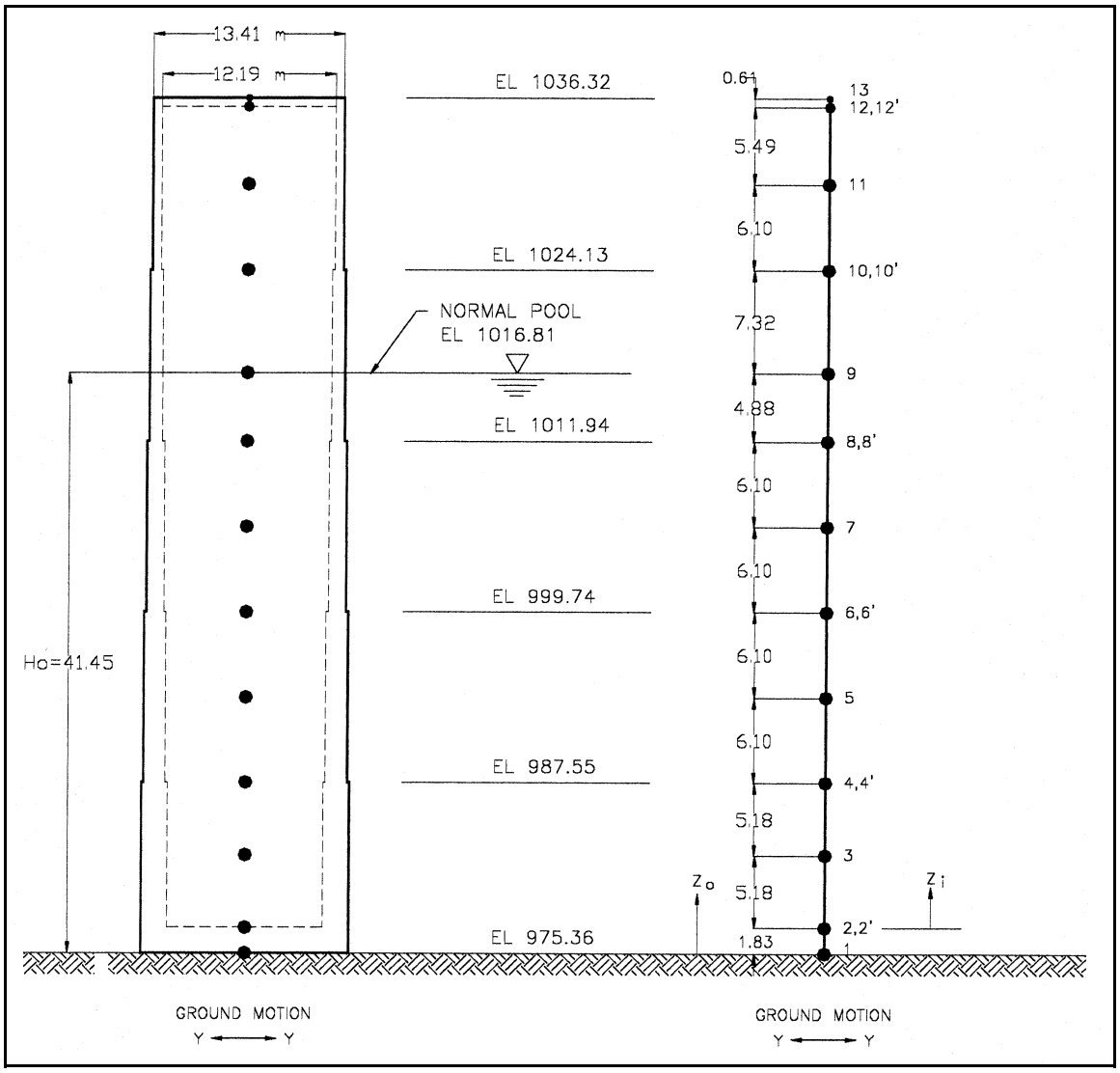

Figure H-4. Structural idealization for excitation along longitudinal axis (y-axis)

Table H-1
Section Properties of Example Tower

Elevation	A m²	A_{sx} m²	A_{sy} m²	I_{xx} m⁴	I_{yy} m⁴	m_o MN-sec²/m²
975.36 to 977.19	214.040	142.69	142.69	3,817.650	3,817.650	0.524
977.19 to 987.55	81.440	32.16	41.17	2,105.190	1,345.334	0.199
987.55 to 999.74	66.698	25.760	33.926	1,697.202	1,029.647	0.163
999.74 to 1011.94	52.802	19.933	27.050	1,324.208	762.525	0.129
1011.94 to 1024.13	38.839	14.335	20.055	961.594	523.045	0.095
1024.13 to 1035.71	25.657	9.262	13.393	626.237	322.521	0.063
1035.71 to 1036.32	118.544	79.029	79.029	1,776.468	771.977	0.290

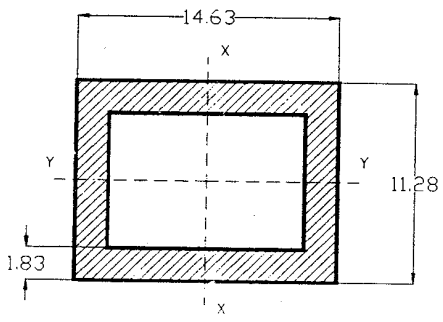

El 977.19 – 987.55

$A = 14.63(11.28) - 10.97(7.62) = 81.44 \quad m^2$

$A_{sx} = 32.16 \quad m^2$

$A_{sy} = 41.17 \quad m^2$

$$m_o = \frac{81.44(0.024)}{9.81} = 0.199 \quad MN - \sec^2 / m^2$$

$$I_{xx} = \frac{1}{12}(11.28 \times 14.63^3 - 7.62 \times 10.97^3) = 2{,}105.190 \; m^4$$

$$I_{yy} = \frac{1}{12}(14.63 \times 11.28^3 - 10.97 \times 7.62^3) = 1{,}345.334 \; m^4$$

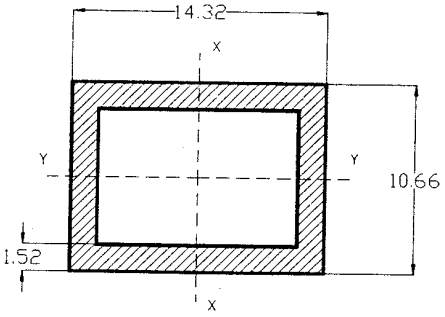

El 987.55 – 999.74

$A = 14.32(10.66) - 11.28(7.62) = 66.698 \quad m^2$

$A_{sx} = 25.760 \quad m^2$

$A_{sy} = 33.926 \quad m^2$

$$m_o = \frac{66.698(0.024)}{9.81} = 0.163 \quad MN - \sec^2 / m^2$$

$$I_{xx} = \frac{1}{12}(10.66 \times 14.32^3 - 7.62 \times 11.28^3) = 1{,}697.202 \; m^4$$

$$I_{yy} = \frac{1}{12}(14.32 \times 10.66^3 - 11.28 \times 7.62^3) = 1{,}029.647 \; m^4$$

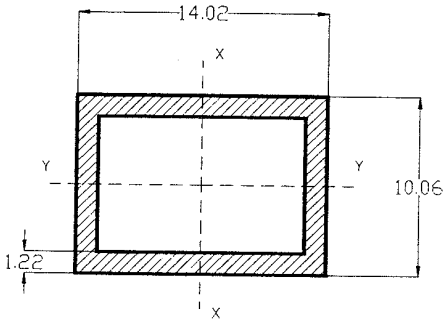

El 999.74 – 1011.94

$A = 14.02(10.06) - 11.58(7.62) = 52.802 \quad m^2$

$A_{sx} = 19.933 \quad m^2$

$A_{sy} = 27.050 \quad m^2$

$$m_o = \frac{52.802(0.024)}{9.81} = 0.129 \quad MN - \sec^2 / m^2$$

$$I_{xx} = \frac{1}{12}(10.06 \times 14.02^3 - 7.62 \times 11.58^3) = 1{,}324.208 \; m^4$$

$$I_{yy} = \frac{1}{12}(14.02 \times 10.06^3 - 11.58 \times 7.62^3) = 762.525 \; m^4$$

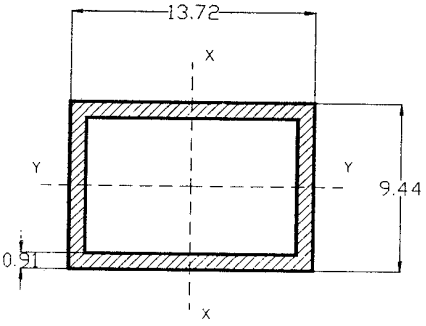

El 1011.94 – 1024.13

$A = 13.72(9.44) - 11.9(7.62) = 38.839 \quad m^2$

$A_{xx} = 14.335 \quad m^2$

$A_{sy} = 20.055 \quad m^2$

$$m_o = \frac{38.839(0.024)}{9.81} = 0.095 \quad MN - \sec^2 / m^2$$

$$I_{xx} = \frac{1}{12}(9.44 \times 13.72^3 - 7.62 \times 11.9^3) = 961.594 \, m^4$$

$$I_{yy} = \frac{1}{12}(13.72 \times 9.44^3 - 11.9 \times 7.62^3) = 523.045 \, m^4$$

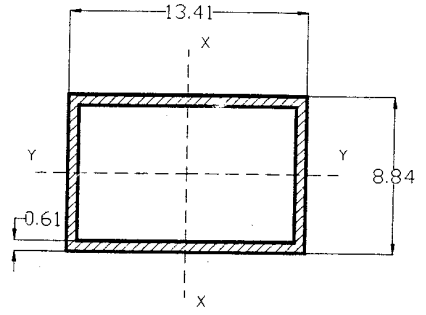

El 1024.13 – 1035.71

$A = 13.41(8.84) - 12.19(7.62) = 25.657 \quad m^2$

$A_{xx} = 9.262 \quad m^2$

$A_{sy} = 13.393 \quad m^2$

$$m_o = \frac{25.657(0.024)}{9.81} = 0.063 \quad MN - \sec^2 / m^2$$

$$I_{xx} = \frac{1}{12}(8.84 \times 13.41^3 - 7.62 \times 12.19^3) = 626.237 \quad m^4$$

$$I_{yy} = \frac{1}{12}(13.41 \times 8.84^3 - 12.19 \times 7.62^3) = 322.521 \quad m^4$$

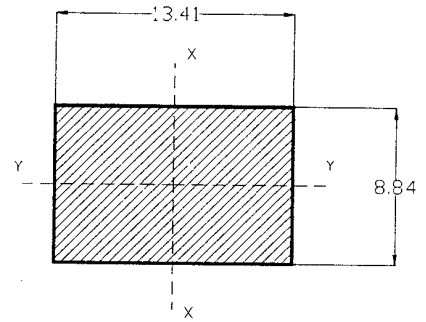

El 1035.71 – 1036.32

$A = 13.41(8.84) = 118.544 \quad m^2$

$A_{xx} = A_{sy} = 79.029 \quad m^2$

$$m_o = \frac{118.544(0.024)}{9.81} = 0.290 \quad MN - \sec^2 / m^2$$

$$I_{xx} = \frac{1}{12}(8.84 \times 13.41^3) = 1{,}776.468 \quad m^4$$

$$I_{yy} = \frac{1}{12}(13.41 \times 8.84^3) = 771.977 \quad m^4$$

b. Added hydrodynamic mass. The hydrodynamic interaction effects of the surrounding and contained water in the analysis of the example tower are approximated by an equivalent added mass of water. This concept assumes the water is incompressible, and provides added hydrodynamic mass functions that represent the inertial effects of water interacting with the tower. The computation of the added hydrodynamic mass is further simplified by the assumption of a rigid tower subjected to unit horizontal ground acceleration. In this example the added hydrodynamic mass functions for the surrounding and contained water are computed using a simplified procedure developed by Goyal and Chopra (1989). The Goyal and Chopra simplified procedure is based on the analytical solutions available for circular cylindrical towers and uniform elliptical towers. The procedure is applicable to the added hydrodynamic mass analysis of both uniform and nonuniform towers of arbitrary cross section with two axes of symmetry. For a tower of arbitrary cross section the added mass analysis is carried out, first by evaluating an "equivalent" uniform elliptical cross section, and then a corresponding "equivalent" circular cylindrical tower for which the analytical solution is available. A summary of Goyal and Chopra's findings and assumptions, which led to their formulation of the simplified procedure, is as follows:

(1) For an infinitely long uniform tower with the same circular cross section, the added mass per unit height is

$$m_{\infty}^{o} = \rho_w \pi r_o^2 \tag{H-1}$$

where ρ_w is the mass density of water. This is equal to the mass of the water displaced by the (solid) tower per unit height.

(2) The normalized added mass $(m_a^o(z)/m_{\infty}^o)$ is influenced by the slenderness ratio (H_o/a_o), the ratio (a_0/b_0) of the cross-sectional dimensions, the cross-sectional area A_0, and the cross-sectional shapes.

(3) The added mass per unit length of an infinitely long uniform tower is two-dimensional in the cross sectional plane of the tower and can be obtained using semianalytical procedures. This led to computation of the added mass per unit length for infinitely long uniform towers with a variety of cross sections.

(4) The computation from Step 3 indicated that the normalized added mass for uniform tower of arbitrary cross section is essentially the same as that for an "equivalent" elliptical tower. This finding led to the conclusion that the normalized added mass for a uniform tower of arbitrary cross section can therefore be obtained from the solution available for an equivalent elliptical tower. The cross-section dimensions ratio $\tilde{a}_o/\tilde{b}_o$ and the slenderness ratio $H_o/\tilde{a}_o$ of the equivalent elliptical tower are related to a_o/b_o, A_o, and H_o for the actual tower by:

$$\frac{H_o}{\tilde{a}_o} = \frac{H_o}{\sqrt{A_o/\pi}} \cdot \sqrt{\frac{b_o}{a_o}} \tag{H-2}$$

$$\frac{\tilde{a}_o}{\tilde{b}_o} = \frac{a_o}{b_o} \tag{H-3}$$

(5) The computation of added mass for elliptical towers, however, requires a large number of graphs and tables in order to cover a wide range of cross-section parameters. To further simplify the solution

process for practical application, the uniform elliptical tower is replaced by an "equivalent" circular cylindrical tower for which a single chart or table will suffice. The slenderness ratio of the "equivalent" circular cylindrical tower is obtained from the slenderness ratio and the ratio of the corresponding elliptical cross-section dimensions.

(6) The procedure is extended to the added mass analysis of nonuniform towers, simply by applying these steps to various portions of the tower that actually are, or assumed to be, uniform.

c. Added hydrodynamic mass of outside water for excitation along longitudinal axis. The added hydrodynamic mass for the outside water is computed separately for excitation along the longitudinal (y) and transverse (x) axes of the tower. The rectangular tower has an outside cross-section area A_o (z), a width of $2a_o$ (z) perpendicular to the direction of excitation, and a dimension of $2b_o$ (z) parallel to the direction of excitation. The following steps illustrate the computation of the added mass for the outside water for excitation along the longitudinal axis:

(1) Select Nodes 1 to 9 along the tower height for computation of added mass $m_a^o(z)$. At the points of discontinuity designate two nodes, one corresponding to the section above and another to the section below. For example Nodes 8 and 8′ are used to account for the section changes at el 1012 m. Compute the height coordinate Z_o, section parameters a_o/b_o, a_o/H_o, and A_o for the selected nodes, as shown in columns 2 to 5 of Table H-2.

(2) Use Equation H-2 and the actual section parameters obtained in Step 1 to determine the ratio of the cross-section dimensions $\tilde{a}_o / \tilde{b}_o$ and the slenderness ratio $\tilde{a}_o / H_o$ for the equivalent elliptical tower (columns 6 and 7 of Table H-2).

(3) From Figure H-5 and the section properties of the equivalent elliptical tower obtained in Step 2, determine the slenderness ratio $\tilde{r}_o / H_o$ of the equivalent circular tower at the selected nodal point (Column 8 of Table H-2).

(4) Use Figure H-6 and section properties obtained in Step 3 to evaluate the normalized added hydrodynamic mass $m_a^o(z) / m_\infty^o$ for the circular cylindrical towers associated with the surrounding water (Column 10 of Table H-2).

(5) Use Table 8.1 of Goyal and Chopra (1989) to compute the added hydrodynamic mass $m_\infty^o(z)$ for an infinitely long tower with its cross section same as that of the actual tower (Column 13 of Table H-2).

(6) Determine the added hydrodynamic mass $m_a^o(z)$ for the actual tower at the location z by multiplying the normalized added mass obtained in Step 4 by $m_\infty^o(z)$ computed in Step 5.

(7) Repeat steps 2 to 6 for all selected nodes along the height of the tower.

d. Added hydrodynamic mass of inside water for excitation along longitudinal axis. The added hydrodynamic mass for the inside water is computed in a manner similar to that described for the outside water. For the example rectangular tower having inside cross sections A_i (z), width $2a_i$ (z) perpendicular to the direction of excitation, and dimension $2b_i$ (z) parallel to the direction of excitation, the computation of added mass for ground motion along the longitudinal axis of the tower is as follows:

(1) Select Nodes 2 to 9 along the tower height for computation of inside added mass $m_i^o(z)$. Compute the height coordinate Z_i, section parameter a_i/b_i, a_i/H_i, and A_i for the selected nodes, as shown in columns 2 to 5 of Table H-3.

Table H-2
Computation of Added Mass for the Outside Water Due to Ground Motion Along Longitudinal Axis (Y)

		Outside Geometry			Equivalent Ellipse		Equivalent Cylinder			Infinitely Long Tower			
Node No.	Z_o m	$\frac{a_o}{b_o}$	$\frac{a_o}{H_o}$	A_o m²	$\frac{\tilde{a}_o}{\tilde{b}_o}$	$\frac{\tilde{a}_o}{\tilde{H}_o}$	$\frac{\tilde{r}_o}{H_o}$	$\frac{Z_o}{H_o}$	$\frac{m_a^o(z)}{m_\infty^o}$	$\rho_w A_o$ MN-sec²/m²	$\frac{m_\infty^o}{\rho_w A_o}$	m_∞^o MN-sec²/m²	$m_a^o(z)$ MN-sec²/m²
1	2	3	4	5	6	7	8	9	10	11	12	13	14
1	0	1	0.176	214.037	1	0.199	0.199	0	0.93	0.218	1.186	0.259	0.241
2	1.83	1	0.176	214.037	1	0.199	0.199	0.044	0.93	0.218	1.186	0.259	0.241
2′	1.83	0.771	0.136	165.026	0.771	0.154	0.175	0.044	0.944	0.168	0.957	0.161	0.152
3	7.01	0.771	0.136	165.026	0.771	0.154	0.175	0.169	0.941	0.168	0.957	0.161	0.152
4	12.19	0.771	0.136	165.026	0.771	0.154	0.175	0.294	0.931	0.168	0.957	0.161	0.150
4′	12.19	0.745	0.129	152.651	0.745	0.145	0.167	0.294	0.936	0.156	0.931	0.145	0.136
5	18.29	0.745	0.129	152.651	0.745	0.145	0.167	0.441	0.916	0.156	0.931	0.145	0.133
6	24.38	0.745	0.129	152.651	0.745	0.145	0.167	0.588	0.878	0.156	0.931	0.145	0.127
6′	24.38	0.717	0.121	141.041	0.717	0.137	0.16	0.588	0.885	0.144	0.903	0.130	0.115
7	30.48	0.717	0.121	141.041	0.717	0.137	0.16	0.735	0.808	0.144	0.903	0.130	0.105
8	36.58	0.717	0.121	141.041	0.717	0.137	0.16	0.882	0.615	0.144	0.903	0.130	0.080
8′	36.58	0.689	0.114	129.517	0.689	0.129	0.153	0.882	0.626	0.132	0.875	0.116	0.073
9	41.45	0.689	0.114	129.517	0.689	0.129	0.153	1	0	0.132	0.875	0.116	0.000

Note:

$$\frac{\tilde{a}_o}{H_o} = \frac{1}{H_o}\sqrt{\frac{A_o}{\pi}\left(\frac{a_o}{b_o}\right)}$$

(2) Use equation given in Table H-3 and the actual section parameters obtained in Step 1 to determine the ratio of the cross-section dimensions $\tilde{a}_i / \tilde{b}_i$ and the slenderness ratio $\tilde{a}_i / H_i$ for the equivalent elliptical tower (columns 6 and 7 of Table H-3).

(3) From Figure H-7 and the section properties of the equivalent elliptical tower obtained in Step 2, determine the slenderness ratio $\tilde{r}_i / H_i$ of the equivalent circular tower at the selected nodal point (Column 8 of Table H-3).

(4) Use Figure H-8 and section properties obtained in Step 3 to evaluate the normalized added hydrodynamic mass $m_a^i(z) / m_\infty^i$ for the circular cylindrical towers associated with the inside water (Column 10 of Table H-3).

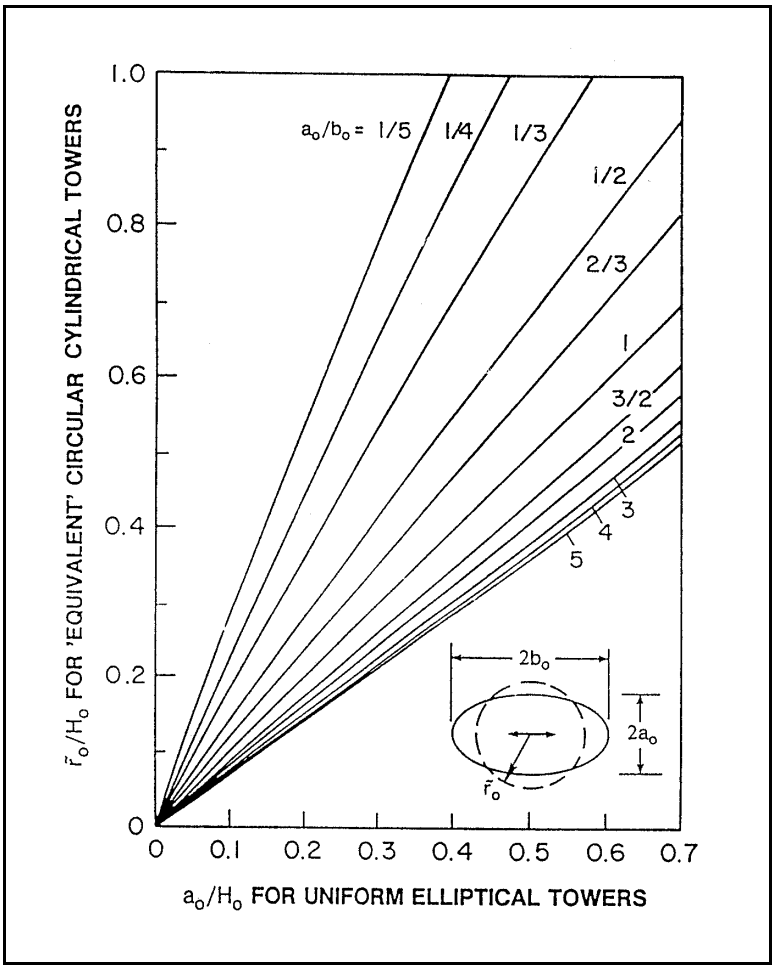

Figure H-5. Properties of "equivalent" circular cylindrical towers for uniform elliptical towers associated with added hydrodynamic mass due to surrounding water (Goyal and Chopra 1989, courtesy of Earthquake Engineering Research Center, University of California, Berkeley)

(5) Determine the added hydrodynamic mass $m_a^i(z)$ for the actual tower at the location z by multiplying the normalized added mass obtained in Step 4 by $m_\infty^i(z) = \rho_w A_i$.

(6) Repeat steps 2 to 5 for all selected nodes along the height of the tower.

e. Added hydrodynamic mass of outside water for excitation along transverse axis. The added hydrodynamic mass for the outside water for excitation along the transverse direction (x-axis) is computed similar to that described for excitation along the longitudinal direction, except that a_o and b_o used previously are switched so that the dimension $2a_o$ remains perpendicular to the direction of excitation. The results are given in Table H-4.

f. Added hydrodynamic mass of inside water for excitation along transverse axis. The added hydrodynamic mass for the inside water for excitation along the transverse direction (x-axis) is computed similar to that described for excitation along the longitudinal direction, except that a_i and b_i used

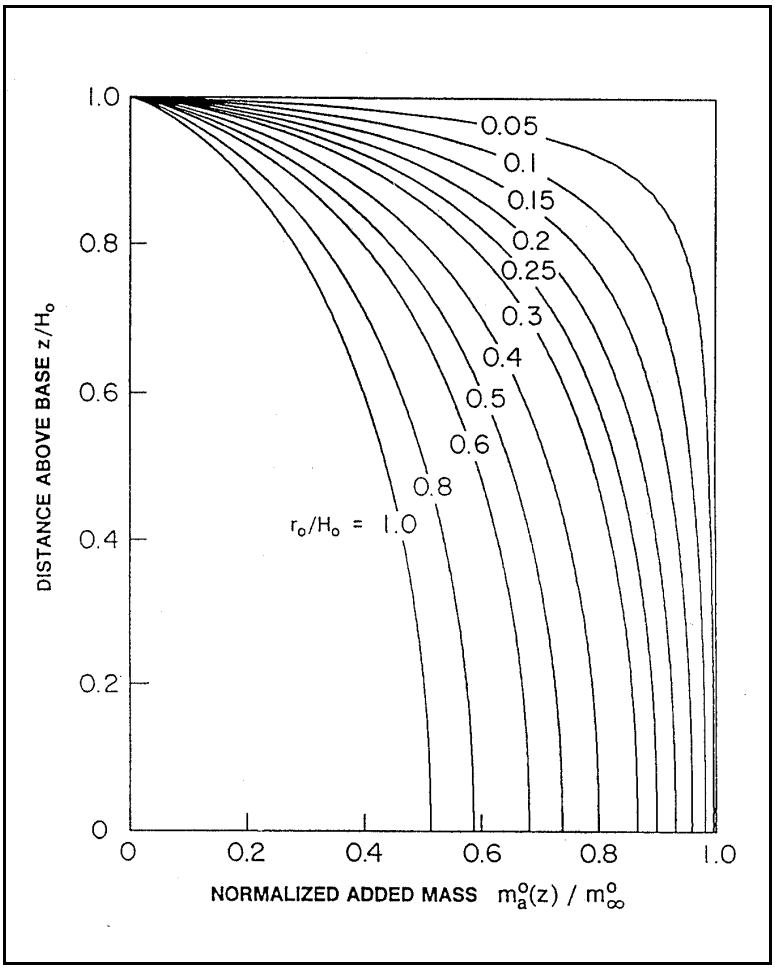

Figure H-6. Normalized added hydrodynamic mass for circular cylindrical towers associated with surrounding water (Goyal and Chopra 1989, courtesy of Earthquake Engineering Research Center, University of California, Berkeley)

previously are switched so that the dimension $2a_i$ remains perpendicular to the direction of excitation. The results are given in Table H-5.

g. Total lumped mass. The added mass per unit length of the tower m_o, outside water m_a^o, and the inside water m_a^i for excitation along the longitudinal and transverse directions are summarized in Tables H-6 and H-7, respectively. The summation of these gives the total effective mass per foot of tower, and when multiplied by the appropriate section length provides the total lumped mass at each nodal point. Note that at the point of discontinuity the mass associated with the upper and lower sections was computed separately and then combined to obtain the total mass at that location, as shown in the last column of the tables.

Table H-3
Computation of Added Mass for the Inside Water Due to Ground Motion Along Longitudinal Axis (Y-axis)

		Outside Geometry			Equivalent Ellipse		Equivalent Cylinder				
Node No.	Z_i m	$\frac{a_i}{b_i}$	$\frac{a_i}{H_i}$	A_i M^2	$\frac{\tilde{a}_i}{\tilde{b}_i}$	$\frac{\tilde{a}_i}{\tilde{H}_i}$	$\frac{\tilde{r}_i}{H_i}$	$\frac{Z_i}{H_i}$	$\frac{m_a^i(z)}{m_\infty^i}$	$m_\infty^i = \rho_w A_i$ MN-sec²/m²	$m_a^i(z)$ MN-sec²/m²
1	2	3	4	5	6	7	8	9	10	11	12
2	0	0.694	0.096	83.59	0.694	0.108	0.156	0.0	1	0.085	0.085
3	5.18	0.694	0.096	83.59	0.694	0.108	0.156	0.131	1	0.085	0.085
4	10.97	0.694	0.096	83.59	0.694	0.108	0.156	0.277	1	0.085	0.085
4′	10.97	0.676	0.096	85.95	0.676	0.109	0.161	0.277	1	0.088	0.088
5	16.46	0.676	0.096	85.95	0.676	0.109	0.161	0.415	0.998	0.088	0.088
6	22.56	0.676	0.096	85.95	0.676	0.109	0.161	0.569	0.993	0.088	0.087
6′	22.56	0.658	0.096	88.24	0.658	0.109	0.165	0.569	0.992	0.090	0.089
7	28.65	0.658	0.096	88.24	0.658	0.109	0.165	0.723	0.961	0.090	0.086
8	34.75	0.658	0.096	88.24	0.658	0.109	0.165	0.877	0.787	0.090	0.071
8′	34.75	0.641	0.096	90.68	0.641	0.109	0.169	0.877	0.780	0.092	0.072
9	39.62	0.641	0.096	90.68	0.641	0.109	0.169	1	0	0.092	0.000

Note:

$$\frac{\tilde{a}_i}{H_i} = \frac{1}{H_i}\sqrt{\frac{A_i}{\pi}\left(\frac{a_i}{b_i}\right)}$$

H-6. Computation of Earthquake Response

Computation of earthquake response of the example tower consists of evaluating the following:

a. The natural periods and mode shapes along the transverse and longitudinal axes.

b. The maximum deflections, shears, and moments due to transverse excitation.

c. The maximum deflections, shears, and moments due to longitudinal excitation.

d. The total response by combining the transverse and longitudinal responses.

The earthquake response of the tower is computed using both the two-mode approximation method carried out by spreadsheet and the computer analysis including 10 modes of vibration. The two-mode approximation method uses the site-specific spectra as the seismic input, whereas both the site-specific and standard spectra are employed in the computer analysis.

a. Frequencies and mode shapes.

(1) The natural periods and mode shapes of the example tower were determined using the structural model and the total lumped masses developed in paragraph H-5. The analyses were performed for two cases, with and without the effect of shear deformations. The results for the 10 lowest periods of

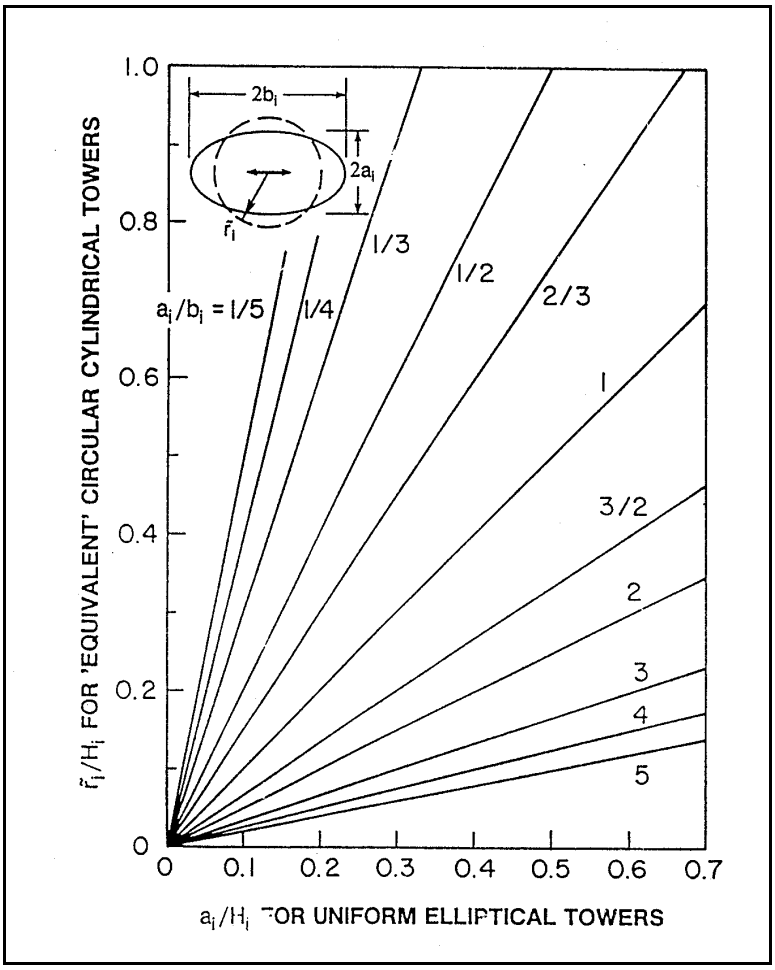

Figure H-7. Properties of "equivalent" circular cylindrical towers for uniform elliptical towers associated with added hydrodynamic mass due to inside water (Goyal and Chopra 1989, courtesy of Earthquake Engineering Research Center, University of California, Berkeley)

vibration along the longitudinal and transverse axes of the tower are summarized in Table H-8. The results show that the shear deformation increases periods of vibration of the example tower by about 10 to 40 percent for the first and second modes, 80 percent for the third mode, and as high as 2.5 to 3 times for the fifth mode. This rather significant effect is not all that surprising, considering that the average slenderness ratio of the example tower is about 16.5 percent in the transverse and 23 percent in the longitudinal direction. The effect of shear deformation can be neglected only if the slenderness ratio is less than 10 percent. The results also show that the effect of shear deformation is most significant in the higher modes where the vibration wavelength approaches the section dimensions of the tower. The normalized mode shapes for the lowest five modes of vibration are displayed in Figure H-9. Each mode shape was normalized to have a maximum value of unity.

(2) Alternatively, the periods and mode shapes for the first two modes may be obtained using the approximate method described in EM 1110-2-2400. In this example, however, the periods and mode shapes computed by the computer program SAP-IV will be used in the approximate two-mode analysis described in the subsequent sections.

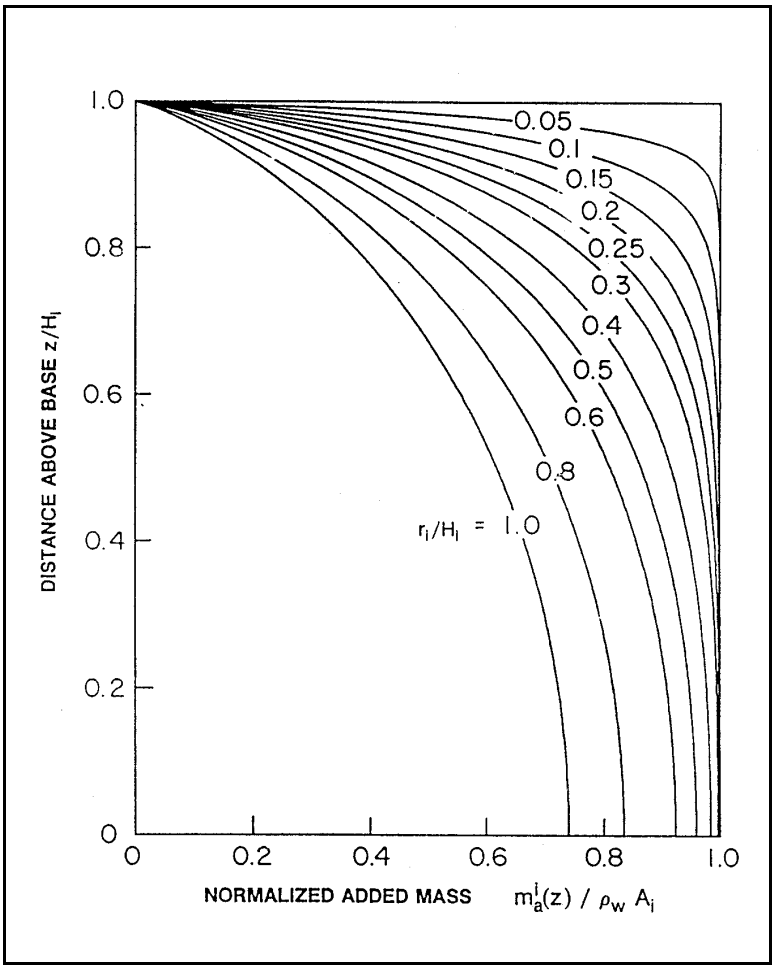

Figure H-8. Normalized added hydrodynamic mass for circular cylindrical towers associated with inside water (Goyal and Chopra 1989, courtesy of Earthquake Engineering Research Center, University of California, Berkeley)

b. Response due to transverse excitation.

(1) Two-mode approximation. The two-mode approximation of the tower response due to the site-specific ground motion along the transverse axis x is illustrated in Tables H-9 to H-11. The Mode-1 and Mode-2 responses are given in Tables H-9 and H-10, respectively, and the total response due to both modes are shown in Table H-11. The computation for Mode-1 response is as follows:

(a) The circular frequency ω_1 is obtained from Table H-8 using:

$$\omega_1 = \frac{2\pi}{T} = 2(3.1416)/(0.504) = 12.467 \text{ rad/sec} \tag{H-4}$$

(b) The spectral acceleration $S_{a1}\left(T_1, \xi_1\right) = 1.289\, g$ for T_1 = 0.504 sec and ξ_1 =5 percent is obtained from the site-specific response spectrum in Figure H-2.

Table H-4
Computation of Added Mass for the Outside Water Due to Ground Motion Along Transverse Direction (x-axis)

		Outside Geometry			Equivalent Ellipse		Equivalent Cylinder			Infinitely Long Tower			
Node No.	Z_o m	$\frac{a_o}{b_o}$	$\frac{a_o}{H_o}$	A_o m²	$\frac{\tilde{a}_o}{\tilde{b}_o}$	$\frac{\tilde{a}_o}{\tilde{H}_o}$	$\frac{\tilde{r}_o}{H_o}$	$\frac{Z_o}{H_o}$	$\frac{m_a^o(z)}{m_\infty^o}$	$\rho_w A_o$ MN-sec²/m²	$\frac{m_\infty^o}{\rho_w A_o}$	m_∞^o MN-sec²/m²	$m_a^o(z)$ MN-sec²/m²
1	**2**	**3**	**4**	**5**	**6**	**7**	**8**	**9**	**10**	**11**	**12**	**13**	**14**
1	0	1	0.176	214.037	1	0.199	0.199	0	0.931	0.218	1.186	0.259	0.241
2	1.83	1	0.176	214.037	1	0.199	0.199	0.044	0.931	0.218	1.186	0.259	0.241
2′	1.83	1.297	0.176	165.026	1.297	0.199	0.184	0.044	0.939	0.168	1.468	0.247	0.232
3	7.01	1.297	0.176	165.026	1.297	0.199	0.184	0.169	0.935	0.168	1.468	0.247	0.231
4	12.19	1.297	0.176	165.026	1.297	0.199	0.184	0.294	0.925	0.168	1.468	0.247	0.228
4′	12.19	1.343	0.173	152.651	1.343	0.195	0.179	0.294	0.928	0.156	1.512	0.236	0.219
5	18.29	1.343	0.173	152.651	1.343	0.195	0.179	0.441	0.907	0.156	1.512	0.236	0.214
6	24.38	1.343	0.173	152.651	1.343	0.195	0.179	0.588	0.866	0.156	1.512	0.236	0.204
6′	24.38	1.394	0.169	141.041	1.394	0.191	0.172	0.588	0.873	0.144	1.560	0.225	0.196
7	30.48	1.394	0.169	141.041	1.394	0.191	0.172	0.735	0.798	0.144	1.560	0.225	0.180
8	36.58	1.394	0.169	141.041	1.394	0.191	0.172	0.882	0.597	0.144	1.560	0.225	0.134
8′	36.58	1.452	0.165	129.517	1.452	0.187	0.166	0.882	0.606	0.132	1.615	0.213	0.129
9	41.45	1.452	0.165	129.517	1.452	0.187	0.166	1	0	0.132	1.615	0.213	0.000

Note:

$$\frac{\tilde{a}_o}{H_o} = \frac{1}{H_o}\sqrt{\frac{A_o}{\pi}\left(\frac{a_o}{b_o}\right)}$$

(c) The normalized mode shape ϕ_{j1} in Column 2 of Table H-9 was determined by the computer program SAP-IV, as described in the previous paragraph. Here the subscript *j* refers to nodal points along the tower height, and subscript *1* is the mode number.

(d) The nodal mass m_j in Column 3 is the combined structural and outside and inside mass of water for excitation in the transverse direction (Table H-7).

(e) The modal earthquake-excitation factor $L_1 = \sum m_j \phi_{j1} = 4.134$ is obtained by multiplying Column 2 by Column 3 and summing the results for all nodes.

(f) The modal mass $M_1 = \sum m_j \phi_{j1}^2 = 1.874$ is computed by multiplying Column 2 by Column 4 and summing the results for all nodes.

(g) When L_1 and M_1 are known, the modal participation factor for Mode 1 is computed from the ratio L_1/M_1=2.206.

Table H-5
Computation of Added Mass for the Inside Water Due to Ground Motion Along Transverse Direction (x-axis)

		Outside Geometry			Equivalent Ellipse		Equivalent Cylinder				
Node No.	Z_i m	$\frac{a_i}{b_i}$	$\frac{a_i}{H_i}$	A_i m²	$\frac{\tilde{a}_i}{\tilde{b}_i}$	$\frac{\tilde{a}_i}{H_i}$	$\frac{\tilde{r}_i}{H_i}$	$\frac{Z_i}{H_i}$	$\frac{m_a^i(z)}{m_\infty^i}$	$m_\infty^i = \rho_w A_i$ MN-sec²/m²	$m_a^i(z)$ MN-sec²/m²
1	2	3	4	5	6	7	8	9	10	11	12
2	0	1.44	0.138	83.59	1.44	0.156	0.109	0.0	1	0.085	0.085
3	5.18	1.44	0.138	83.59	1.44	0.156	0.109	0.131	1	0.085	0.085
4	10.97	1.44	0.138	83.59	1.44	0.156	0.109	0.277	1	0.085	0.085
4′	10.97	1.48	0.142	85.95	1.48	0.161	0.109	0.277	1	0.088	0.088
5	16.46	1.48	0.142	85.95	1.48	0.161	0.109	0.415	1	0.088	0.088
6	22.56	1.48	0.142	85.95	1.48	0.161	0.109	0.569	1	0.088	0.088
6′	22.56	1.52	0.146	88.24	1.52	0.165	0.109	0.569	1	0.090	0.090
7	28.65	1.52	0.146	88.24	1.52	0.165	0.109	0.723	0.991	0.090	0.089
8	34.75	1.52	0.146	88.24	1.52	0.165	0.109	0.877	0.894	0.090	0.080
8′	34.75	1.56	0.150	90.68	1.56	0.169	0.109	0.877	0.894	0.092	0.082
9	39.62	1.56	0.150	90.68	1.56	0.169	0.109	1	0	0.092	0.000

Note:

$$\frac{\tilde{a}_i}{H_i} = \frac{1}{H_i}\sqrt{\frac{A_i}{\pi}\left(\frac{a_i}{b_i}\right)}$$

(h) The maximum modal displacement is obtained from

$$Y_1 = \frac{\frac{L_1}{M_1}}{\omega_1^2} S_{a1}(T_1,\xi_1) = \frac{2.206}{(12.467)^2}(1.289 \times 9.81 \times 1000) = 179 \text{ mm} \qquad \text{(H-5)}$$

(i) The maximum nodal displacements of the tower u_{j1} are obtained by multiplying Y_1 computed in Step h by the mode shape ϕ_{j1} in Column 2. The results are shown in Column 6.

(j) The Mode-1 elastic forces given by $f_{j1} = \frac{L_1}{M_1} m_j \phi_{jn} S_{a1}(T_1,\xi_1)$ are obtained by multiplying L_1/M_1 (from Step g) and S_{a1} (from Step b) by Column 4. The results are listed in Column 7.

(k) The shear force at each section along the tower height is obtained from the summation of elastic forces above that section $V_{j1} = \sum_{k=j}^{13} f_{k1}$. For example $V_{13,1} = f_{13,1} = 2.427$ *MN*, and $V_{12,1} = f_{12,1} + f_{13,1} = 2.427 + 7.152 = 9.579$ *MN*. The shear force at all nodal points is given in Column 8.

Table H-6
Total Lumped Mass for Ground Motion Along Longitudinal axis (y-axis)

Node No.	m_o	m_a^o	m_a^i	$m_o + m_a^o + m_a^i$	Length, m	$m_o + m_a^o + m_a^i$	Total Mass at Point of Discontinuity
1	0.524	0.241		0.765	0.91	0.696	
2	0.524	0.241		0.765	0.91	0.696	2 + 2′ =
2′	0.199	0.152	0.085	0.436	2.59	1.129	1.825
3	0.199	0.152	0.085	0.436	5.18	2.258	
4	0.199	0.150	0.085	0.434	2.59	1.124	4 + 4′ =
4′	0.163	0.136	0.888	0.387	3.05	1.180	2.304
5	0.163	0.133	0.088	0.384	6.10	2.342	
6	0.163	0.127	0.087	0.377	3.05	1.150	6 + 6′ =
6′	0.129	0.115	0.089	0.333	3.05	1.016	2.166
7	0.129	0.105	0.086	0.320	6.10	1.952	
8	0.129	0.080	0.071	0.280	3.05	0.854	8 + 8′ =
8′	0.095	0.073	0.072	0.240	2.44	0.586	1.440
9	0.095	0	0	0.095	6.10	0.580	
10	0.095			0.095	3.66	0.348	10 + 10′ =
10′	0.063			0.063	3.05	0.192	0.540
11	0.063			0.063	5.79	0.365	
12	0.063			0.063	2.74	0.173	12 + 12′ =
12′	0.290			0.290	0.30	0.087	0.260
13	0.290			0.290	0.30	0.087	

(l) Finally the moment at each section is computed from multiplication of elastic forces acting above that section by their associated moment arms $M_{j1} = \sum_{k=j}^{13} h_k f_{k1}$. For example $M_{13,1}$ = 0*2.427 = 0.00 *MN-m*, and $M_{11,1}$ = 0*8.676 + 5.49*7.152 + 6.10*2.427 = 54.070 *MN-m*. The results are given in Column 9.

The computation of Mode-2 response follows the same steps and is shown in Table H-10. The total response of the tower due to excitation along the transverse axis is then obtained by combining the Mode-1 and Mode-2 response quantities listed in Tables H-9 and H-10 by the simplified response spectrum analysis (SRSS) method. For example, the total response quantities at Node 10 are determined as follows:

$$u_{10} = \sqrt{u_{10,1}^2 + u_{10,2}^2} = \sqrt{129^2 + (-7)^2} = 129 \text{ mm} \qquad \text{(H-6)}$$

Table H-7
Total Lumped Mass for Ground Motion Along Transverse Axis (x-axis)

Node No.	m_o	m_a^o	m_a^i	$m_o + m_a^o + m_a^i$	Length, ft	$m_o + m_a^o + m_a^i$	Total Mass at Point of Discontinuity
1	0.524	0.241		0.765	0.91	0.696	
2	0.524	0.241		0.765	0.91	0.696	2 + 2′ =
2′	0.199	0.232	0.085	0.516	2.59	1.336	2.032
3	0.199	0.231	0.085	0.515	5.18	2.668	
4	0.199	0.228	0.085	0.512	2.59	1.326	4 + 4′ =
4′	0.163	0.219	0.088	0.470	3.05	1.434	2.760
5	0.163	0.214	0.088	0.465	6.10	2.836	
6	0.163	0.204	0.088	0.455	3.05	1.388	6 + 6′ =
6′	0.129	0.196	0.090	0.415	3.05	1.266	2.654
7	0.129	0.180	0.089	0.398	6.10	2.428	
8	0.129	0.134	0.080	0.343	3.05	1.046	8 + 8′ =
8′	0.095	0.129	0.082	0.306	2.44	0.747	1.793
9	0.095	0.000	0.000	0.095	6.10	0.580	
10	0.095			0.095	3.66	0.348	10 + 10′ =
10′	0.063			0.063	3.05	0.192	0.540
11	0.063			0.063	5.79	0.365	
12	0.063			0.063	2.74	0.173	12 + 12′ =
12′	0.290			0.290	0.30	0.087	0.260
13	0.290			0.290	0.30	0.087	

$$f_{10} = \sqrt{f_{10,1}^2 + f_{10,2}^2} = \sqrt{10.817^2 + (-5.360)^2} = 12.072 \text{ MN} \quad \text{(H-7)}$$

$$V_{10} = \sqrt{V_{10,1}^2 + V_{10,2}^2} = \sqrt{29.072^2 + (-22.828)^2} = 36.964 \text{ MN} \quad \text{(H-8)}$$

$$M_{10} = \sqrt{M_{10,1}^2 + M_{10,2}^2} = \sqrt{165.426^2 + (-164.920)^2} = 233.590 \text{ MN-m} \quad \text{(H-9)}$$

The results for other nodes are given in Table H-11.

(2) Computer analysis. The results for computer response analysis using the SAP-IV program are displayed in Figures H-10 to H-12. Figure H-10 clearly demonstrates that the total displacements of the tower are due essentially to the first mode response and that the displacements for the third and higher modes are practically zero. Figure H-11 provides a comparison of shear forces for four different cases.

Table H-8
Natural Periods of Vibration for Example Tower, sec

Mode No.	Without Shear Deformation		With Shear Deformation	
	Transverse	Longitudinal	Transverse	Longitudinal
1	0.4588	0.3493	0.504	0.388
2	0.1186	0.0865	0.161	0.124
3	0.0468	0.0335	0.082	0.063
4	0.0240	0.0173	0.052	0.041
5	0.0154	0.0110	0.040	0.032
6	0.0104	0.0075	0.033	0.026
7	0.0071	0.0051	0.030	0.023
8	0.0056	0.0039	0.026	0.021
9	0.0046	0.0034	0.023	0.019
10	0.0040	0.0028	0.019	0.015

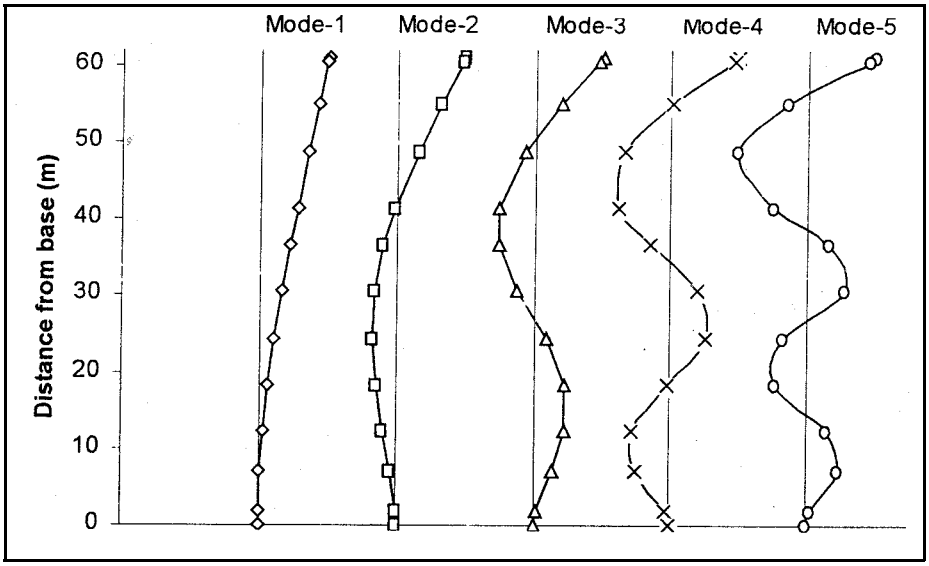

Figure H-9. Normalized lowest five mode shapes of example tower

The two-mode approximation of shear forces was computed manually in the previous paragraph, whereas those based on 10 modes of vibration were evaluated using SAP-IV. The computer analyses of shear forces were carried out for the standard and the site-specific ground motions with and without the effects of shear deformations. As expected, the shear forces for the standard response spectra are the largest, mainly because the standard response spectra show higher spectral accelerations than the site-specific spectra do (Figure H-2). The results also show that ignoring the effect of shear deformation would result

Table H-9
Mode-1 Nodal Displacements, Lateral Forces, Shears, and Overturning Moments Due to Ground Motion Along Transverse Axis (x-axis)

Node No.	ϕ_{j1}	m_j MN-sec²/m²	$\phi_{j1} \times m_j$ MN-sec²/m²	$\phi_{j1}^2 \times m_j$ MN-sec²/m²	u_{j1} mm	f_{j1} MN	V_{j1} MN	M_{j1} MN
1	2	3	4	5	6	7	8	9
13	1.000	0.087	0.087	0.087	179	2.427	2.427	0.000
12	0.986	0.260	0.256	0.253	177	7.152	9.579	1.481
11	0.852	0.365	0.311	0.265	153	8.676	18.255	54.070
10	0.718	0.540	0.388	0.278	129	10.817	29.072	165.426
9	0.555	0.580	0.322	0.179	100	8.981	38.052	378.232
8	0.451	1.793	0.809	0.365	81	22.560	60.612	563.927
7	0.329	2.428	0.799	0.263	59	22.286	82.898	933.662
6	0.219	2.654	0.581	0.127	39	16.215	99.113	1439.338
5	0.128	2.836	0.363	0.046	23	10.127	109.240	2043.928
4	0.059	2.760	0.163	0.010	11	4.543	113.783	2710.295
3	0.020	2.668	0.053	0.001	4	1.489	115.272	3299.693
2	0.001	2.032	0.002	0.000	0	0.057	115.329	3896.802
1	0.000	0.696	0.000	0.000	0	0.000	115.329	4107.854

Note: L_1 = 4,134
M_1 = 1.874
L_1/M_1 = 2.206
S_a = 1.289 g
ω = 12.467 rad/sec

in 10 percent less base shear, but has negligible effect on the overturning moments. The two-mode approximation gives slightly smaller shear forces and overturning moments than the computer analysis, which considers 10 modes of vibration. The shears and moments due to the probabilistic seismic hazard analysis (PSHA) spectra are also smaller than those due to the standard spectra.

c. Response due to longitudinal excitation.

(1) Two-mode approximation. The two-mode approximation of the tower response due to excitation along the longitudinal axis is given in Tables H-12 to H-14. The computation steps are identical to those described in *b*(1) above, except that the periods, mode shapes, and the mass distribution associated with the vibration along the longitudinal axis of the tower are used. Again the Mode-1 (Table H-12) and Mode-2 responses (Table H-13) are computed separately and then combined using the SRSS method to obtain the total response due to the longitudinal excitation (Table H-14).

(2) Computer analysis. The results of computer response analysis for excitation along the longitudinal axis are given in Figures H-13 and H-14. The highest shear forces are obtained for the standard response spectra and the lowest shear forces for the case without shear deformation. The magnitudes of shear forces for the two-mode approximation and the 10-mode computer analysis are

Table H-10
Mode-2 Nodal Displacements, Lateral Forces, Shears, and Overturning Moments Due to Ground Motion Along Transverse Axis (x-axis)

Node No.	ϕ_{j2}	m_j MN-sec^2/m^2	$\phi_{j2} \times m_j$ MN-sec^2/m^2	$\phi_{j2}^2 \times m_j$ MN-sec^2/m^2	u_{j2} mm	f_{j2} MN	V_{j2} MN	M_{j2} MN
1	2	3	4	5	6	7	8	9
13	1.000	0.087	0.087	0.087	-20	-2.657	-2.657	0.000
12	0.967	0.260	0.251	0.243	-19	-7.678	-10.335	-1.621
11	0.640	0.365	0.234	0.150	-13	-7.134	-17.469	-58.360
10	0.325	0.540	0.176	0.057	-7	-5.360	-22.828	-164.920
9	-0.006	0.580	-0.003	0.000	0	0.106	-22.722	-332.025
8	-0.170	1.793	-0.305	0.052	3	9.309	-13.414	-442.909
7	-0.287	2.428	-0.697	0.200	6	21.281	7.867	-524.732
6	-0.308	2.654	-0.817	0.252	6	24.964	32.831	-476.743
5	-0.252	2.836	-0.715	0.180	5	21.825	54.656	-276.477
4	-0.151	2.760	-0.417	0.063	3	12.727	67.393	56.924
3	-0.067	2.668	-0.179	0.012	1	5.459	72.842	405.969
2	-0.006	2.032	-0.012	0.000	0	0.372	73.215	783.293
1	0.000	0.696	0.000	0.000	0	0.000	73.215	917.276

Note: L_2 = -2.397
M_2 = 1.295
L_2/M_2 = -1.851
S_a = 1.682 g
ω = 39.026 rad/sec

essentially the same. The moments for the standard response spectra are the largest, but are about the same for the other three. The results indicate that the two-mode approximation method and shear deformation affect the shear forces more than they do the moments.

d. Response due to transverse and longitudinal excitations.

(1) The peak value of any resultant response quantity R due to the combined gravity and ground motion components is obtained from one of the following equations:

$$R = R_o \pm R_x \pm 0.5R_y \quad \text{(H-10)}$$

$$R = R_o \pm 0.5R_x \pm R_y \quad \text{(H-11)}$$

$$R = R_o \pm \sqrt{R_x^2 + R_y^2} \quad \text{(H-12)}$$

Table H-11
Combined Mode-1 and Mode-2 Responses Due to 1000-year San Francisco Bay Area Ground Motion Applied Along Transverse Axis (x-axis)

Node No.	$u_j = \sqrt{u_{j1}^2 + u_{j2}^2}$ mm	$f_j = \sqrt{f_{j1}^2 + f_{j2}^2}$ MN	$V_j = \sqrt{V_{j1}^2 + V_{j2}^2}$ MN	$M_j = \sqrt{M_{j1}^2 + M_{j2}^2}$ MN-m
13	181	3.599	3.599	0.000
12	178	10.493	14.092	2.195
11	153	11.232	25.267	79.558
10	129	12.072	36.964	233.590
9	100	8.981	44.320	503.289
8	81	24.405	62.079	717.065
7	59	30.814	83.270	1071.013
6	40	29.768	104.409	1516.238
5	24	24.061	122.150	2062.543
4	11	13.514	132.239	2710.892
3	4	5.658	136.359	3324.573
2	0	0.377	136.606	3974.747
1	0	0.000	136.606	4209.021

where

R_0 = peak response due to gravity loads

R_x = peak response due to the x-component of ground motion

R_y = peak response due to the y-component of ground motion

Equations H-10 and H-11 are used with the standard response spectra, and Equation H-12 is employed with the site-specific response spectra. These equations are particularly applicable to the computation of section stresses.

(2) For the example tower with two axes of symmetry, gravity loads do not produce shears and moments. The x-component of ground motion produces shear only in the x-direction V_x and bending moment only about y-axis M_y. Similarly, the y-component of ground motion generates shear only in the y-direction V_y and bending moment only about the x-axis M_x. Therefore, for evaluation only the following combination of shears and moments need to be considered: V_x and 0.5 V_y, with M_x and 0.5 M_y and 0.5 V_x and V_y with 0.5 M_x and M_y.

(3) For the purpose of this example, the fault normal and the fault parallel components of ground motion response spectra (see paragraph 3-3*b*(4)) were assumed to be respectively 15 percent higher and 15 percent lower than the average equal-hazard spectra shown in Figure H-2. However, the standard response spectra were assumed to be the same for both horizontal directions. The combination of shear forces V_x and $0.5V_y$ and bending moments M_x and $0.5M_y$ for the site-specific and standard response spectra of ground motion are shown in Figures H-15 and H-16, respectively. The combination of shear forces $0.5V_x$ and V_y and bending moments $0.5M_x$ and M_y are presented in Figures H-17 and H-18, respectively.

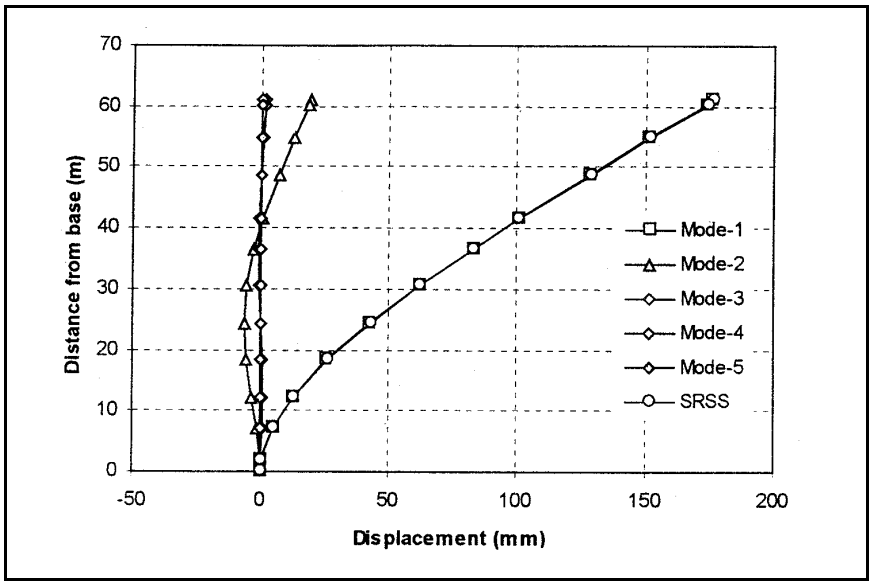

Figure H-10. Modal and SRSS displacements due to 1000-year San Francisco Bay area response spectra motion applied along x-axis (transverse direction)

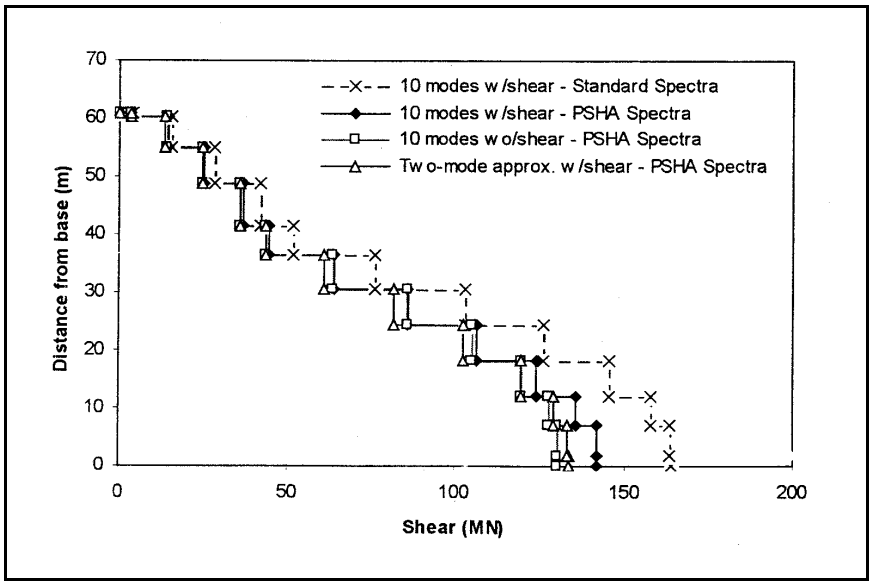

Figure H-11. Maximum shears due to 1000-year San Francisco Bay area response spectra applied along x-axis (transverse direction)

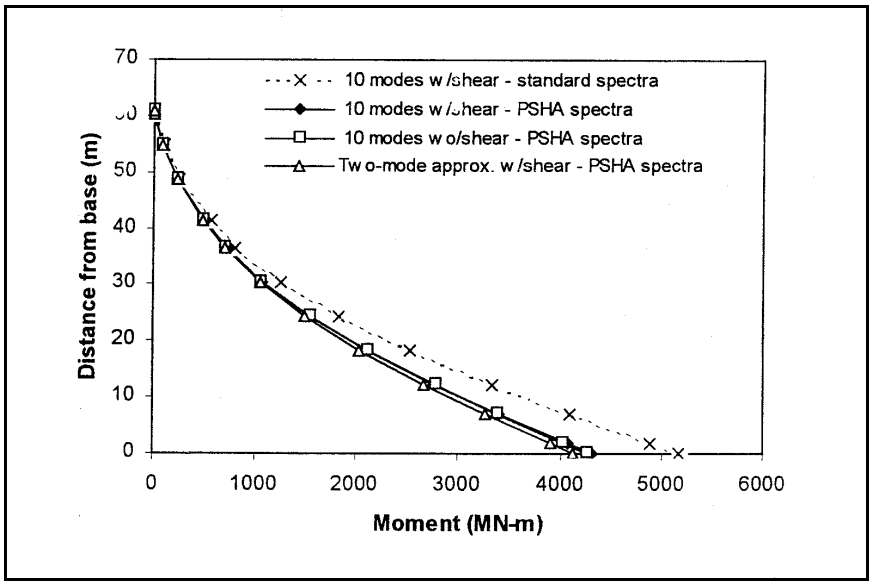

Figure H-12. Maximum moments due to 1000-year San Francisco Bay area response spectra applied along x-axis (transverse direction)

Table H-12
Mode-1 Nodal Displacements, Lateral Forces, Shears, and Overturning Moments Due to Ground Motion Along Longitudinal Axis (y-axis)

Node No.	ϕ_{j1}	m_j MN-sec^2/m^2	$\phi_{j1} \times m_j$ MN-sec^2/m^2	$\phi_{j1}^2 \times m_j$ MN-sec^2/m^2	u_{j1} mm	f_{j1} MN	V_{j1} MN	M_{j1} MN
1	2	3	4	5	6	7	8	9
13	1.000	0.087	0.087	0.087	116	2.645	2.645	0.000
12	0.987	0.260	0.257	0.253	114	7.801	10.446	1.613
11	0.857	0.365	0.313	0.268	99	9.509	19.954	58.960
10	0.726	0.540	0.392	0.285	84	11.917	31.872	180.682
9	0.567	0.580	0.329	0.186	66	9.997	41.869	413.984
8	0.464	1.440	0.668	0.310	54	20.311	62.180	618.304
7	0.343	1.952	0.670	0.230	40	20.353	82.533	997.603
6	0.233	2.166	0.505	0.118	27	15.342	97.875	1501.054
5	0.140	2.342	0.328	0.046	16	9.967	107.842	2098.089
4	0.067	2.304	0.154	0.010	8	4.693	112.534	2755.924
3	0.025	2.258	0.056	0.001	3	1.716	114.250	3338.851
2	0.002	1.825	0.004	0.000	0	0.111	114.361	3930.668
1	0.000	0.696	0.000	0.000	0	0.000	114.361	4139.949

Note: $L_1 = 3.762$
$M_1 = 1.794$
$L_1/M_1 = 2.097$
$S_a = 1.478$ g
$\omega = 16.194$ rad/sec

Table H-13
Mode-2 Nodal Displacements, Lateral Forces, Shears, and Overturning Moments Due to Ground Motion Along Longitudinal Axis (y-axis)

Node No.	ϕ_{j2}	m_j MN-sec^2/m^2	$\phi_{j2} \times m_j$ MN-sec^2/m^2	$\phi_{j2}^2 \times m_j$ MN-sec^2/m^2	u_{j2} mm	f_{j2} MN	V_{j2} MN	M_{j2} MN
1	2	3	4	5	6	7	8	9
13	1.000	0.087	0.087	0.087	-10	-2.187	-2.187	0.000
12	0.969	0.260	0.252	0.244	-9	-6.332	-8.519	-1.334
11	0.648	0.365	0.237	0.153	-6	-5.945	-14.464	-48.104
10	0.326	0.540	0.176	0.057	-3	-4.425	-18.889	-136.335
9	-0.017	0.580	-0.010	0.000	0	0.248	-18.641	-274.602
8	-0.195	1.440	-0.281	0.055	2	7.058	-11.583	-365.570
7	-0.328	1.952	-0.640	0.210	3	16.093	4.510	-436.227
6	-0.359	2.166	-0.778	0.279	4	19.545	24.054	-408.718
5	-0.304	2.342	-0.712	0.216	3	17.895	41.950	-261.987
4	-0.192	2.304	-0.442	0.085	2	11.119	53.068	-6.095
3	-0.092	2.258	-0.208	0.019	1	5.221	58.290	268.799
2	-0.009	1.825	-0.016	0.000	0	0.413	58.703	570.740
1	0.000	0.696	0.000	0.000	0	0.000	58.703	678.166

Note: L_2 = -2.336
M_2 = 1.407
L_2/M_2 = -1.661
S_a = 1.543 g
ω = 50.671 rad/sec

Table H-14
Combined Mode-1 and Mode-2 Responses Due to 1000-year San Francisco Bay Area Ground Motion Applied Along Longitudinal Axis (y-axis)

Node No.	$u_j = \sqrt{u_{j1}^2 + u_{j2}^2}$ mm	$f_j = \sqrt{f_{j1}^2 + f_{j2}^2}$ MN	$V_j = \sqrt{V_{j1}^2 + V_{j2}^2}$ MN	$M_j = \sqrt{M_{j1}^2 + M_{j2}^2}$ MN-m
13	116	3.432	3.432	0.000
12	115	10.048	13.479	2.093
11	100	11.214	24.645	76.094
10	84	12.712	37.049	226.348
9	66	10.000	45.831	496.779
8	54	21.503	63.250	718.291
7	40	25.947	82.656	1,088.809
6	27	24.847	100.787	1,555.704
5	16	20.484	115.713	2,114.383
4	8	12.069	124.420	2,755.931
3	3	5.496	128.261	3,349.654
2	0	0.427	128.548	3,971.888
1	0	0.000	128.548	4,195.127

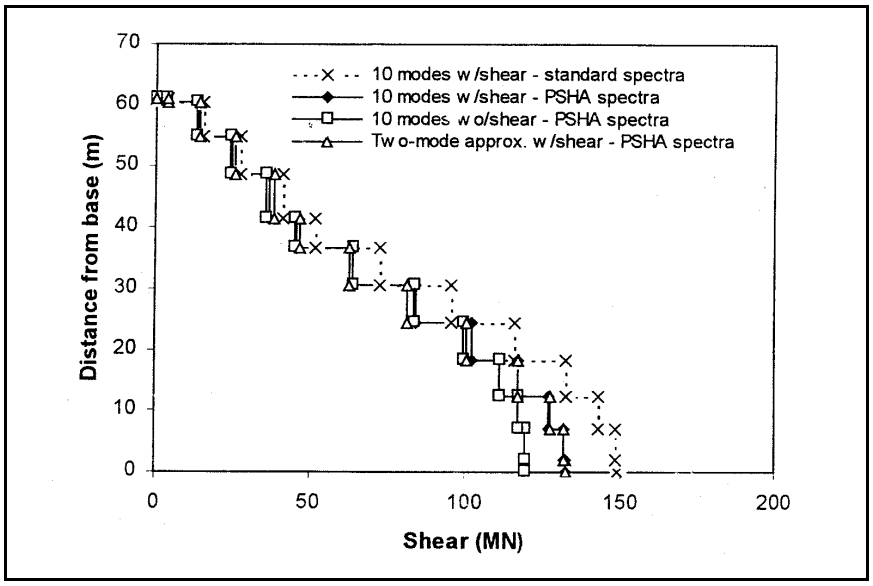

Figure H-13. Maximum shears due to 1000-year San Francisco Bay area response spectra applied along y-axis (longitudinal direction)

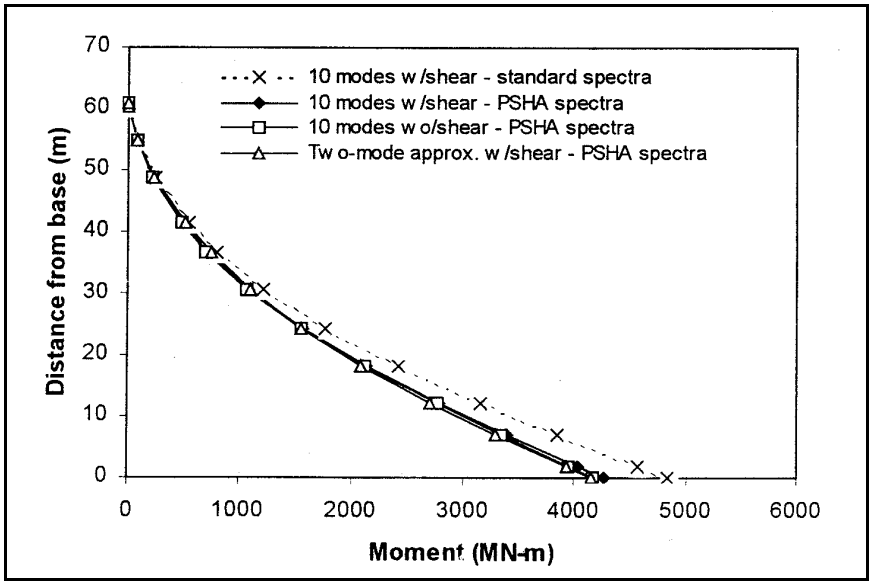

Figure H-14. Maximum moments due to 1000-year San Francisco Bay area response spectra applied along y-axis (longitudinal direction)

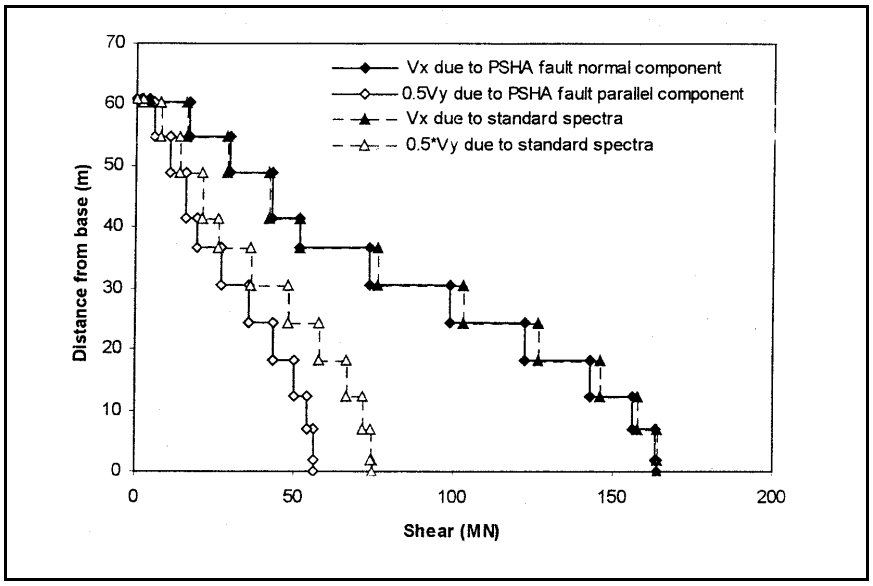

Figure H-15. Combination of shear forces V_x and 0.5V_y for site-specific and standard ground motions

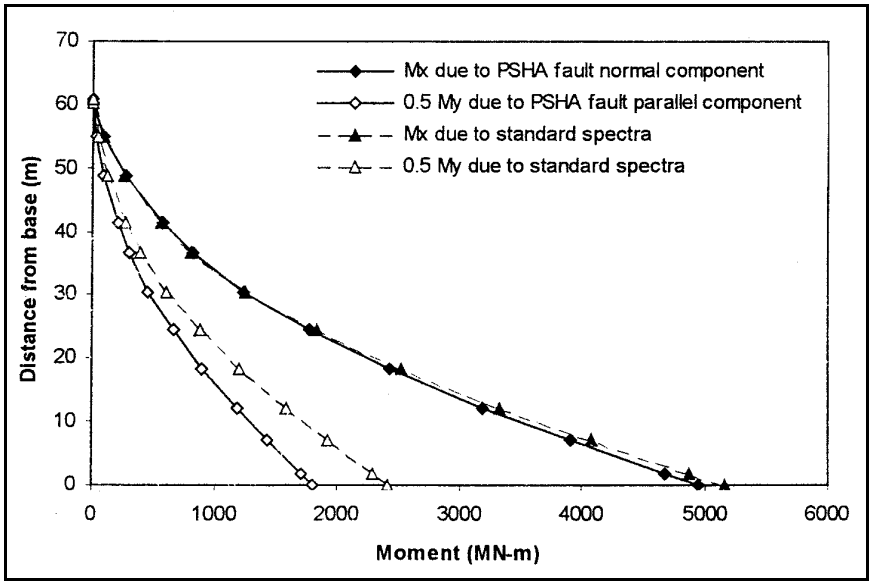

Figure H-16. Combination of moments M_x and 0.5M_y for site-specific and standard ground motions

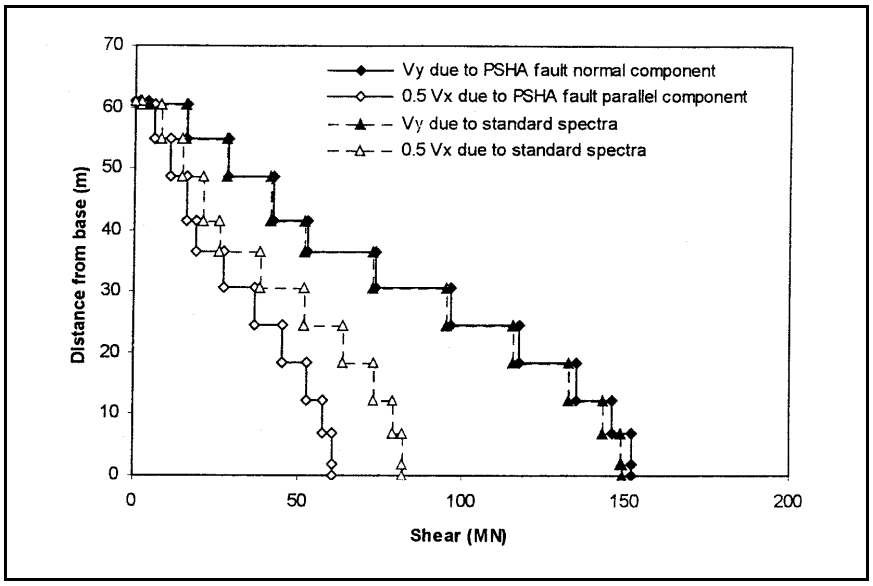

Figure H-17. Combination of shear forces $0.5V_x$ and V_y for site-specific and standard ground motions

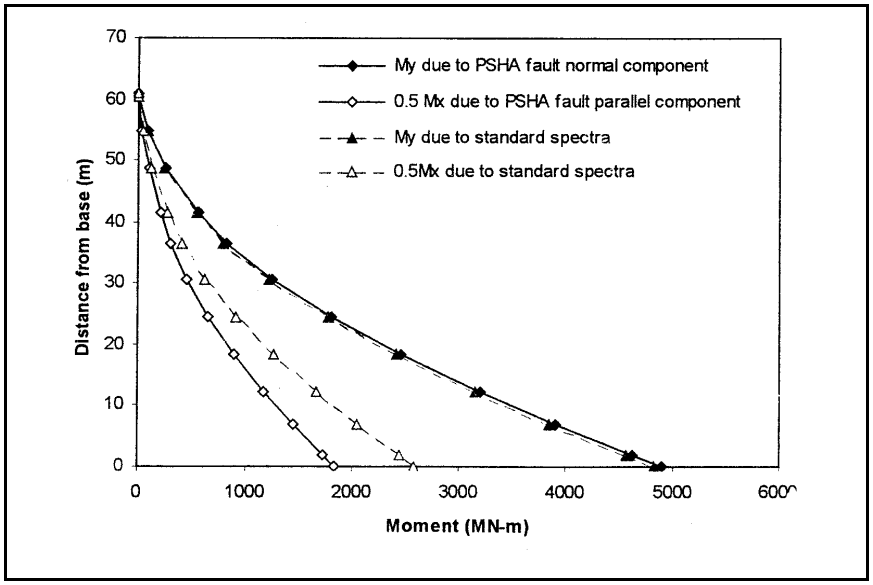

Figure H-18. Combination of shear forces $0.5M_x$ and M_y for site-specific and standard ground motions

H-7. Conversion Factors

To Convert	Into	Multiply By
Meter (m)	ft	3.281
m^2	ft^2	10.764
m^4	ft^4	115.884
Mega Newton (MN)	kip	224.81
Mega Pascal (Mpa)	psi	145.038
MN-m	kip-ft	737.562
MN-sec^2/m	k-sec^2/ft	68.488
MN-sec^2/m^2	k-sec^2/ft^2	20.875
MN/m^3	pcf	6250

Appendix I
Glossary

I-1. Sources

The following definitions were assembled from glossaries in Bolt (1978), ICOLD Bulletin 72 (1989), and EERI Committee on Seismic Risk (1984).

I-2. Terms

Acceleration Time-History
A time series of accelerations that is either recorded during an actual earthquake or synthesized to be representative of that recorded during an earthquake.

Accelerometer
A seismograph for measuring ground acceleration as a function of time.

Acceptable Risk
A probability of social or economic consequences due to earthquakes that is low enough (for example in comparison with other natural or man-made risks) to be judged by appropriate authorities to represent a realistic basis for determining design requirements for engineered structures or for taking certain social economic actions.

Active Fault
A fault, reasonably identified and located, known to have produced historical earthquakes or showing geologic evidence of Holocene (11,000 years) displacements and which, because of its present tectonic setting, can undergo movement during the anticipated life of man-made structures. Differences of opinion regarding the definition of activity are acknowledged. For the purpose of earthquake engineering application, a seismogenic or earthquake fault is distinct from other types of fractures such as those resulting from landslides, ice thrusting, groundwater withdrawal effects, etc. (Alternate: a fault that may produce an earthquake within a specified exposure time, given the assumption adopted for a specific seismic-risk analysis.)

Aftershocks
Smaller earthquakes following the largest earthquake of a series concentrated in a restricted crustal volume.

Attenuation
Decrease in amplitude and change in frequency content of the seismic waves with distance because of geometric spreading, energy absorption, and scattering. Also designates a decrease of signal magnitude during transmission, and a reduction of amplitude or energy without change of wave form.

B-value
A parameter indicating the relative frequency of occurrence of earthquakes of different sizes. It is the slope of a straight line indicating absolute or relative frequency (plotted logarithmically) versus earthquake magnitude or meiszoseismal Modified Mercalli Intensity. (The B-value indicates the slope of the Gutenberg-Richter recurrence relationship.)

Bedrock
Any sedimentary, igneous, or metamorphic material represented as a unit in geology, consisting of a sound and solid mass, layer, or ledge of mineral matter, with shear wave threshold velocities greater than 750 m/sec. Bedrock can be exposed at the ground surface or underlie soil layers.

Coefficient of Variation
The ratio of standard deviation to the mean.

Critical Damping
The least amount of damping that will prevent free oscillatory vibration in a one-degree-of-freedom system.

Damage
Any economic loss or destruction caused by earthquakes.

Damping
Resistance that reduces or opposes vibrations by energy absorption. There are different types of damping, such as material (viscous, Coulomb) and geometric (radiation) damping.

Damping Ratio
The ratio of the actual damping to the critical damping.

Design Response Spectrum
A smooth response spectrum developed from a deterministic or probabilistic ground motion analysis and used as a basis for seismic design.

Dispersion (wave)
The spreading out of a wave train due to each wave length traveling with its own velocity.

Duration
A qualitative or quantitative description of the length of time during which ground motion at a site shows certain characteristics (perceptibility, violent shaking, etc.).

Earthquake
A sudden motion or vibration in the earth caused by the abrupt release of energy in the earth's lithosphere. The wave motion may range from violent at some locations to imperceptible at others. (Alternate: The vibrations of the earth caused by the passage of seismic waves radiating from some source of elastic energy.)

Elastic Rebound Theory
The theory of earthquake generation proposing that faults remain locked while strain energy slowly accumulates in the surrounding rock, and then suddenly slip, releasing this energy.

Epicenter
The point on the surface of the earth directly above the focus (hypocenter) of an earthquake.

Equal-Hazard Response Spectrum
A response spectrum developed from a probabilistic ground motion analysis that has an equal probability of being exceeded at each period of vibration

Exceedance Probability
The probability that a specified level of ground motion or specified social or economic consequence of earthquakes will be exceeded at a site or in a region during a specified exposure time.

Expected
Mean, average.

Expected Ground Motion
The mean value of one or more characteristics of ground motion at a site for a single earthquake (mean ground motion).

Exposure Time
The time period of interest for seismic-risk calculations, seismic-hazard calculations, or design of structures. For some categories of structures such as buildings, the exposure time is often chosen to be equal to the design lifetime of the structure.

Fault
A fracture or zone of fractures in rock along which the two sides have been displaced relative to each other parallel to the fracture. The total fault offset may range from centimeters to kilometers.

Fault Plane
The plane that most closely coincides with the rupture surface of a fault.

Focal Depth
The vertical distance between the epicenter and the hypocenter.

Focus
See Hypocenter.

Free Field
The regions of the ground surface not influenced by man-made structures. Also designates a medium that contains no structure (free-field profile), or a region where boundary effects do not influence the behavior of the medium significantly.

Frequency
Number of hertz or equivalent cycles per second.

Geologic Hazard
A geologic process (e.g., landsliding, liquefaction, soil compaction, surface fault rupture) that during an earthquake or other natural event may produce adverse effects in structures.

Hertz
The unit of frequency equal to one cycle per second or 2π radians per second.

Hypocenter
The point within the earth at which an earthquake initiates.

Intensity
A numerical index describing the effects of an earthquake on man-made structures or other features of the surface of the earth. The assignment of intensity values is subjective and is influenced by the quality of construction, the ground surface condition, and the individual perception of the observer. Different intensity scales are used in various countries, such as the Modified Mercalli Intensity scale, which is the most widely used in the United States.

Left-lateral Fault
A strike-slip fault on which the displacement of the far block is to the left when viewed from either side.

Liquefaction (of Soil)
Process of soil behaving like a dense fluid rather than a wet solid mass during an earthquake.

Love Waves
Seismic surface wave with only horizontal shear motion transverse to the direction of propagation.

Magnitude (of Earthquakes)
A measure of earthquake size, determined by taking the common logarithm (base 10) of the largest ground motion recorded during the arrival of a seismic wave type and applying a standard correction for distance to the epicenter. Three common types of magnitude are Richter (or local) (M_L), P body wave (m_b), and surface wave (M_s). Moment magnitude (M_W), which is directly determined from the logarithm of the seismic moment (see definition below), is another type of magnitude often used.

MCE
The Maximum Credible Earthquake.

MDE
The Maximum Design Earthquake.

Mean Recurrence Interval, Average Recurrence Interval
The average time between earthquakes or faulting events with specific characteristics (e.g., magnitude $\geq$ 6) in a specified region or in a specified fault zone.

Mean Return Period
The average time between occurrences of ground motion with specific characteristics (e.g., peak horizontal acceleration $\geq$ 0.1g) at a site (equal to the inverse of the annual frequency of exceedance).

Moment (of Earthquakes)
The rigidity of rocks times the area of faulting times the amount of slip. A measure of earthquake size.

Near-Field Motion
Ground motion recorded in the vicinity of a fault.

Normal Fault
A dip-slip fault in which the rock above the fault plane has moved downward relative to the rock below.

OBE
The Operating Basis Earthquake.

Oblique-Slip Fault
A fault that combines some strike-slip motion with some dip-slip motion.

PGA
Peak Ground Acceleration.

P-Wave
The primary or fastest wave traveling away from a seismic event through the rock, and consisting of a train of compressions and dilations of the material.

Period (Wave)
The time interval between successive crests in a sinusoidal wave train; the period is the inverse of the frequency of a cyclic event.

Phase
The angle of lag or lead of a sine wave with respect to a reference. The phase response is the graph of the phase shift versus frequency.

Plate (Tectonic)
A large, relatively rigid, segment of the lithosphere of the earth that moves in relation to other plates over the deeper interior. Plates meet in convergence zones and separate at divergence zones.

Plate Tectonics
The theory of plate movement and interaction; the attempt to explain earthquakes, volcanoes, and mountain building as consequences of large horizontal surface motions.

Rayleigh Waves
Seismic surface waves with ground motion only in a vertical plane containing the direction of propagation of the waves.

Refraction (Wave)
The departure of a transmitted wave from its original direction of travel at an interface with a material of different wave velocity.

Response Spectrum
A plot of the maximum values of acceleration, velocity, and/or displacement response of an infinite series of single-degree-of-freedom systems subject to a time-dependent dynamic excitation, such as but not limited to ground motion. The maximum response values are expressed as a function of undamped natural period for a given damping. Approximate response spectrum acceleration, velocity, and displacement values may be calculated from each other assuming a sinusoidal relationship between them. When calculated in this manner, these are sometimes referred to as pseudo-acceleration, pseudo-relative velocity, or pseudo-relative displacement response spectrum values.

Reverse Fault
A dip-slip fault in which the rocks above the fault plane move up and over the lower rocks, so that older strata are placed over younger strata. A low-angle (less than 45 deg from horizontal) reverse fault is termed a thrust fault.

Right-Lateral Fault
A strike-slip fault on which the displacement of the far block is to the right when viewed from either side.

Risk (Seismic)
The relative risk is the comparative earthquake hazard from one site to another. The probabilistic risk is the odds of earthquake occurrence within a given time interval and region.

S-Wave
The secondary seismic wave, traveling more slowly than the P-wave, and consisting of elastic vibrations transverse to the direction of travel. It cannot propagate in a liquid.

Seismic Hazard
Any physical phenomenon (e.g., ground shaking, ground failure) associated with an earthquake that may produce adverse effects on human activities. In the context of a probabilistic ground motion analysis (often termed a probabilistic seismic hazard analysis, or PSHA), hazard refers to the probability or frequency of exceeding a certain amplitude of ground motion.

Seismicity
The occurrence of earthquakes in space and time.

Seismic Risk
The probability that social or economic consequences of earthquakes will equal or exceed specified values at a site, at several sites, or in an area during a specified exposure time.

Seismic Wave
An elastic wave in the earth usually generated by an earthquake source or explosion.

Seismograph
An instrument for recording as a function of time the motions of the surface of the earth that is caused by seismic waves.

Seismology
The study of earthquakes, seismic sources, and wave propagation through the earth.

Seismoscope
A simple seismograph recording on a plate without time marks.

Seismometer
The sensor part of the seismograph, usually a suspended pendulum.

Slip (Fault)
The relative motion of one face of a fault relative to the other.

Standard Deviation
The square root of the variance of a random variable.

Strain (Elastic)
The geometrical deformation or change in shape of a body. The change in an angle, length, area, or volume divided by the original value.

Stress (Elastic)
A measure of the forces acting on a body in units of force per unit area.

Stress Drop
Initial shear stress acting across a fault plane minus the residual shear stress across the same fault plane after occurrence of slippage.

Strike-Slip Fault
A fault in which movement is principally horizontal.

Strong Ground Motion
The shaking of the ground made up of large-amplitude seismic waves of various types.

Strong Motion
Ground motion of sufficient amplitude to be of engineering significance in the evaluation of damage due to earthquakes.

Subduction Zone
A dipping ocean plate descending into the earth away from an ocean trench. It is usually the locus of intermediate and deep earthquakes defining the Benioff zone.

Surface Wave (of Earthquakes)
Seismic waves that follow the earth's surface only, with a speed less than that of S-waves. There are two types of surface waves: Rayleigh waves and Love waves.

Swarms (of Earthquakes)
A series of earthquakes in the same locality, no one earthquake being of outstanding size.

Synthetic Acceleration Time-History
An acceleration time-history that is not recorded during an actual earthquake but is developed to be representative of one that could be recorded during a design earthquake. One form of synthetic time-history is modified from a recorded time-history using spectrum matching techniques so that its response spectrum is a close match to the design response spectrum. Another form of synthetic time-history is developed from ground motion modeling methods to be similar to a time-history that might be recorded during an actual earthquake. Such modeling methods simulate the rupture process at the earthquake source and the seismic wave propagation from the earthquake source to the site.

Tectonic Earthquakes
Earthquakes resulting from sudden release of energy stored by major deformation of the earth.

Tectonic Province
A geologic area characterized by similarity of geologic structure and earthquake characteristics.

Tectonics
Large-scale deformation of the outer part of the earth resulting from forces in the earth.

Tsunami
A long-period ocean wave usually caused by sea floor movements in an earthquake.

Variance
The mean squared deviation of a random variable from its average value.

Wavelength
The distance between two successive crests or troughs of a wave.